The University Of Sheffield.

Department Of Mechanical Engineering

PhD Mechanical Engineering PhD Thesis

Sand Particle Entrainment and its Effects on the Wheel/Rail Interface

William **SKIPPER**

September 2021

PhD Thesis submitted to the Department of Mechanical Engineering, University of Sheffield in fulfilment of the requirements for the degree of PhD

ABSTRACT

Low adhesion in the wheel/rail contact has long been a problem for the rail industry in Great Britain as it causes significant scheduling and safety issues; this is especially true in Autumn. Applying sand to the wheel/rail contact has long been used to mitigate against low adhesion, however there is not a common consensus on what makes a "good" particle for restoring adhesion.

The aim of this project was to optimise the sanding process by investigating what constitutes an ideal adhesion restoring particle. The structure of this investigation included characterising a range of particles and assessing their effect in a small scale tribological test, namely the high pressure torsion rig. Additionally, work was undertaken to study the entrainment of particles into the wheel/rail contact; this was achieved through particle characterisation and the use of a scaled-wheel test set-up. Finally, the extended creep-force model was parameterised using data accrued from high pressure torsion testing to predict full-scale wheel/rail behaviour when sand is present; these predictions were validated using data from a full-scale wheel/rail rig.

A literature review was conducted to assess previous sanding research, this resulted in the identification of knowledge gaps in the understanding of the sanding process. The identified knowledge gaps included: the effect different particle characteristics have on wheel/rail adhesion; the mechanisms surrounding the restoration of adhesion by particles; and modelling the effect of particles with regards to their full-scale behaviour.

A particle characterisation framework was formulated based off key particle properties for sanding that were identified during the literature review. A range of particles from the international rail industry and other marketed abrasive products were assessed using the particle characterisation framework and the measured data was used in later chapters to compare the importance of different characteristics on adhesion and damage during high pressure torsion testing.

High pressure torsion (HPT) testing has previously been used to simulate the wheel/rail contact by using a rail and wheel specimen to create a flat, annular contact under high normal pressures with the two specimens then rotated over one another and the torque required to do this measured. As part of this project, the test methodology was adapted for testing with granular material and with low adhesion conditions present. An ordinary least squares model was used to assess which particle characteristics had a statistically significant effect on traction and damage. Through this, harder and more circular particles were found to increase

traction in dry and wet conditions, whilst in leaf contaminated conditions harder, and less circular particles of an optimum size increased traction. With regards to damage, less circular particles produced rougher surfaces, with larger particles creating more roughness on the surface of the wheel specimen surface.

Further HPT tests were conducted to assess the effects of multiple wheel passes and varying normal pressure on traction using one type of rail sand. It was observed that in dry and wet conditions multiple passes had little effect on traction, whereas in leaf contaminated conditions traction decreased. In dry and wet conditions, increasing normal pressure saw an increase in traction, in contrast with leaf contaminated conditions where an increase in normal pressure resulted in a decrease in traction.

Scaled-wheel tests were performed to corroborate findings concerning particle entrainment observed during particle characterisation and HPT testing. In dry conditions, much of the sand particle was expelled out of the contact upon being crushed. In comparison, wet conditions saw a greater amount of the particle being retained in the contact.

Finally, HPT data was used to parameterise the extended creep-force (ECF) model. Good agreement was seen between the HPT data and ECF model, indicating the parameterisation process was successful. The parameterised ECF model was then used to generate predicted creep curves for a typical real-world wheel/rail contact; in dry, sanded conditions, adhesion was estimated to be between 0.4-0.5; in wet, sanded conditions, between 0.3-0.4; and in sanded, leaf contaminated conditions, between 0.1-0.2.

Full-scale validation of the ECF predictions was hampered by unusually low traction measurements on the FSR, however the trends between contact conditions and normal loads were similar to the ECF predictions. In addition, field data from unsanded and sanded, leaf contaminated conditions matched up very well with ECF predictions.

ACKNOWLEDGEMENT

The author would like to sincerely thank Professor Roger Lewis and Mr Anup Chalisey for their steadfast support and exceptional guidance throughout this PhD project.

The author would also like to express his gratitude for the funding and support received from the Engineering and Physical Sciences Research Council & the Rail Safety and Standards Board. In the case of the latter, special mention should be made with regards to the support afforded by the adhesion research group.

Thanks must also go to the integrated tribology CDT, with respect to their help and provision of tribology training, special thanks must go to the CDT manager Ms Kimberly Matthews-Hyde.

Use of the ECF model has proved vital for the success of this project, therefore the author would like to extend his sincere gratitude to those Virtual Vehicle Research, particularly Dr Klaus Six and Dr Alexander Meierhofer whose enthusiasm for the project and hospitality was much appreciated.

The author would like to thank all those fellow PhD students and Research Associates who provided help and support during this project, especially with regards to Dr Sadegh Nadimi and Dr Michael Watson for their invaluable help with particle characterisation and statistical analysis.

Gratitude must also be expressed for the technicians in the mechanical engineering department who assisted with this project. Special recognition in particular is reserved for Mr Richard Kay and Mr Dave Butcher.

Finally, I would like to thank all my friends & family for their comradeship and support during the writing of this thesis.

TABLE OF CONTENTS

LIST OF FIGURES

LIST OF TABLES

1 INTRODUCTION

1.1 Statement of Problem

Low adhesion[1] within the wheel/rail contact of a train is estimated to cost the British rail industry ~£345 m/annum [1]; the loss of traction when accelerating and braking can lead to timetable delays [2] and safety issues (e.g. signals passed at danger or in the worst case collisions [3]) respectively. These low adhesion conditions are created by the presence of contaminants in the wheel/rail contact, such as: oil [4], water [5], water and oxides [6], and leaves on the line which bond tightly to the rail [7].

A well-established method for mitigating against low adhesion has been the application of sand particles to the wheel/rail contact. As sand is an insulating material, there is the possibility it may negatively affect track circuits; sand may also create wheel/rail surface damage. However, there is currently little consensus on what makes a "good" sand for increasing traction in the wheel/rail contact, or whether sand particles are necessarily the best type of particle for mitigating low adhesion. Therefore, greater knowledge of the sanding process is necessary.

1.2 Aim & Objectives

Aim:

The purpose of the work undertaken in this thesis is to develop an understanding of how to optimise the sanding process, with an emphasis on what makes an ideal traction enhancing particle.

Objectives:

1. Review academic and industrial literature to identify knowledge gaps and key particle characteristics for optimal traction increase (Chapter 3);
2. Identify and conduct characterisation tests on prospective particles (Chapters 3 & 4);
3. Conduct small-scale, high pressure torsion (HPT) testing to understand the key mechanisms of particles in the interface and assess particle performance (Chapter 5);
4. Record particle entrainment into a scaled wheel/rail contact using high speed video footage (Chapter 6);

[1] The term "adhesion" is an industry term, defined as the amount of traction present in the wheel/rail contact. The terms "adhesion" and "traction" are used interchangeably in this thesis, unless specifically stated otherwise.

5. Parameterise the extended creep-force (ECF) model using HPT tribological test data and compare with FSR tribological test data (Chapter 7).

1.3 Approach

Figure 1.1 breaks down the sanding process and what techniques are being used to assess each part of this process. Particle characterisation is linked to how the particles behave throughout the process and the effect of the particles on the wheel/rail contact. High speed video (HSV) of particles applied to the scaled wheel rig (SWR) will provide information on particle entrainment. The small (HPT) and full scale (FSR) tribological tests will provide insight into the particles' effect on traction and damage; the full scale test also provides data on the amount of material active in the contact. The extended creep force model focusses on the effect of the particles on traction.

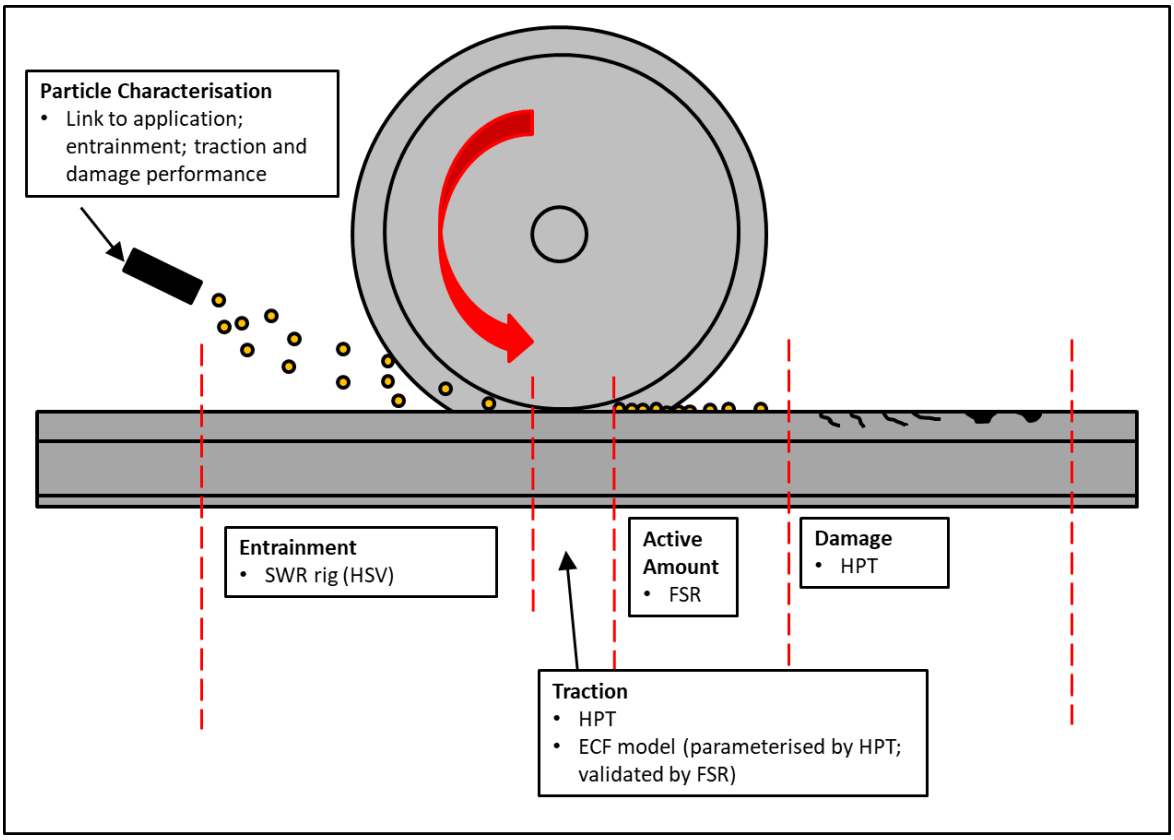

Figure 1.1. Schematic of Approach to Thesis.

1.4 Novelty

The work presented in this thesis outlines a new particle characterisation framework for use on potential future particle-based products. In addition, a novel method for assessing the tribological effect of particles has been presented, with a wide range of particles having been tested. Lastly, the outputs from a newly

parameterised ECF model have been included where a comparison with full-scale data has been made. Overall, it is hoped that this thesis will serve as a foundation for understanding why certain particles have their respective effects in the wheel/rail interface.

1.5 Thesis Outline

The following thesis has been split into eight chapters, as follows:

1. **Introduction**

An overview of the purposes and novelties of the work included in this thesis, and the aim, objectives, and approach to be undertaken.

2. **Technical Background**

An overview of technical knowledge that puts the project in context. This includes basic information on the wheel/rail contact, low adhesion within it, and mitigation methods. Included also, is information on British standards for sanding that are currently used. Lastly, a brief assessment of common test methods for simulating the wheel/rail contact has been incorporated.

3. **Literature Review**

This chapter reviews literature surrounding three areas key to this project: work assessing the effect of particles on the wheel/rail contact, particle characterisation properties and techniques, and modelling of the wheel/rail contact.

Chapter 3 fulfils objective 1 and partly fulfils objective 2.

4. **Particle Characterisation**

This chapter lists the particles being tested as part of this project. The particle characterisation techniques are fully detailed and particles are characterised and results of these characterisations are shown.

Chapter 4 partly fulfils objective 2.

5. **High Pressure Torsion Testing**

A detailed explanation of the HPT rig and how it was developed to fit this work is included. Traction data and post-surface analysis is taken for each particle type and correlations between particle characteristics and HPT outputs are extracted.

Chapter 5 fulfils objective 3.

6. Scaled-Wheel Rig Testing

High speed video stills of particle entrainment into the scaled wheel/rail are included in this chapter. Particle entrainment in both dry and wet conditions are assessed, with pictures of the wheel/rail surface after the passing of the scaled-wheel also included.

Chapter 6 fulfils objective 4.

7. Extended Creep-Force Model

In this chapter, HPT results are used to parameterise the ECF model, which then allows direct comparison with FSR and field data as a means of validating.

Chapter 7 fulfils objective 5.

8. Conclusions

An overview of the project findings, including the strengths and weaknesses of the work, conclude the thesis. Also, included are proposals for how the work can be developed in the future and its wider impact.

2 TECHNICAL BACKGROUND

2.1 Introduction

The following section details the technical background needed to put the topic of this thesis into context. A brief summary of the wheel/rail contact, and what causes low adhesion within it, are discussed before detail is provided on some adhesion enhancing systems, including sanding. Current international sanding standards and common sanding research methods are also described.

2.2 Wheel/Rail Contact

The wheel/rail contact between the train and the track is complex. It is hard to analyse and is hard to describe geometrically due to: the variety of vehicles, wheel and rail profiles, the curve of the rail, and railhead conditions. Typically, the contact area is less than 1 cm^2 with contact pressures reaching 1500 MPa in some cases [8].

The areas where contact between the wheel and rail occurs can be split into three separate regions, which are illustrated in Figure 2.1. Region A is the most common region for contact to occur, and is also the most desirable, as contact stresses are lower, therefore less wheel/rail damage occurs. Contact in region C is very unlikely to occur; contact stresses and damage can be very high whilst in this region. Lastly, contact in region B, which usually occurs when the rail curves, can lead to high stresses and two-point contact when significant wear or plastic flow occurs.

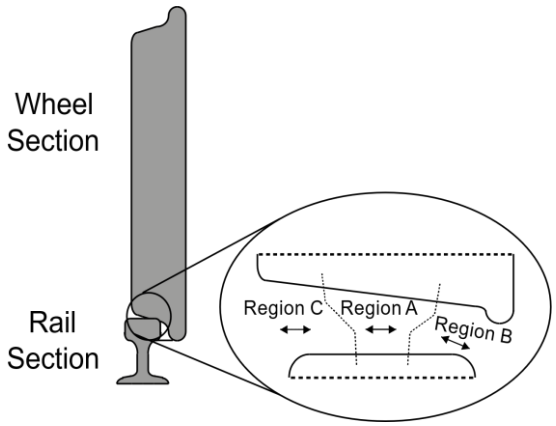

Figure 2.1. Contact Regions in Wheel/Rail Contact.

Within the contact itself there are different mechanisms which can take place, all of these have been illustrated in Figure 2.2 where the wheel and rail are imagined as discs running together. A purely rolling contact results in no tractive force and can also be described as a sticking contact, this behaviour happens when the train is "coasting" i.e. undergoing no tractive effort; this mechanism has been illustrated in

Figure 2.2(a) where points on the wheel and rail enter and exit the contact together, sticking throughout. A full sliding contact will either result in wheel spin when accelerating and a locked wheel when braking, both of which can damage the wheel and rail respectively and is therefore not ideal; in Figure 2.2(b) this is represented in similar fashion to Figure 2.2(a), where the wheel is spinning whilst trying to accelerate. In cases where acceleration or braking are desired the contact needs to be rolling/sliding and therefore imparting tractive force. The acceleration case being represented in Figure 2.2(c); during movement through the contact the wheel point slips ahead of the rail point as the wheel surface undergoes elastic deformation.

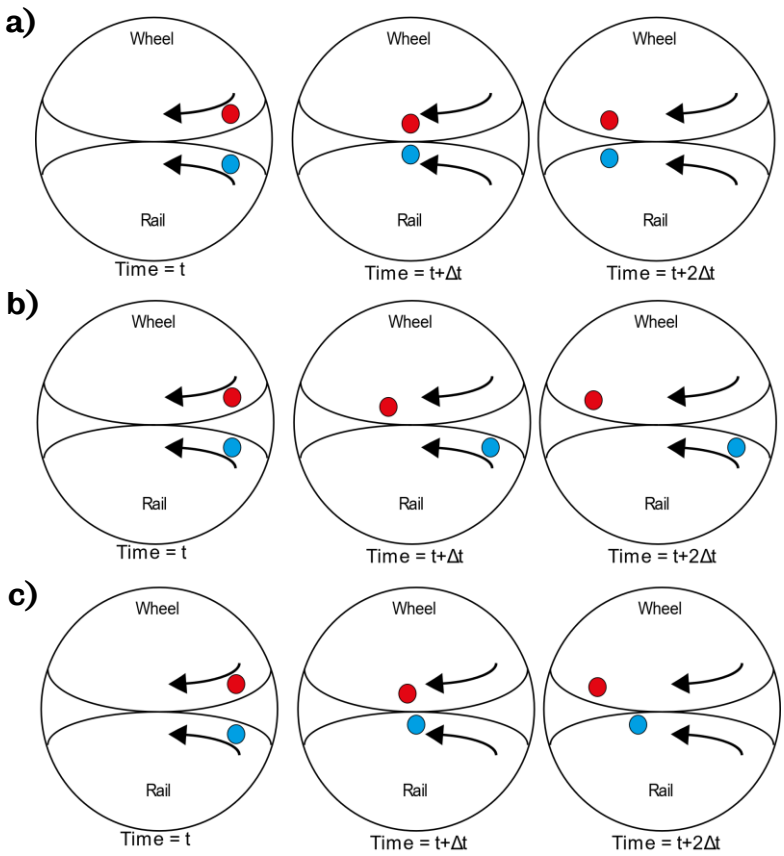

Figure 2.2. *(a)* Illustration of a Pure Rolling Contact; *(b)* Illustration of a Pure Sliding Contact; *(c)* Illustration of a Rolling/Sliding Contact.

The rolling/sliding effect occurs when the wheel is moving at a different speed to the wheel speed at which pure rolling occurs, the ratio between these two speeds is known as the creep rate, or slip rate, that is occurring in the contact. Figure 2.3 shows how traction changes with increasing creep and includes a diagram of the stick/slip behaviour at certain creep rates. Ideally, it is best to maximise traction whilst limiting damage thus the aim would be to keep the creep rate on the curved section of the creep curve without entering full slip.

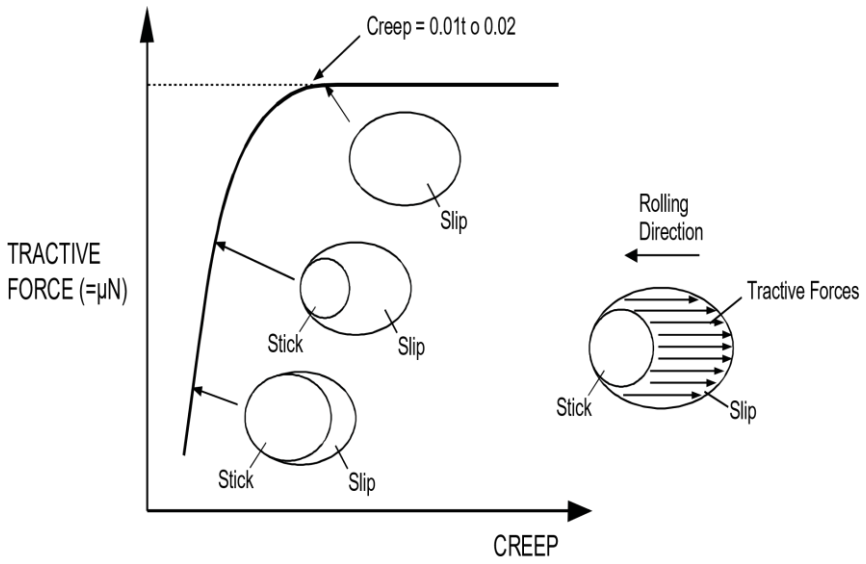

Figure 2.3. Generic Creep Curve [8].

A safety feature of railway operations is the use of train detection. Track sections are bounded using insulated rail joints and an electrical signal is sent along this track section, this is a track circuit. If a train is present the track circuit is shorted out and the train is detected, this set-up is summarised in Figure 2.4. Wheel/rail isolation, otherwise known as wrong side track circuit failure (WSTCF), occurs when the train's wheels are insulated by a contaminant layer, resulting in no short circuit occurring and the appearance of no train on the track section which can lead to safety issues.

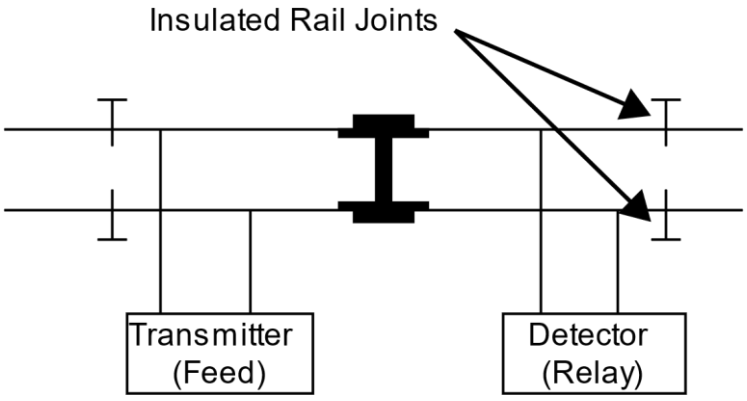

Figure 2.4. Track Circuit Schematic.

2.3 Low Adhesion: Causes & Consequences

The presence of friction modifiers can drastically affect the creep curve introduced in section 2.2. When lubricants enter the wheel/rail interface the amount of creep that can be sustained lessens as the contact friction is lowered, this can result in a contact undergoing pure slip when the driver expects normal braking or

acceleration behaviour. A drop in friction is generally referred to as a reduction of adhesion by the railway industry.

Low adhesion in the wheel/rail contact leads to both performance and operational issues in the railway industry and is estimated to cost the British rail industry ~£345m/annum [1]. Performance issues arise as a lack of adhesion leads to reduced traction, therefore it takes longer for trains to accelerate up to a desired speed, thus leading to delays [2]. Safety issues occur due to the presence of low adhesion increasing braking distance, potentially leading to SPADs (signals passed at danger) or in the worst case collisions [3].

The minimum accepted adhesion values in Great Britain are 0.09 and 0.2 for braking and traction respectively [2], with problems occurring under this limit; adhesion values have been found to go as low as 0.05 in poor conditions [2]. Low adhesion conditions exist when a third body layer is present on the track, such as: oil [4], water [5], water and oxides [6], and leaves on the line which bond tightly to the rail [7]. These third body layers can also cause isolation, especially when leaves insulate the wheel and rail; a recent near miss occurred in Norfolk due to leaf contamination isolating the train [9]. Third body layers can also create surface damage as full slip occurs, leading to possible wheel flats and/or rail damage.

2.4 Adhesion Materials & Their Application

Typically, dry sand particles are applied to the wheel/rail contact by means of an air stream running through a hose directed at the contact [10]. Figure 2.5 shows a typical sander set-up for a train-borne system.

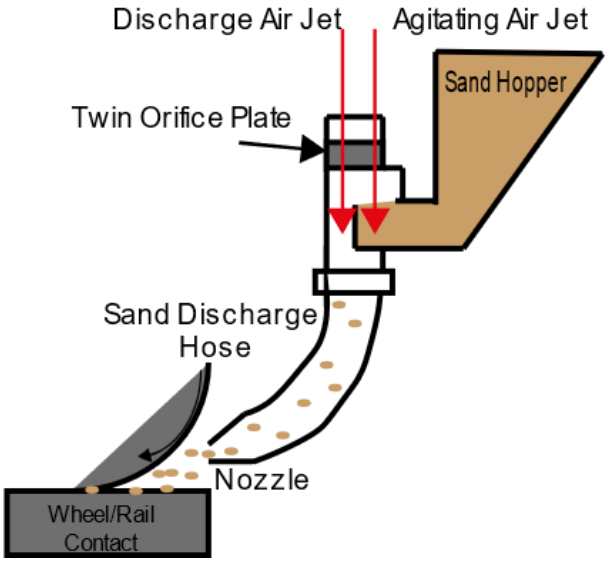

Figure 2.5. Schematic of a Typical Sander.

Particles can also be applied to the wheel/rail contact within a gel, these are generally called friction modifiers (FM) [2]. These are typically applied using track-side applicators, applying FM directly onto the rail head via a pumping system. These can also be applied using train-borne applicators.

The use of sanding on railways has the potential to result in unwanted negative effects, such as wheel/rail isolation and/or wheel/rail surface damage; though these effects occurring catastrophically are rare. Isolation can occur if the insulating sand completely covers the contact and results in the loss of train detection by the track circuit. Damage can occur as sand particles are mostly comprised of quartz [11], which is harder than rail steel [12]. When hard particles go through a contact, they can abrade the surface causing damage [13].

2.5 International Sanding Standards

2.5.1 Standards Pertaining to Particle Characteristics

In Great Britain, the only dry particles applied to the wheel/rail contact are sand particles that meet the sanding equipment standards set by the Rail Safety and Standards Board (RSSB) [11]. The criteria for sand particles to be used in braking and traction in Great Britain are summarised in Table 2.1.

Table 2.1. Sand Specifications Provided by the RSSB [11].

Parameter	Sand Specification for Braking	Sand Specification for Traction
Size	<5% of particles should be <0.71mm	100% of particles must be able to pass through a 1.25mm sieve
		≤15% of particles should be >1.18mm
	<5% of particles should be >2.8mm	≤15% of particles should be <0.15mm
		≤1% of particles should be <75µm
Shape	Rounded and Irregular	Sharp
Uniformity Coefficient	<1.5	N/A
Mineralogy	≥90% Quartz or some other silicate	Silicate
	≤2% Contaminant Particles	
Source	Quarry sands preferable	Quarry sands preferable

Braking sand is used in multiple units with combined braking and traction sanding systems; this is done to simplify the design.

France and Germany also have standards relating to the sand particles' characteristics. The French standard [14] differs from the GB standard in a few places: the sand origin must be alluvial as opposed to from a quarry; sand must be round and unbroken and not sharp, contradicting the GB standard for traction sand; French sand must be free of any additives whereas GB sand can be contaminated up to 2%; and the specified grain size distribution is more strict and calls for smaller grain sizes than is seen in the GB (see Table 2.2 for more details).

Table 2.2. Specified Grain Size Distribution provided by SNCF [14].

Sieve Aperture Size (mm)	Maximum Percentage Passing Value (%)	Minimum Percentage Passing Value (%)
3.15	100	100
2.5	100	98.5
2	99	90
1.25	85	60
0.63	50	25
0.315	10	0
0.08	1	0

The German standard [15] surrounding particle characteristics is much closer to the GB standard than the French version. The German standard also specifies that the sand must be sharp, that it must be ≥90% quartz and does not specify a particle size distribution though it does recommend the distribution included in Table 2.3). The German standard also specifies that the moisture content of the sand must not exceed 0.5%wt and similarly to the French standard specifies that no contaminants can be present.

Table 2.3. Specified Grain Size Distribution provided by German Operators [15].

Grain Size (mm)	Maximum Share (Mass %)
>2.5	0.1
>2	5
1.6-2	30
0.8-1.6	50
0.63-0.8	30
<0.63	5
<0.1	0.5

Australia also has standards [16] pertaining to sanding, but these do not cover the characteristics of the sand being applied.

2.5.2 Standards Pertaining to Sanding Equipment

Current sanding equipment standards encompass the application of the particles onto the rail as well as the mechanical design of the sanders. The GB standards depend on whether the locomotive is undergoing braking or traction and in the case

of the former whether the multiple unit has 8 or more wheelsets. All of the British [11], French [14], German [15] and Australian [16] standards specifically outline that sand must not interfere with the track circuit, i.e. cause isolation.

The British standard specifying the necessary criteria for sand application under braking has been summarised in Table 2.4.

Table 2.4. Sanding System Standards under Braking [11]**.**

	≥8 Wheelsets	**<8 Wheelsets**
Feed Rate (kg/min/rail)	2	2
Minimum Number of Wheelsets between Sanders	6 (≥14 wheelsets)	4 (<14 wheelsets)
Location of First Sander	To the rear of the second wheelset in direction of travel	In front of the leading wheelset in direction of travel
Location of Last Sander	>6 wheelsets before rear of the train	>4 wheelsets before rear of the train
Minimum Train Speed (mph)	10	10

The traction requirements are less complex; the standard requires the sand to be fed at 2kg/min/rail for a pure traction system. It should be noted that this discharge rate does not need to be continuous e.g. a discharge rate of 4kg/min/rail for 30 seconds followed by 30 seconds of inactivity would meet the standard.

The absolute minimum sanding requirements, set out by GMRT 2461, state that the sand should be applied by the leading vehicle after the third wheelset in the direction of travel.

Though the sand is normally applied automatically, the British standard states that the driver can override the automatic application in certain areas such as through switches and crosses to avoid damaging bearer surfaces. It should be noted that the application of sand is not used in anticipation of low adhesion, as there are no benefits and in the worst case can cause train isolation.

The British standard also deals with mechanical aspects of the sander. These mostly focus on achieving a steady sand application rate directed just in front of the wheel/rail contact.

The guidance from the RSSB concerning sand boxes encompasses the following:

- The sand box should not consist of shallow angles; this is a way of avoiding blockages;
- Sand boxes that operate on the Venturi principle should have adequately sized breathers that are positioned away from areas where contamination is likely;
- Care should be taken to keep the sand dry; this includes preventative measures such as using adequate seals or curative measures such as heating within the sand box;
- Sand box storage capacity should be adequate for the journey being undertaken, a sand level monitoring system can assist with this.

The same standards also provide guidance on the hose and nozzle sand delivery system:

- The hose length should be as small as possible;
- The sand needs to be applied to both rails, this means two hoses are needed per sander;
- The combining of a large diameter hose with a smaller diameter nozzle can increase the amount of sand going into the wheel/rail contact, though small bore sizes can reduce the flow rate;
- The nozzle should be straight and made of stainless steel;
- The discharge nozzle should be kept at an angle of 10-15° relative to the rail;
- Sags in the hose should be eliminated to keep up the discharge rate;
- The discharge nozzle should be as close to the wheel/rail interface as possible;
- The nozzle should be aimed at the centre of the rail head;
- Non-corrosive materials should be used as much as possible to maintain performance.

It should be noted that an RSSB report into sander set-ups [17] found that many sanding systems were not dispensing the required amount of sand out of the hose. The report specified the lack of regular maintenance and ineffective design as the root causes with the current sanding standards detailed in this section being a response to this.

2.6 Common Test Methods Used in Sanding Research

When investigating the wheel/rail contact, careful consideration needs to be taken to ensure any experiment is as accurate a representation of the contact as possible, whilst being simple enough to infer reliable conclusions. Field tests give real world results, but it is hard to control all the possible variables, whereas a simple test rig simulating the contact in lab conditions allows these variables to be controlled and therefore specific variables can be isolated and tested.

For significant conclusions to be drawn from testing a range of scales is needed, starting small and simple and then becoming larger and more complex. In this way results can be corroborated and conclusions can be drawn. For the wheel/rail contact there are four types of commonly used tests: high pressure torsion, twin-disc, full-scale, and field.

2.6.1 High Pressure Torsion Rig

The high pressure torsion (HPT) rig has previously been used to assess the effect of sand in a simulated tribological contact [18], though only to a limited extent. A schematic showing the operation of the HPT rig is shown in Figure 2.6, where the wheel and rail specimens are constructed from actual cuts of wheel and rail material. The contact area and pressures achievable are similar to what might be found in an actual wheel/rail contact, though the contact geometry is very different. A great deal of control over the third body layer is achievable also i.e. no recycling layer and exact control over the quantity of material in the contact. Only a few sweeps are possible with the HPT rig before complete degradation of the contact, though as the effects of sand are of most interest for the first few sweeps this does not present a problem for testing sanding.

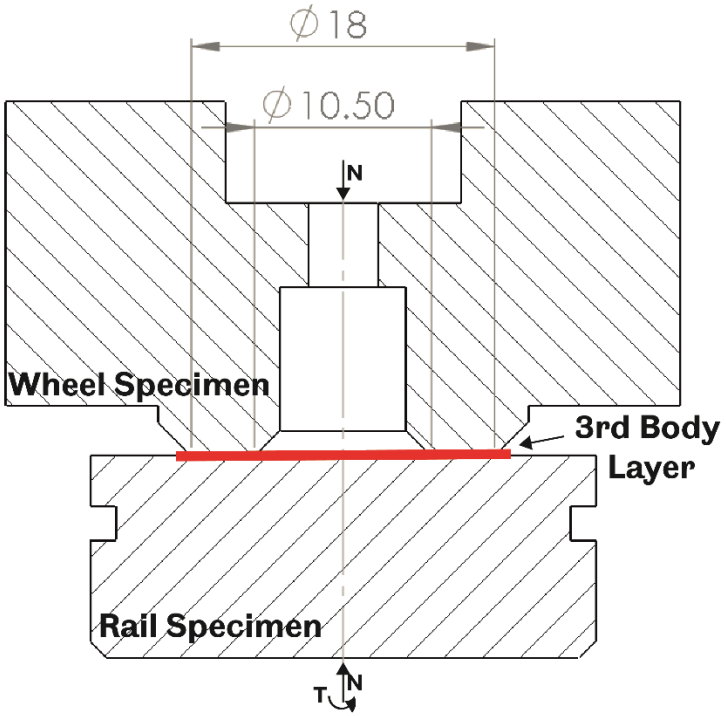

Figure 2.6. Schematic of the HPT Rig.

2.6.2 Twin Disc Set-Up

A typical twin disc set-up uses two discs rolling against each other to simulate a wheel running over a rail, with one disc representing the wheel and the other the rail. This testing method has been used extensively in many sanding investigations [19]–[23]. A typical schematic of such a machine is shown in Figure 2.7 (Top). The twin discs are usually cut from actual wheel and rail sections to achieve the same surface material, though the geometries of the disc are very different to that of actual wheels and rails. The actual geometries of the discs are very small compared to an actual wheel and rail with drawings of the discs included in Figure 2.7 (Bottom).

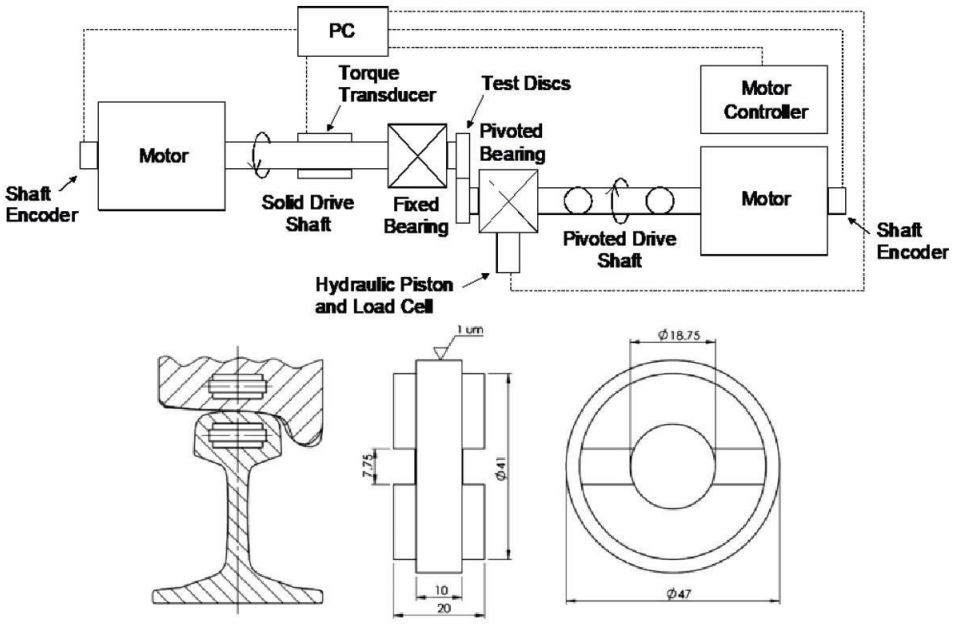

Figure 2.7. Twin Disc Tests: *(Top)* Twin Disc set-up, *(Bottom)* Wheel and Rail Disc Geometry [23]**.**

The contact between the discs is a line contact, differing from that of an actual wheel and rail; the line contact has a width of 10mm. The actual geometry of the contact will not be stable, due to the curving rail head and wheel profiles, this cannot be simulated using twin-disc methods. However, the contact pressure between the discs is similar to those of an actual wheel/rail contact; mean contact pressures of 900-1500MPa can be achieved. Another limitation of the twin disc tests is the lack of a realistic velocity between the surfaces, with speeds typically only reaching ~2mph.

When sanding is being applied to the twin-disc contact the results garnered for adhesion, isolation, and damage will all be exaggerated due to several factors [19]:

- *Twin-disc geometry;* As mentioned above the geometry of the actual contact will be smaller than a realistic wheel/rail contact. As the sand is not scaled down it will be artificially large and therefore have a larger effect on the contact;
- *Sand application;* In many cases the sand application method used a similar principle to that of a real-world sanding system, but the hose is much closer to the contact. This will result in more particles being entrained into the contact and subsequently affecting the mechanics of the contact. A typical example of the application set-up can be seen in Figure 2.8;

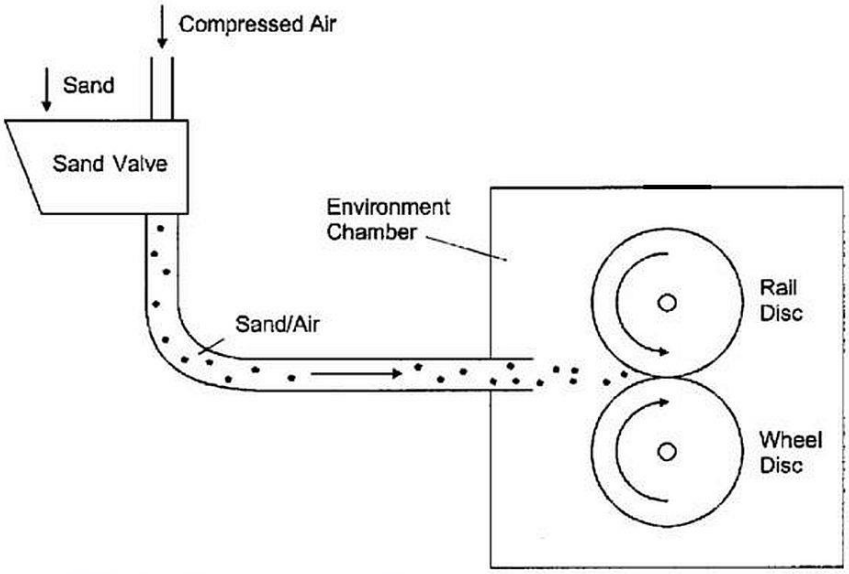

Figure 2.8. Particle Application Set-up [19].

- *Lab conditions;* Whilst the indoor conditions of the lab offer control over the testing procedure, the realism of the experiment is the necessary trade off. There is no way to account for: crosswinds, air turbulence, curves etc. What can be accounted for will only be in an artificial way; contaminants, moisture, temperature etc.

2.6.3 Linear Full-Scale Rig

Linear full-scale rigs use actual wheels and rails with realistic contact pressures (900-1500 MPa) and geometries. The limitation to these machines is the lack of realistic wheel velocity, due to the truncated length of rail used (600mm for one such rig [24]) and safety issues; for the rig used by British rail and the University of Sheffield [24] the top speed of the wheel is <1mph. The rig is beneficial for studies concerning the actual application of particles [24], [25] into the contact, due to its realistic geometries. Even the effect of prevailing winds and cross winds can be simulated with the use of fans. An example of a full-scale rig (as used by Lewis et al. [24]) is included in Figure 2.9; *(1)* denotes the wheel and *(3)* is a 1010mm length of rail which is moved by a linear slider bed *(4)*, the sand is fired from the hopper *(10)* into the contact via the hose *(12)* and nozzle *(14)*.

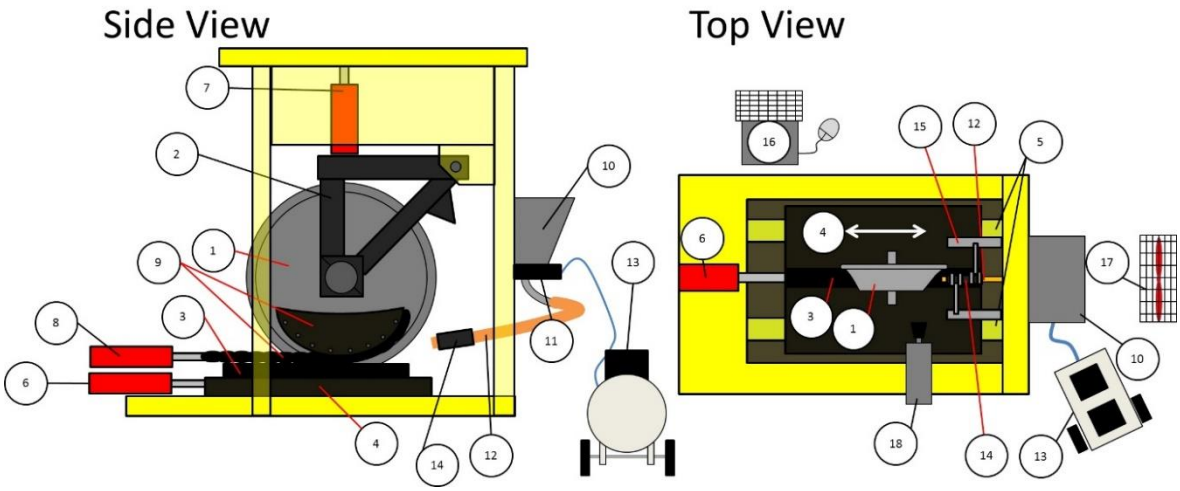

Figure 2.9. Schematic of Full-scale Rig Sanding Set-up [24]**.**

2.6.4 Field Tests

A large portion of industry field tests that have been carried out have been qualitative in nature [26]–[30], in large part due to the difficulty of running experiments on working lines. Most quantitative work there is comes either in the form of tribometer trains [31] (providing actual adhesion values), or actual train performance [32]–[35] (journey time, slip detection, braking distances). Whilst there is inherent realism in field tests, the lack of control over variables leads to results that could be misleading, therefore many field test conclusions have to come with caveats.

2.7 Summary

In this chapter, the technical background of this project has been detailed, thereby couching the work within its surrounding context. Low adhesion and low adhesion mitigation methods were introduced, with the latter being later reviewed in detail as part of chapter 3. In addition, international standards around the current use of traction enhancing particles were covered. Lastly, different test methods for assessing the effect of sanding were reviewed with discussion surrounding their respective advantages and disadvantages.

3 LITERATURE REVIEW

3.1 Introduction

The following literature review has been split into three parts:

- *Sanding;* This section will focus on the research conducted on adhesion restoring particles in both academia and industry, as well as at a range of scales. The research will be analysed to ascertain what knowledge gaps are present in this field.
- *Particle Characterisation;* A set of key particle properties will be identified, with the help of the sanding literature section. The literature surrounding the measurement of each property will then be assessed to determine the best methodologies for a particle characterisation framework.
- *Modelling;* A brief overview of potential modelling methods will be presented. This section will look at various contact models for analysing the wheel/rail interface and distinct element methods for modelling particle behaviours.

3.2 Sanding Literature

3.2.1 The Effect of Particles on Wheel/Rail Adhesion

There have been multiple laboratory investigations that have found that the use of sand generally has an augmentative effect on adhesion in the wheel/rail contact when low adhesion conditions exist [12], [19], [20], [22], [36]–[42]. Additionally, field tests have also shown that sand improves adhesion levels [25], [27], [29], [30], [34], [35], [43]. The following sections will describe these investigations in more detail.

3.2.1.1 Dry Particles

3.2.1.1.1 Twin-Disc Set-up

A large amount of the work utilising twin-disc measurements of adhesion has been undertaken by Arias-Cuevas who has conducted multiple studies into the use of sand particles in the wheel/rail contact.

In dry[2] tests, Arias-Cuevas et al. [20] found that sand reduced friction in the contact at all sand densities (0.75-7.5 g/m), particle sizes (0.06-2 mm) and at all creep rates (1-10%). Arias-Cuevas et al. also showed the effect particle size had on adhesion; it was found that larger particles generally led to better adhesion. The same work

[2] Throughout this thesis "dry" tests refer to tests where no extra addition of liquid has been applied outside of any constituent part of an applied adhesion material.

suggested that there is an upper limit on the discharge rate of sand from the hose after which the sand within the contact was creating a solid lubricant, reducing the adhesion between the wheel and the track further still. A summary of the particle size categories used throughout all of Arias-Cuevas' et al. work has been included in Table 3.1, these categories will be referenced throughout this review.

Table 3.1. Particle Size Categories used in Arias-Cuevas et al. work.

	Particle Size Band (μm)	Location of Particle Size Distribution Peak (μm)
S sand	60-300	150
M sand	300-600	350
L sand	850-1600	1200
R sand	250-1400	600-1000

Furthermore, Arias-Cuevas et al. found that in dry tests higher slip rates enhanced the interlocking action of the sand particles leading to much higher adhesion values compared to similar tests at lower slip rates. It should be noted that the effect of further increasing the slip at already high slip rates was minor in comparison to the significant increase in adhesion when increasing the slip at low slip rates, thus suggesting that there is not much benefit from increasing the slip rate past a certain point. The influence of both slip and particle size is summarised in Figure 3.1.

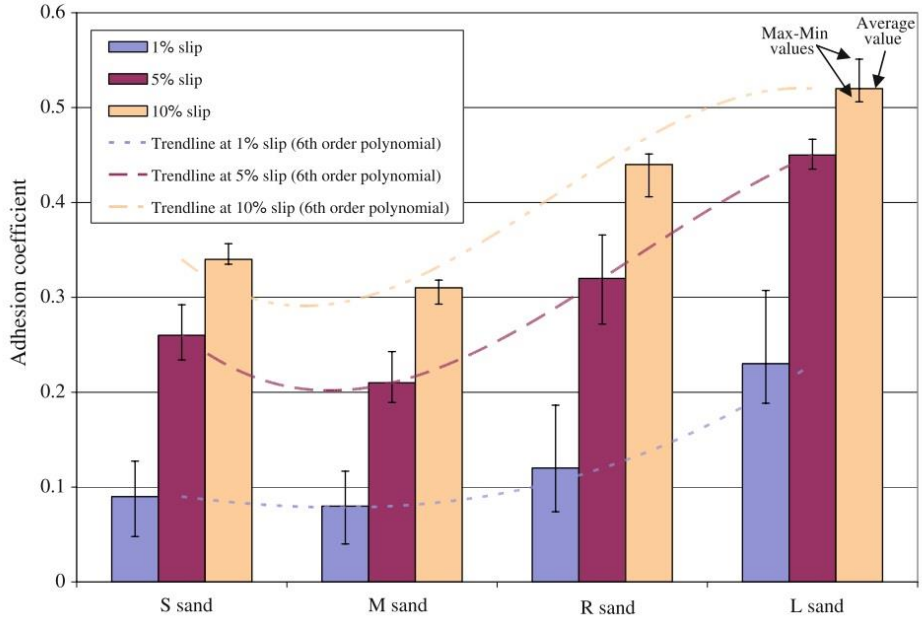

Figure 3.1. Summary of Adhesion Results from Twin-disc Tests from Arias-Cuevas et al. [20].

The conclusion that larger particles lead to greater adhesion, held true in another twin-disc study conducted by Huang et al. [44] though these tests were conducted

in wet[3] conditions. There sand particles ranged in size from 50-900 µm with the smaller sands barely improving adhesion compared to an unsanded, wet contact; the larger particles increased adhesion somewhat, but were still considerably less than dry conditions, possibly due to the low slip rates used (<1%). Their tests also suggested that increasing feed rate also increased adhesion, though this relationship appeared very minimal in their tests.

In another paper, Arias-Cuevas et al. [45] ran a twin disc study with more focus on the effect particle size had on improving adhesion in a leaf contaminated contact. In these tests they found that for all particle sizes the leaf layer was being removed, yet the adhesion values still increased with particle size as the sand started acting on the actual rail due to the removal of the leaf layer. This may have an impact on particle size selection as any sand remaining after the leaf layer removal could negatively affect adhesion, as sand in a dry contact has been shown to reduce adhesion values in the previously discussed paper [20].

Omasta et al. [46] undertook twin-disc work concerning the effect sand had on various adhesion reducing contaminants. In a wet contact, it was observed that changing the application rate of the sand did not have a large effect on adhesion recovery at low slips and low surface speeds. As the slip rate and surface speeds increased so did the effect of the application rate on adhesion recovery. These results are included in Figure 3.2.

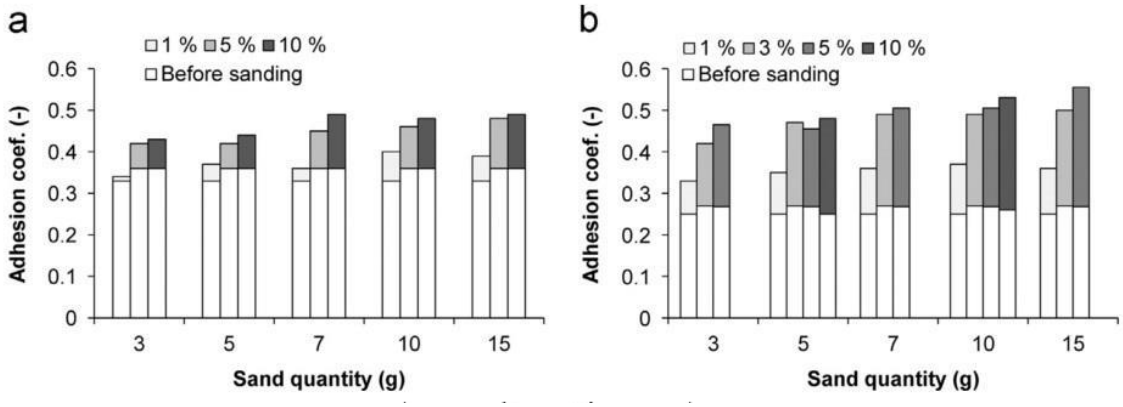

Figure 3.2. The Effect of Sanding in a Wet Contact at Surface Speeds of: *(a)* 1 m/s, and *(b)* 3 m/s [46]**.**

Kumar et al. [41] also found that the application of sand into oil contaminated contacts had the effect of restoring adhesion, again only at higher slip rates. Similar results have been found in work conducted on a full-scale rig by Zobel [47], which will be discussed in section 3.2.1.1.2.

[3] Throughout this thesis "wet" tests refer to tests conducted with the addition of an amount of water to the tested contact.

More work assessing the performance of sand in different liquid contaminated contacts has been undertaken by Wang et al. [42]; it was found that sand had a positive adhesive effect on wet contacts, but less so when oil was present perhaps due to the higher viscosity of the oil preventing entrainment into the contact; these results were summarised in Figure 3.3. They also found that sanding was most effective at restoring adhesion at lower speeds and higher normal loads.

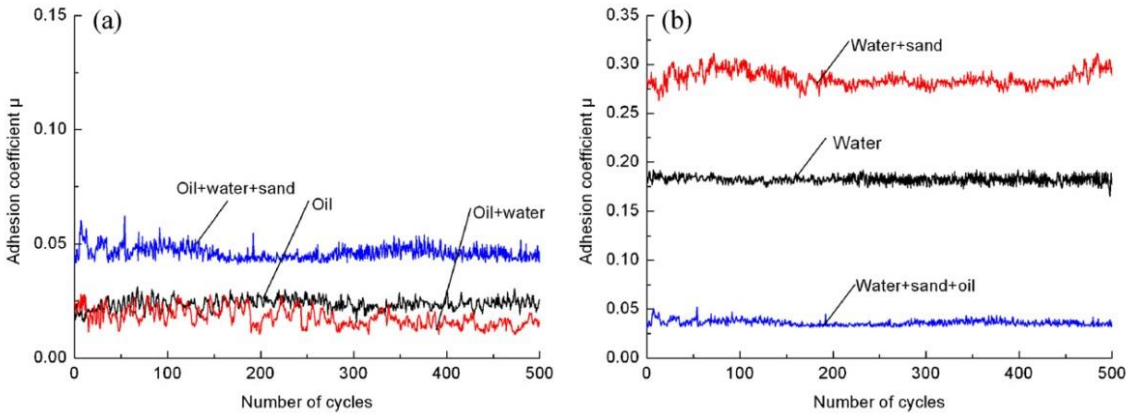

Figure 3.3. *(a)* The Effect Sanding has in an Oiled Contact; *(b)* The Effect Sanding has in different Low Adhesion Conditions [42].

The results obtained from the studies described above clearly indicate that there is a relationship between slip, particle size and discharge rate at which the adhesion between wheel and rail will be optimised.

A study by Shi et al. [48] had a slightly different focus than aforementioned studies, assessing the effect of micro-fragments (0.1-30 μm) of silica sand compared to its uncrushed state (600-2000 μm). In this study, micro-fragments were suspended in a water mixture. This study found that in wet, oil, and leaf contaminated contacts, single applications of both sand and its fragments produced similar adhesion values, though the effect of the micro-fragments was shorter lasting. In tests in wet conditions with a continuous application of material, the micro-fragment slurry produced higher adhesion than sanded tests at a similar ratio of water to adhesion material; even a small concentration of micro-fragments in the slurry produced greater adhesion compared to a wet, unsanded contact. It was necessary for micro-fragments to be applied in a different manner to uncrushed sand (i.e. via slurry) which may contribute to its effect on adhesion levels being similar to uncrushed particles, however even small concentrations of micro-fragments improving adhesion suggests that crushed particles make a considerable contribution to adhesion recovery.

Contrary to other papers in this section, Wang et al. [36] studied the effect alumina particles had in recovering adhesion in contaminated contacts. They found evidence

that suggested alumina performed better than sand in oiled and wet contacts, possibly due to the alumina being harder and according to Zobel's research [47] harder particles are more effective at restoring adhesion. However, in the leaf layered contact Wang et al. [36] found that the alumina underperformed compared to sand; as the sand particles ranged from 0.5-1.3 mm compared to an alumina particle size of 0.1mm this may have been due to the alumina not being sufficiently large enough to penetrate the leaf layer and break it up.

Further work assessing alumina particles was conducted by Cao et al. [49], where a particles ranging between 75-550 μm in size were applied in wet conditions. Their work suggested that the smaller alumina particles had a greater effect on adhesion levels (reaching ~0.45), though all particles increased adhesion compared to wet, unsanded conditions. This study also investigated how feed rate affected adhesion; it was surmised that adhesion peaked at 3 g/min (reaching ~0.4), a very low feed rate compared to other sanding studies.

Another study using alumina particles was conducted by Shi et al. [50], where the effects of a single application of alumina particles into a wet contact with differing particle quantity and size were investigated. The application amounts tested were between 0.03-25g, and their results suggested that initial improvement in adhesion reached a plateau at 8g of ~0.6, however after this initial improvement all application amounts saw adhesion level off to a similar amount (~0.3); larger quantities did, however, produce longer lasting effects. When investigating the effect of particle size (0.02-0.8 mm), a peak was reached at 0.15 mm of ~0.7, before tapering off for larger particles, and all particles eventually produced similar adhesion levels after initial application (~0.3); a similar trend was observed for the duration of the particles' effect. As a different range of particle sizes was used in this study, it is hard to directly compare with Cao et al. [49]; the particle size range used by Shi et al. was broader than Cao et al., possibly to allow inferences about the effect of particle size to be made for smaller and larger particles than could be made from the work undertaken by Cao et al. Where ranges do overlap a similar trend in particle size vs adhesion can be observed, i.e. smaller alumina particles produce greater adhesion values.

Work to establish the link between particle crushing strength and adhesion in wet conditions was undertaken by Wang et al. [51]. The study showed that particles with higher crushing strength also produced higher traction, though this relationship became less prominent after a certain crushing strength (in this study minimal increases in traction were observed for particles with a higher crushing strength than sand).

3.2.1.1.2 Linear Full-Scale Rig

Lewis et al. [37] focussed on the effect application rate had on improving adhesion in a full-scale rig; the low adhesion situation was created using wetted paper tape. They found that the minimum sand density needed on the rail (in this context sand density refers to the amount of sand per metre of rail) to remedy low adhesion situations was 7.5 g/m. In tests run with sand densities of 106 g/m there was still adhesion recovery, but the peak adhesion reached was lower than the 7.5 g/m test. Lewis et al. summarised that this may be due to the increased quantity of sand mixing with the low adhesion layer thereby creating a lubricating paste. Lewis et al. concluded that the optimal sand density will be somewhere between 7.5 g/m and 106 g/m; these results have been included in Figure 3.4.

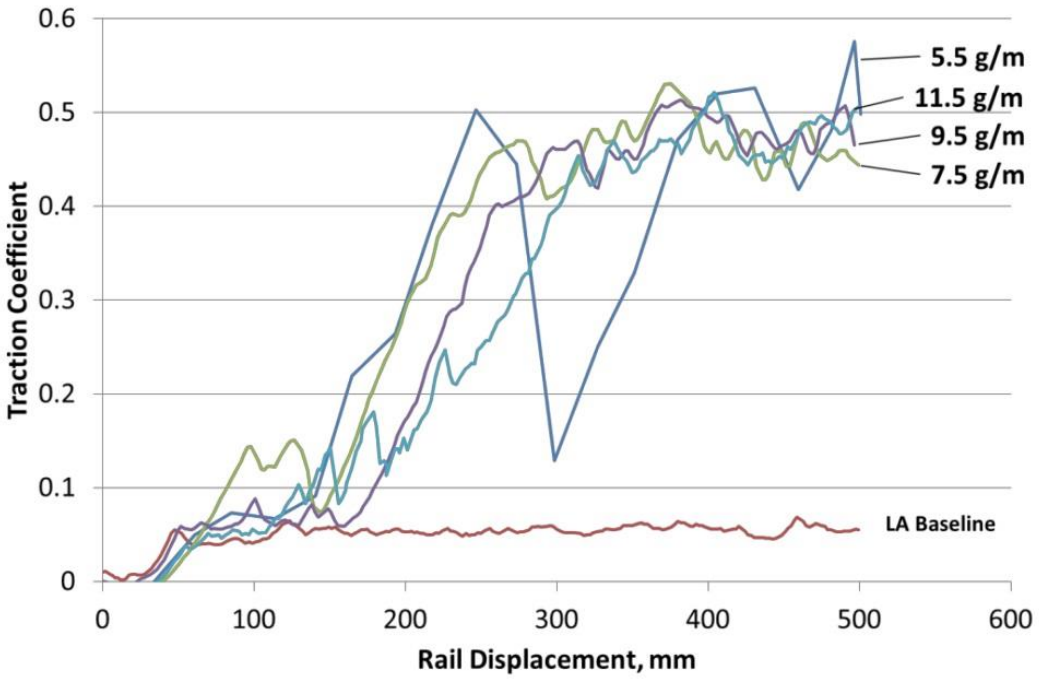

Figure 3.4. Investigation of the Effect of Sand Density in Restoring Adhesion [37]**.**

Zobel's full-scale tests [47] looked at different types of sand in an oiled contact, including research into the relationship between particle hardness and adhesion improvement. Zobel found that whilst harder particles generally offered higher adhesion there was a critical hardness after which there was very little adhesion improvement. The critical hardness seems to be between 6000-8000 kg/mm^2 in his tests, or around the same hardness of quartz.

Both Lewis et al. [37] and Zobel [47] found that the amount of sand actually needed to improve adhesion is very small compared to the amount that is actually being discharged from the hose. This suggests that a focus on the accuracy of sanding

system will have a beneficial effect on adhesion and waste less sand; this was discussed in another review paper [52].

In work done by Cooper [53], it was found that increasing sand particle size produced greater friction in an oiled contact, which reinforces conclusions from multiple papers in section 3.2.1.1.1. This relationship was especially pronounced for particle sizes below 53 μm suggesting that particles may not be effective below this size. It should be noted that this test was run with a low quantity of sand on the rail (0.05-0.1 kg/m^2), so these results may be hard to compare to other results mentioned in this review as they mostly used a lower limit of 0.15 kg/m^2.

There has been some full-scale work looking at particles other than sand, Tanvir used a full-scale rig to measure the adhesion recovery properties of different types of unnamed "fines" in an oiled wheel/rail contact [54]. These fines differed from sand in that they were amorphous and crumbled very easily. Tanvir found that these fines did not improve the adhesion at all in the wheel/rail contact whilst the crystalline sand offered improvements, but not to the extent of completely recovering adhesion. From these results Tanvir surmised that amorphous particles gave lower adhesion values than crystalline particles.

3.2.1.1.3 Field Tests

Whilst there has been a lot of field work conducted looking at sanding in the wheel/rail contact, most of this has centred on qualitative research into the effect sanding has on improving adhesion [25].

Schofield et al. [33], Marks [34] and Waring [35] reported on tests conducted by British Rail Research with an emergency one shot sander system to understand how effective it would be when braking was critical and adhesion was low. Schofield et al. found stopping distances were halved when the emergency sander was applied, suggesting an increase in adhesion; Marks also found improvements when receiving feedback from drivers. Waring went into more detail and found the emergency sander, using a discharge rate of 5 kg/min/rail, resulted in a train retardation increase from 2%g to 9%g, allowing full braking. In comparison, a typical sander with a discharge rate of 2kg/min/rail increased retardation from 1.5%g to 4.5%g considerably less, perhaps due to the lower amount of sand going into the contact.

Studies looking at the braking performance of 2 & 3 car class 165/166 stock with attached sanders were conducted by British Rail Research in 1996 and are included in reports by Tunley [55], [56] and Peat [57]. These tests showed the application of sand at 2 kg/min in low adhesion conditions improved deceleration by 3%g

compared to the unsanded case. Tests run with lower application rates found "insufficient" improvement in braking performance.

Recent field work carried out by the RSSB [58] has verified the findings of Waring i.e. higher discharge rates result in more effective braking. They found that two 4 kg/min/rail sanders on a 4 car train comfortably achieved a train retardation of above 6%g even in very low adhesion conditions (μ<0.02). There set-up was variable, in that the 4 kg/min/rail rate was only active above 20 mph so as not to exceed the 7.5 g/m amount currently specified by RSSB standards [11], when slowing down between 10-20 mph the discharge rate ramped back down to 2 kg/min/rail. It may be the case that even higher discharge rates at high speed are even more effective based on the field work conducted, however the upper limit may be decided by the chance of isolation and unwanted damage occurring.

3.2.1.2 Traction Gels

3.2.1.2.1 Twin-Disc Set-up

Traction gels are generally deposited on the rail in areas with low adhesion problems. Most traction enhancers consist of hard, abrasive particles suspended in an aqueous gel. Most gels will also have other chemical elements designed to improve its performance i.e. corrosion inhibitors.

In a twin-disc study conducted by Lu et al. [59], a friction modifier with graphite and molybdenum disulphide particles was applied to a contact with grease present. They found evidence that 2-3 mg of friction modifier would eventually bring traction values towards dry values for up to 24 mg of grease. These tests were conducted at 3% slip only, and even when grease was present, traction barely dropped below 0.2.

Arias-Cuevas et al. [23] ran twin-disc experiments that investigated the effect two different traction gels had in a dry and a wet contact. In dry contacts, they found that adhesion was reduced in comparison with a clean rail, he did find that the gel with larger particles gave higher adhesion values than the other gel. These results seem to be very similar to the results found from research with dry particles, though the improvement could be for other reasons to do with the gel.

In wet contacts, Arias-Cuevas found that the traction gel with smaller particles had a stronger matrix between said particles and its polymers and had a longer lasting effect on adhesion than the traction gel with larger particles. This effectively meant the adhesion recovery in wet conditions was quicker for the smaller particle traction gel, but was still lower than the peak adhesion reached in the bare rail. These results could either show that: smaller particles had a greater effect than larger particles (unlikely when looking at the results garnered from dry particle tests), or the

strength of the matrix between the particles and the gel has a large part to play in a traction enhancer's efficacy.

A study conducted by Lewis et al. [60], analysed the effect of applying a solid stick friction modifier called high positive friction (HPF) that is intended to mitigate against undesirably high friction in the wheel/rail contact; no details on the type of particles within the friction modifier were provided. They found that, in dry conditions, upon application of the product that measured traction came to just below 0.3 at both 1% and 3% slip; this constituted a drop in the coefficient of traction compared to a clean contact, where values of ~0.4 and ~0.5 were measured at 1% and 3% respectively. In comparison, at 0.1% slip HPF made little difference, the coefficient of traction remaining at ~0.1 before and after application.

This study using HPF was further expanded by Hardwick et al. [61] who conducted similar tests at lower contact pressures (900 MPa vs 470 MPa). A summary of their results between 0-0.5% slip is included in Table 3.2. At all slip values tested HPF reduced adhesion in the contact. In both studies using HPF only dry conditions were used, as this is not a product designed for use in low adhesion conditions.

Table 3.2. Summary of Traction Data from Hardwick et al. [61]**.**

Slip (%)	Average Traction	
	Dry	HPF
0.0	0.00	0.00
0.1	0.19	0.14
0.2	0.25	0.16
0.3	0.35	0.23
0.5	0.40	0.27

Lewis et al. [62] conducted studies using diluted hydrophobic products, with the idea that this would repel excess moisture and increase adhesion up to that of a dry contact. No increase in adhesion was found with these products in wet conditions, thus the authors concluded that they showed next to no benefit.

Lewis et al. [21] conducted experiments primarily designed to investigate traction gel's efficacy at removing leaf layers. They found that there was a drop in adhesion upon application of the gel followed by an increase in adhesion as the leaf layer was removed (see section 3.2.2.2.1 for more detail). A possible reason for this phenomenon was put forward and is explained using Figure 3.5; the timeline for the traction gel is: *(a)* the gel is entrained in to the contact, but the particles are resisted by the hydrodynamic pressure of the gel, *(b)* as the gel evaporates particles begin to enter the contact, *(c)* the gel has fully evaporated resulting in crushed, embedded particles.

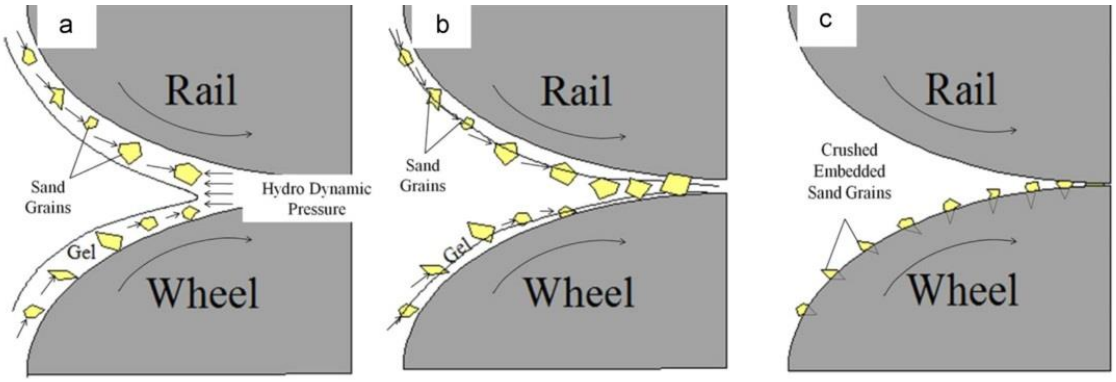

Figure 3.5. Mechanism of Traction Gel Entrainment [21].

In a different vein to the rest of this sub-chapter, Galas et al. [63] conducted a ball-on-disc study of two different oil based friction modifiers with metal particles suspended within. The use of ball-on-disc testing was justified by the authors due to the low contact pressures and small particle sizes being used (4-10 μm). This study found similar results as Lewis et al. [21], where upon initial application of the friction modifier adhesion was lowered to a similar adhesion value as pure oil, and after multiple cycles adhesion was slowly recovered. They also saw that as more friction modifier was applied, the level of adhesion stayed low throughout the test runs.

In a further study by Galas et al. [64], a similar set-up was used to assess water-based friction modifiers. In this study, a range of different particles were assessed with zinc oxide providing greater and faster adhesion recovery than talc and bentonite. Zinc oxide was considerably harder than both other particles, with all possessing similar sizes; from the information given hardness seems the clearest reason as to why these particles produce different adhesion levels.

3.2.1.2.2 Field Tests

Most of the field studies on traction gels centre around “Sandite”, a mixture of sand and aluminium particles suspended in a silicate clay called Laponite, which becomes a gel when water is added. It is currently approved for use in Great Britain.

Tunley [32] conducted field work comparing the ability of sanding, Sandite, and water jetting at restoring adhesion when a leaf layer was present. The Sandite was applied to the rail using train-borne applicators. In his work, he found that water jetting alone offered no adhesion improvements at all and that Sandite and water jetting combined offered the best adhesion recovery system, this was summarised into the graph shown below in Figure 3.6. It should be noted that Tunley does not go into any detail about methodology or what is defined by a train slipping, so it is hard to draw any definitive conclusions about this work.

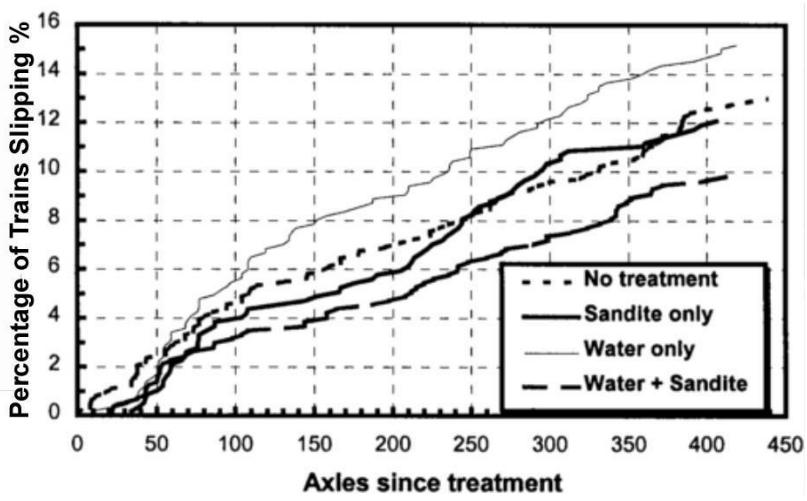

Figure 3.6. Performance of Different Leaf Layer Removal Methods [32]**.**

Sandite was also used in a study by Marshall for Network Rail [65]. Using on-train monitoring and recording, it was found that sandite restored adhesion after Lignin mixture (a component of leaves that can bond firmly to the rail [7]) was applied to produce low adhesion. The amount of information that can be drawn from this finding is limited by the lack of repetition of results and the methodology used is unknown.

Looking at different traction gels, a now defunct traction gel, known as "slipmaster", was tested to find the adhesion improving properties. Zobel [47], conducted field work that found that after 20 wheelset passes the traction gel actually seemed to lower adhesion. Zobel conducted more tests using a twin disc set-up and concluded that the presence of ethylene glycol and the gel were responsible for lowering the adhesion as the gel was crushed and particles removed from the contact.

Fulford conducted an in-depth review into the use of traction gels in improving adhesion in the wheel/rail contact [2]. He found that almost all traction gels offered some improvement in adhesion when dry, but would cause a decrease in adhesion when freshly applied or too much gel was applied to the rail.

In addition to Fulford's review, Garner [66] also found that traction enhancers were only beneficial in a limited climatic range. Garner's study concerned two different traction enhancer products: U5® and Alleviate®; the study took place during Autumn and the products were applied every axle. Garner found that both products provided little benefit in warm weather (~20°C) as the traction enhancers dried out quickly resulting in their quick breakdown and removal by subsequent wheel passes. Additionally, in freezing temperatures there was no improvement in adhesion, possibly due to the applied gels freezing to create an icy layer though this was not verified in her thesis. Lastly, Garner found that the traction enhancers were at their

most effective in dry conditions backing up the conclusions of Tunley and suggesting that applying traction enhancers directly after water jetting, whilst the rail head is moist, is detrimental to the efficacy of the gels.

It can be concluded that in ideal conditions (dry contaminant layer, time since application neither too short or long, cold but not freezing temperature) traction gel benefit adhesion levels. In future, more thought will need to be applied as to how and when to utilise traction enhancers in low adhesion conditions. In addition, the chemical structure of the gel is an important indicator as to how the traction enhancer will perform.

3.2.2 The Effect of Particles on Leaf Layer Removal

Leaves on the line are a problem for the rail industry as they dramatically reduce the amount of adhesion between the wheel and rail by forming a layer that bonds to the rail surface that is hard to remove [2], [7], [38]. Sand is a valuable tool, as it can indent into the leaf layer, breaking it away from the rail and restoring adhesion. The following sections investigate previous research that studied the effect particles in the wheel/rail contact have on removing leaf layers.

3.2.2.1 Dry Particles

3.2.2.1.1 Twin-Disc Set-up

Particle size is critical when breaking up the leaf layer. Laboratory work undertaken by Arias Cuevas et al. [39] and operational experience [11] have shown medium size sand grains (<0.6 mm) to be the most effective at removing leaf layers in braking. This is possibly due to:

- The grain size being larger than the contaminant thickness, thereby penetrating the leaf layer, providing a mechanical link between the wheel and rail;
- The particles being more easily entrained compared to larger particles, thereby increasing the number of particles affecting the layer.

In reference to the latter point, Arias-Cuevas et al. [39] found that the number of sanding axles in use (in this study this is proportional to the amount of particles being applied) has a proportional relationship with adhesion recovery, suggesting that one train pass with enough sanding axles may eradicate the leaf layer entirely. Contrary to this, Omasta et al. [46], in a study with a 1:3 scale twin-disc, found that whilst the application rate of sand into the contact had an effect this was much less important than slip rate and disc speed at determining the amount of adhesion recovery.

Higher slip rates mean a particle embedded in the wheel will abrade the surface on the rail for longer. This means that high slip rates could be an effective way of removing the leaf layer, both with and without sand being present in the contact as shown by the Arias-Cuevas et al. [39] study; though they admitted this would need to be balanced against increasing wear and RCF at higher creeps. A complete summary of this paper has been presented in Table 3.3 and uses the number of cycles till adhesion restoration as the basis for the effect the particles have had on leaf layer removal.

Table 3.3. Number of Cycles Required to Reach Minimum Adhesion Levels at Different Slip rates, Particle sizes, and Application amounts [39].

Mass of Sand Applied (g)	1% slip	5% slip				10% slip
	R sand	R sand	S sand	M sand	L sand	R sand
0	880	418				308
1.108	1000	315	80	66	440	249
2.216	528	117	<65	<65	308	117
4.432	286	<65	<65	<65	117	<65

Arias-Cuevas et al. [45] also conducted sanding tests with a twin-disc set-up which used a continuous application of sand into the contact, as opposed to the tests described above which used a set amount. They found that all particle sizes eventually removed the leaf layer, though under continuous application it seems like large particles gave the highest adhesion after recovery, probably due to the particles actually acting on the dry rail after the leaf layer was removed, thus agreeing with the conclusions from section 3.2.1.1.1 that larger particles lead to greater adhesion recovery [20].

Sanding equipment standards [11] recommend that small grain sizes (the sizes specified in Table 3.1) should be used in traction as it forms a paste between the wheel and the rail that is more effective at transferring tractive effort from the wheel to the rail. This seems to run counter to the results gained from Arias Cuevas et al. [39], who found fine particles were not as effective as medium particles for adhesion recovery and in the worst case seemed to lubricate the contact as the fine particles tended to mix with the leaf layer creating a lubricating paste.

It can be concluded that whilst there is a given amount of sand that will remove a given leaf layer, any extra sand will not aid in increasing adhesion and may cause unwanted effects e.g. damage and wheel/rail isolation. In addition, high slip rates aid the sand in the removal of the leaf layer. It should be noted that, due to the nature

of twin-disc testing, sand embedded in the leaf layer will stay in the layer throughout, possibly giving an unrealistic idea of what a single application of sand will do over multiple cycles.

3.2.2.1.2 Linear Full-Scale Rig

Tunley [32] conducted work comparing sanding with a variable discharge rate set-up to Sandite (traction gel); these results were summarised in Figure 3.7. They found that sand alone was enough to remove a significant amount of the leaf layer as multiple wheel sets passed over. Tunley also found evidence that whilst Sandite had an immediate impact on the leaf layer, the leaf layer quickly rose back to pre-treatment levels. There are limitations as to what conclusions can be drawn from this testing: Tunley does not explain how they measured the percentage of leaf contaminated rail or explain the specifics of the test methodology. The conclusion that can be drawn from this work is that both sanding and Sandite can remove the leaf layer under the correct conditions.

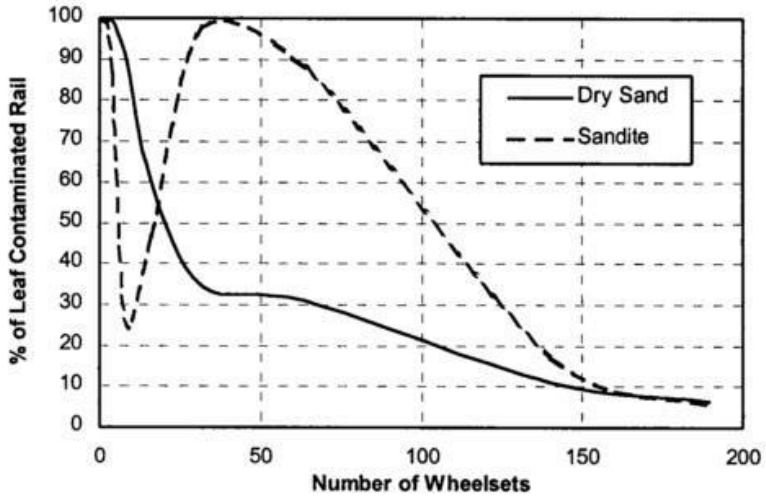

Figure 3.7. Efficacy of sand vs Sandite for removing the leaf layer [32]**.**

3.2.2.1.3 Field Tests

Most of the field work investigating leaf layer removal is qualitative in nature [25]–[27] with most research occurring in the 70's when measurement techniques were not as advanced. Thus, conclusions drawn from these studies must be treated with some scepticism.

In recent field tests, Arias-Cuevas & Li [43] looked at the influence of particle size on removing leaf layers; these tests used actual sanders and actual leaves. They found that sand was more effective at removing leaf layers compared to not using sand. They also saw that the optimal particle size (0.3-0.6 mm) for removing leaf layers was the same as in their laboratory work [39], adding credence to the twin disc

method. Another finding was that the sand was effective for the wheelsets after the sanding axle, showing the sand was staying in the running band.

3.2.2.2 Traction Gels

3.2.2.2.1 Twin-Disc Set-up

The effects of an unnamed traction gel on leaf layer removal have been studied by Lewis et al. [21] in a twin disc set-up, the results of which are included in Figure 3.8. They found that the traction gel eventually removed the leaf layer and increased adhesion. Initially the gel reduced adhesion due to the lubricating effects of the gel; however, once the gel had evaporated the particles started to have an effect on leaf layer removal.

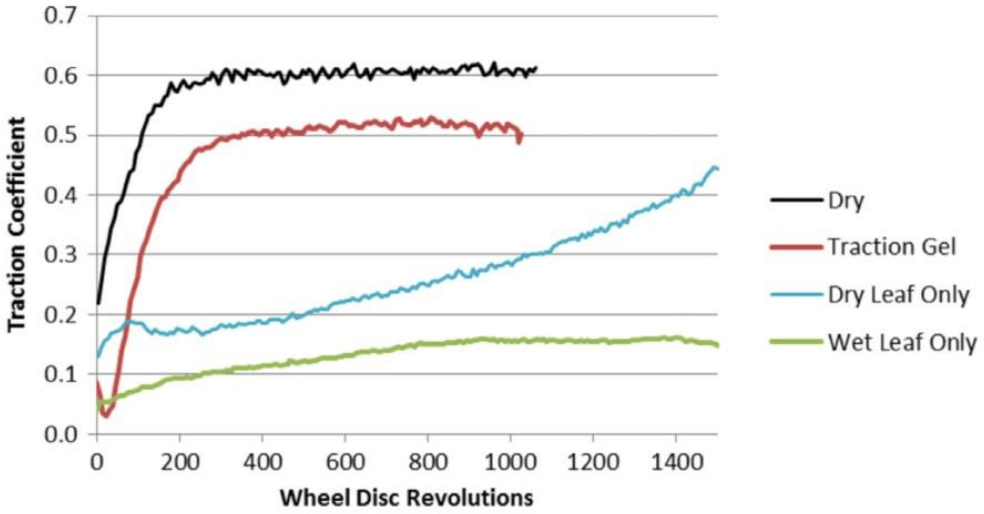

Figure 3.8. Restoration of Adhesion in a Leaf Contaminated Contact [21]**.**

More twin disc work was undertaken by Li et al. [12] looking at the effectiveness of two types of traction gel on leaf layer removal and restoring traction. The two types of traction gel can be summarised thusly:

- *FMA*; small particles with relatively strong bonds between its abrasive particles and its polymeric matrix.
- *FMB*; a mixture of gelling agent, stainless steel and sand particles of a larger size than those in FMA.

They found that when low slip conditions were present the friction modifiers were more likely to mix with the leaf layer, keeping adhesion levels low. FMB was shown to recover adhesion better than FMA, possibly due to the greater particle size. These results can be seen in Table 3.4.

Table 3.4. Number of Cycles Needed to Achieve Adequate Adhesion in a Leaf Contaminated Contact [12].

	Braking (μ=0.09)			Traction (μ=0.2)		
	0.5% slip	1% slip	2% slip	0.5% slip	1% slip	2% slip
Untreated	515	115	0	2255	982	667
FMA	245	207	220	N/A	1884	1151
FMB	187	35	70	1965	65	145

The same research also took Vickers hardness measurements: the leaf layer was 47-68 HV_{10g}, the stainless steel 320 HV_{10g}, and the sand was 1500 HV_{10g}. It can be inferred that the FMB particles were successful at removing the leaf layer because they more easily indented the leaf layer due to their hardness and size.

Higher slip rates seemed to more easily remove leaf layers. It may be possible that the gel can have a negative effect on adhesion under the wrong conditions. As with dry particles, the continued presence of traction gel during the cycles may exaggerate the effect on leaf layer removal over a number of cycles.

3.2.2.2.2 Field Tests

McEwen [29], conducted field research into the effects of Sandite in recovering adhesion in leaf affected sections of track. Overall, it was concluded that Sandite did improve the adhesion, but due to limitations in the testing method they did not expand any more than this. They did report that they saw an increase in adhesion level to about 0.03, but qualified this with reports of the Sandite sometimes reducing the adhesion level and that these adhesion increases were not much more than that seen on an untreated rail.

Work by Garner [66], found that Alleviate® traction gel, when applied every axle, was effective at removing a leaf layer. Traction enhancer carried down on the wheel was creating clear patches with the spacing between each clear patch being equal to the circumference of the wheel. It should be noted that Garner did not see any wheel slips or slides during her testing period, suggesting the leaf layer was not built up enough to cause low adhesion, which means the leaf layer Garner observed is not fully representative of "problem" leaf layers.

McEwen et al. [30] also investigated the effect entrained sand in a water jetting system had on removing leaf layers. They found that whilst the water-sand system was detaching the leaf layers from the rail, it was leaving a paste on top of the rail which could be rubbed away with a finger. This paste, however could be re-compacted, thus not solving the adhesion problem completely.

Further field work on this water-sand system carried out by Pollicott and Taylor [26]–[28], found that whilst the system was effective at removing "thick" leaf layers, it was less effective at removing tightly bonded "thin" leaf layers. In most of their work the system did not consistently remove all of the leaf layer.

These field studies corroborate the findings from the laboratory: traction gels may be partly effective, but could be counter-productive if not applied correctly or under the right conditions.

3.2.3 The Effect of Particles on Wheel/Rail Isolation

Trains on the track are sensed via an electrical current running through sections of rail known as track circuits. If these rails are short circuited by the wheels of a train then detection has occurred, when the wheels are insulated from the rail by a contaminant then the train cannot be detected and isolation has occurred. As sand is insulating, too large a quantity between the wheels and the rails can result in the loss of train detection, potentially leading to accidents [11].

The sanding equipment standards supplied by the RSSB [11] state that the factors affecting isolation include:

- The position of the first sander on the train formation;
- The number of wheelsets between sanders;
- The number of wheelsets after the last sander on the train formation;
- Sanding feed rate;
- Properties of the sand being used;
- Axle load.

It should be noted that in work conducted by RSSB [67], using field data, the viability of applying sand during braking was assessed using RSSB's Network Modelling Framework Safety Module. This approach calculated that reduction in risk of signals passed at danger (SPADs) was 170 times greater than the risk of isolation occurring, in fact it was found that only 3% of isolations were caused by sanding with the rest coming from contamination. These findings suggest that whilst it is important to consider isolation when designing a sanding system, the ability of the system to remove contaminants is of much greater importance.

The following sections detail the research that has previously been carried out to assess the effect particles have on isolation in the wheel/rail contact.

3.2.3.1 Dry Particles

3.2.3.1.1 Twin-Disc Set-up

The laboratory tests studying isolation have mostly been conducted on twin-disc set-ups, such as the study by Arias-Cuevas et al. [20]. The investigation showed that sand size plays an important part in the likelihood of isolation occurring in the contact, with fine and medium sized sand particles (0.06-0.3 mm and 0.3-0.6 mm respectively) being more likely to cause isolation, this was shown in Figure 3.9.

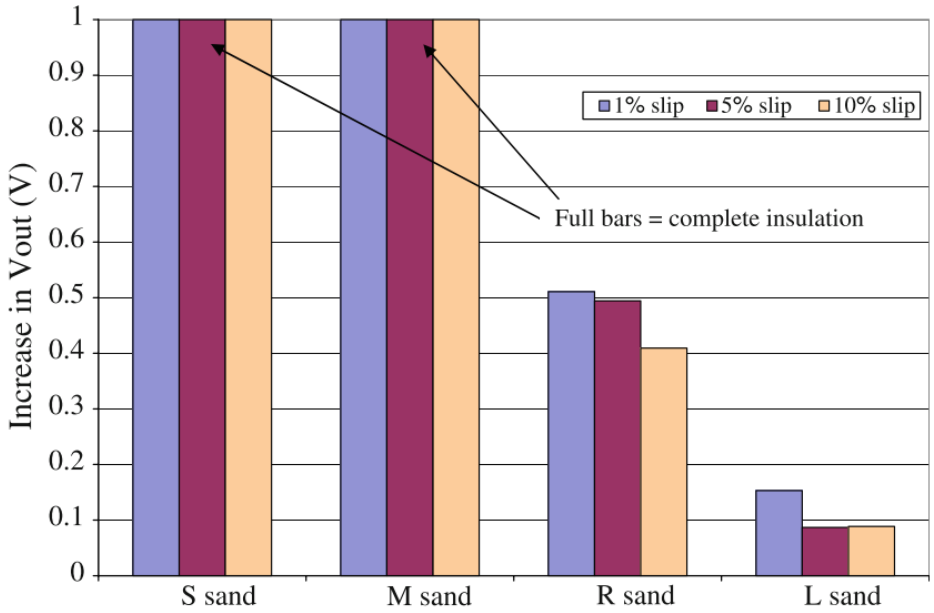

Figure 3.9. Electrical Isolation Occurrence for Different Particle Sizes [20].

Arias-Cuevas et al. [20] suggested this may be due to smaller particles not breaking up and being ejected upon entering the contact thus allowing a layer of sand to build up on the disc. The schematic Arias-Cuevas et al. used to illustrate this hypothesis is shown in Figure 3.10.

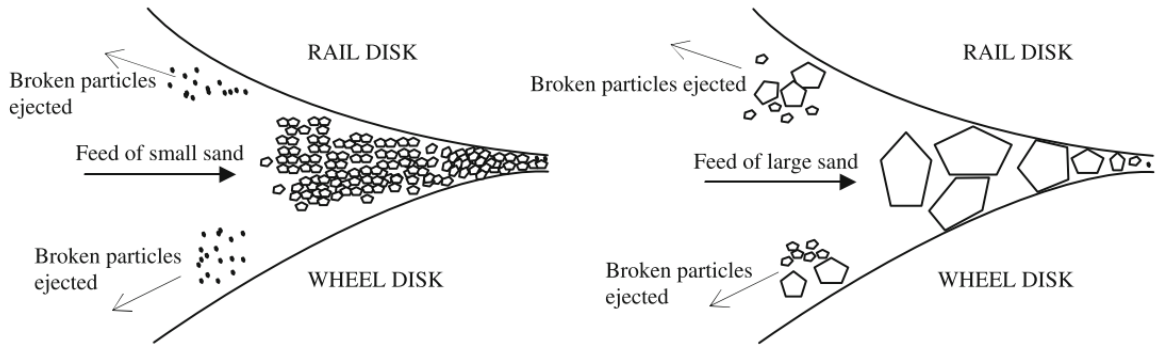

Figure 3.10. Schematic of Sand Entrainment at Different Particle Sizes [20].

As well as particle size, the amount of sand entering the contact will affect the possibility of isolation occurring. Previous field work [11] identified a critical sand density of 7.5 g/m above which isolation would occur. Lewis & Masing [68] and Lewis et al. [19] found that the amount needed to cause isolation was significantly higher than the 7.5 g/m mark. Their results are converted into sand concentrations (kg/m^2) with the "rail at 10 mph" value being obtained by dividing the sand density (7.5 g/m) by an estimate of rail head width (50 mm), there results have been summarised in Table 3.5.

Table 3.5. A comparison of critical sand concentrations calculated with different testing regimes [68]**.**

Experimental Method	Critical Sand Concentration (kg/m^2)
Static	0.3
Twin Disc at 2mph	0.75
Rail at 10mph	0.15

On a twin disc set-up, Lewis et al. [19] conducted a more detailed and fundamental investigation into isolation caused by sanding. Their experimental work found that there was a critical discharge rate at which isolation would occur, the same conclusion surmised by the Arias-Cuevas et al. study previously discussed in this section. Lewis et al. also formulated a simple model of isolation in the contact which was based largely on work by Bowden and Tabor [69]. This model predicts that the amount of contact points needed for effective conductance between wheel and rail is in the order of magnitude of 100 points; this is a tiny proportion of the nominal contact area and suggests that for isolation to occur there needs to be a complete separation of the surfaces. This also means that the voltage across the surfaces is effectively binary; the voltage being either at 0 V or at the open circuit voltage.

Work has been conducted studying the effect that the addition of both water and sand had on isolation; whilst water is conductive, so should therefore decrease the likelihood of isolation, this was not the case. Both static tests by Lewis et al. [68] and dynamic tests by Lewis et al. [19] have shown that the presence of water reduces the amount of sand needed to cause isolation. In the static case, it was put forward that this was due to some form of the meniscus effect holding neighbouring particles together and preventing them from being pushed out of the contact under load; in the dynamic case, it was suggested that capillary action was entraining particles into the contact. However, these conclusions are affected by the contact conditions; the same static study found that under lower contact loads the conductance between surfaces increased with the presence of moisture.

The previously mentioned static tests by Lewis & Masing [68] suggested that leaves and sand mixed together were more likely to cause isolation than either individually. This conclusion is not surprising on a static test, where the powder created could not be carried away through the contact by the presence of shear forces such as in the experiments conducted by Arias-Cuevas et al. [39] which found that the presence of sand in a leaf layer removes said leaf layer thus reducing the risk of isolation.

Another static test, performed by Broster and Taylor [70], suggested that sand, “black” abrasive fines, “mixed” abrasive fines, and silicon carbide particles of two different sizes all isolated the contact, though larger silicon carbide particles produced the highest conductivity.

3.2.3.1.2 Field Tests

A project primarily conducted by British Rail Research produced several technical reports outlining conductivity tests performed using class 165 trains fitted with sanders [57], [71]–[73]. These tests were performed between November 1995 and August 1996. The series of tests were performed at the Old Dalby test track at different times of the year with different sanding configurations.

The first trials [71] were conducted with a sander operating outside its intended specification; the findings presented in this report detailed that the use of sanding in dry conditions increased shunt resistance compared to a dry uncontaminated track, but not above unacceptable levels, however when sand was applied to previously sanded track under wet conditions unacceptable levels of shunt resistance were observed.

A further report [72] was later prepared that superseded these tests. These tests utilised a similar track circuit and measurement method but found that sand would decrease the likelihood of train detection in subsequent passes over a previously sanded area, though only on day one of their testing (they posited this may be due to windy conditions on day two of testing). It should be noted that this report fails to mention what sand application rate was used, which makes any interpretation of this report difficult. This work also conducted tests using a mixture of sand and cast iron grit (7%/wt.). Whilst no evidence of unacceptable shunt resistance was observed, only one test over previously applied material was presented from day one and this was also at the end of the day, meaning the track had been previously cleaned twice and possibly reducing the likelihood of the loss of train detection; the effects of sand on shunt resistance were found to nearly halve after the rail was cleaned once. The authors concluded these tests with iron particles were inconclusive.

In a further report [57], similar tests were then conducted when the sander was properly instrumented to ensure a 2 kg/min application rate. All the tests performed in this report were performed at 10 mph. Detection issues were observed for trains following sanding for up to 16 wheelsets though this was not observed when no wind was present. The conclusions in this report deemed these results "inconclusive" and suggested further tests were needed.

A final report [73] was produced that explored the effect of different train speeds whilst applying sand. These tests were run in what the author called an "extreme case" in that: a low voltage track circuit was utilised, the sand was applied continuously at a steady speed, and the rail was dry; this latter point is potentially spurious, whilst dry conditions are shown to be worse for train detection in unsanded contacts there is evidence to suggest that wet conditions are worse for train detection in sanded contacts [19], [68], [71]. The findings presented in this report were that after sanding at 10 mph the next three trains experienced some issues with train detection; above 15 mph these issues were not observed. Some doubt is valid when viewing these results, the amount of rust present on the rail head was high enough that train detection was not possible in even unsanded conditions without the aid of track circuit assisters, suggesting the effect of sand on track circuit performance may have been exaggerated in this report.

Aside from this collection of British Rail Research reports, more recent field work studying the effect of sand particles on track conductivity was conducted by Bombardier, in 2011, using 142 and 153 class trains [74]. The results in this work indicated important thresholds for sand application rates; application rates below 6 g/m had little to no effect on train shunt, whereas above this rate effects could be seen, furthermore above an application rate of 7.5 g/m it was found that there was an increased likelihood of the shunt resistance exceeding 500 mΩ. This work also recorded no examples of shunt resistance exceeding 500 mΩ for the preceding train after sanding had occurred, though it was noted that some runs came very close to this limit.

In work package 1 of the T797 project report [10], two reports of field testing carried out in Ireland and Germany are included. The summary of the tests from Ireland suggest that at sand application rates of 1.2 kg/min at ~15 mph effective isolation of the leading wheelset occurs i.e. a limit of 0.5 Ω is reached, though with these conditions train detection was still possible at the rear wheelset. The summary of the tests from Germany suggest that at sand application rates of 0.9 k/min at <37 mph and 2.3 kg/min at >37 mph no loss of train detection occurred.

3.2.3.2 Traction Gels

3.2.3.2.1 Twin-Disc Set-up

In a study performed by Lewis et al. [60] the effect of applying Kelsan® high positive friction (HPF) solid stick friction modifier on the conductivity between wheel and rail was assessed. A twin-disc set-up and a static set-up were used for performing tests. The study saw no evidence that HPF had any negative effect on conductivity in either test set-up. The study also saw evidence that, at increasing slip rates, impedance in the HPF applied contact decreased; in the study this was explained by the greater metal-to-metal contact occurring at higher slips.

Further to the aforementioned study, Hardwick et al. [61] expanded on this work by analysing the effect of HPF on conductivity at lower axle loads than previously investigated. The difference in measured impedance between dry conditions vs conditions where HPF was applied was minimal, though seems to be more apparent than the previous study. Any slight increase in impedance due to the presence of HPF was more noticeable at higher speeds and slip values. Unlike the previous study, static tests showed a noticeable, though slight, increase in impedance when HPF was present. There was no explanation for the increased effect of HPF on impedance presented in the Hardwick et al. paper but one possible reason may have been due to less friction modifier being squeezed out at lower contact pressures.

A study by Lewis et al. [62] assessed the effect of "wet" friction modifiers (different dilutions were used through the testing) on measured impedance in a twin-disc set-up. A notable observation from this study was that the frequency of the AC circuit being used affected the impedance for both friction modifiers; in almost all cases, the lower frequency circuit was more negatively impacted by the presence of friction modifier, no explanation for this was provided in the paper. The concentration of each product, with respect to water, affected impedance in different ways; friction modifier "A" gave a higher impedance at higher concentrations whilst friction modifier "B" showed the opposite effect. Overall, this study showed no clear relationship between the presence of friction modifier and impedance, any possible relationship seems to heavily depend on the exact details of the friction modifier being used.

In a twin-disc study by Lewis et al. [21]. They found evidence that the presence of traction gel in a leaf contaminated contact was effective at decreasing impedance between the wheel and rail. The results, shown in Figure 3.11, also suggest that 5-10 s after traction gel application, the impedance falls close to uncontaminated levels, which according to Lewis et al. occurred when the excess gel started to evaporate

suggesting that the gel was responsible for creating more impedance than the sand though this may also be due to more of the isolating leaf layer being removed.

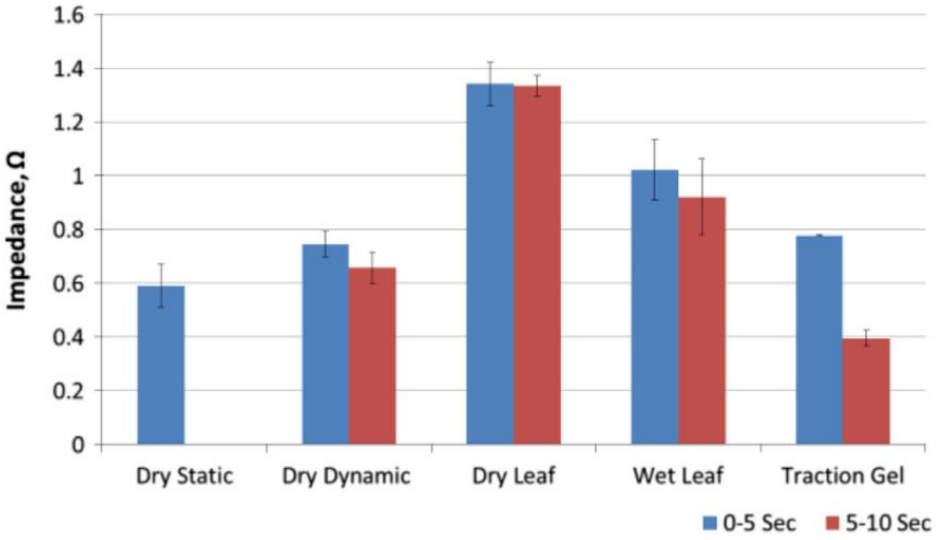

Figure 3.11. Impedance between Wheel and Rail with Different Intermediary Layers [21].

3.2.3.2.2 Field Tests

The only identified field work on isolation was by Zobel [31], who studied the effects a traction gel called "slipmaster" had on isolation. Slipmaster is made up of sand suspended in an aqueous fluid which includes thickeners and corrosion inhibitors. Zobel found that as the train speed decreased the traction gel had a larger effect on isolation, however one layer alone was never enough to cause isolation. He also saw evidence that trains at lower speeds did not remove the gel suggesting that slipmaster applied at low speeds would build up, resulting in an isolation problem.

3.2.4 The Effect of Particles on Wheel/Rail Damage

As the traction restoring effect of the hard particles is dependent on them indenting and transferring traction from wheel to rail, inevitably there will be some damage to the surface. The amount of damage is important, but only as important as the damage mechanism that is occurring, for example abrasive wear could present a maintenance issue, but it is unlikely to cause a safety issue unlike a high amount of ratchetting fatigue.

3.2.4.1 Dry Particles

3.2.4.1.1 Twin-Disc Set-up

The exact amount of damage sand can cause is hard to quantify on twin-disc set-ups, due to almost all the sand being entrained into the interface and the much smaller geometry of the discs resulting in much more severe wear than would be

expected in the field. Kumar et al. [41], found that the application of sand into the wheel/rail contact increased the amount of wear by an order of magnitude of between 1 and 2, a very large and potentially costly increase.

Similarly, Lewis & Dwyer-Joyce [22] found that sand particles being fired into the wheel/rail contact greatly increased damage compared to an unsanded contact. In Lewis & Dwyer-Joyce's tests three different scenarios were tested: dry with no sand, dry with sand, and wet with sand. In all scenarios, the wear at the wheel was always more than at the rail, this is unsurprising for the case with no sand as the wheel surface was softer, with a measured hardness of 1.9 GPa (193.7 HV), compared to the rail surface, with a measured hardness of 2.9 GPa (295.7 HV). In the sandless scenario the wear mechanism seemed to be ratchetting of the surface, with the wheel undergoing more delamination than the rail. The full results have been shown in Figure 3.12 where the amount of damage is analogous to the wear rate.

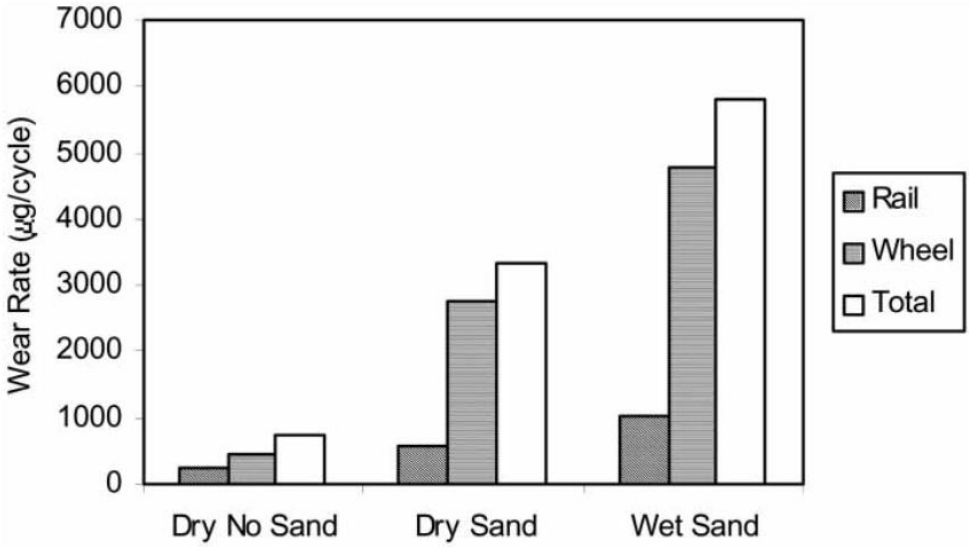

Figure 3.12. Wear Rates Under Different Sanding Conditions [22].

Furthermore, Lewis & Dwyer-Joyce found evidence of two body abrasion occurring in the contact as the sand indented the wheel and caused abrasion scars along the rail. It would be expected that this would result in higher wear rates in the rail (harder surface) than the wheel (softer surface) which was untrue in this case. Instead, Lewis & Dwyer-Joyce concluded that the sand indentation at the wheel surface was causing fatigue damage leading to spalling at the wheel surface. The damage features they identified are shown in Figure 3.13. This observation has been backed up in similar work by Arias-Cuevas et al. [45] and Wang et al. [36].

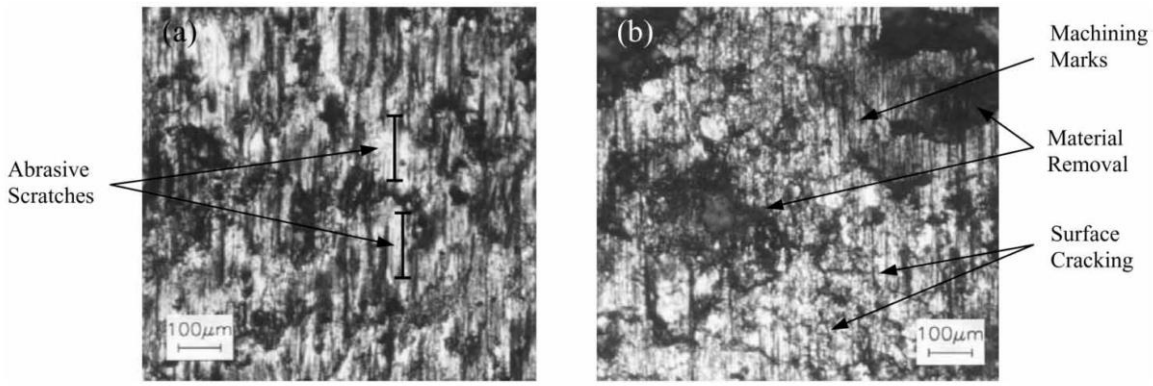

Figure 3.13. Damage Features for *(a)* Rail Disc and *(b)* Wheel Disc [22]**.**

The Lewis & Dwyer-Joyce experiments [22] also assessed the effect that the presence of moisture had on the damage. Results indicated that wet conditions seemed to almost double the wear rate at both wheel and rail compared to dry conditions, it was posited that this was due to sand particles sticking to the wheel and rail via meniscus effects and entrained via capillary action; a schematic of this effect has been included in Figure 3.14.

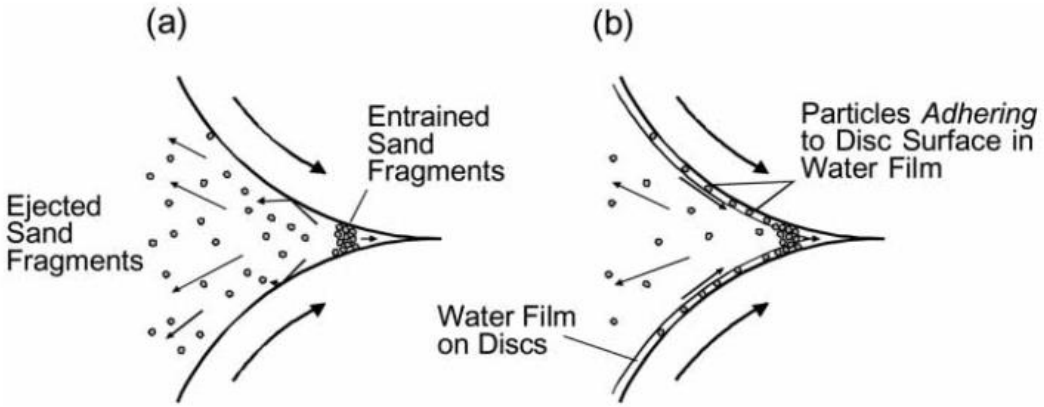

Figure 3.14. Schematic of Particle Entrainment in *(a)* Dry Contacts & *(b)* Wet Contacts [22]**.**

Arias-Cuevas et al. [45] conducted a study to assess the effects particle size and slip in the contact had on the damage being caused to the wheel/rail surfaces. They found that smaller particles (<0.3 mm) at lower slip rates (1%) produced a coating of crushed sand that was embedded into the disc surfaces, this may have been due to: the lower slips not abrading the surface as much therefore leaving the coatings intact; or that less of the smaller particles are being entrained into the contact thus not being present in large enough numbers to be able to form the coating. At higher slips and larger particle sizes indentations in the surface were observed with no coating being present.

Furthermore, Arias-Cuevas eat al. seemed to show that when the sand separated the surfaces fully (when isolation was present) there was little plastic deformation

compared to instances with metal to metal contact at similar adhesion levels. Arias-Cuevas et al. posited that this may be due to the sand acting as a solid lubricant, protecting the surfaces whilst still being embedded into them, transferring traction and keeping adhesion high. Where large particles and slips were applied to the contact there was evidence of greater work hardening being present which correlated with a high adhesion coefficient. The images Arias-Cuevas et al. drew these conclusions from have been included in Figure 3.15 and Figure 3.16.

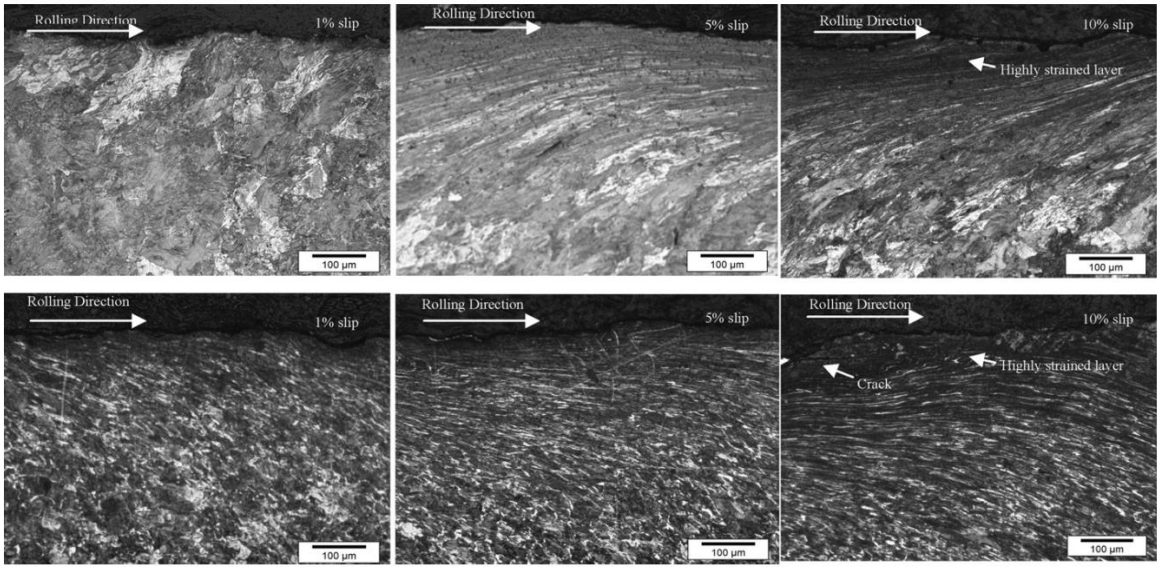

Figure 3.15. Sections Parallel to Rolling Direction Using R Sand: *(Top)* Rail section, *(Bottom)* Wheel Section [45]**.**

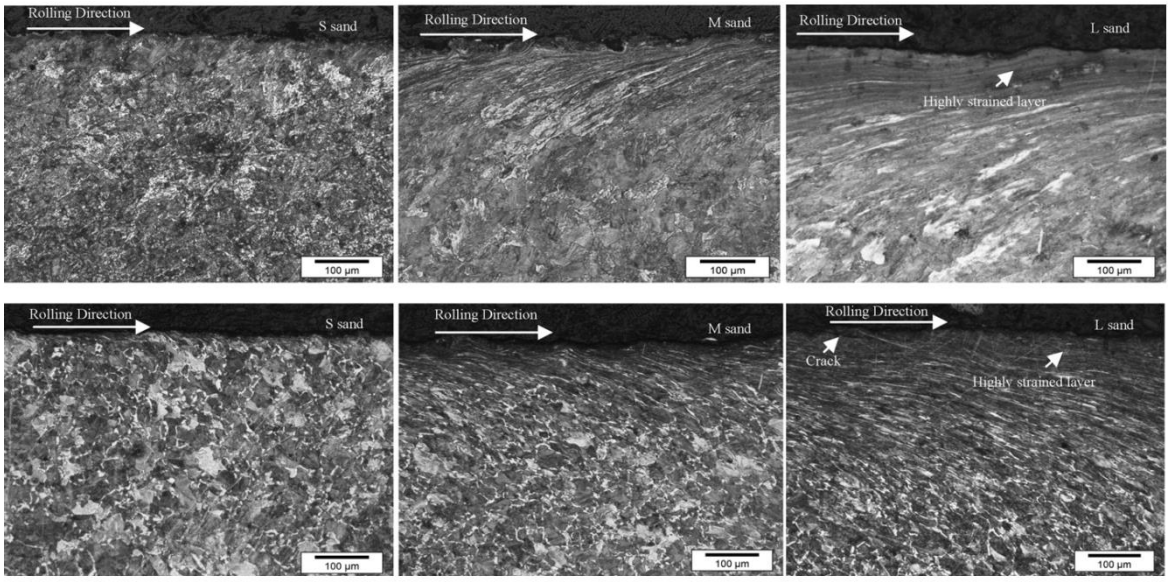

Figure 3.16. Sections Parallel to Rolling Direction Using 5% Slip: *(Top)* Rail section, *(Bottom)* Wheel Section [45]**.**

Arias-Cuevas also took surface roughness measurements of all the discs and found that higher slips caused greater roughening, probably due to the lengthened

abrasion scars caused by the sand in the contact. The same measurements also showed the medium sized particles (0.3-0.6 mm) caused the most wear, possibly because they struck the balance between causing larger indentations than the small particles and being more easily entrained into the contact than large particles, therefore greater damage due to sheer number of particles will occur.

Lastly, Arias-Cuevas et al. saw that at high slips the larger particles created greater damage (measured through mass loss), in large part because of plastic deformation and spalling due to ratchetting at these higher slips being aggravated by larger particles. However, this trend did not exist at low slips as the only observed wear mechanism was abrasion and fewer large particles entered the contact compared to medium and small particles thus less abrasion occurred. These results are shown in Figure 3.17 where the size categories are those described in Table 3.1.

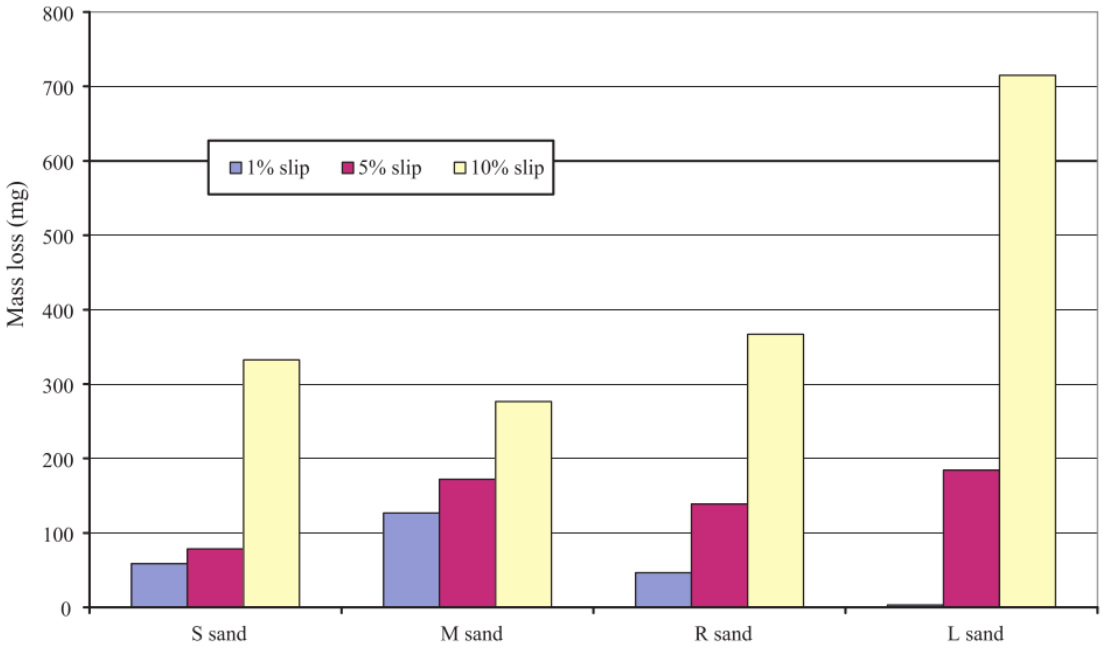

Figure 3.17. Mass Loss due to Wear at a range of particle sizes and slip rates [45]**.**

Huang et al. [44] have also conducted tests assessing the effect of particle size (using a range of 50-900 μm) on damage, with these tests being conducted in wet conditions at low slip rates (<1%) with a continuous feed of sand. Their work found larger particles and higher feed rates created more damage, and in all sanded cases damage was greater than the unsanded, wet case.

A study by Shi et al. [48] analysed the effect on wheel/rail surface damage of micro-fragments (0.1-30 μm) of silica sand compared to its uncrushed state (600-2000 μm) in wet conditions. Their work found evidence that uncrushed sand created much greater wear than micro-fragments under similar feed rates, and as less micro-fragments were applied wear rate also decreased. However, these

micro-fragments appeared to create severe rolling contact fatigue, thus it was their conclusion that micro-fragments would not be suitable for real-world use. These findings do suggest that most wheel/rail damage is caused by the initial crushing of particles, as opposed to damage caused by crushed particles.

Faccoli et al. [75], assessed the effects of sand on different grades of wheel steels. Their study found that wheel damage was much greater for softer wheel steels with lower ultimate tensile strengths. They proposed that this was due to increased ratchetting of the wheel steel.

More particles than just sand have been assessed. A study by Wang et al. [36], investigated the effect alumina particles had on wheel/rail damage when applied to the contact, these results are shown in Figure 3.18. Though it should be noted that though the alumina particles were five times smaller than the sand particles, the alumina caused 3 times less wear whilst still being a more effective adhesion enhancer than the sand particles in some situations. These results are promising and may bear greater scrutiny going forward.

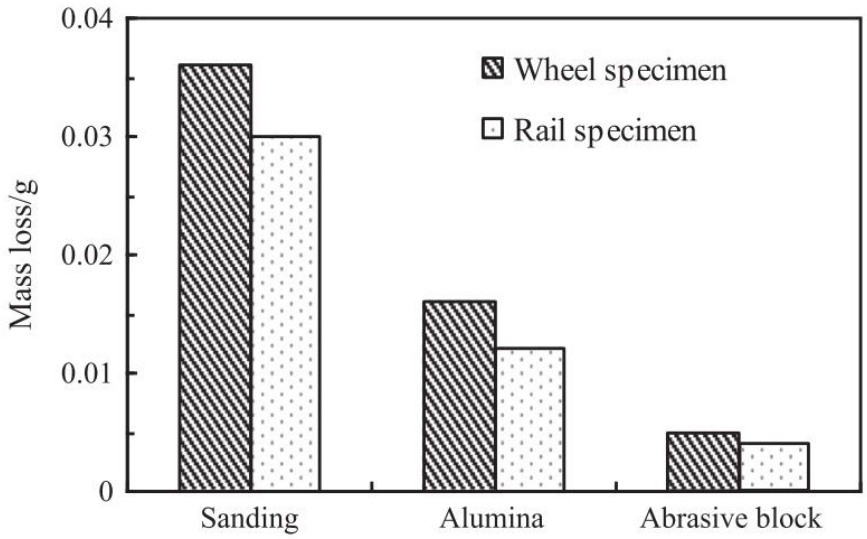

Figure 3.18. Mass Loss for Different Particle Systems [36].

A further study using alumina particles was conducted by Cao et al. [49], where a range of particle sizes (75-550 μm) were assessed in wet conditions with varying feed rates (1-10 g/min). Here, they found that increasing particle size and feed rate increased both wear rate and surface roughness, whilst making no difference to surface hardness. This combined with the study's adhesion data, discussed in sub-chapter 3.2.1.1.1, suggest that smaller alumina particles provide a greater benefit than larger particles when considering adhesion and damage.

Shi et al. [50] conducted similar tests, though with a single application of alumina, as opposed to a continuous application. Through conducting tests in this manner, they

saw that surface damage was highest upon initial crushing of the particles and generally lessened as the number of runs increased.

Alumina, as well as sand, zinc oxide, and spinel, was also tested in a twin-disc set-up by Wang et al. [51]; these tests were conducted with the primary aim of assessing the relationship between particle crushing strength and surface damage. This work found that particles with a higher crushing strength produced larger damage, with any corresponding increase in adhesion being negligible for particles with a higher crushing strength than sand.

Wear tests conducted with crushed granite ballast (~290 μm) were carried out by Grieve et al. [76]. This work found that granite particles agglomerated in the contact, producing flakes that ploughed the surfaces of the wheel/rail contact. Wear of the rail disc was observed to be greater than the wheel disc, possibly due to particles embedding into the softer wheel material and abrading the rail material; a similar hypothesis was put forward by Lewis & Dwyer-Joyce [22].

3.2.4.2 Traction Gels

3.2.4.2.1 Twin-Disc Set-up

Traction enhancers reduce the amount of damage in the contact compared to a dry rail. This was the case in a study carried out by Lewis et al. [21], though this may have been due to the traction gel particles abrading the leaf layer as opposed to the rail itself, whereas traction enhancer on a dry contact may cause more damage. The results have been included in Figure 3.19.

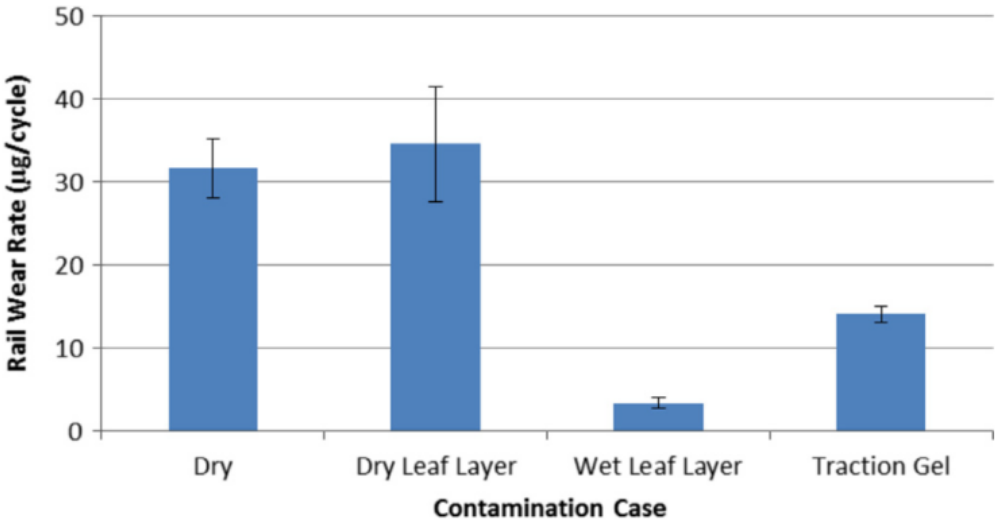

Figure 3.19. Wear Rates with Different Intermediary Layers [21].

Further damage research was conducted by Li et al. [12] who found correlation between particle sizes in the traction enhancer and the amount of damage to the

surface. The conclusion was that larger, harder particles seemed to cause more damage, which is in line with what was found for dry particles and may be due to the gel aiding entrainment of these larger particles.

Arias-Cuevas et al. [23] have also conducted work into the effect traction gels have on damage in both a wet and a dry conditions. In dry contacts they found evidence that the traction gels reduced the amount of wear, on both wheel and rail by effectively lubricating the contact whilst keeping adhesion at an acceptable value; this reduction in damage was especially prevalent in traction gels with particles <100 μm, corroborating the Li et al. results. The results from Arias-Cuevas et al. have been summarised in Table 3.6 where FMA and FMB are two types of commercially available traction enhancers.

Table 3.6. Mass Loss Comparison Between Different Traction Gels [23]**.**

	Dry		FMA		FMB	
	Wheel	**Rail**	**Wheel**	**Rail**	**Wheel**	**Rail**
Mass Loss (mg)	114.9	90.1	30.3	28.4	109.6	70.5

In a ball-on-disc study conducted by Galas et al. [63], they found that oil based friction modifiers with small metal particles (4-10 μm) reduced wear rate and surface damage compared to a clean contact, a similar conclusion to the aforementioned study by Arias-Cuevas et al. [23].

3.2.5 Application of Particles into the Wheel/Rail Contact

The sanding system's ability to aid adhesion will be very dependent on the amount of sand it can deliver into the wheel/rail interface. Any sand not going into the interface is increasing cost and reducing effectiveness. Much of the work cited in this section was undertaken by Lewis et al. [24], [37], who studied the entrainment of sand into the wheel rail contact on a full-scale rig; in all their tests the full-scale rig (see section 2.6.3) was utilised.

3.2.5.1 Dry Particles

3.2.5.1.1 Location & Frequency of Application

Usually the frequency with which the sanding procedure is used is dependent on the levels of adhesion being measured in the interface, i.e. when significant sliding occurs between the wheel and rail (significant sliding is defined as the wheelset rotational speed being ≤95% of the true train speed [11]). In addition, the sand application will normally engage whenever the train is undergoing emergency braking.

3.2.5.1.2 Mechanical Aspect

The application of sand into the wheel/rail contact will depend heavily on the amount of sand being discharged from the hose; the T796 RSSB report [17] undertaken in 2009 found a large variance in discharge rates of sanders, with the average discharge rate being measured at 1.148 kg/min (it should be noted that industry believes this situation has improved since this report). The report also investigated different sanding system parameters to try and diagnose the cause of low discharge rate.

The effect of hose lengths on discharge rate is dependent on the type of system being used. The work in T796 found that shortening or removing hoses on Venturi plate systems generally increased discharge rate, whilst for pressurised air systems there was no discernible difference; overall it was recommended that short hose lengths should be used. The report also studied the hose configuration, i.e. straight, bent, sag, no sag: the existence of sag in the hose reduced the discharge rate whereas tight bends seemed to have no effect.

The same study analysed the effect the diameter of the sand exit point had on discharge rates. On-site testing produced some weak evidence to suggest that discharge rates increase with exit diameter. This was partly validated by a controlled test of a sand hose with a 19 mm nozzle and a 25 mm nozzle; the discharge rate more than doubled for the larger nozzle. A smaller diameter nozzle reduced the discharge rate but this can potentially be compensated for by using a higher regulator pressure.

Tests carried out on a full-scale rig by Lewis et al. [24] have shown a marked increase in the amount of sand going through the contact with a nozzle (exit diameter smaller than that of the main hose) attached to the end of the hose, these results are shown in Figure 3.20. This was due to the nozzle focusing the sand stream more precisely at the contact. The optimum hose configuration derived from these results was a 25 mm bore diameter hose with a nozzle attached.

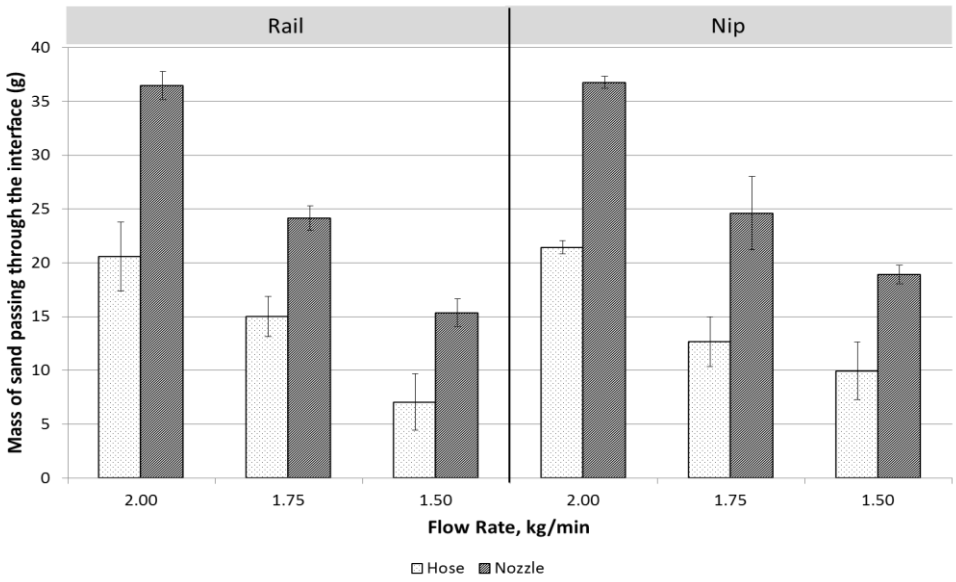

Figure 3.20. Effect of the Nozzle on Sand Entrainment [24].

A common sand application system uses an orifice plate to discharge sand from the sandbox. The orifice plate has two holes in it: one hole directs the air into the sand reservoir to agitate it; the other hole uses the Venturi effect to draw the agitated sand into the hose. A typical orifice plate is shown in Figure 3.21.

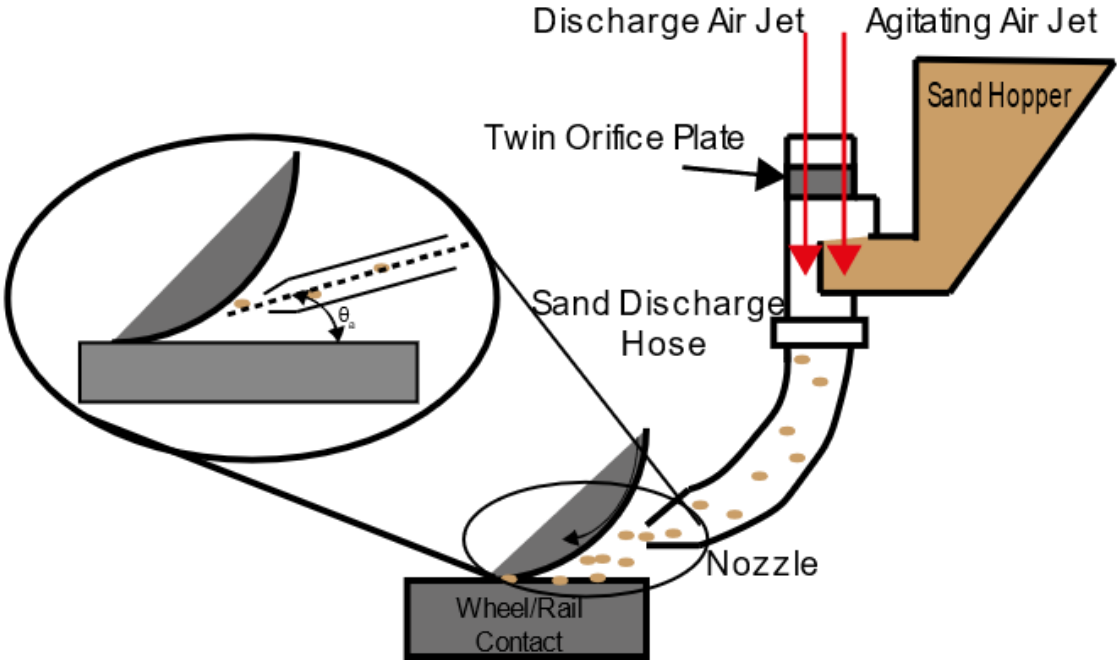

Figure 3.21. Orifice Plate Sanding Valve with Angle of Attack (θ_a).

All sandbox designs that use the Venturi effect to draw sand into the hose require a breather to prevent the formation of a vacuum [17]. The breather design has a large effect on the discharge rate as it must shield the sand from contaminants whilst allowing enough air to pass through to prevent vacuum within the hopper. It is vital to ensure that the moisture content in the sander is kept very low; Zobel found that

as little as 2-3% moisture content could prevent sand being ejected from the sand box [47].

3.2.5.1.3 Angle of Attack

The angle of attack can be defined as the angle between the rail and the direction of discharge, a schematic has been included as part of Figure 3.21.

The angle of attack between the hose and rail does not affect the discharge rate [17], but it does affect the entrainment of sand into the contact. Lewis et al. [24], found that shallower angles of attack resulted in an increased amount of sand entering the contact. These results are summarised in Figure 3.22 where the angles of attack were varied with target area: the rail, the nip (where the wheel and rail meet), and the wheel. Each measurement of sand passing through the interface was conducted after one wheel pass. A shallow angle of attack aimed at either the rail or nip seems to entrain more particles with the latter doing so more consistently.

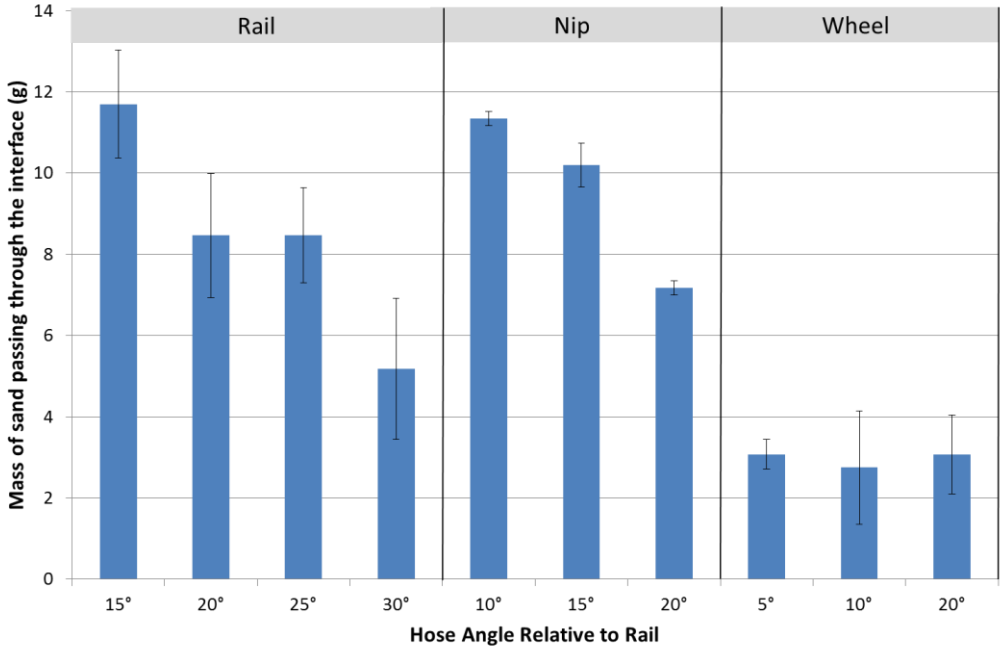

Figure 3.22. Effect of Angle of Attack and Application Direction on Entrainment over one Wheel Pass [24].

High speed stills taken from the Lewis et al. work [24] have been included in Figure 3.23. With higher angles of attack, the particles bounced away from the contact and when aimed at the wheel the particles bounced straight off and away from the contact. These stills corroborate the findings from Figure 3.22, particles bouncing on the rail may go anywhere and will do so unpredictably whereas those particles hitting the wheel will just bounce away.

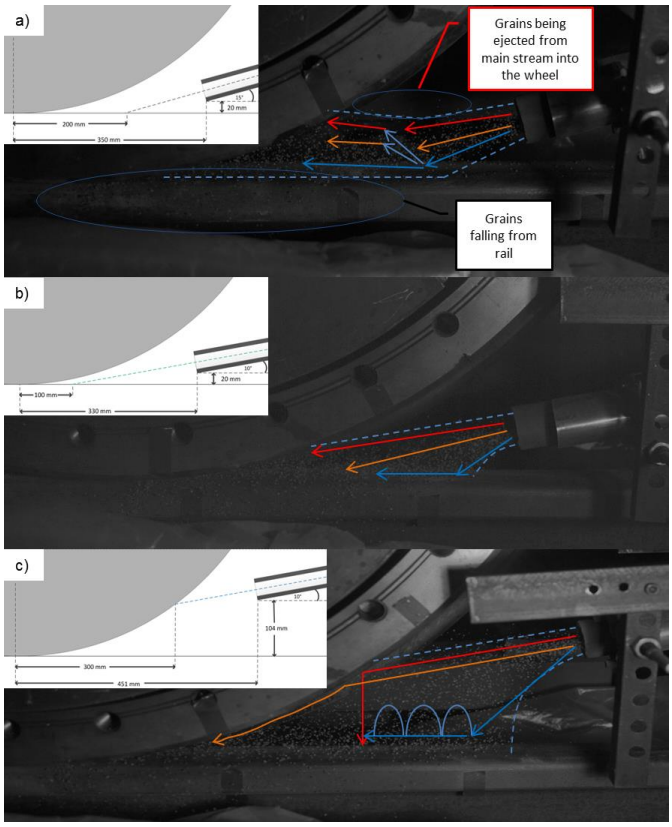

Figure 3.23. High Speed Stills; *(a)* hose aimed at rail with 15° angle; *(b)* hose aimed at wheel/rail nip with 10° angle; *(c)* hose aimed at wheel with 10° Angle [24].

3.2.5.1.4 Nozzle Alignment

Lewis et al. [24] investigated the effect the hose alignment and position had on the amount of sand being entrained into the wheel/rail contact. Unsurprisingly, the amount of sand entering the contact increased the closer the hose exit was placed to the contact.

The hose alignment was shown to have a large effect on entrainment, the optimum condition found by Lewis et al. was a hose pointed directly at the wheel/rail centreline with the hose running parallel to the rail. Any slight misalignment was shown to have a detrimental effect on entrainment. The effect of the hose's lateral position from the centre line is shown in Figure 3.24 (Top) and effect of the nozzle alignment angle is shown in Figure 3.24 (Bottom).

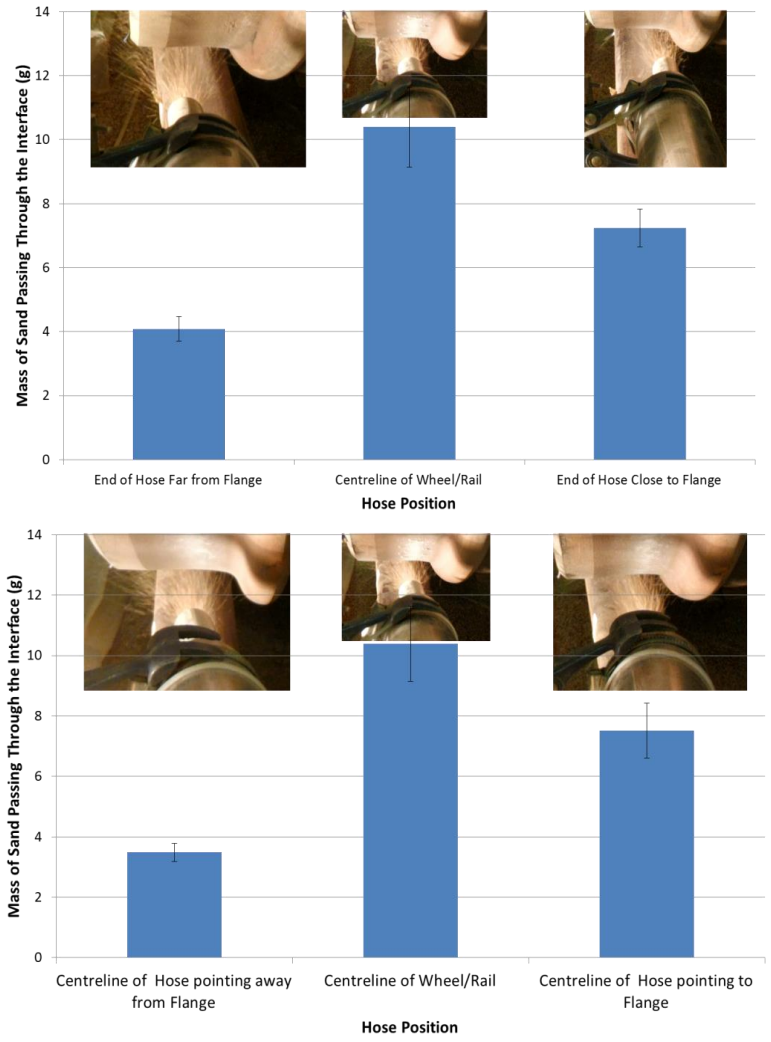

Figure 3.24. Effects of Changing: *(Top)* Lateral Alignment, *(Bottom)* Nozzle Alignment Angle with Respect to the Rail Direction over one Wheel Pass [24].

3.2.5.1.5 Discharge Pattern

The discharge pattern from the nozzle to the rail head is an important parameter for optimum sand entrainment into the wheel/rail interface. In static tests conducted indoors, nozzles focused the sand stream more precisely onto the rail head [17], though it should be noted that the lack of real world complications from crosswind etc. were not accounted for. The comparison between wide and narrow discharge patterns and the subsequent amount of sand being entrained can be seen in Figure 3.25, where more sand is clearly entering the contact when the discharge pattern is narrow.

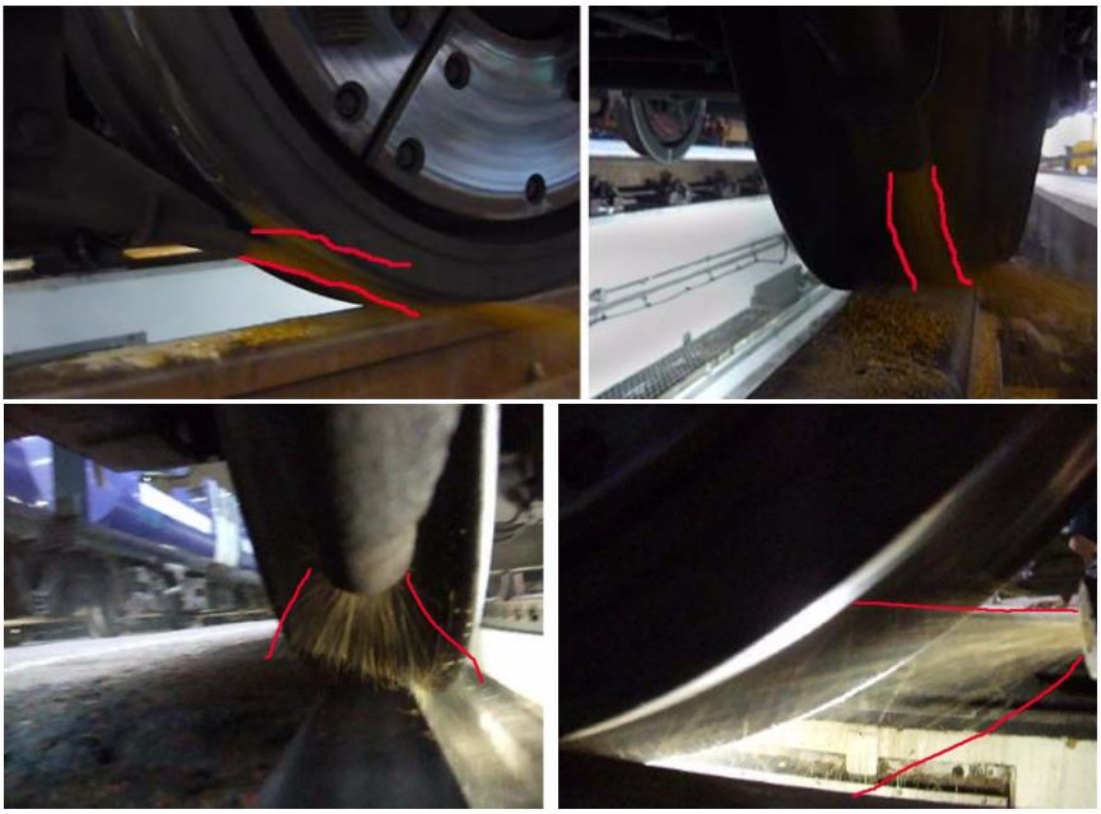

Figure 3.25. ***(Top)*** **Narrow Discharge Pattern vs** ***(Bottom)*** **Wide Discharge Pattern** [17]**.**

3.2.5.1.6 Wind

The research conducted by Lewis et al. [24], looked at the effect wind had on the application of sand into the contact. The work suggests that increasing the velocity of the air flowing parallel to the train's direction of travel gradually decreased the amount of sand entering the contact when dry conditions were present. This trend was reversed in wet conditions where higher air velocities increased the quantity of sand being entrained. Generally, wet rail seems to increase the quantity of sand being entrained, possibly due to the same mechanisms described by Figure 3.14. All these observations were obtained from the results shown in Figure 3.26.

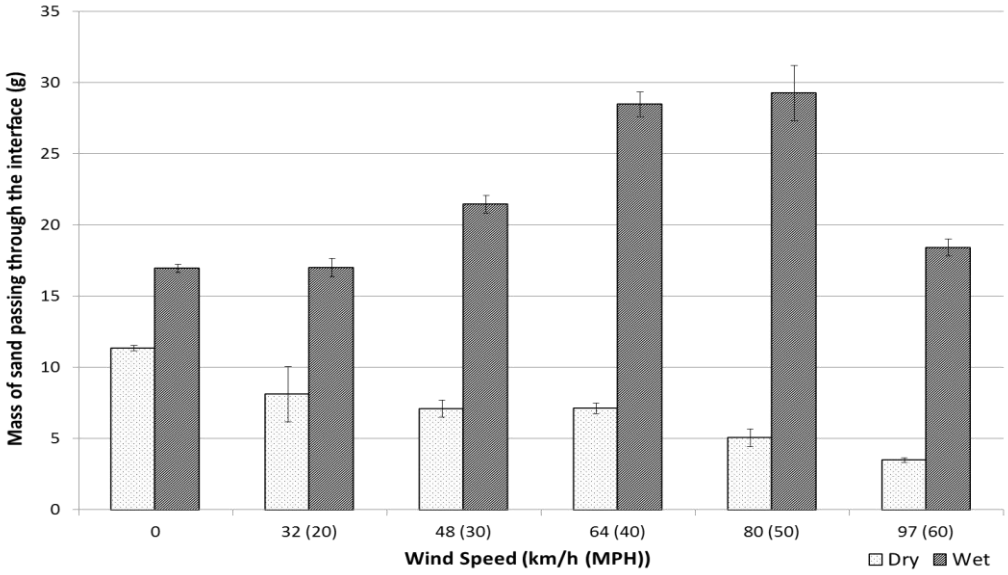

Figure 3.26. The effect of Head Wind on Sand Entrainment over one Wheel Pass [24].

The same study also investigated the effect of cross-wind on the amount of sand applied to the rail. The findings were that even a moderate amount of cross-wind may remove all the sand from the rail, making the sanding system effectively useless. The study suggested that these findings may have significant consequences for sanding systems being used at high train speeds; the speed of the train may cause the air flow to become turbulent, blowing all the sand away from the rail; evidence of this was found at head winds of 60mph as seen in Figure 3.26.

The speed at which the particles are discharged at seems to have a positive effect on the entrainment of particles into the contact [25], [77], possibly due to lessening the effects of crosswind.

3.2.5.2 Traction Gels

An early example of a traction gel system included mixing sand into a water jetting system which was applied to the track by a specially modified train [26]–[28], [30].

A common traction enhancer used by the British rail industry is a liquid-sand mixture known as sandite (sand and aluminium particles suspended in a silicate clay called Laponite which becomes a gel when water is added) [29], [32]. Sandite can be applied using modified trains or by trackside applicators, the former method can also utilise water jetting to first blast off contamination, initially improving adhesion, before applying sandite to maintain this higher adhesion level [32].

In work conducted by Garner [66], the application of traction enhancers was studied, specifically application using traction gel applicators (TGA's). TGA's use a peristaltic pump to send traction enhancer up a hose and onto the rail head; Garner found that pumping losses increased with hose length and pumping time. They also

found that the traction enhancer with a higher viscosity did not flow as well through the pipe, leading to a decrease in output. However, the higher viscosity traction enhancer stayed on the rails more meaning less wasted material and contamination of the ballast.

A Network Rail project conducted by Marshall [65] looked at certain aspects of traction enhancer application using TGA's. They found that a new type of cylinder applicator bar is more effective at delivering traction enhancer as it can apply across the rail with a length equal to the circumference of a typical wheel, meaning more gel can be carried down by the wheel making it effective for a larger length of rail section. They also found that there was no link between the flow rate of the traction enhancer and the amount of traction enhancer in the hopper, he did however find a weak correlation between rising climatic temperatures and increasing flow rate.

There are some yet untested traction foams, based on US 6,297,295 B1 patent [78], the idea being that the sand particles are suspended in the foam allowing more control of dispersion onto the rails.

3.2.5.3 Future Application Techniques

New technologies for improving particle entrainment into the wheel/rail contact have been discussed in a report written by Barnard and Cooke [79], to the authors' best knowledge, none of these techniques are currently under consideration in the railway industry. Some of these measures include:

- *Electrostatic particles.* This would use a similar technique to traditional electrostatic coating, the particles are charged using a high DC voltage. These charged particles repel each other, aiding uniformity, and are attracted to the nearest ground, the wheel. The particles could be picked up by an electrode of opposite charge on the other side of the wheel;
- *Magnetically responsive particles.* Radial electromagnets would be present in selected wheels; iron particles would then be fired at the wheel and stick through the contact. The particles could be picked up by an electromagnet of opposite charge on the other side of the wheel;
- *"Smart Sand".* A mixture of iron particles and ceramic particles attracted to the wheel electromagnetically, the presence of ceramic may give greater adhesion;
- *Particle wedge.* This wedge of particles in front of the contact would be created by a build-up of magnetically responsive powder, thus absorbing the rotational energy;
- *Magneto-Rheological Fluid.* Small ferrous particles suspended in a carrier fluid, when subjected to a magnetic field the viscosity of the fluid will increase to the

point that it acts as a viscoelastic solid. This solution would have the benefit of providing relatively precise adhesion control in the contact.

In regards to electrostatic particles, a model of electrostatic particle application was developed by Gorbunov et al. [80] which was validated experimentally. Their electrified sand set-up was estimated to decrease the consumption of sand by up to 12 times, with the electrified sand dispersing more evenly on the surface of the rail.

3.2.6 Gap Analysis

3.2.6.1 Paper Grading

To successfully identify the current knowledge gap present in sanding research a paper grading system proposed by Harmon & Lewis [81] has been employed in this review. The aim of this paper grading system is not to assess a paper's quality but to understand what areas research has been conducted into and whether the conclusions have been validated by testing at multiple scales and/or through modelling work.

The papers have been graded according to seven criteria, summarised below in Table 3.7. The first two criteria have been chosen to assess whether they have correct conclusions and stand up to scrutiny, the last five indicate how much the conclusions or hypotheses are validated through different approaches.

Table 3.7. Paper Grading Criteria.

	Criteria
1	Peer Reviewed
2	Conclusions match with results
3	Theory supported by testing
4	Theory supported by modelling
5	Scaled test
6	Full size test
7	Real world test

Each graded paper was marked out of 7 and split into three categories: "A" papers had a score of 5/7 or higher; "B" papers had a score of 4/7; "C" papers had a score of 3/7 or below. The papers with higher grades have conclusions which are validated across a range of scales and/or modelling; this does not mean lower grade papers

have no useful conclusions but that more work is needed to assess the validity of their conclusions.

Each paper was put into a primary category and a secondary category so the knowledge gap areas could be more easily identified. The primary categories were: adhesion, leaf layer removal, isolation, damage, and application. The secondary categories were “dry particles” and “traction enhancers”. There were multiple papers which overlapped into various categories, in these cases the papers were entered separately into each category.

3.2.6.2 Outcomes

In the following schematics: “A” literature is represented in green, “B” literature is represented in yellow, and “C” literature is represented in red. The numbers represent the reference numbers of each piece of literature as presented in this thesis. The primary categories have been split into separate figures to aid clarity.

The gap analysis for literature pertaining to wheel/rail adhesion has been included in Figure 3.27. None of the literature in this category were considered “A” papers, though there were many papers within the category. All “C” papers were adjudged so, due to their lack of peer review; all these papers were from industrial literature. The fact that these are “C” papers can belie that some of these papers offer useful studies.

None of the academic literature offered studies undertaken at either a range of test scales or reinforced by modelling work. However, work by Arias-Cuevas et al. was conducted in laboratory tests [45] and field tests [43], which when taken together would form an “A” paper. This work found at both test scales, smaller sands produced greater adhesion mitigation than larger sands (see Table 3.1 for size ranges). The work undertaken by Arias-Cuevas et al. was particularly useful as the particle size ranges were consistent throughout all their projects, allowing for a quick comparison to be made between their papers. Comparing the effect of particle size between papers by different authors was made more challenging by the different particle size ranges being used by different authors, thereby complicating the ability to draw conclusions from the wider body of sanding research.

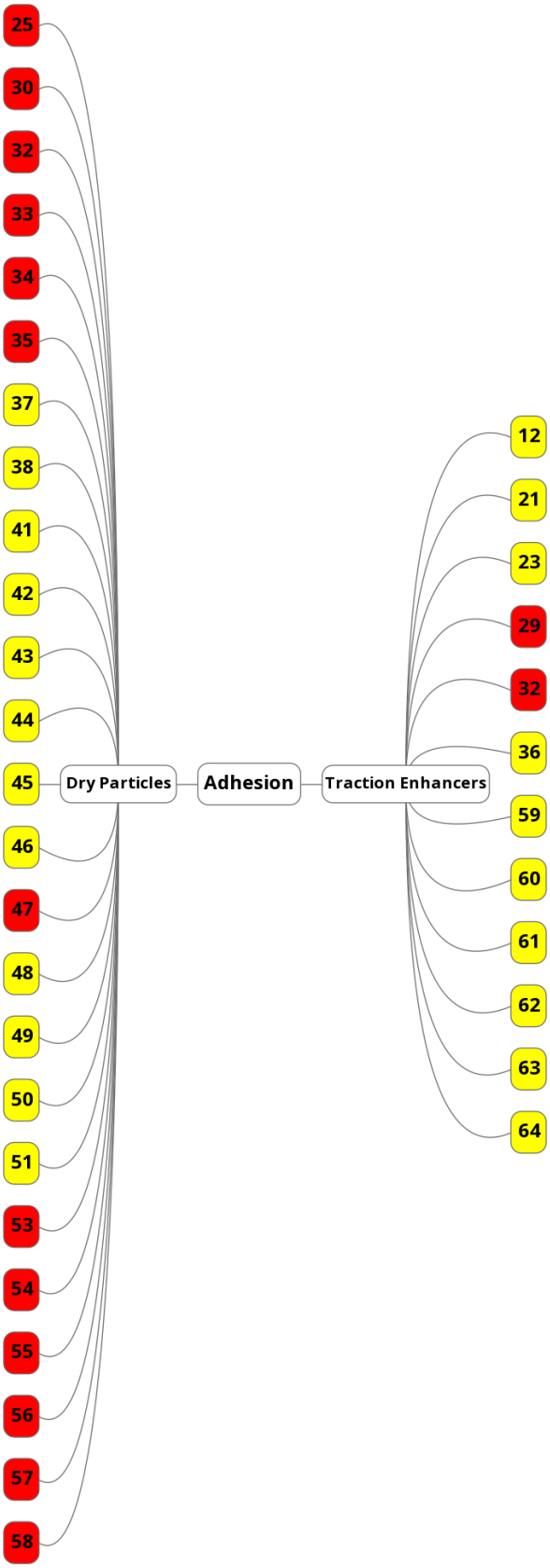

Figure 3.27. Gap Analysis of Literature Pertaining to the Effect of Particles on Adhesion within the Wheel/Rail Contact.

The gap analysis for literature pertaining to leaf layer removal has been included in Figure 3.28. As before, “C” papers are from industrial literature where a peer review process has not been undertaken, and all literature has not been performed at a variety of test scales or supported by modelling.

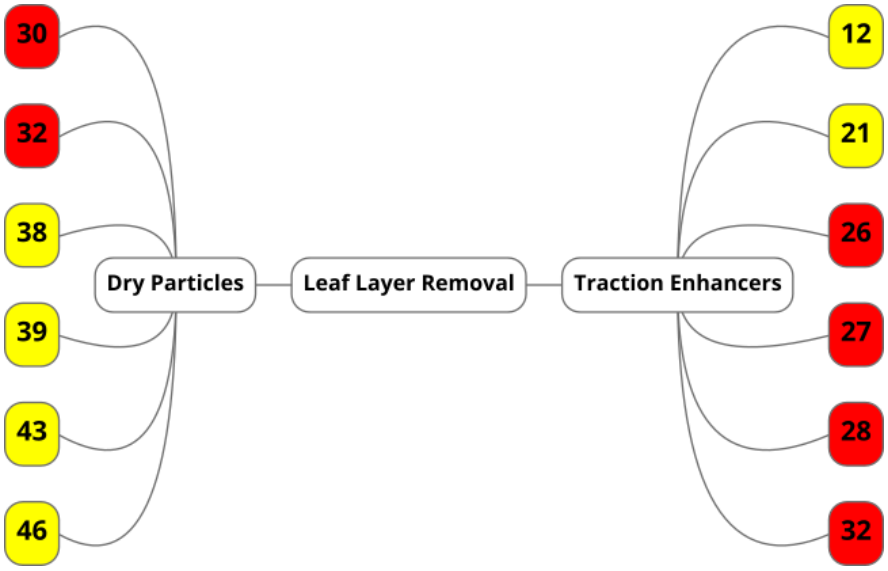

Figure 3.28. Gap Analysis of Literature Pertaining to the Effect of Particles on Leaf Layer Removal within the Wheel/Rail Contact.

The gap analysis for literature pertaining to wheel/rail isolation has been included in Figure 3.29. This gap analysis shows one paper that was adjudged to be an “A” paper; the paper by Lewis et al. [19], presents experimental, twin-disc work paired with a model estimating the likelihood of wheel/rail isolation. This work concluded that complete wheel/rail isolation was unlikely, as both discs would have to be completely separated by a contaminant third body layer.

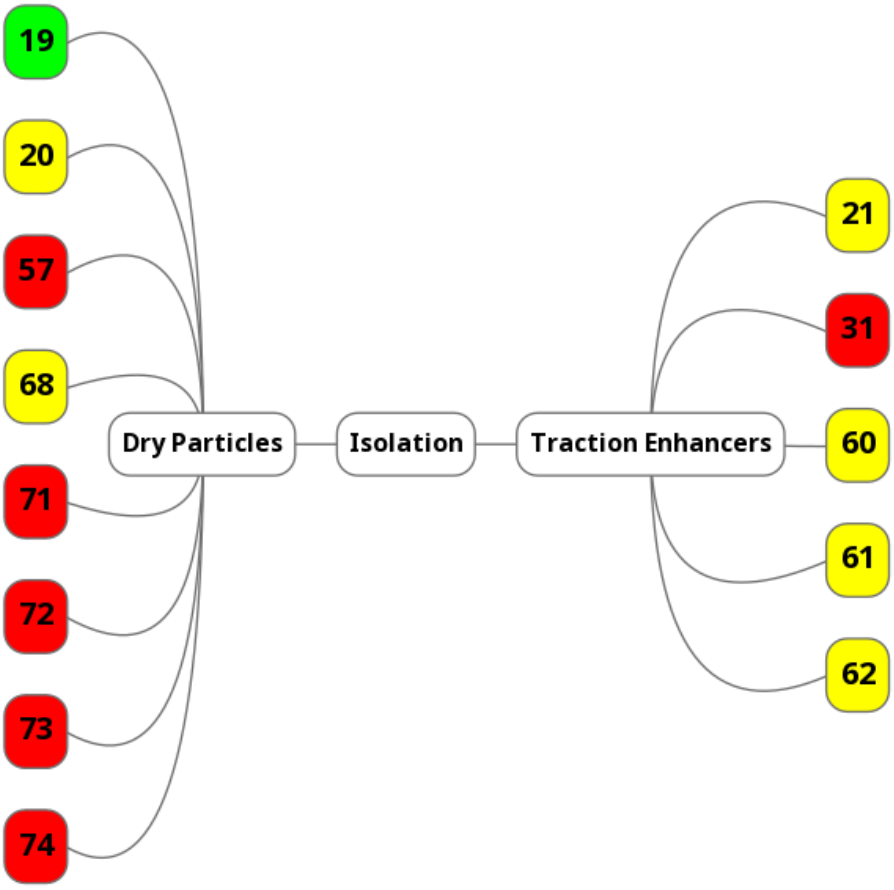

Figure 3.29. Gap Analysis of Literature Pertaining to the Effect of Particles on Isolation within the Wheel/Rail Contact.

The gap analysis for literature pertaining to wheel/rail damage has been included in Figure 3.30. The lack of "C" papers in this category is due to a lack of industrial literature, unsurprising when the majority of industrial literature comprises of field testing where it is difficult to assess damage in-situ. The three "A" papers in this category paired laboratory twin-disc tests with complementary models. In studies by Lewis & Dwyer-Joyce [22] and Grieve et al. [76], evidence of sand particles indenting into wheel material and abrading rail material was found; the latter study also observed that granite particles would agglomerate upon crushing a create a flake of applied material that would plough the surface. The third "A" paper was by Faccoli et al. [75] who predicted that surface damage occur on two different layers at different scales; a top layer with severe ratchetting and a sub-surface layer with milder ratchetting whose thickness was dependent on wheel/rail contact geometry and cyclic yield stress of the wheel/rail material.

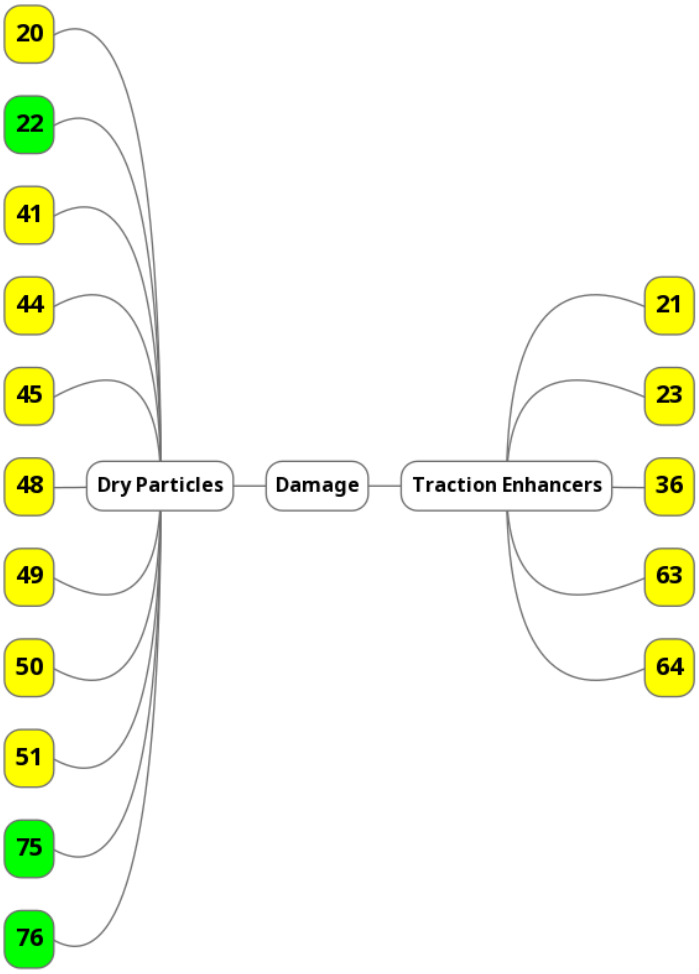

Figure 3.30. Gap Analysis of Literature Pertaining to the Effect of Particles on Damage within the Wheel/Rail Contact.

The gap analysis for literature pertaining to particle application has been included in Figure 3.31. The "A" paper, was the study carried out by Gorbunov et al. [80] assessing the effect of pre-electrifying sand particles before applying to the contact, they found that this method helped spread sand more evenly on the rail head.

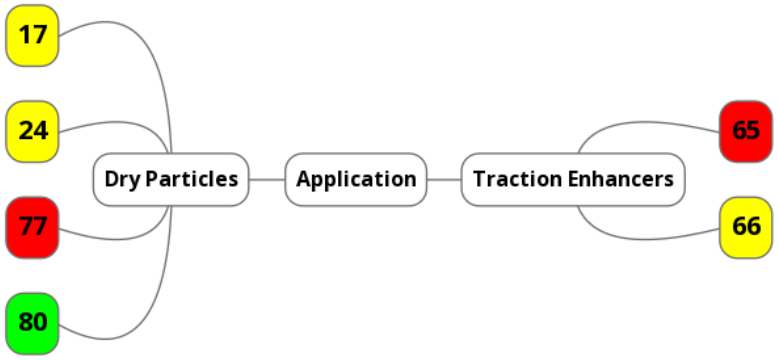

Figure 3.31. Gap Analysis of Literature Pertaining to the Application of Particles to the Wheel/Rail Contact.

3.2.7 Summary

The literature review presented in this sub-chapter has been analysed and subsequently assessed using a gap analysis method to identify knowledge gaps. Overall the results of the gap analysis seem to show that current research lacks in both quantity and breadth.

All literature found that sand (or other abrasive particles) were effective at increasing traction in low adhesion conditions and mitigating against leaf layers, but would create more surface damage. Wheel/rail isolation caused by sand seemed to be plausible, but unlikely. Most laboratory studies, found that smaller sands increased adhesion, the opposite of the current GB advice on particle size.

Particle properties have been under researched, with the exception of particle size. The influence of particle shape, toughness, and to a lesser extent hardness have either not been looked at or looked at very briefly. Related to this is the relatively small amount of research conducted on particles that are not sand.

The identified knowledge gaps can be summarised thusly:

- The effect that different particle characteristics have on the contact;
- The effect of different particles other than sand;
- A greater understanding of how sand behaves within the contact;
- A model that is able to predict the behaviour of sand within the wheel/rail contact.

3.3 Particle Characterisation Literature

3.3.1 Key Particle Properties

Work undertaken by Arias-Cuevas et al. [39] and Arias-Cuevas et al. [45], found particles between 600-1000 μm in size to have the most positive impact on low adhesion conditions when applied to the wheel/rail contact. It should be noted that larger particles generally caused more damage also.

The shape of the particle in question has shown to be an important parameter in 3rd body abrasion [13]. 3rd body abrasion can be thought of as embedded particles ploughing the surface or surfaces, thus increasing the friction between them. It can be surmised that what affects the amount of abrasive wear may also affect the traction in the wheel/rail interface. Work by Zobel [47], found evidence of harder particles generally performing better in restoring adhesion, but at the cost of increasing damage.

Lewis & Dwyer-Joyce [22], have done some work on the effect of sand in the contact, they summarised that a low crushing strength may be ideal as it would keep damage low whilst still providing adequate traction improvement, this crushing strength will be characterised by the particle's fracture toughness.

Both geometric and physical properties are an effect of the mineralogy of the particle being used. Thus, this needs to be looked at to help identify particles by their chemical composition.

How much the particle bounces off the rail will have a large effect on entrainment according to Lewis et al. [24], with lower bouncing particles being more easily entrained. This bounce measurement is referred to as the coefficient of restitution, the ratio between the velocity of the particle before and after impact.

How a particle adheres to the wheel/rail surface could be important in predicting how the presence of particles in the wheel/rail contact affect traction within the contact. For this reason, measuring particle adhesion with steel will be of interest.

This flowability is also affected by particle-particle adhesion and particle-surface adhesion. This will be very important for assessing the compatibility of a particle system with current sanding systems.

Bulk compression will also be of use when assessing how a particle system behaves as a whole. By measuring bulk compression, an idea of the stiffness of a particle system and how it does or does not rearrange within a confined space can be inferred.

These properties will be the basis of the particle characterisation framework going forward. Each selected particle will need to be characterised according to this framework with the outputs being fed into any modelling and being used as variables during tribological testing.

3.3.2 Characterisation Techniques

3.3.2.1 Mineralogy

The study of mineralogy concerns the chemical composition and crystal structure of a particle [82], more specifically, for particles that are minerals. Minerals are defined as "naturally occurring homogeneous solids with a highly ordered atomic arrangement" [83]. Understanding how mineralogy affects the properties of a particle can narrow down the list of potential mineral-type particles based on mineralogy alone.

Sand is classically defined as rock fragments with irregular shapes that have a grain size between 0.063-2 mm [84]. Particles larger than 2 mm are referred to as granules and particles smaller than 0.063 mm are called silt.

Sand particles can generally be classified into two separate types of minerals: detrital minerals and chemical minerals [85]. Detrital minerals come from the erosion and weathering of pre-existing rock, whereas chemical minerals are grown as crystals. Detrital minerals are generally harder and more durable, precisely because they have already survived erosion over a large amount of time.

Silicate is incredibly abundant in the earth's crust, making up just over a quarter of this crust [84], [86]. Silicate is most often found as quartz, which is made up of tetrahedral groups of SiO_4; these groups are linked together by a shared oxygen atom, thus giving the overall form SiO_2 [87]. In a quartz crystal these tetrahedral groups are bonded very strongly making quartz a very hard material; quartz is rated as a 7 on the Moh's scale [88].

Feldspar is another very common form of silicate. Feldspar encompasses a range of aluminium-silicate base minerals, which can be classified into sodium, potassium, calcium, iron, barium, aluminium-silicate [89]. All the types of feldspar are softer than quartz; feldspar is at 6 on the Mohs' scale [88] which is directly below quartz. This means quartz can scratch and, given enough time, erode away feldspar.

Non-silicate materials are generally weak and brittle [90]. These minerals usually only exist outside harsh environments and most are soluble in water [84].

Two common methods for studying the mineralogy of naturally occurring particles are: polarising microscopy and X-ray diffraction [84]. Polarising microscopy

requires an expert geologist to understand what different features may represent in terms of mineral identification, therefore this method is clearly implausible for general engineering work.

X-ray diffraction measures the interatomic spacing of the crystalline lattice by transmitting X-rays at the sample at a range of angles and plotting the angle against the reflected intensity of the wave [91]. Different minerals have different lattice spacing, therefore possesses different intensity peak locations. X-ray diffraction has been shown to be the best tool for mineral identification and quantification as it allows a detailed analysis of the crystal structure as well as the mineral's chemical makeup [92].

3.3.2.2 Particle Morphology

3.3.2.2.1 Particle Size

Particle size has already been shown to be an important factor in wheel/rail adhesion, damage, and isolation [22], [39]. There are many different measures of particle size as it is hard to characterise a complex 3D object using a single value. Sieving, image analysis techniques and laser diffraction will all measure slightly different dimensions therefore it is hard to compare one measurement technique against another. Usually particle dimensions are reported in terms of their median size, 10^{th} percentile size, 90^{th} percentile size, and their uniformity coefficient (UC). The latter is calculated using Equation 3.1 where D_x denotes the xth percentile of particle size.

$$UC = \frac{D_{60}}{D_{10}}$$

Equation 3.1

Particle sizes can be measured using either mechanical, imaging or diffraction methods.

Mechanical methods employ a system of sieves to sort the particles into size bands, down to a minimum size of 63 μm. ASTM C136 [93], combines this sieve system with a mechanical shaker to ensure particles are able to get through openings that are large enough them. The weight of the sand in each sieve is measured and compared to the total weight to get a size distribution. This method may not be precise, as it is dependent on the number of sieves, and the particle only needs to be small enough in one dimension to fit through the aperture, giving slightly inaccurate results. The advantages to sieve analysis are that it is quick, simple, and sorts the particles into size categories for later testing.

Image analysis does not have the disadvantages of sieve analysis as it can be done very precisely and with good accuracy [94] and this method can also be used to measure particle shape thus saving some time. Image analysis also make allowances for particle clusters [95], thus improving accuracy even more compared to sieve analysis.

Laser diffraction is a common particle size analysis technique, as it promises excellent precision compared to sieving. However, work done by Blott et al. [96] suggests that diffraction measurement is dependent on particle shape, thus it has the potential to create more inaccurate results than sieve or image analysis.

3.3.2.2.2 Particle Shape

The shape of the particle in question has shown to be an important parameter in 3rd body abrasion [13]. 3rd body abrasion can be thought of as embedded particles ploughing the surface or surfaces, thus increasing the friction between them. It can be surmised that what affects the amount of abrasive wear will also affect the traction in the wheel/rail interface.

Krumbein and Sloss [97], have proposed a visual inspection regime that compares test samples with particles of known form and roundness. Whilst this may seem crude, the operator variability has been shown to be less than the variability associated with the particle shape [98], hence it should have no effect on the average particle form calculated. This chart can be seen below in Figure 3.32, and uses the Wadell's definitions of sphericity and Krumbein roundness [99] parameters.

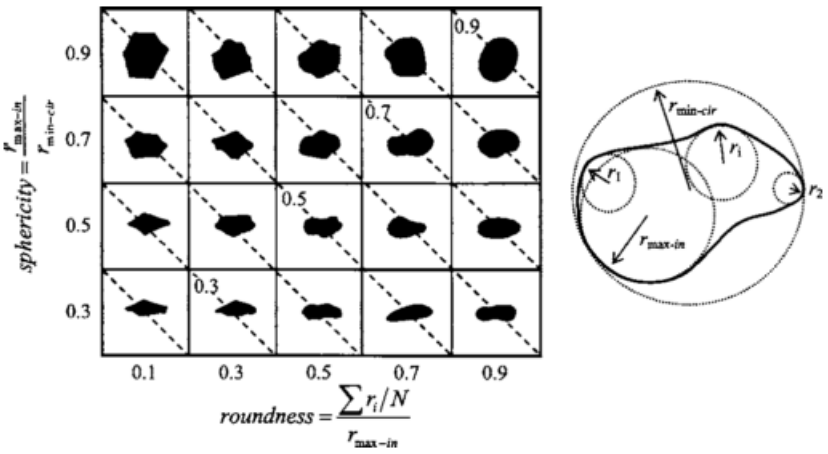

Figure 3.32. Krumbein/Sloss Visual Inspection Chart Taken from Cho et.al [98]**.**

Particle form can also be analysed using computational methods. The shape analysis would comprise of measuring the short, medium and long orthogonal axes of a 2D projection of the particle. Krumbein's intercept sphericity, Ψ, [100], adapted Wadell's sphericity to improve measurability:

$$\Psi = \sqrt[3]{\frac{I \cdot S}{L^2}}$$

Equation 3.2

where *S*, *I* & *L* are the small, intermediate and large orthogonal axes respectively. This measure also has the advantage of being directly measured using mechanical methods, such as ASTM D4791, which uses sieves to measure the relevant lengths [101].

The roundness would have to be measured using image analysis, either using the chart above or with computational methods. Stachowiak [102], proposes a measure that only takes into account the large protruding corners of a particle, called "spike parameter quadratic-fit". This method finds the average centre, x_{bar}, y_{bar}, and radius, r_{bar}, of the particle and measures the angles of the spikes, θ, protruding outside of this circle, a visualisation of this can be seen in Figure 3.33.

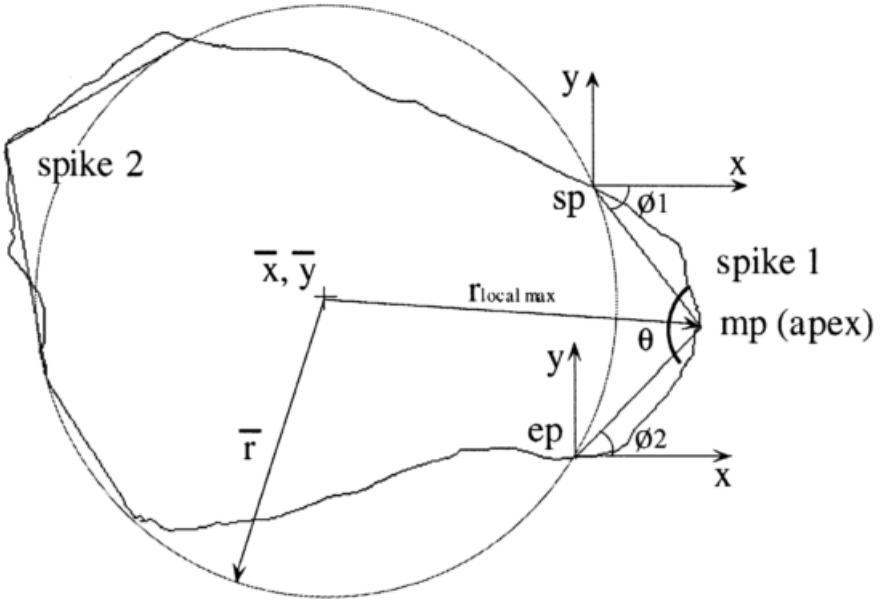

Figure 3.33. Visualisation of SPQ Method [102].

The SPQ factor is the average spike value ($sv_{average}$), where spike value is solely a function of the spike angle:

$$sv = \cos\left(\frac{\theta}{2}\right)$$

Equation 3.3

Overall, the shape parameters of interest here are:

- Major axis; a line passing through the centre of mass with an orientation corresponding to the minimum rotational energy [103];

- Minor axis; a line through the centre of mass that is 90° to the major axis;
- Length; all the points on the perimeter of the shape are projected onto the major axis, the maximum distance between any two points is the length;
- Width; same as length but the points are projected onto the minor axis;
- Aspect Ratio; the ratio between width and length;
- Circle Equivalent Diameter; the diameter of a circle with the same area of that of the measured particle;
- High Sensitivity Circularity; Defined by Equation 3.4, where A is the particle area and P is the particle perimeter. Examples of particles of different circularity are included in Figure 3.34.

$$HS\ Circularity = \frac{4\pi A}{P^2}$$

Equation 3.4

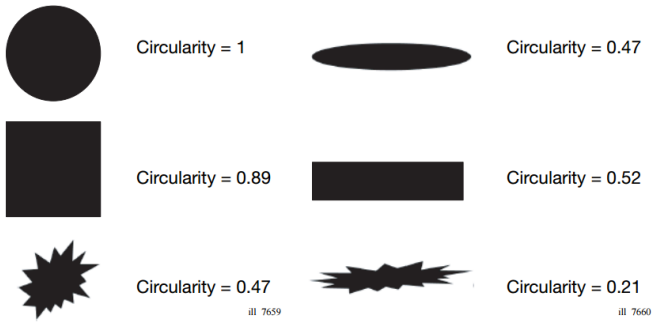

Figure 3.34. Examples of Particles with Different Circularities [103].

- Convexity; found by dividing the complex hull perimeter of the particle by the particle's actual perimeter [103]. The complex hull perimeter can be imagined as the perimeter of an elastic band placed around the particle. Examples of convexity are shown in Figure 3.35.

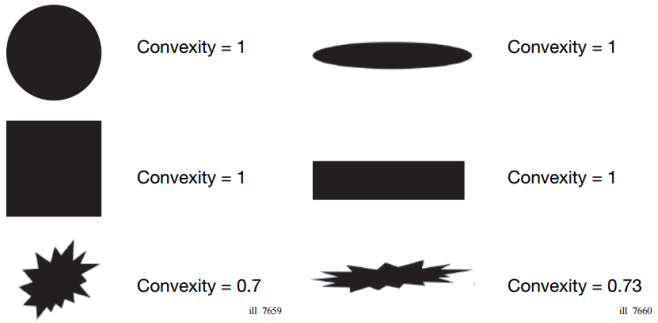

Figure 3.35. Examples of Particles with Different Convexities [103].

3.3.2.3 Physical Properties

3.3.2.3.1 Single Particle Crushing Strength

The crushing strength of a particle will determine how the particle is entrained into the contact upon crushing, and may even effect its ability mitigate against low adhesion. Ultimately, the crushing strength will be most dependent on the number of defects in the particle.

The crushing strength can be estimated using a 1 dimensional crushing test, between either: two flat platens, or a rail segment and a wheel segment to simulate more realistic conditions. Jaeger [104] has previously quantified the crushing strength (σ_{SP}) of a single particle using:

$$\sigma_{SP} = \frac{F}{d^2}$$

Equation 3.5

where F is the force at failure and d is the initial distance between the compacting surfaces. This method does assume that the particle is a sphere, which is not entirely valid, so care should be taken to try and test particles with similar shape throughout the test to eliminate this unwanted variable.

McDowell [105], went on to define a probabilistic model of a particles survival based on a given load:

$$P_{SC} = \frac{number\ of\ particles\ crushing\ at\ \sigma_{SP} \geq \sigma_C}{total\ number\ of\ particles\ tested}$$

Equation 3.6

where P_{SC} is the probability of survival at a given crushing strength, σ_C. This method analysing the data allows survival probability curves to be generated that may be more useful in analysing the data than one single average value due to the large amount of variance for each sample.

3.3.2.3.2 Particle Hardness & Fracture Toughness

Particle hardness is an important parameter as it affects the crushing strength of the particle which in turn will affect the wear and adhesion increase in the wheel/rail contact [13]. Generally, sand is hard enough to cause abrasive wear on a martensitic surface [13], such as that of the rail, however the load is so large the particle will almost certainly be crushed at some point in the contact.

Whilst Hutchings [13], suggests hardness can be derived from the yield strength of the particle this is fairly impractical to accurately measure. All previous work on the

hardness of individual sand particles has used nanoindentation techniques to derive hardness, as well as other properties [106], [107].

Nano-indentation can potentially give values for the particle's hardness, Young's modulus, and fracture toughness [108]. Though from operator experience the indentation force from the nano-indenter may not be sufficient to measure fracture toughness for hard particles such as those being measured in this report. Therefore, a micro-indenter may be used in conjunction with the nano-indenter to give a full range of properties.

Nanoindentation techniques plot load displacement data on a graph, and derive the hardness, *H*, using:

$$H = \frac{P_{max}}{A}$$

Equation 3.7

where *P* is the applied load and *A* is the contact area of the indenter on the particle. This can be either a maximum or continuous measurement. Results have been accurate when measuring the hardness of single particles [106].

Yield strength can then be found using the Oliver-Pharr method where reduced Young's modulus, E_r, can be calculated from:

$$\frac{dP}{dh} = \frac{2}{\sqrt{\pi}} E_r \sqrt{A}$$

Equation 3.8

where h is the elastic displacement of the indenter. The reduced Young's modulus can then be fed into:

$$\frac{1}{E_r} = \frac{(1-\nu^2)}{E} + \frac{(1-\nu_i^2)}{E_i}$$

Equation 3.9

where the Young's modulus of the indenter, E_i, the samples poissons ratio, ν, and the indenters poissons ratio, ν_i, can all be found from literature. Fracture toughness can be found by inducing cracks at the corners of the indent and then analysing these cracks using methods outlined by Sebastiani et al. [109].

3.3.2.4 Coefficient of Restitution

The coefficient of restitution (CoR) is a measure of the energy lost when one body collides with another, it can be expressed as:

$$CoR = \frac{Velocity\ After\ Collision}{Velocity\ Before\ Collision}$$

Equation 3.10

Previous work undertaken by Lewis et al. [24] has found evidence to suggest particles with a low coefficient of restitution (i.e. particles that keep low) tend be more easily entrained into the contact as it is more likely to enter into the nip (see Figure 3.36), therefore CoR is of import when considering sanding efficiency. The coefficient of restitution is usually measured by the use of a high speed camera system [110], [111].

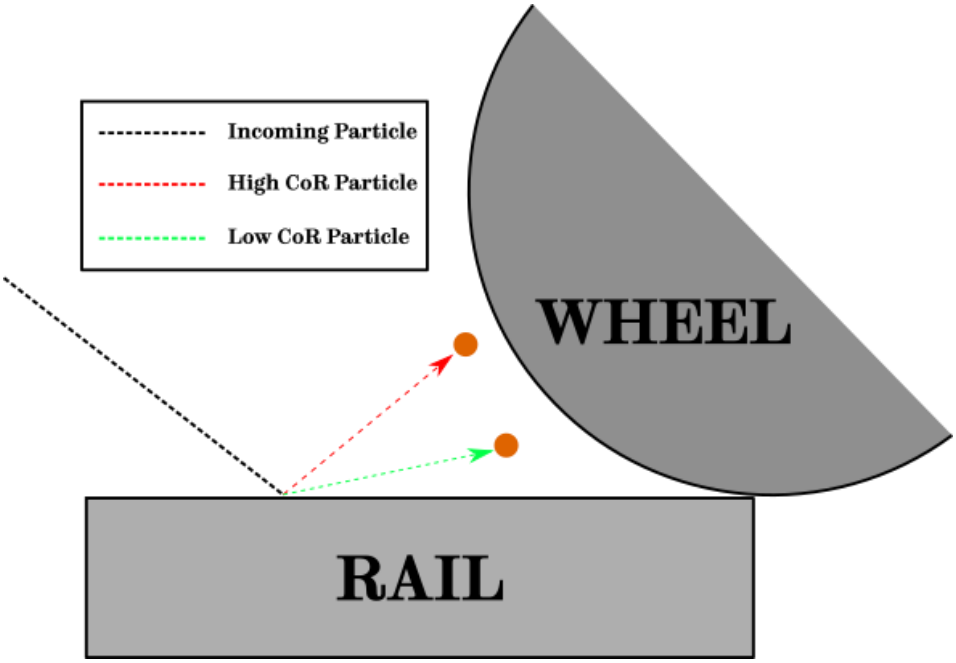

Figure 3.36. Effect of Coefficient of Restitution on Particle Behaviour.

3.3.2.5 Particle Adhesion

Particle adhesion measures the interface energy between it and a surface. According to Krupp [112], the dominant forces in adhesion are the Van der Waals force and the electrostatic force.

Krupp describes the particle adhesion steps thusly:

- The particle and the surface come into contact at one point and an atomic bond is formed;
- The long range attractive forces, as well as any outside forces, cause several more contact points to form;
- As the contact area increases as more bonds are formed up to the point at which the attractive forces and the internal forces resisting deformation are at equilibrium.

The capillary force, or meniscus force [113], can also be significant in humid conditions. The meniscus can either form: from vapour condensing in the small gap between the particle and the surface, or from a thin fluid layer present on the surface being drawn into the gap. The first mechanism is only applicable to lyophilic surfaces and volatile fluids.

There are several ways of measuring particle adhesion to a surface, some more applicable than others. These methods include:

- Atomic Force Microscopy [114], [115]; though it is both expensive and time consuming and heavily dependent on the local geometry of a single particle;
- Centrifugal techniques [116], [117]; the particles adhesion is related to the rotational energy needed to detach them. The equipment is costly and this method can also be time consuming but the technique is well defined;
- Electric field detachment methods [117]; particles adhesion energies are equated to the electric field energy needed to displace them. It can only be used on electrically conductive particles;
- Aerodynamic detachment methods [118]; the particle is subjected to air flow in a tube and the drag force on the particle from the air is compared to the adhesion force of the particle. However, the close proximity of one particle to another can affect the air flow and particle collisions also decrease result accuracy;
- Vibration methods [115], [119]; A sinusoidal signal is set up in the wall which causes the particle to undergo alternating detachment and compression forces, these are then related to the adhesion force. The vibration can cause the particle to flatten, resulting in an increased adhesion measurements [120];
- Drop test [114]; The particles are mounted onto a substrate that is dropped from a height to impact onto a stopper, causing the adhered particles to undergo a tensile force which is then equated to the adhesive force. The method is relatively quick and inexpensive, though not widely used due to its novelty.

3.3.2.6 Angle of Repose

Flowability is a measure of a granular material's ability to flow [121], in the context of the sanding mechanism it is an important parameter for the transportation of the sand from the hopper and through the hose. A simple, cost efficient way of measuring the flowability of a material is to measure it's angle of repose [122], the steepest angle at which the slope of the bulk material is stable. The angle of repose can be measured a number of ways from simple methods (tilting box, revolving cylinder) to more complex methods (fixed funnel, hollow cylinder) [122], [123].

3.3.2.7 Bulk Compression

Information on the bulk behaviour of a particle system can be obtained using confined compression tests, that can measure the stiffness of a particle system; this test method has previously been analysed by Hassanpour & Ghadiri [124]. This information can provide knowledge on how a particle system will settle within a hopper e.g. the amount of particle rearrangement.

3.3.3 Summary

In this sub-chapter, key particle characteristics were identified from the sanding literature review in sub-chapter 3.2. The literature surrounding effective measurement methods for analysing these characteristics was discussed and from this literature test methods will be assessed in sub-chapter 4.1.2 to create an effective particle characterisation framework for assessing prospective particles for use in the sanding process.

3.4 Modelling Literature

Various modelling approaches to understanding the effect of low adhesion have previously been proposed. This section briefly examines a few of these approaches and analyses their applicability to model low adhesion contacts with traction restoring particles.

In the FASTSIM approach [125] the elastic half space is modelled as a bed of springs where the tangential surface displacement of said springs is proportional to the traction in the contact. The stiffness of the springs is such that tangential forces calculated with FASTSIM equal that of half space theory. Third body layers are taken into account by adjusting the stiffness of the springs.

The Polach model [126] is based on FASTSIM but can describe changes in the initial slope of the traction curve as well as decreasing traction with high slips. It is more computationally efficient than FASTSIM also.

The Tomberger model [127] uses an interfacial fluid model, temperature model, and micro-contact model alongside FASTSIM to give a better representation of the effect of fluid in the wheel/rail contact.

A model predicting sub-surface stresses in the presence of sand particles was developed by Mazzù & Battini [128], included in a study by Faccoli et al. [75], has been partly used to predict friction behaviour. There model did not take particle crushing into effect, so it does not seem particularly relevant and the simulated values of

friction seem very low (<0.3) when compared to typical values of dry, sanded contacts from experimental work.

The extended creep force (ECF) model was first proposed by Meierhofer [18], the core of the model was the assumption that the contact could be modelled as a homogeneous and isotropic 3rd body layer with temperature and normal load dependent elasto-plastic behaviour. This 3rd body layer includes actual 3rd body contaminants (sand, wear debris, leaves, etc.) and the top layers for both wheel and rail that undergo tribological plasticity as described by Six et al. [129]. This simulated 3rd body layer is assumed to act elastic-plastically, whereas the surrounding wheel and rail material are assumed to act elastically. The 3rd body layer is described by Voce's hardening law [130], with the parameters of the model comprising of a temperature and pressure dependency. Lastly, the 3rd body layer can be amended to a brush type model allowing prediction of creep curves.

The ECF model can be seen as the most appropriate for modelling the influence of particles in the contact as it can accurately describe the effect of solid third body layers and can model complex traction characteristics. It is also more accurate for describing creep curve behaviour at higher creep rates, with traction predicted to fall due to temperature effects. The temperature dependency will be parameterised from previous field tests run at high creep rates, pressure dependency can be parameterised by high pressure torsion testing conducted at three different normal pressures.

3.5 Summary

In this chapter, three areas of literature were reviewed. The sanding literature review found knowledge gaps associated with the lack of understanding as to how particle characteristics affected their performance in the wheel/rail contact, and highlighted a lack of validation of results from using different test scales and models.

The particle characterisation literature review identified key particle characteristics and assessed the most viable techniques for measuring these characteristics, creating a particle characterisation framework.

Lastly, the modelling literature review discussed different modelling approaches for predicting traction behaviour in the wheel/rail contact. The extended creep-force model was identified as the most suitable model for this work, due to its accuracy and ability to be parameterised by high pressure torsion testing.

4 PARTICLE CHARACTERISATION

4.1 Introduction

The following chapter details the particle characterisation testing undertaken as part of this thesis. Each sub-chapter will concern different particle characteristics and will include the methodology for measuring said characteristic and the results of these measurements for each particle type. A discussion sub-chapter will assess what findings can be taken from the characterisation method. The results obtained from this chapter will go on to inform discussion in later chapters.

For all appropriate tests a representative sample of particles was produced using a chute splitter (as outlined in ASTM C702 [131]) which reduces the maximum error due to variations in the sand particles to <5% [132].

4.1.1 Aims & Objectives

The primary aim of the work discussed in this chapter was to characterise a group of particles with wide ranging properties to use for comparing each particles' effect in tribological tests. A secondary aim is to create a framework that can be used for assessing future prospective particles for use in the rail industry.

The objectives for completing these aims include:

- Defining a particle characterisation framework based on the review of literature included in sub-chapter 3.3;
- Selecting particles for testing, where attention was paid to ensure a range of particle characteristics and industry products were included;
- Conducting particle characterisation measurements.

4.1.2 Particle Characterisation Framework

The test methods discussed in the sub-chapter 3.3 were assessed to find their suitability for the measurement of particles in the wheel/rail contact. The summary of the comparison is included in Table 4.1, with the methods highlighted in green being methods that will be used going forward. The methods were assessed according to the criteria included in Table 4.1, the judgement was subjective due to the uniqueness of the framework. In the mechanical properties section two indentation methods will be carried on as their findings can be used to complement one another. For the size analysis sieving will be used alongside the best method, image analysis, as it is simple and quick to run and can help validate image analysis results.

Table 4.1. Test Method Comparison

Particle Property	Test Method	Criteria						Score
		Cost Effective	Time Effective	Accessible	Simple	Realistic	Accurate	
Mineralogy	Polarising Microscopy	Yes	No	Yes	No	No	No	2
	X-ray Diffraction	Yes	Yes	Yes	No	Yes	Yes	5
Size	Sieve Analysis	Yes	Yes	Yes	Yes	Yes	No	5
	Image Analysis	Yes	Yes	Yes	Yes	Yes	Yes	6
	Laser Diffraction	Yes	Yes	Yes	Yes	No	No	4
Shape	Krumbein Chart Comparison	Yes	No	Yes	Yes	No	No	3
	Image Analysis	Yes	Yes	Yes	Yes	Yes	Yes	6
Mechanical Properties	Single Particle Crushing	Yes	No	Yes	Yes	No	Yes	4
	Nanoindentation	Yes	Yes	Yes	Yes	Yes	Yes	6
	Microindentation	Yes	Yes	Yes	Yes	Yes	Yes	6
Coefficient of Restitution	High Speed Camera	Yes	No	Yes	Yes	Yes	No	4
Adhesion	Atomic Force Microscopy	Yes	Yes	Yes	No	No	Yes	4
	Centrifuge	Yes	Yes	No	Yes	Yes	Yes	5
	Electric Field Detachment	Yes	Yes	No	Yes	No	Yes	4
	Aerodynamic Detachment	Yes	Yes	No	Yes	No	Yes	4
	Vibration	Yes	Yes	No	Yes	No	Yes	4
	Drop Test	Yes	Yes	Yes	Yes	Yes	Yes	6
Angle of Repose	Funnel Method	Yes	No	Yes	No	Yes	Yes	4
	Dynamic Test	No	Yes	No	No	No	Yes	2
	Vibrating Funnel	Yes	Yes	Yes	Yes	No	Yes	5
Bulk Compression	Confined Compression	Yes	Yes	Yes	Yes	No	Yes	5

4.1.3 List of Particles

Particles were sourced from multiple areas: some particles were taken directly from the railway industry, some for their abrasive properties, and some for providing an extreme point of difference from typical abrasive particles i.e. lubricating particles. The list of particles that were tested included:

- Various rail sands:
    - British rail sand from Leighton Buzzard (LB);
    - Central European rail sand (CE);
    - Derbyshire sand previously used in sanding tests (DY);
    - Austrian rail sand (AT);
    - Finnish rail sand (FI);
    - Lithuanian rail sand (LT);
    - Californian rail sand (CA);
    - Illinoisan rail sand (IL);
    - Japanese rail sand, no longer in use (JPD);
    - Japanese rail sand, currently in use (JPA);
- Other particles:
    - Rubber crumb (AC);
    - Aluminium oxide (AL);
    - Diatomaceous earth (DE);
    - Natural abrasive (NA);
    - Steel (NSS);
    - Zeolite (ZL);
- Soda lime glass beads:
    - Large glass beads, 1.75-2 mm (GBL);
    - Medium glass beads, 0.75-1 mm (GBM);
    - Small glass beads, 0.2-0.4 mm (GBS);
    - Crushed glass beads (GBC).

These particles will be characterised in the rest of this chapter, thereby providing more detailed information on the particles.

4.2 Mineralogy: X-Ray Diffraction

4.2.1 Methodology

XRD measurements of each particle type were used to find the major constituent mineral phases. The measurements were performed using a Siemens D5000 and were scanned using Cu Kα1 radiation between slit angles of 5-80°. The data was then

assessed using ICDD PDF-4+ software to identify and match characteristic peaks to elements in the software's database.

XRD was not appropriate for all particles and some particles came with chemical consist data as part of their respective technical data sheets, so XRD has not been performed on all particles exhaustively.

4.2.2 Results

The XRD results for all tested rail sands has been included in Figure 4.1, where the intensity peaks have been normalised against each sand's respective maximum intensity to aid clarity and comparison. The largest peak for each mineral phase is labelled for each rail sand. The majority of the rail sands have a strong peak at roughly 25°, indicating a quartz phase; as both British and German standards have a requirement that the sand be mostly silicate based (see chapter 2.5.1) this is to be expected. Several rail sands also have other mineral phases present: AT, FI, CA, and JPA; all other mineral phases were silicate based and in the case of JPA it differs from all other rail sand by not having a peak indicating pure silica, but two identified mineral phases that are silicate based. In the case of CA, its non-quartz phase appears to be relatively minimal compared to other non-pure quartz sands.

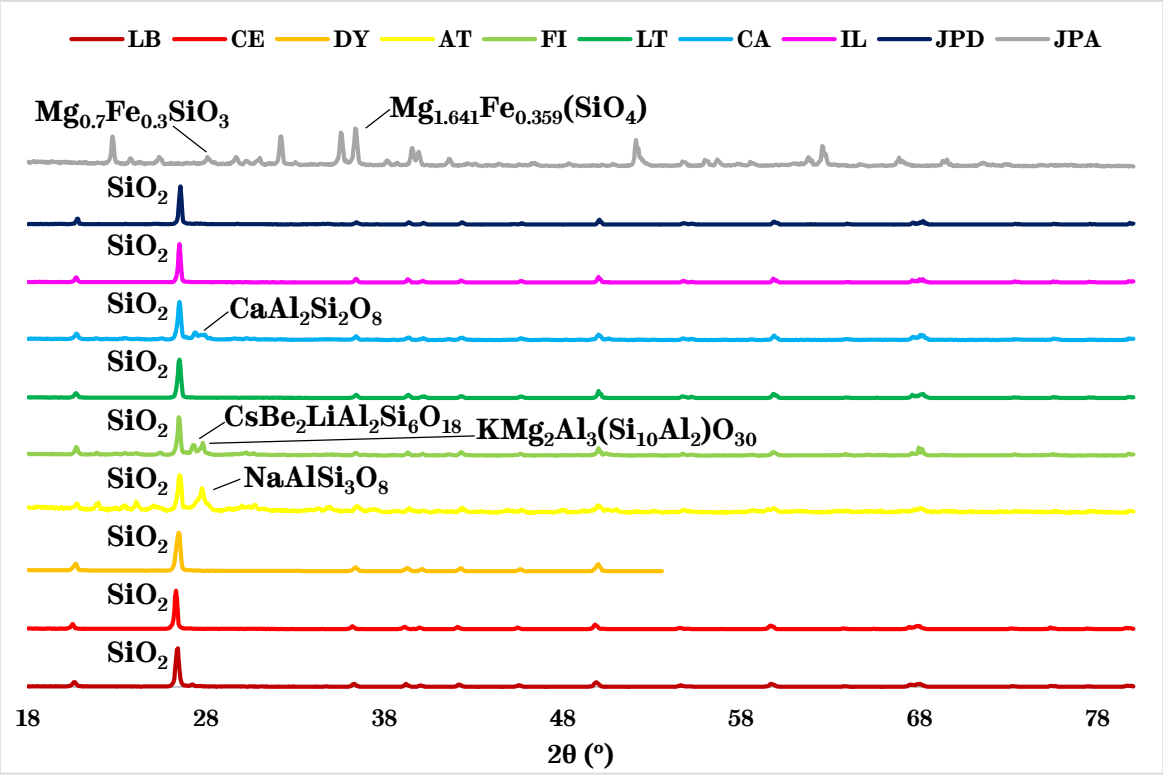

Figure 4.1. XRD Analysis of Rail Sands.

Out of the non-rail sand materials, AC and NSS were not suitable for XRD analysis and DE, NA, and ZL came with data sheets detailing their chemical content. This

leaves AL, the XRD data for which is included in Figure 4.2. The peaks characterised AL as pure alumina.

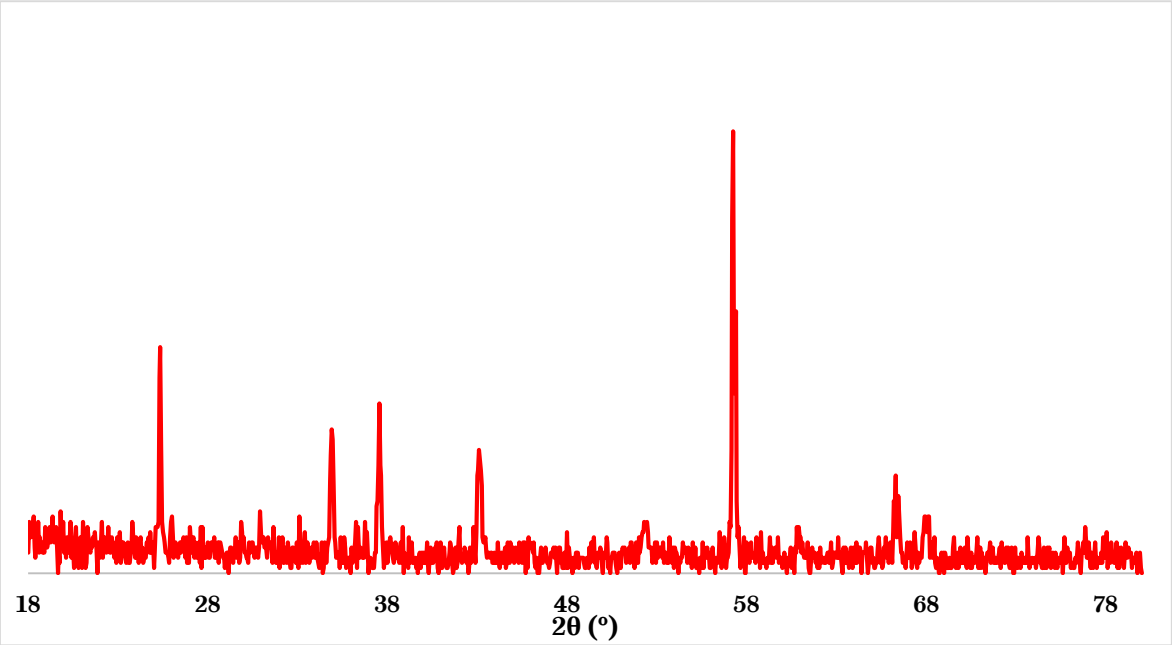

Figure 4.2. XRD Analysis of AL.

Other particles that came with necessary information on data sheets include:

- *AC;* recycled tyre tread;
- *DE;* calcined natural diatomaceous earth (silicium dioxide) with up to 1% crystalline silica;
- *GB;* soda lime glass with 70% quartz (SiO_2), 10% sodium oxide (Na_2O), 5% calcium oxide (CaO), 5% Potassium oxide (K_2O), 5% Barium oxide (BaO), and 5% of other material;
- *NA;* Juglans Regia shell powder, Prunus Armeniaca seed powder, and Prunus Amygdalus Dulcis shell powder;
- *NSS;* EN8D mid-carbon steel;
- *ZL;* calcium potassium sodium aluminosilicate ($(CaK_2Na_2Mg)_4Al_8Si_{40}O_{96}.24H_2O$).

4.3 Particle Size: Sieve Analysis

4.3.1 Methodology

Sieving was carried out to assess particle size distribution as it is a simple, cost effective way of comparing different sand samples, the method used for sieving follows the method for sieving fine grained soils set out in BS1377-2:1990 [133]. The sieve apertures ranged from 2 mm to 63 µm. All the sieves were placed, in order from largest to smallest, onto a sieve shaker for 20 minutes to ensure the sand had

been adequately sieved. A minimum of sample size of 100g was sieved for each particle type.

4.3.2 Results

4.3.2.1 Rail Sand Comparisons

Figure 4.3 includes the sieve analysis of rail sands sourced from international industrial sources. There is a spread in the different sizes of rail sands being used, with some interesting geographical trends; sands from Austria and Germany, from California and Illinois, and two different Japanese sands are fairly close in size.

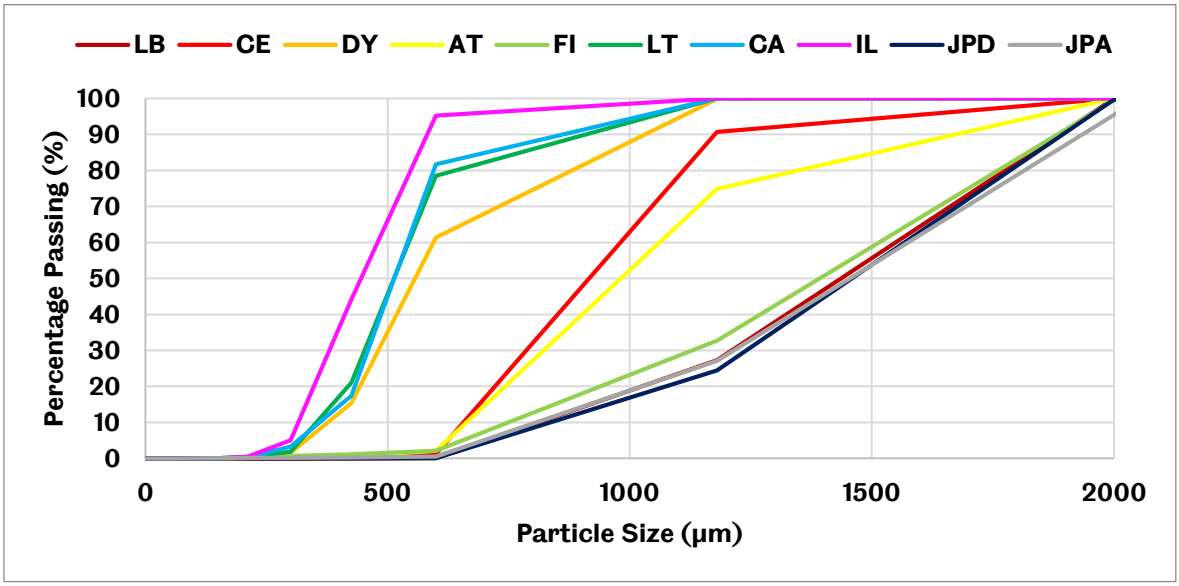

Figure 4.3. Sieve Analysis of Rail Sands.

Table 4.2 includes the measure of each rail sands 10th, 50th, and 90th percentile size (D_{10}, D_{50}, and D_{90} respectively), as well as their uniformity coefficients (UC). As could be seen visually in Figure 4.3, there is a spread in measured size across the different rail sands; D_{50} ranged from ~0.5 mm up to ~1.5 mm. UC tends to be between 1.5-2 for the rail sands.

Table 4.2. Sieve Analysis of Rail Sands.

	LB	CE	DY	AT	LT	FI	CA	IL	JPD	JPA
D_{10} (µm)	811	657	376	663	353	750	359	316	837	807
D_{50} (µm)	1437	916	557	982	513	1393	514	445	1459	1455
D_{90} (µm)	1888	1175	1032	1674	910	1883	863	582	1894	1935
UC	1.91	1.49	1.58	1.60	1.54	2.02	1.50	1.52	1.87	1.95

4.3.2.2 Other Particles

Whilst is not useful to compare the remaining non rail sand particles, as their sources and characteristics are plainly different, all results have been included together to aid clarity. From Figure 4.4, it can been seen that there is a similar spread in size to the rail sands, this is partly a deliberate attempt on the part of the author to allow easier comparison with rail sands based on the intrinsic properties of the different particles being used.

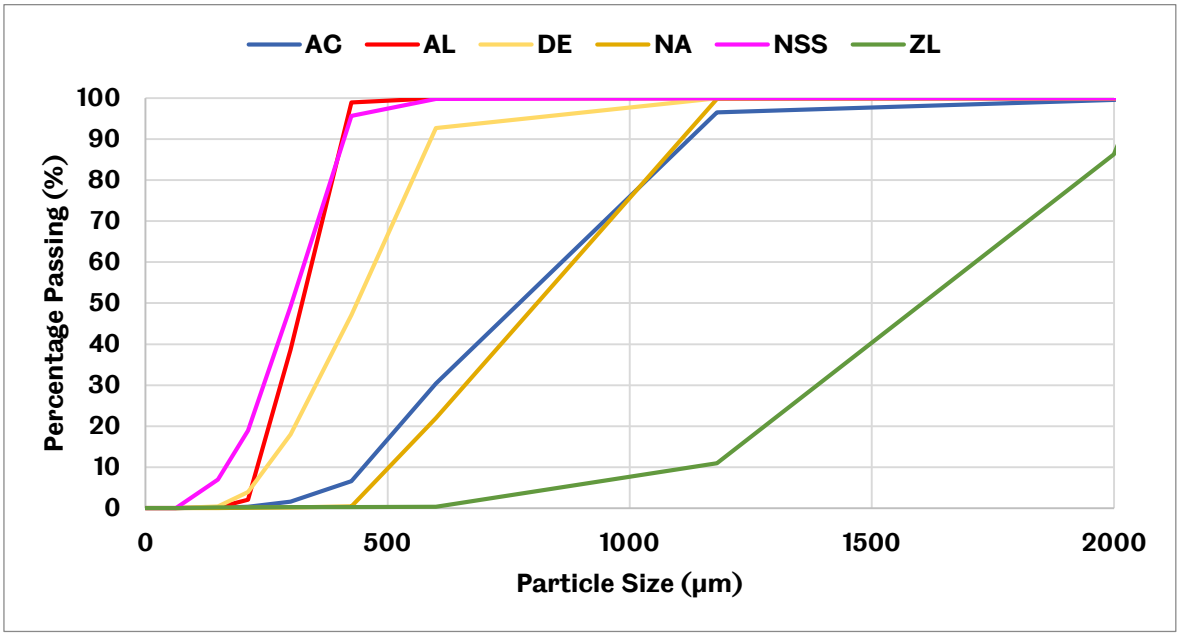

Figure 4.4. Sieve Analysis of Other Particles.

Table 4.3 includes detailed sieve size data on the other particles. Some particles such as AL, DE, and NSS are slightly smaller than the lower limit of the rail sands, being less than <0.5 mm. ZL was slightly larger than all rail sands, at 1.6 mm in size. Measured uniformity coefficients are all similar to rail sands, all being between 1.5-2.

Table 4.3. Sieve Analysis of Other Particles.

	AC	AL	DE	NA	NSS	ZL
D_{10} (µm)	450	231	250	503	166	1128
D_{50} (µm)	772	323	436	809	302	1605
D_{90} (µm)	1123	406	590	1107	410	2135
UC	1.91	1.49	1.90	1.76	1.98	1.52

4.4 Particle Size & Shape: Image Analysis

4.4.1 Methodology

The image analysis was carried out using the Morphologi G3S. The sand being tested was dispersed onto a sample plate using high pressures to separate particles and the image analysis machine scanned the area that particles were dispersed over. The images were subsequently binarised which allowed measurements to be taken of each individual particle. The circle equivalent diameter has been used in this study to characterise sand size. The circular equivalent diameter is the diameter of a circle with the same area as the measured particle.

In addition to particle size, particle shape measurements were taken from the image analysis as well. The measurements taken included:

- *Circularity;* the ratio between the perimeter of a circle of equivalent area to the particle and the actual perimeter of the particle. Circularity can take a value between 0-1 with 1 denoting a perfectly circular particle;
- *Convexity;* the ratio between the convex hull perimeter of the particle shape and its actual perimeter. The convex hull can be thought of as the shape an elastic band would take if put onto the 2D particle shape [134]. Convexity can take a value between 0-1 with 1 denoting a perfectly non-convex particle.

4.4.2 Results

4.4.2.1 Size Analysis

4.4.2.1.1 Rail Sands

The circle equivalent diameter measurements of tested rail sands are included in Figure 4.5. This size measurement compares well to sieving, though it appears the largest sands are measured at slightly more than 1.5 mm, compared to sieving which had this as an upper limit. The relative size order of the sands has remained broadly the same using image analysis compared to sieving.

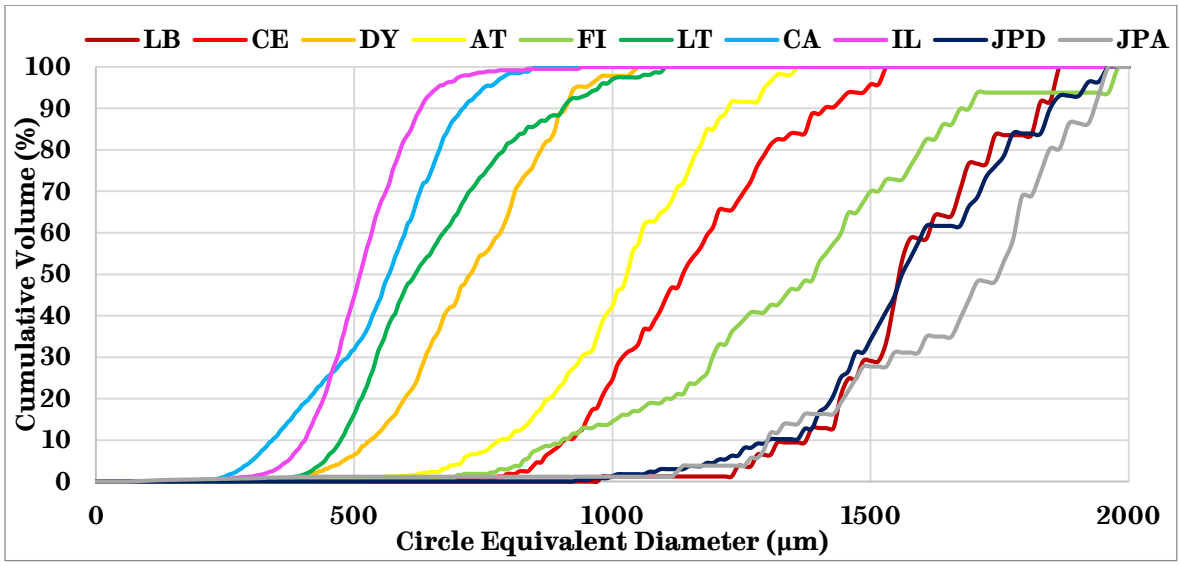

Figure 4.5. Circle Equivalent Diameter of All Rail Sands.

4.4.2.1.2 Other Particles

The circle equivalent diameter measurements for all other particles aside from rail sand are included in Figure 4.6. Results were relatively similar to sieving results, with a range of sizes and size distributions being observed between the disparate particles.

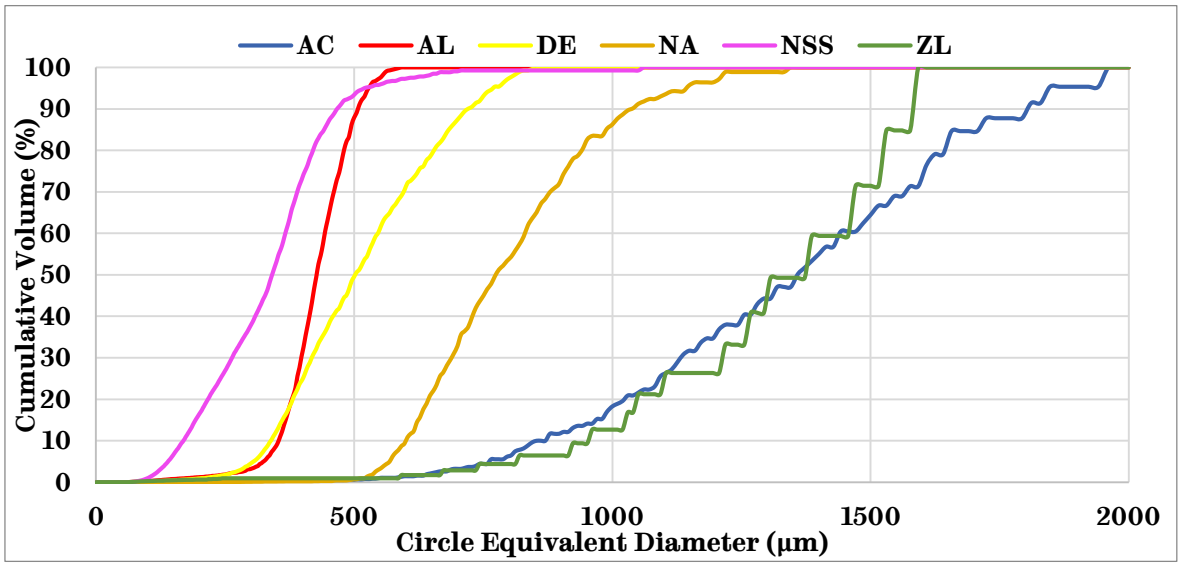

Figure 4.6. Circle Equivalent Diameter of Other Particles.

4.4.2.2 Shape Analysis

4.4.2.2.1 Rail Sands

The measured circularity of the rail sands, included in Figure 4.7, show a spread in values ranging from 0.7-0.9, notably some sands exhibit a larger spread in circularity values, for example, JPD ranges from 0.5-0.7. When considering a perfectly circular

particle (circularity=1), these circularity values indicate that these rail sands range from fairly circular to circular in shape.

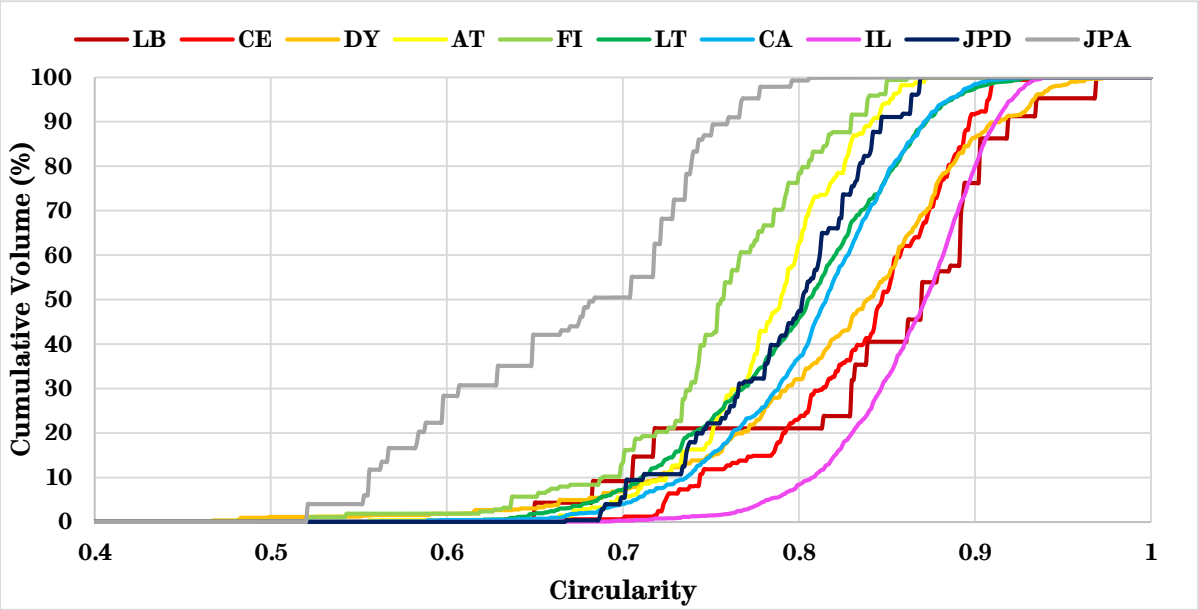

Figure 4.7. Circularity of All Rail Sands.

The convexity values for all rail sands are included in Figure 4.8. Compared to the measured circularity values, the spread of convexity values is smaller, ranging from 0.9-0.97. These values indicate that all rail sands are relatively non-convex, due to how close they are to the perfect non-convex particle (convexity=1).

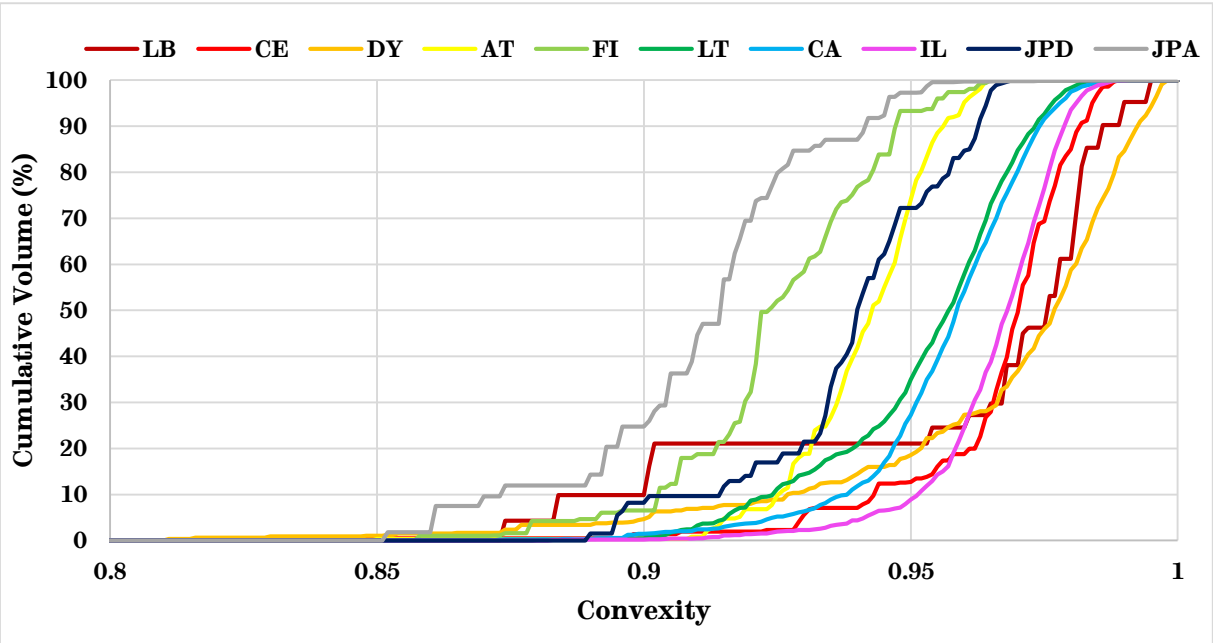

Figure 4.8. Convexity of All Rail Sands.

4.4.2.2.2 Other Particles

The circularity of all other particles not including rail sands are included in Figure 4.9. Most particles are between 0.7-0.8 and can be considered fairly circular, however AC was measured to be non-circular; a quick visual inspection of the particle shows AC exhibits a long flake-like shape.

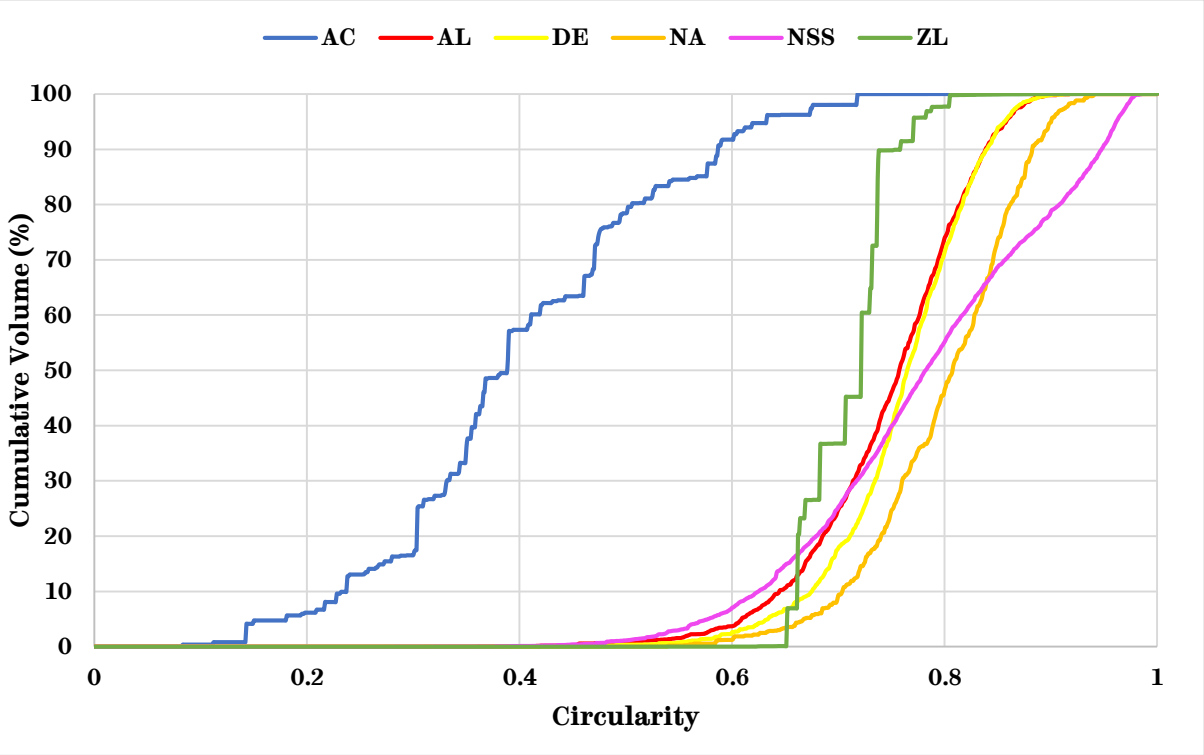

Figure 4.9. Circularity of Other Particles.

The convexity data for other particles is included in Figure 4.10. All of these particles are relatively non-convex, with values ranging from 0.85-0.97.

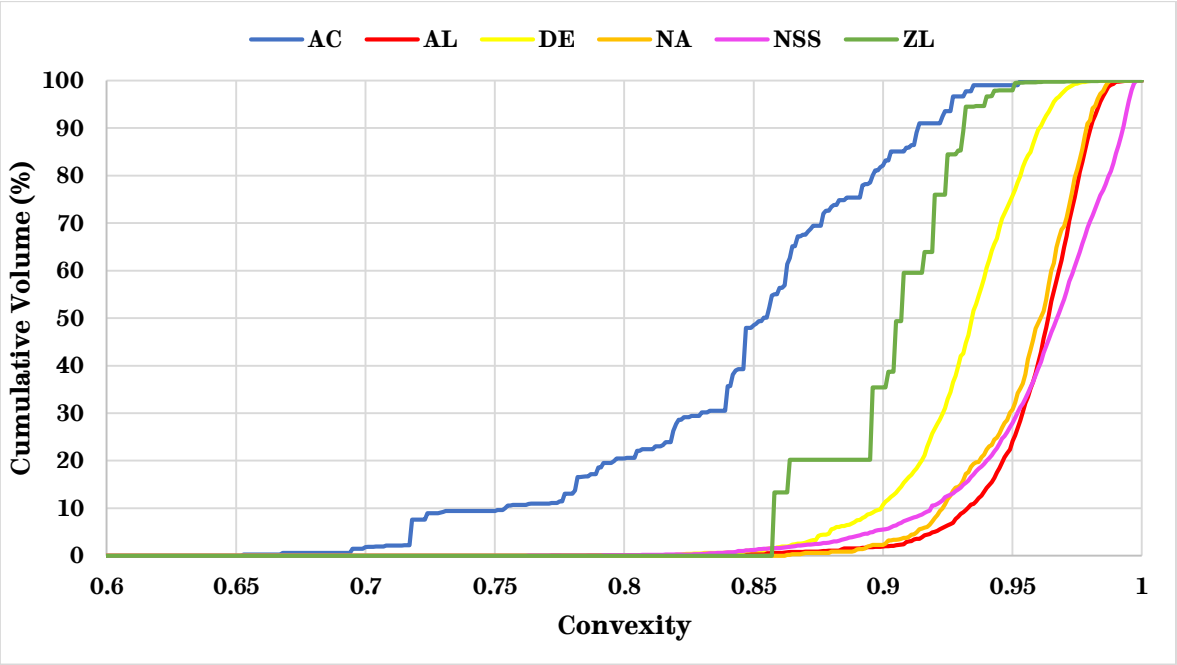

Figure 4.10. Convexity of Other Particles.

4.5 Nano-Hardness & Stiffness: Nano-indentation

4.5.1 Methodology

Nanoindentation was carried out on a Hysitron TI Premier from Bruker using a Berkovich indenter and a 10,000 μN load. Nine indentations were performed on >5 particles for each specimen. The raw load vs displacement data was then analysed using the Oliver-Pharr method [108] to produce hardness results.

Due to a combination of pre-existing hardness data and incompatibility with the nano-indentation technique not all particles underwent nano-indentation. Comparison with micro-indentation techniques will be made as part of sub-chapter 4.12.2.

4.5.2 Results

The hardness data for select rail sands has been presented in Figure 4.11. The rail sands which were found to not be purely quartz (AT, FI, and CA) showed a larger variation in hardness measurements being observed, possibly due to the indentation of their different phases. AT in particular was measured to be noticeably less hard than the other materials, with the pure quartz materials being the hardest measured.

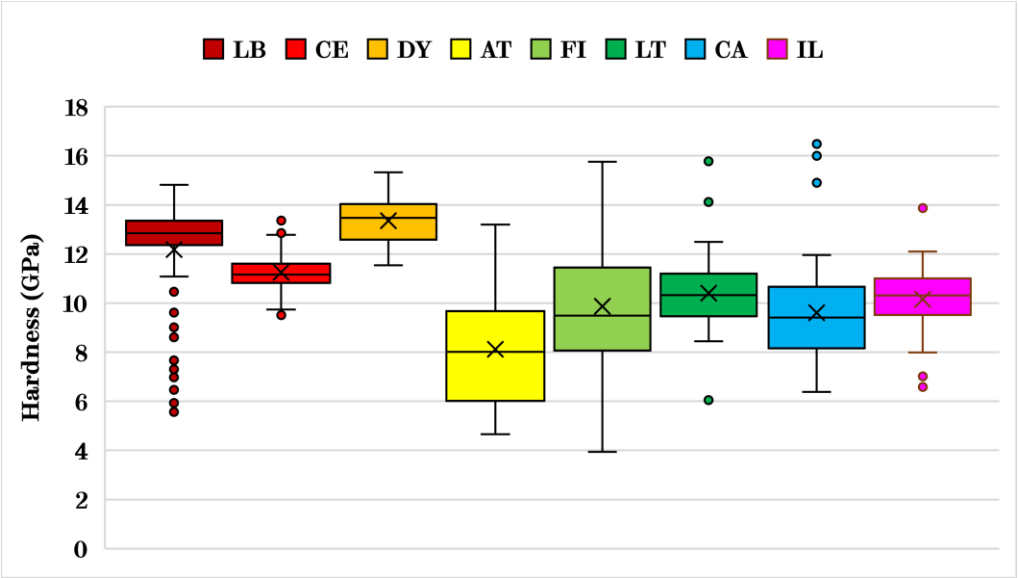

Figure 4.11. Nano-Hardness Measurements of Select Rail Sands.

Assuming Poisson's ratio of ν= 0.3, the stiffness measurements of the rail sands can be derived using Equation 3.9. The stiffness measurements are presented in Figure 4.12; Outliers and mean markers have been removed from this plot to aid clarity. A large spread can be seen in both the range of stiffness measurements for each sand as well differences between the sands themselves.

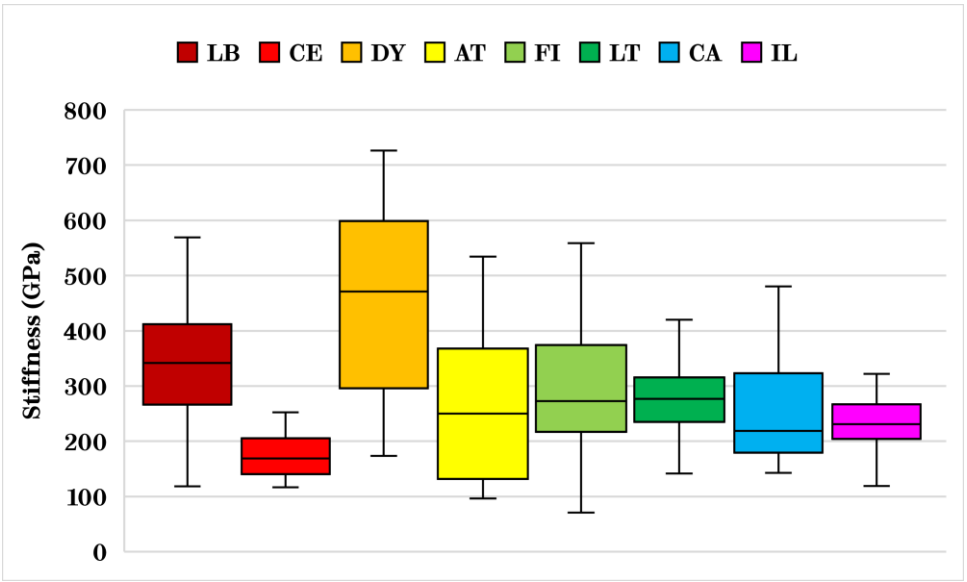

Figure 4.12. Stiffness Measurements of Select Rail Sands.

4.6 Micro-Hardness & Fracture Toughness: Microindentation

4.6.1 Methodology

Microindentation was carried out on a Durascan 70 G5 from Struers using a HV0.3 loading conditions. The indentation was measured optically to produce a hardness value and the cracks at each corner were subsequently measured to find a value for fracture toughness from a formula derived by Antis et al. [135]:

$$K_C = \alpha \left(\frac{E}{H}\right)^{0.5} \left(\frac{P}{c^{\frac{3}{2}}}\right)$$

Equation 4.1

where K_C is fracture toughness, α is an empirical constant varying with tip indenter geometry (α =0.032 in this case), E is the Young's modulus (obtained from the Oliver-Pharr nano-indentation method [108]), P is the load and c is the crack length. Daphalapurkar et al. [107] found this produced data that could be used to characterise sand at the granular level but is ineffective for bulk characterisation, something which is less of a problem in this case where the sand does not act as a bulk material when discharged from the sanding hose.

Comparison with nano-indentation techniques will be made as part of sub-chapter 4.12.2.

4.6.2 Results

The micro-hardness measurements of rail sands are presented in Figure 4.13. Most sands show average hardness values of ~12 GPa, with the exception of AT, FI, and JPA. AT in particular showed a particularly large spread of hardness values.

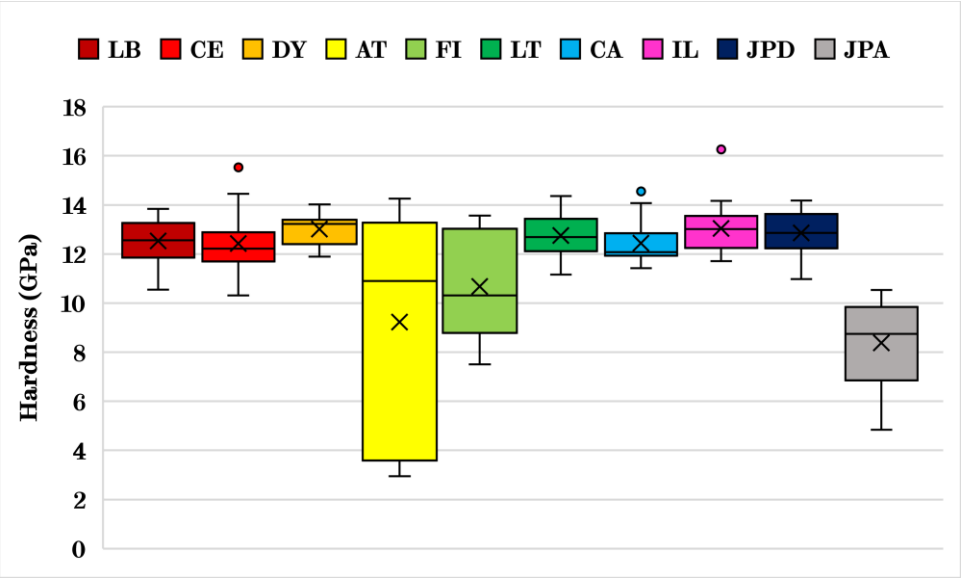

Figure 4.13. Micro-Hardness Measurements of Rail Sands.

Fracture toughness results for selected rail sands are presented in Figure 4.14; outlier points have been removed from the plot to aid clarity. Fracture toughness results are more spread when compared to their respective micro-hardness measurements. Fi is noticeably less tough compared to other sands.

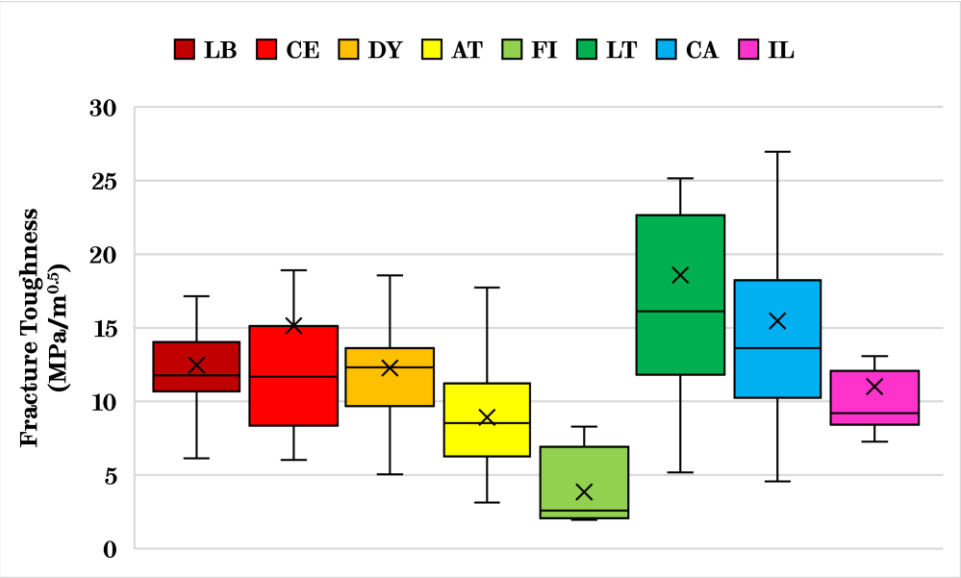

Figure 4.14. Fracture Toughness Measurements of Select Rail Sands.

In addition to the rail sands AL, DE, and NA particles were also tested; these data are shown on different plot due to aid clarity. The data for AL is presented in Figure 4.15(a), the median value confirming that this alumina is considerably harder than all rail sands. The data for DE and NA is presented in Figure 4.15(b). these measurements indicate that these particles are considerably softer than all rail sands.

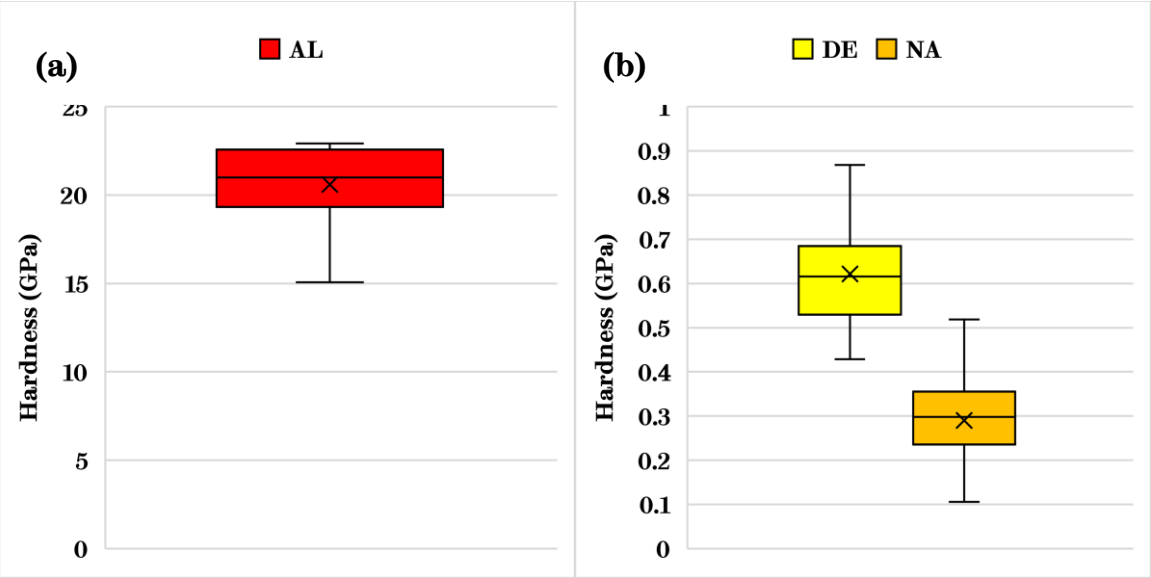

Figure 4.15. Micro-Hardness Measurements of *(a)* AL; *(b)* DE & NA.

AC was not appropriate for either indentation method but a previous study [136] of tyre tread hardness estimates a shore A hardness of 65. In a previous study [137], GB material was found to be ~6 GPa. NSS & ZL had given hardness measurements of 1.7-2.2 GPa and 0.6-1.5 GPa respectively.

4.7 Coefficient of Restitution: High Speed Camera

4.7.1 Methodology

The coefficient of restitution (as defined in sub-chapter 3.3.2.4) was tested by carefully pushing a sand particle off of a platform and onto a rail; a high speed camera recorded the particle bouncing on the rail. A set of lights and white background were used to ensure sufficient contrast in order to clearly see the particle, a schematic of this set-up is included in Figure 4.16.

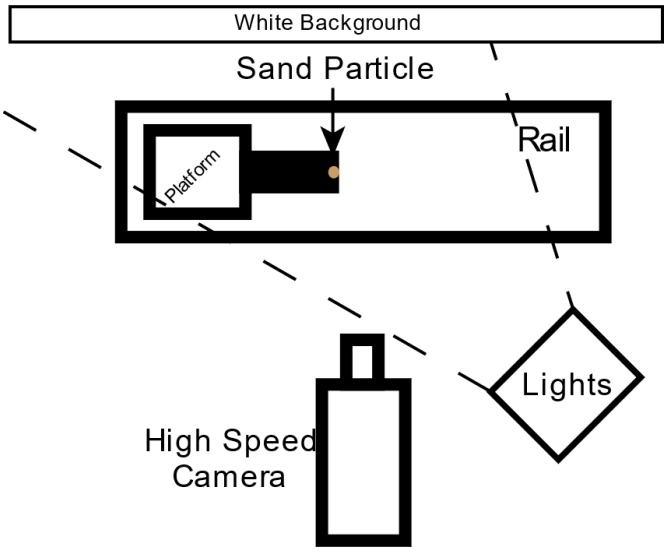

Figure 4.16. Coefficient of Restitution Test Set-up.

The coefficient of restitution was measured using image analysis of video recorded with a Phantom V210 high speed camera at frame rates of 2230 fps. Particle velocities were measured immediately before and after bouncing using the mtrackJ plugin in ImageJ software, thus the coefficient of restitution (CoR) could be calculated:

$$CoR = \frac{Velocity\ After\ Collision}{Velocity\ Before\ Collision}$$

Equation 4.2

20 particles from each sand were tested, repeats on a single particle were found to be impractical due to the difficulty in locating sand particles after use.

It has been found that particles that bounce lower tend to be more easily entrained into the wheel/rail contact [24], therefore identifying particles with lower CoRs, or even just characterising particle behaviour when keeping low, may help improve understanding of how to improve entrainment.

4.7.2 Results

The results from the coefficient of restitution tests for rail sands are shown in Figure 4.17. The median values for all tested sands are between 0.3-0.51, though all sands exhibited a notable spread in measured values.

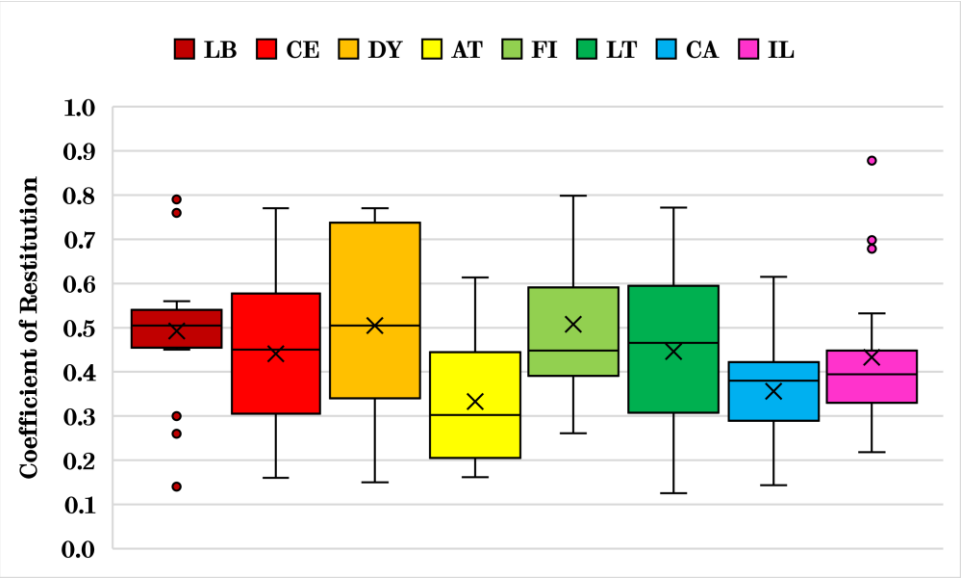

Figure 4.17. Rail Sand Results from Coefficient of Restitution Testing.

The coefficient of restitution results for other particles are shown in Figure 4.18. Generally, the other particles had lower values of coefficient of restitution that the sand particles and showed a lower spread of measured values.

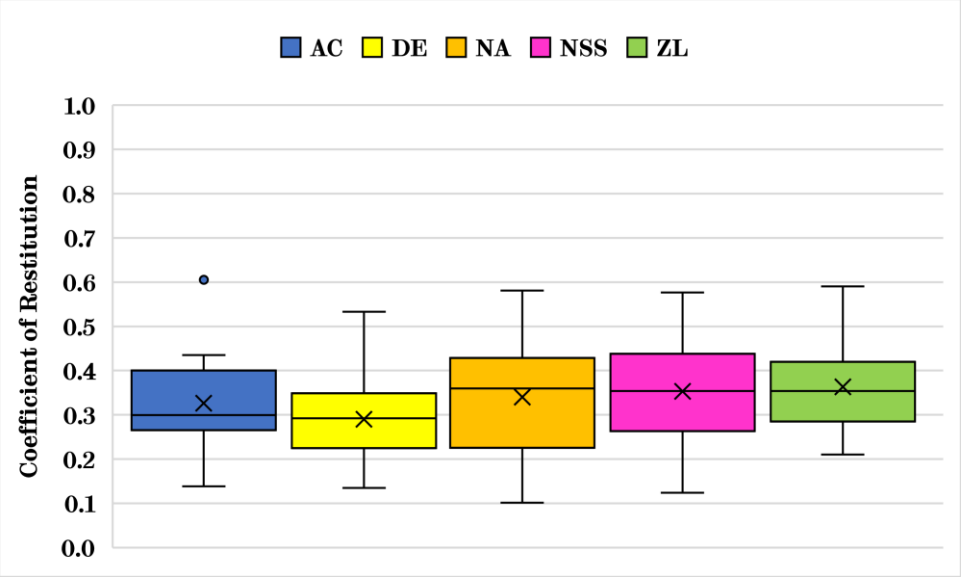

Figure 4.18. Other Particles Results from Coefficient of Restitution Testing.

It can be expected that some natural variation may occur in coefficient of restitution testing, Hastie [68] posited that one reason may be the angular velocity after impact. In Figure 4.19, two particles are shown, the left particle's point of contact is directly below its centre of mass (CoM) thus the only forces acting on the sand (R) are straight up; the right particle has contacted the surface at a point away from its centre of mass creating a force couple which will cause the particle to have a greater angular velocity. Without knowing the exact shape and at what point each particle is impacting the rail it is impossible to account for this variation.

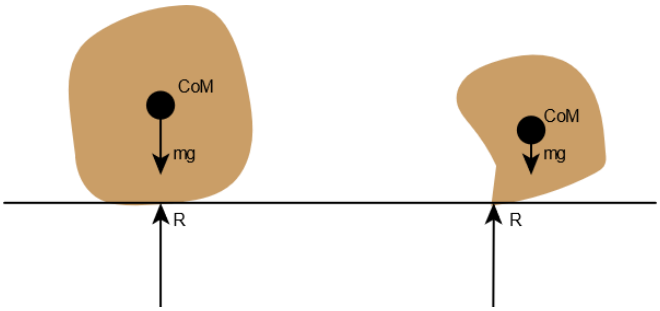

Figure 4.19. Diagram of Particle Bounce Behaviour.

Another reason for a variation in measured coefficient of restitution is the velocity measurements being conducted in 2D, thus not accounting for any velocity component parallel to the direction of filming. This may mean in cases where this velocity component is higher the coefficient of restitution is underestimated.

4.8 Particle Adhesion

4.8.1 Methodology

The particle drop test, utilised in this project to assess adhesion, was sourced from work conducted by Zafar et al. [114]. Particles are applied to a steel plate (6×6×2 mm) which is then dropped onto a ring which exerts a transient force on the particles causing some, larger particles, to become unattached. By equating the detachment force of a particle to adhesive force from JKR theory [138] an equation for interfacial energy, Γ, can be derived:

$$\Gamma = \left(\frac{mv}{\Delta t}\right) / \frac{3}{2}\pi R$$

Equation 4.3

where m is the estimated mass of a particle based on its size and density, v is the impact velocity, Δt is half the contact time between the steel plate and the stopper, and R is the reduced particle radius.

A critical particle diameter is determined by the average between the largest particle remaining on the steel plate and the smallest particle that has become unattached; this can then be used to estimate particle mass. This means the steel plate and the particles on it be must be evaluated pre-test and post-test by the Morphologi G3, previously mentioned in the Particle Size & Shape: Image Analysis sub-chapter.

The impact velocity and half contact time are measured using high speed video footage recorded by a Photron FASTCAMSA5 at 75,000 frames per second.

Three repeats were taken for each particle tested. All tests were performed by Sadegh Nadimi due to access to the relevant equipment.

4.8.2 Results

For all three rail sands being tested (LB, CE, and DY) a critical particle diameter of ~85 μm was measured. Using Equation 4.3 the interfacial energy for all three rail sands was calculated as 0.1 mJ/m^2 on a steel surface.

All samples giving similar values does indicate that this test method was successful at measuring particle adhesion as an intrinsic characteristic of each sands material i.e. as they are all pure quartz they should have similar values. As the values for all rail sands were relatively similar, only these three rail sands were used as an indication of the adhesion between rail sand and steel.

4.9 Single Particle Crushing

4.9.1 Methodology

As a means of characterising the crushing characteristics of LB, a simple test was set-up to measure the amount of crushing stress needed for initially breaking the particle. As this test was to serve as a more fundamental examination of how a typical rail sand gets crushed only LB was analysed as this could be considered a fairly typical rail sand.

The test set-up is illustrated in Figure 4.20. A Shimadzu EZ-LX tensile tester with a 500 N load cell was used as the basis for the set-up with the tested particle positioned between two flat steel platens.

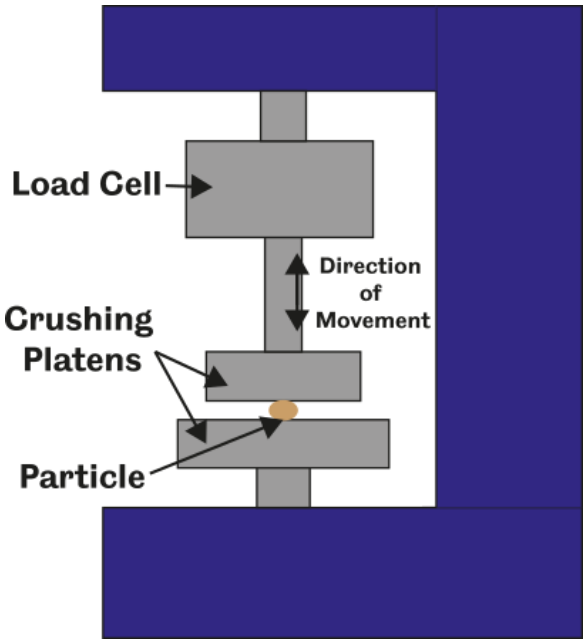

Figure 4.20. Test Set-up for Single Particle Crushing.

20 particles from 6 different sieve sizes (0.71-0.85 mm, 0.85-1 mm, 1-1.18 mm, 1.18-1.4 mm, 1.4-1.7 mm, and 1.7-2 mm) were tested to allow later analysis of the effect of size on crushing characteristics.

A single particle was placed on the bottom platen and the top platen was brought down until it was in contact with the particle, the distance between the platens was then taken as the individual particle's characteristic dimension. The upper platen was then moved down at 1 mm/min until fracture was detected by the Shimadzu software i.e. a sudden drop in applied force was detected.

4.9.2 Results

Figure 4.21 shows how the crushing stress varies according the measured particle dimension. Here, crushing stress was calculated using crushing force divided by a circular area with the diameter of the measured particle dimension. There is a weak inverse correlation between particle size and crushing stress and there seems to be a greater spread in crushing stress with smaller particle sizes.

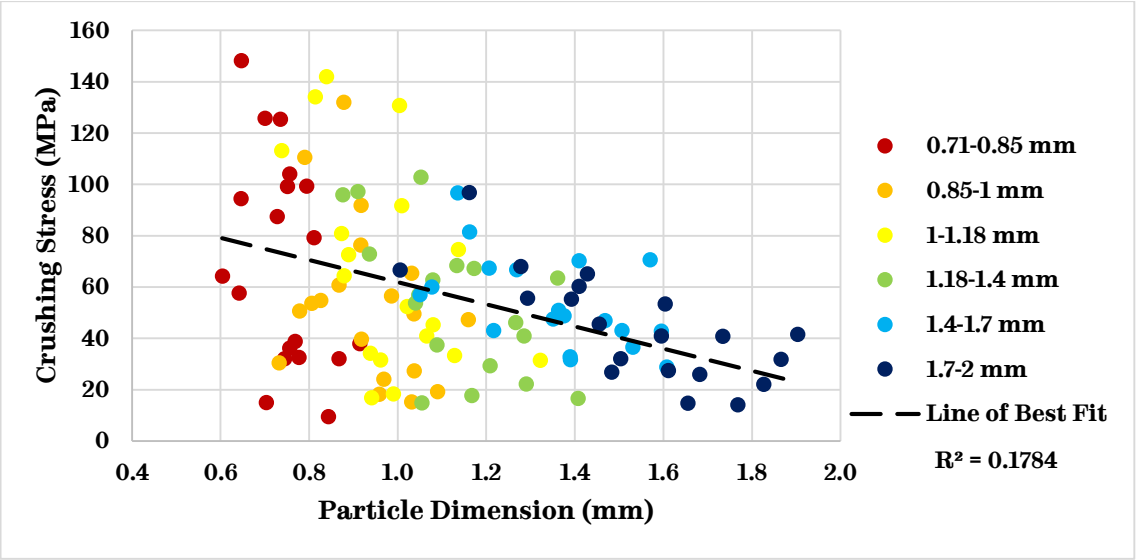

Figure 4.21. Relationship between Particle Size and Crushing Stress for LB.

Figure 4.22 plots the characteristic stress against the probability of survival at this given characteristic stress. Again, a relationship between particle size and the consistency of fracture at a given stress is shown as proportional i.e. the larger the particle the more predictable its crushing stress; this can be inferred from the gradient of each line. In general, the smaller particles seem to have a slightly greater chance of surviving higher stresses, as is shown by their respective characteristic stresses being slightly higher at a probability of survival of 50%.

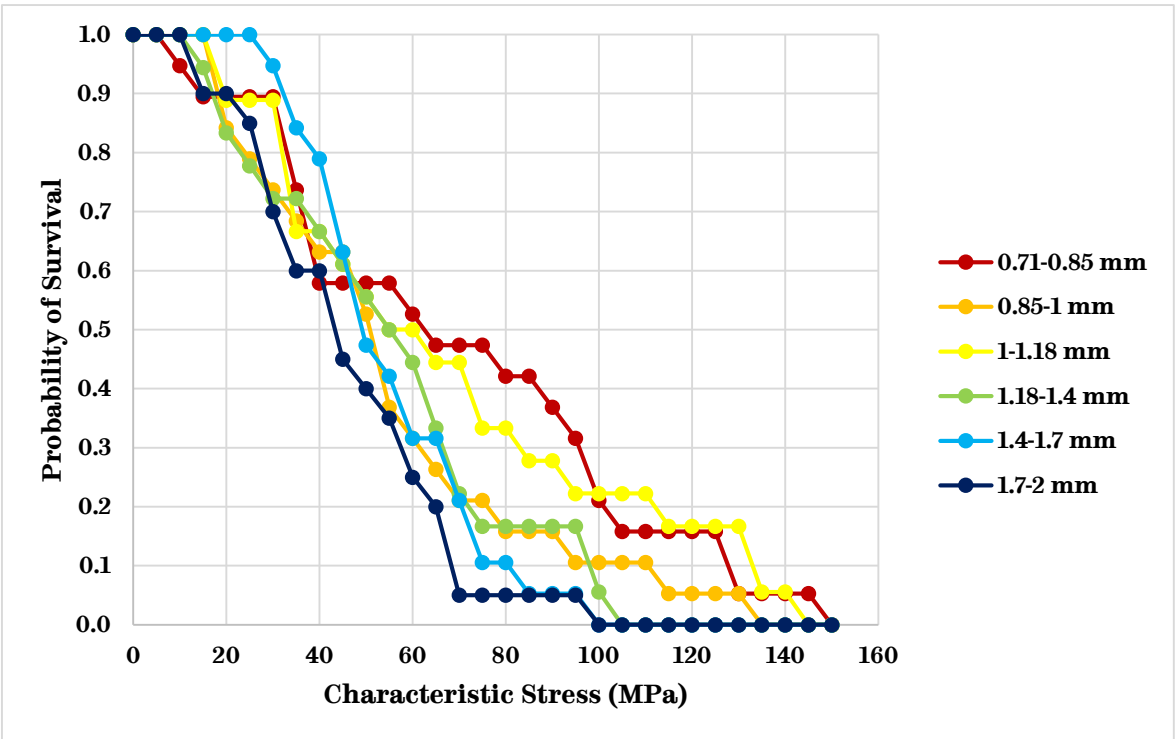

Figure 4.22. Relationship between Characteristic Stress and Probability of Survival for LB.

Figure 4.23 plots probability of survival vs the normalised stress, where normalised stress is equal to a characteristic stress divided by the characteristic stress at which the probability of survival is 1/e. The plot shows the variability of normalised stresses at which LB will crush, ranging from 0.5-2.5 its respective normalised stresses.

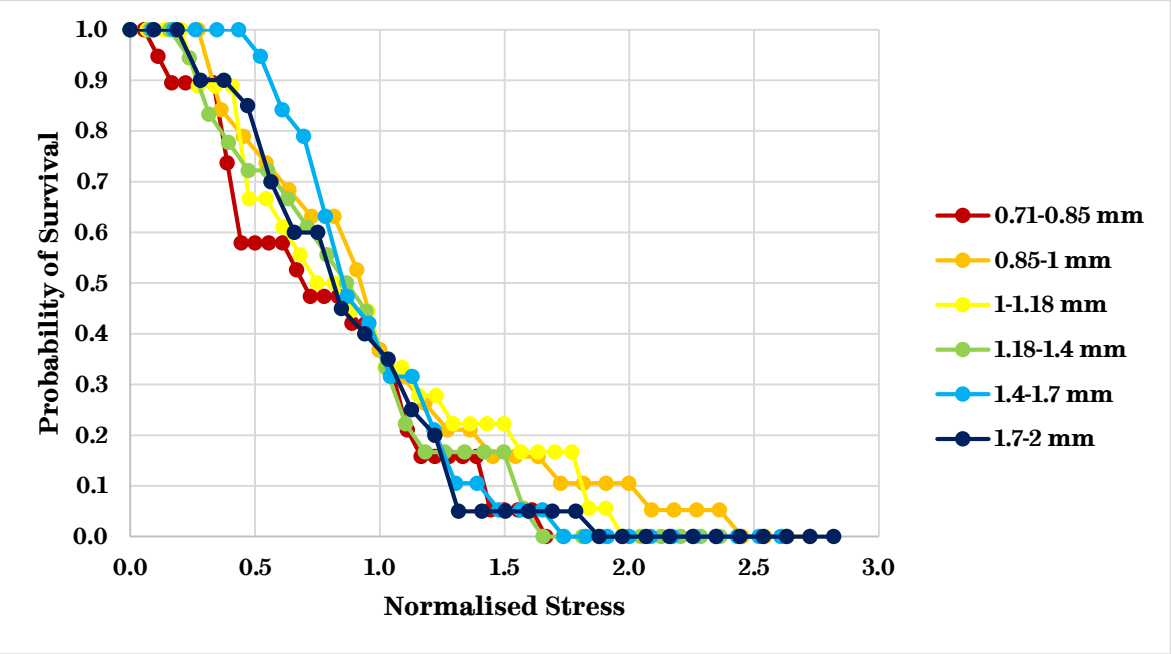

Figure 4.23. Relationship between Normalised Stress and Probability of Survival for LB.

By comparing the data in Figure 4.23 to Weibull function curves produced in a study by Nakata et al. [105] a value of Weibull modulus [139] can be estimated as between 2-3. This Weibull modulus indicates middling variability, for comparison brick, pottery, and cement have a Weibull modulus of ~5.

4.10 Angle of Repose

4.10.1 Methodology

Measurement of angle of repose (defined in sub-chapter 3.3.2.6) was conducted using the method first described in work by Geldart et al. [122]. 200 g is applied to a vibrating chute which feeds into a funnel, the particles then fall onto a flat surface backed by a vertical wall. The angle of the mound made by the particles is then measured and pictures taken. Three tests were carried out for each particle type.

Due to this test serving as a general assessment of how bulk characterisation of rail sands could be carried out not all particles were tested. All tests were performed by Sadegh Nadimi due to access to the relevant equipment.

4.10.2 Results

Figure 4.24 shows all three tests for selected rail sands. LB had the smallest angle of repose at 26° ± 1° (Figure 4.24(a)), whereas DY had the highest angle of repose at 36° ± 1° (Figure 4.24(c)); CE was in the middle with a measured angle of repose at 30° ± 1° (Figure 4.24(b)).

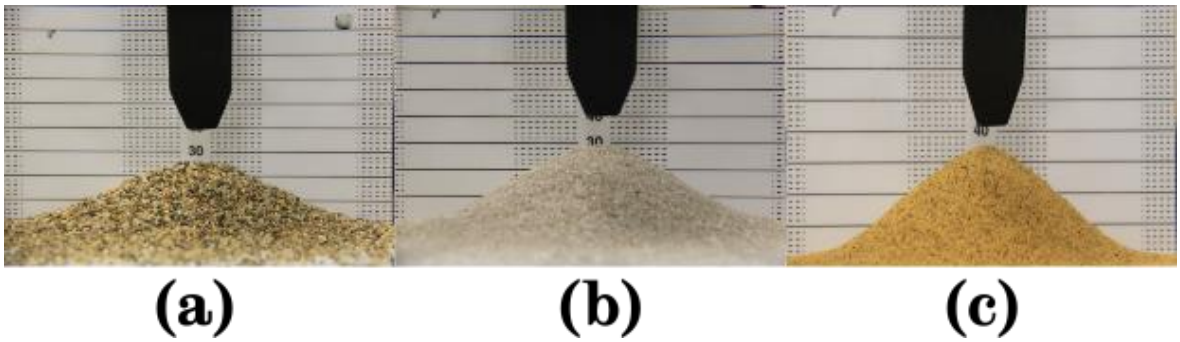

Figure 4.24. Angle of Repose Tests for: *(a)* LB, *(b)* CE, *(c)* DY.

4.11 Compacted Bulk Density

4.11.1 Methodology

An Instron 5566 test machine was used for measuring compacted bulk density, in a similar method to the one used by Hassanpour et al. [124]. A representative amount of particles, weighing ~60 g, was placed into cylindrical die with a diameter of 40 mm and then tapped until a bulk height of 25 mm of particles was produced; die filling was conducted using air pluviation to maintain similar conditions for all tests. A 10 kN load cell was used for all tests and compression was applied at a rate of 0.1 mm/min. Two repeats for each particle type being tested were carried out.

Due to this test serving as a general assessment of how bulk characterisation of rail sands could be carried out not all particles were tested. All tests were performed by Sadegh Nadimi due to access to the relevant equipment.

4.11.2 Results

The results from confined compression tests are summarised in Figure 4.25. DY shows the highest amount of stiffness, whereas LB was measured as the least stiff. LB shows some plastic behaviour, indicative of rearrangement of the particles in the compacted mass.

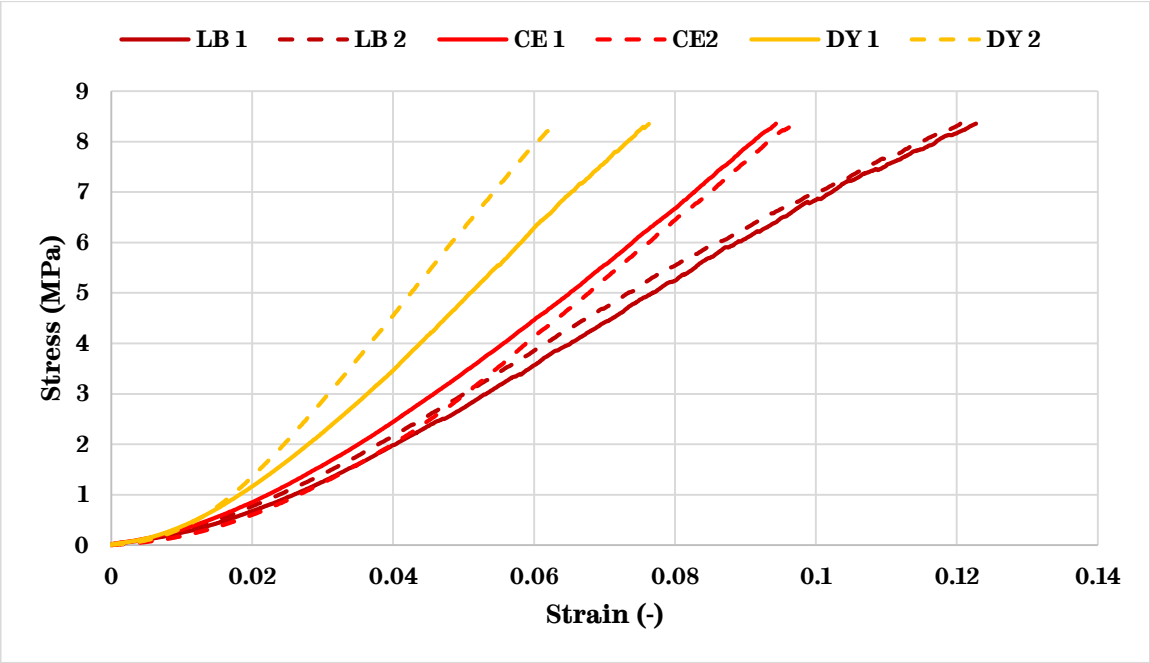

Figure 4.25. Confined Compression Results for Selected Rail Sands.

After the confined compression test each sample was sieved, the results of which are included in Figure 4.26. Comparing these results to the sieving results from Table 4.2 there seems to be very little difference in sand size after the confined compression test. This suggests that little particle breakage occurred during test and bulk strain was due to the respective material properties alone.

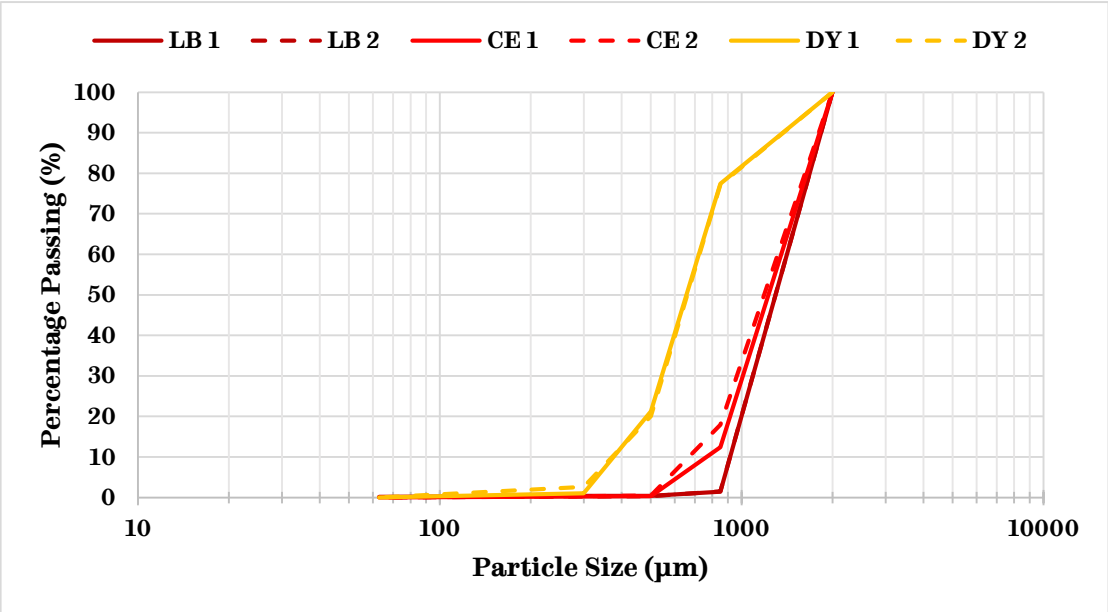

Figure 4.26. Particle Size Distribution Post Confined Compression Test.

4.12 Discussion

4.12.1 Sieve vs Image Analysis

Qualitatively, sieve and image analysis produced similar results in terms of the relative sizes of the particles, however image analysis tended to give larger measurements of particle size compared to sieve analysis. This is due to the analyses measuring different dimensions and therefore not being directly comparable; image analysis measures the circle equivalent diameter, whereas the sieve analysis measures the second smallest dimension of a particle; this is particularly noticeable for AC, a needle like, non-circular, particle where the sieve measured particle size is close to double the image analysis measured particle size.

Both analysis methods are relatively simple and quick to use, though the initial set-up of an image analysis method can be costly or time consuming. Sieving is also more ubiquitous when compared to image analysis, so may be more applicable for size characterisation in industry. Image analysis, however offers greater granularity of data and also provides data on shape characteristics.

In image analysis the sand is lying on a 2D surface and it is settled on its most stable base, generally its largest surface, leading to an image being taken of this surface. For more informative measurements, future research could try to take a 3D image of the particle.

4.12.2 Comparison of Indentation Scales

Two different scales of indentation were used in this particle characterisation framework: indentation at the nanoscale and indentation at the microscale.

Practically, the micro-indenter is a much simpler piece of equipment to use and much quicker, though if many indentations are being performed it is relatively laborious. These factors make micro-indentation possibly more appropriate to be widely adopted as a particle characterisation method in the railway industry.

With regards to the range of samples that can be used, there are advantages and disadvantages associated with either scale. Nano-indentation can be used on smaller and/or softer particles where micro-indentation may only succeed in completely destroying a particle. Nano-indentation also does not require a reflective surface as the indentations are not being measured post-test. The sample preparation associated with micro-indentation is also marginally simpler with less polishing required to supply an appropriate surface for indentation.

Comparing the hardness measurements for both scales, nano-indentation measurements gave a wider spread of hardness values compared to micro-indentation for pure quartz particles. This could be due to each nano-indentation taking place over a much smaller area, allowing small variations in a particle's structure making a noticeable difference when compared to micro-indentation. For non-pure quartz materials, the larger spread of hardness values will be due to the different mineral phases present, this was apparent for both indentation scales.

Using a combination of both scales does offer advantages, by using nano-indentation a value for particle stiffness can be calculated. Using this value, in conjunction with measurements taken from micro-indentation gives a value for fracture toughness. Both of these are useful data sets to have for characterising particles.

4.12.3 Bulk Properties

Three different rail sands were characterised according to bulk tests: LB, CE, and DY. The two bulk properties measured, angle of repose and compacted bulk density, apply to the performance of the rail sand whilst in the sand hopper, as opposed to in the wheel/rail contact where particles will be acting almost individually.

There were differences in bulk characteristics between all sands. The main point of difference between all these rail sands was their morphology, suggesting this plays an important role when considering how compatible a particle system is with sander design.

4.12.4 Comparison of Rail Sands

Ten different rail sands were analysed in particle characterisation tests, with three rail sands (LB, CE, and DY) being analysed in extra tests also. These rail sands can be broadly split into two different categories: pure and non-pure quartz sands.

The pure quartz sands (LB, CE, DY, LT, IL, and JPD) were generally harder according to both scales of indentation and showed a lesser spread of physical properties measured from indentation tests. CA was the closest of the non-pure quartz sands to acting like a pure quartz sand, possibly due to having a higher percentage of a quartz mineral phase than other non-pure quartz sands. JPA, the only rail sand to not have any quartz mineral phase, also demonstrated the lowest measured hardness and unlike other non-pure quartz rail sands its spread of measured values did not reach the value of pure quartz sands.

The difference between pure and non-pure quartz sands can also be seen in their respective shape characterisation measurements. JPD, FI, and AT were both less

circular and less convex than other sands. Whilst, there seems to be no difference in shape between CA and pure quartz sands, this may be due to the amount of non-quartz phase being less than other non-pure quartz sands.

Comparing the rail sands by countries of origin produces some points of difference. The sands from the USA (CA & IL), tend to be smaller than other sands from the rest of the world, whereas Japanese sands (JPD & JPA) tend to be the largest. The sands from central European countries (CE & AT) are both very similar in size, suggesting they were meant to suit the same standard.

The difference between JPD and JPA is also of interest, the decision to change from a harder pure quartz sand (JPD) to a softer (JPA) may have been justified by the latter being paired with AL in a new particle system that is being used in Japan.

4.12.5 Possible Improvements to Characterisation Framework

The particle characterisation framework introduced in this chapter may not be entirely appropriate for wider use in the rail industry; some characterisation methods utilised here may be overly technical or expensive for particle suppliers to implement. Further thought may be needed on what would constitute the bare minimum needed to characterise new products for use in industry, this will be dependent on analysing the effect of particle characteristics in tribological tests, which will take place in subsequent chapters. Currently, according to different countries' standards for rail sands it seems, at a bare minimum, a particle system's mineral content and morphology should be characterised.

Useful improvements to the particle characterisation framework in this work might include:

- *Mineralogy;* using a test method to accurately measure percentage mineral content for each phase may further help understanding on the effect that mineral ratios (e.g. quartz content) may have on particle performance in the wheel/rail contact;
- *Morphology;* characterising the 3D morphology of a particle would give a more accurate and complete picture of particle morphology than 2D analysis methods;
- *Coefficient of Restitution;* a two-camera set-up would allow particle velocity to be measured in 3D, possibly improving the accuracy of the data being acquired.

4.13 Summary

In this chapter a particle characterisation framework was detailed and results from a selection of rail sands and other particles have been presented. Differences between rail sands seem to depend on the quartz content of each particular sand.

The particle characterisation presented in this chapter will feed into further chapters that will assess the effect of each particle system on traction measurements in tribological tests.

5 HIGH PRESSURE TORSION TESTING

5.1 Introduction

The high pressure torsion (HPT) rig compresses two flat test specimens together and subsequently applies torsion. The HPT rig at Sheffield can supply 400 kN of normal load and 1000 Nm of torque, thus it can simulate contact stresses up to 900 MPa, equivalent to a 60 kN load on a single wheel according to a study conducted by Zhou et al. [140].

Traditionally, the HPT rig has been used to study the effect of high plastic strain where the large compressive forces prevented failure [141]–[143]. Previous research concerning the setting up of the rig for rail work has previously been conducted at The University of Sheffield [144], [145]; As the high contact pressures and stick-slip nature of the HPT contact simulate some aspects of the wheel/rail contact. HPT rigs have also been used to study the effects of sand, such as work conducted by Meierhofer [18], though this work was limited in its scope as only one sand type was considered and not with realistic application amounts.

5.1.1 Aim & Objectives

The aim of the work described in this chapter was to use a scaled tribological test to assess the effect of particle systems on traction and contact conditions. Achieving this aim would also allow further work analysing the effect of particle characteristics on a particle system's performance and gather data for use in parameterising the extended creep-force model.

The objectives needed to be completed to achieve this aim included:

- Adapting the previously used HPT methodology and procedure for the use of granular material and very low adhesion conditions;
- Testing a range of particles in different contact conditions and measure how coefficient of traction (CoT) changes;
- Analysing the post-test surfaces and measure surface roughness.

5.1.2 HPT Concept

The HPT rig is controlled by electro-hydraulic servo valves to provide the required accuracy when controlling load and displacement in both the axial and torsional directions. The axial and torsional directions are controlled by two separate channels which can control the force or position in that specific direction. The channels send a command signal to the servo valves which respond and send

feedback of the actual position or force the HPT is undergoing. The response of the feedback compared to the command being sent is set by the values inputted into a proportional-integral-derivative (PID) loop.

The HPT rig compresses a bottom specimen together with a top specimen to create an annulus contact, thereby allowing third bodies to be uniform within the contact, unlike a pin-on-disc type test. A torque is applied to the bottom specimen until it has moved through a set sweep length at a low speed (<1 mm/s), a schematic of this action is included in Figure 5.1.

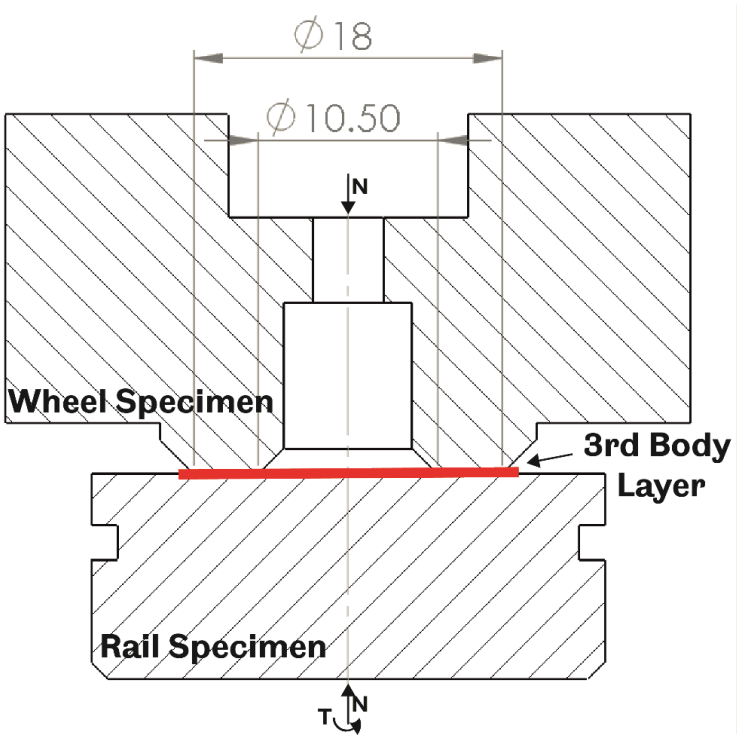

Figure 5.1. Schematic of HPT Concept.

The typical output of a single HPT test run has been included in Figure 5.2. The "elastic" region (ER) is characterised by an initial steep linear increase. The "pseudo-plastic" region (PPR) begins when asperity level contacts begin to plastically deform, work hardening the contact and leading to the coefficient of traction continuing to increase in the PPR. This asperity level plasticity was referred to as "local" or "tribological" plasticity by Six et al. [129], who also specify that this plasticity should not be confused with "global" plasticity, i.e. plastic deformation in the bulk material. For clarification: "global" plasticity can occur in the HPT contact during initial load cycles until reaching a shakedown limit, this will be discussed in further detail in later sections.

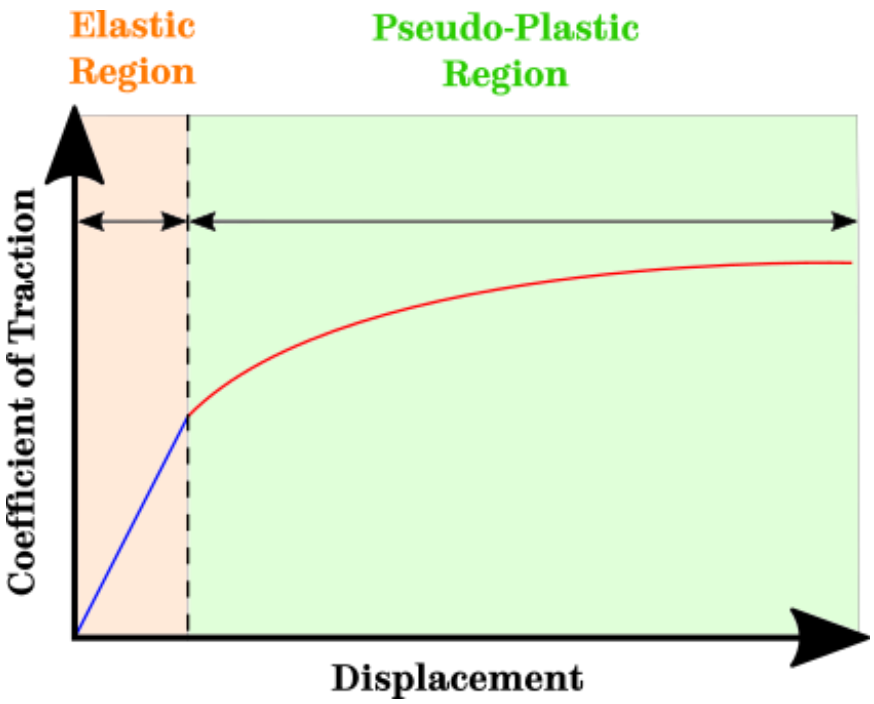

Figure 5.2. Typical Example of HPT Output.

5.1.3 Apparatus & Specimens

The HPT rig is shown in Figure 5.3, where (1) and (2) denote the wheel and rail specimens, shown in Figure 5.1, respectively. The two specimens are held in place by sample holders (3) made of 431 martensitic stainless steel. The axial position/force is controlled by a linear hydraulic actuator (5) and the actual axial position/force is measured by a linear variable differential transducer (LVDT)/load cell (7). The torsional position/force is controlled by a rotational hydraulic actuator (4) and the actual torsional position/force is measured by a rotary variable differential transducer (RVDT)/load cell (6). The attached controller (8) regulates the movement/applied force and records both command signals and feedback signals. The crosshead (9) can be moved up and down to accommodate test apparatus between 500 mm and 2000 mm in length. The actuators are pressurised by a hydraulic ring main (10).

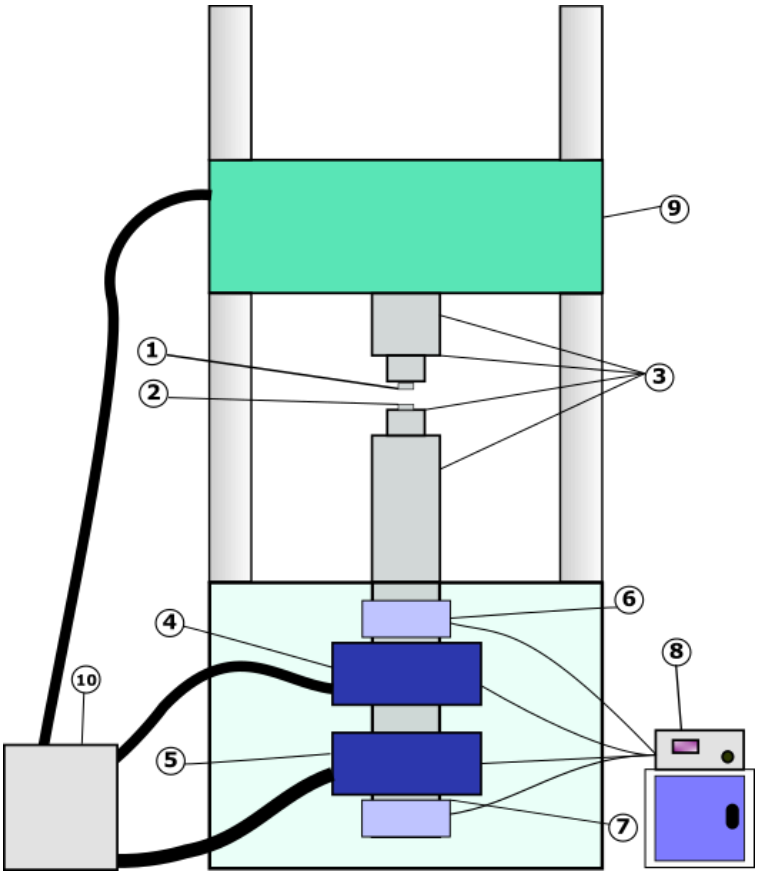

Figure 5.3. Schematic of HPT Rig.

The wheel specimen (see Figure 5.1) is made of R8T steel cut directly from an actual train wheel; the contacting surface of the wheel specimen is annular with an inside diameter of 10.5 mm and an outside diameter of 18 mm. The rail specimen (see Figure 5.1) is made from R260 steel cut directly from an actual rail; the contacting surface is flat. The dimensions of the annular contact between these specimens were produced from an iterative method, which is fully outlined by Evans [144].

5.2 Methodology

In this sub-chapter, an overview of the HPT procedure is presented that discusses the procedure at a high-level, i.e. what tests were conducted and the general procedure on for typical test; a more detailed test procedure can be found in Appendix A.

This sub-chapter will also include information on how the test method developed by Evans [144] was adapted for testing granular material and low adhesion conditions produced by new 3rd body layers.

In addition, the methodology for analysing the specimen surfaces post-test will also be discussed.

5.2.1 HPT Test Procedure Overview

The procedure for a typical HPT test is thus:

1. Three run-in sequences to bring the specimen surfaces to their shakedown limit;
2. Two dry runs to further condition the surfaces and provide a simple test to determine if the specimens are behaving in a typical manner. The second test start point is moved forward 10° from the previous test start point to avoid running over the same surface;
3. Any third body material is applied in the manner described in sub-chapter 5.2.4;
4. Three test runs are performed, traction data is accrued for each test and the effect of third body materials over several runs can be deduced. Each subsequent test start point is moved forward 10° from the previous test start point to avoid running over the same surface;
5. Test specimens are analysed post-test in the manner described in sub-chapter 5.2.6.

A full description of the HPT test procedure has been included in Appendix A and test parameters have been included in sub-chapter 5.2.5.

5.2.2 Adapting HPT Test for Granular Material & Low Adhesion

When Evans [144] was developing his HPT test methodology, he found that the impact the stick-slip phenomenon was having on test results was unacceptable. An example of what he was encountering is included in Figure 5.4, with X marking stick-slip events, where a low adhesion layer is present.

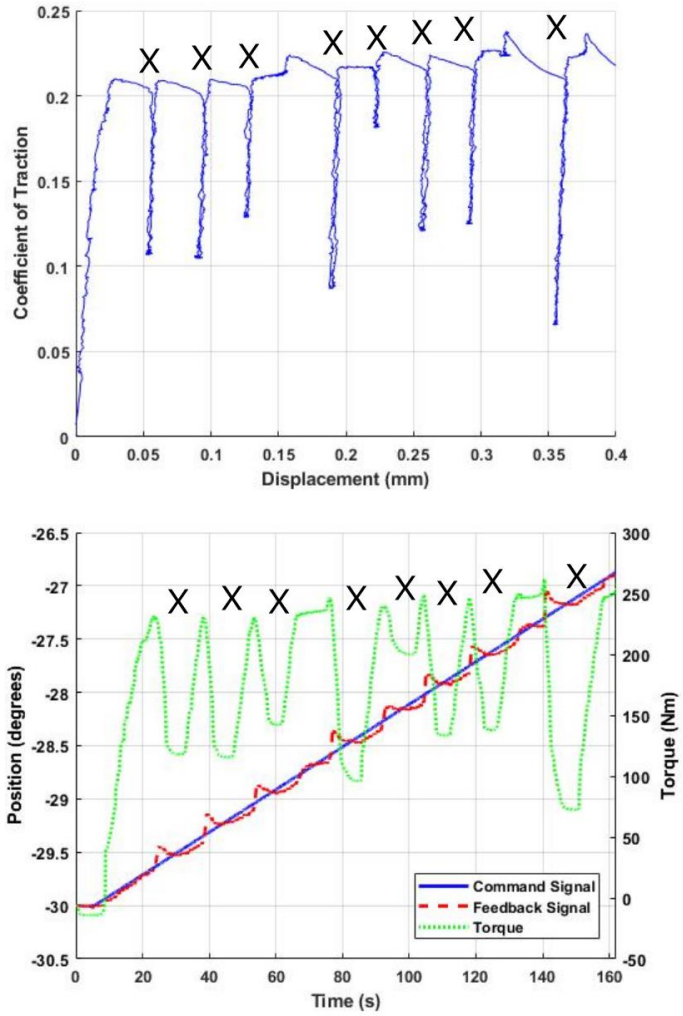

Figure 5.4. Example of the Stick-Slip Phenomenon, where X denotes stick-slip events.

The angular displacement is controlled by specifying a set-point and a set-point rate limit. The controller will send a command signal to the RVDT which will increase linearly at the set-point rate limit until it reaches the set-point. The controller will receive a feedback signal from the RVDT which shows where the rig actually is at that moment in time. When the PID loop is set so that feedback closely follows command signal, then the feedback signal should increase similarly to the command signal.

However, Figure 5.4 illustrates the effect of stick-slip on how the feedback signal follows the command signal. When slip occurs the feedback signal goes above the command signal, the controller will then try to bring feedback back to the command signal, in Figure 5.4 this can be seen as the torque reducing rapidly; if a particularly large slip occurs then the rig can start turning backwards to try and reach the command signal. As the torque rapidly drops, the coefficient of traction also rapidly drops as seen in Figure 5.4. All this effectively means instead of the rig behaving in the manner demonstrated in Figure 5.2, where an “elastic” region (ER) is followed

by a “pseudo-plastic” region (PPR) once during the test run, the rig is instead cycling in and out of the ER and the PPR. Therefore, over one test sweep length many small test runs occur instead of just one test run.

The solution Evans devised to this problem was to set the PID loop so that feedback did not follow the command signal closely, an example run has been included in Figure 5.5 where water was applied to produce stick-slip behaviour. The command still ramps up linearly, but as the PID loop is tuned “loose” there is a delay in the feedback trying to catch up to the command signal, and therefore the actual angular movement of the rig happens very quickly once the HPT contact enters the PPR. Whilst, this method eliminates the stick-slip problems seen in Figure 5.4 there is no control over the sweep rate of the rig and when low adhesion products are applied to the contact there is little control over the sweep length, potentially resulting in a gross slip event that can destroy the surfaces of the test specimens.

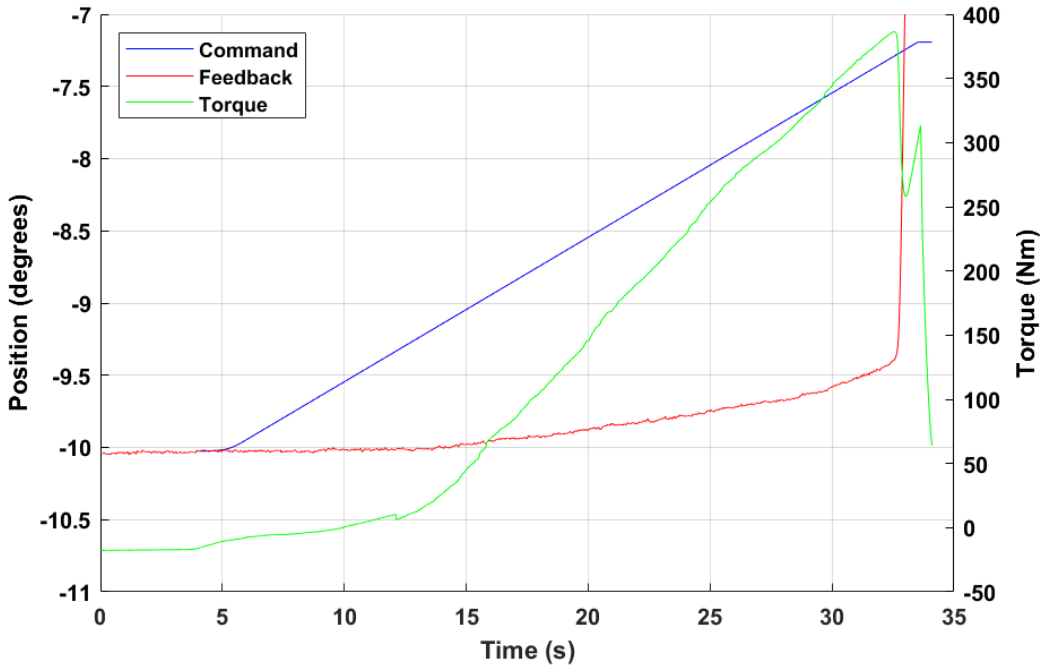

Figure 5.5. Example of Evans' Test Method.

A new method has been devised to combat the stick-slip phenomenon, whilst keeping greater control over test parameters. As the problem with stick-slip occurring was due to the reaction of the controller when feedback went above the command signal, a secondary control was added to the test script; if feedback is greater than command, then the torsional channel is changed semi-instantaneously (therefore not allowing time for force control to have any non-negligible effect) from position control, to force control, then back to position control. As position control is activated the command signal is set to be equal to the feedback signal, therefore

the feedback signal can never be above the command signal and the torque does not rapidly drop. As the PID loop is still tuned “tight” there is greater control of sweep rate and sweep length during a test run. Figure 5.6 shows an example of the revised test method in the presence of low adhesion, whilst there is still a drop in torque it is much reduced compared to Figure 5.4 and there is greater control over the test sweep compared to Figure 5.5.

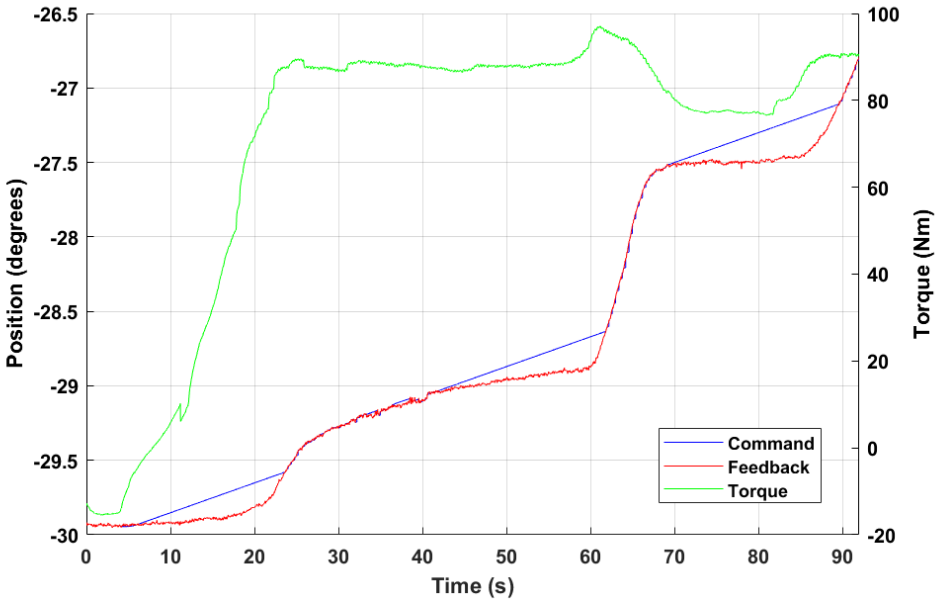

Figure 5.6. Example of Revised Test Method.

It should be noted that all three test methods produce similar results in dry conditions and their different effects are only apparent when low adhesion layers are present. The revised method has been used for all HPT tests conducted in this thesis.

5.2.3 Leaf Layer Development

Developing a repeatable method for creating a leaf layer in a simulated tribological test allows inferences about particles’ effects on leaf layer removal to be made. In Figure 5.7, multiple different methods for simulating a leaf layer are presented.

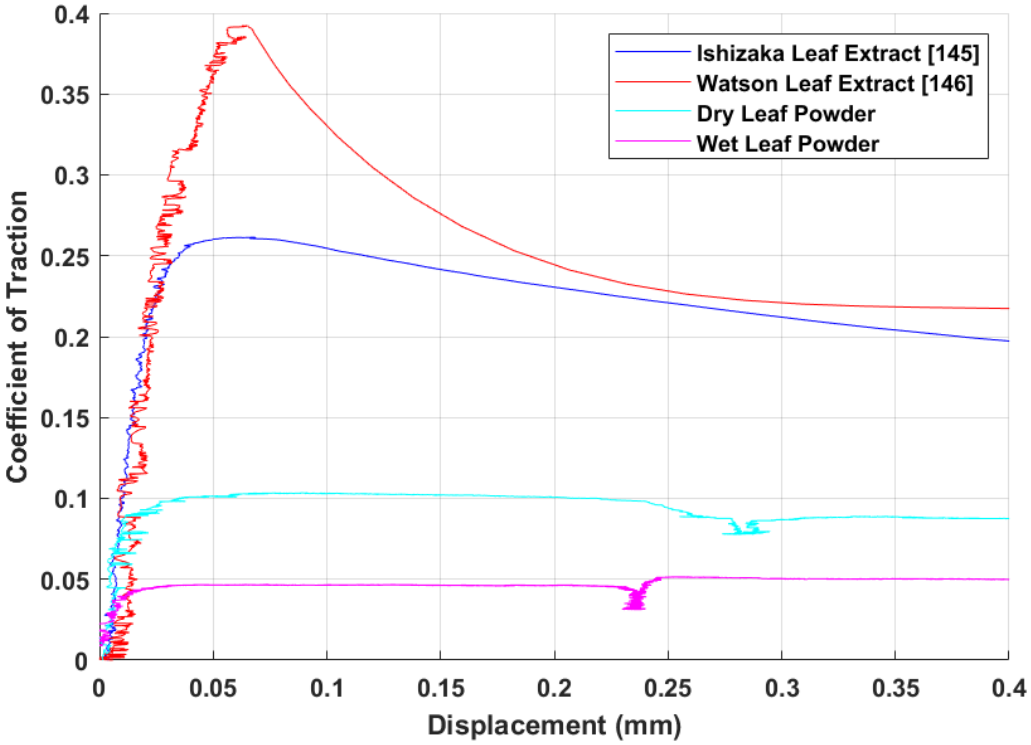

Figure 5.7. Example HPT Data from Tests with Different Leaf Contamination Methods.

Initially, the creation of a leaf layer for use in the HPT contact was attempted using a liquid leaf extract layer produced using a method proposed by Ishizaka et al. [146], i.e. leaf mulch was soaked in water overnight after which large particles were sieved out of the extract through a 50 µm filter. Tests were run with 100 µl of leaf extract applied to a conditioned HPT contact, an example of these tests has been included in Figure 5.7. The peak coefficient of traction was not below the minimum adhesion limit for traction of 0.2, though traction did reach that point eventually, and was not close to being under 0.09, the minimum adhesion limit for braking. As low adhesion was not achieved a new method for simulating leaf layers was needed.

The leaf extract produced by Watson et al. [147] is subtly different in that it was filtered to 0.2 µm. Another difference between the application of this leaf extract to the leaf extract created using the Ishizaka et al. was that only 20 µl was applied. An example of HPT data from this leaf extract has been included in Figure 5.7. As with the previous leaf extract, low adhesion was not achieved.

As the two liquid leaf extracts had not succeeded in creating low adhesion in the HPT contact, a leaf powder was tried instead. The leaf powder was formed by blended sycamore leaves and 0.025 g was applied to the contact; this amount was chosen as it completely covered the HPT contact. An example of a test with leaf powder has been included in Figure 5.7. A significant drop in traction was achieved when compared to the liquid leaf extracts.

In an attempt to lower the traction being produced further, 20 µl of distilled water was applied on top as previous work suggests that the presence of moisture promotes leaf to rail bonding. An example of this has been included in Figure 5.7. The traction dropped significantly further when compared to a dry leaf powder layer.

However, one issue remained, as time was needed to apply any particles to the contact the leaf layer would dry out in that time. This drying out can be seen in the data, in Figure 5.8 after inserting a 3 minute pause to represent the time to apply particles, the traction notably increases with each subsequent run seeing increasing traction, up to above 0.1 on the last run.

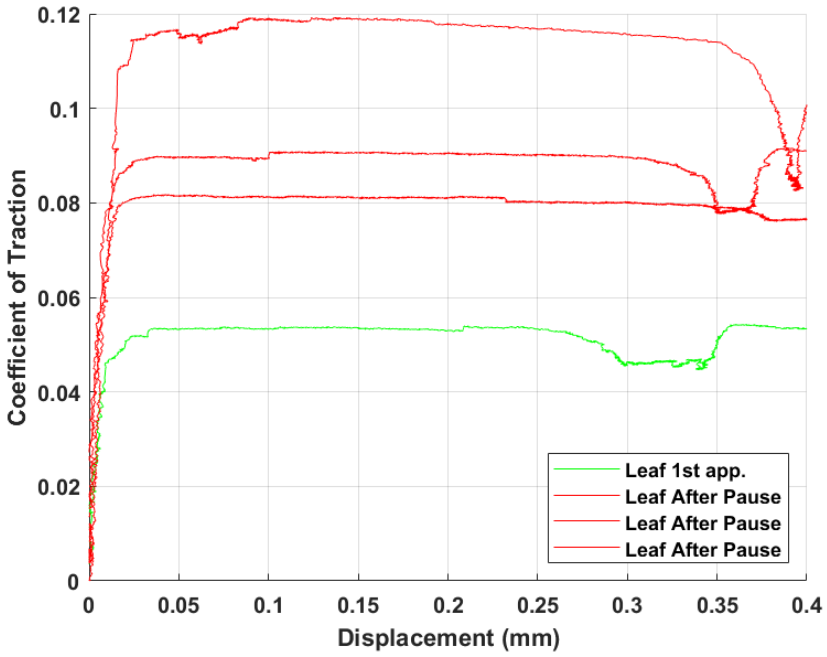

Figure 5.8. Example of HPT Data from Leaf Powder Tests where a 3 Minute Pause was inserted before continuing Testing.

The effect of drying out was also present in the leaf layer itself, Figure 5.9 shows the aftermath of a test run with a drying leaf layer, where the characteristic black leaf layer is not present.

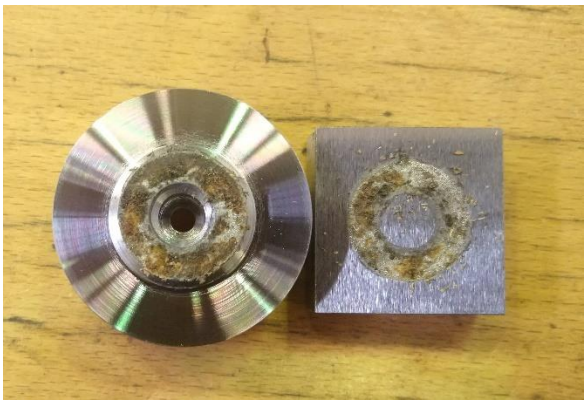

Figure 5.9. Drying out of Leaf Powder Layer.

Finally, it was decided that an extra application of 20 µl just before recommencing the test after the particle application pause could limit the dehydration of the leaf powder layer. The data from these test runs has been included in Figure 5.10, here the traction does not see any difference between initial application and after a 3 minute pause. The level of adhesion from these runs can be characterised as ultra-low (coefficient of traction <0.05).

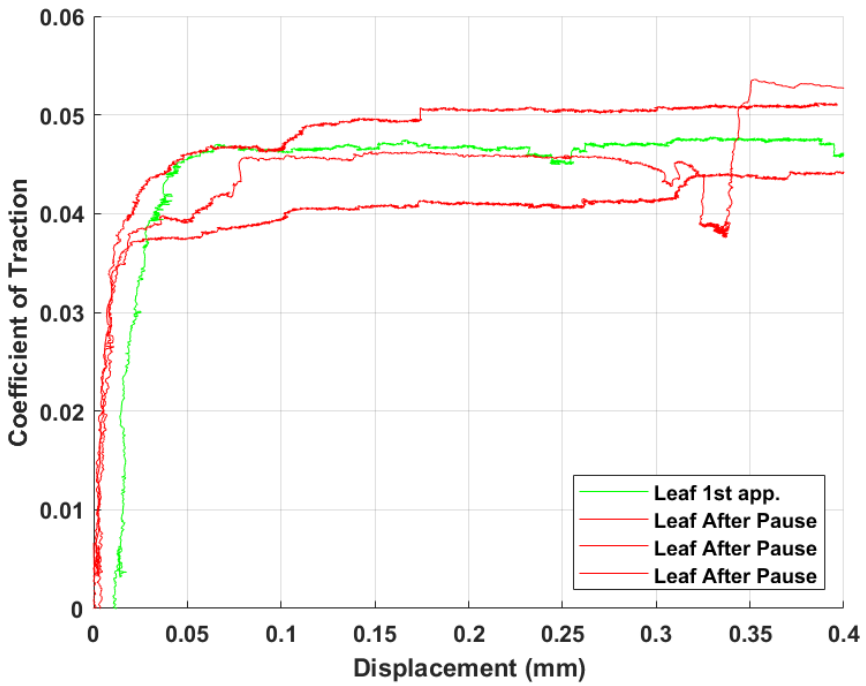

Figure 5.10. Example of HPT Data from Leaf Powder where an Extra 20 µl of Distilled Water was Applied after a 3 Minute Pause.

The difference the extra application of distilled water made can also be seen in the leaf powder layer itself. Figure 5.11 shows the specimens after testing with two 20 µl applications of distilled water and 0.025 g of leaf powder. The characteristic black leaf layer is present and its removal from the surface was very difficult, showing some degree of bonding with the specimen surfaces.

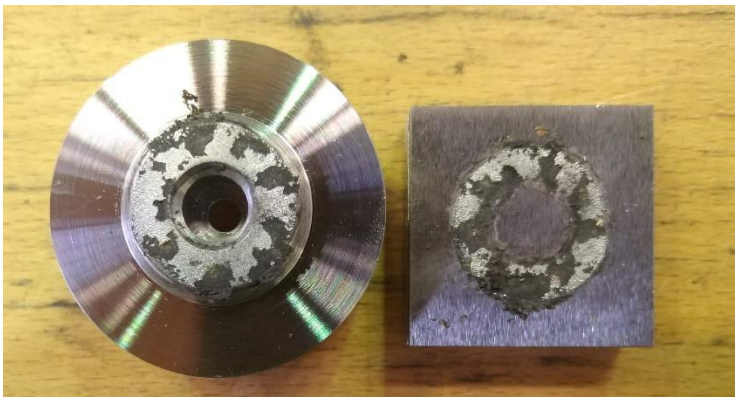

Figure 5.11. Characteristic Black Leaf Layer.

This final method for generating a leaf layer was utilised in all further testing with a leaf layer present. That there is an actual solid layer, as opposed to a liquid layer, is more realistic to actual leaf layers found on track and is more relevant for testing with granular material as their effect on leaf layer removal can be assessed.

5.2.4 Third Body Application

Particles were applied to the contact by hand, ensuring an even spread throughout the annular contact. A typical example of sand placement in dry conditions is included in Figure 5.12.

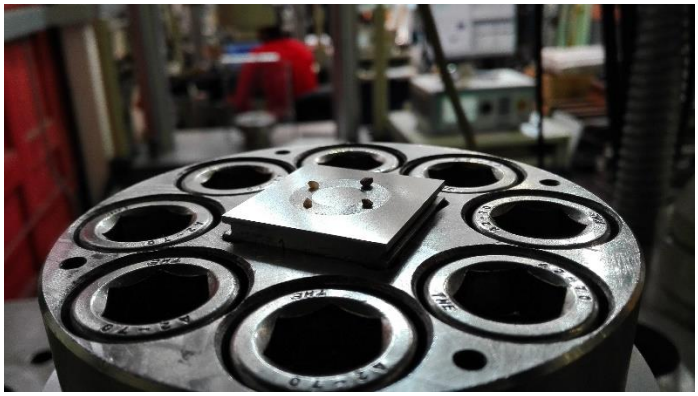

Figure 5.12. Example of Sand Placement.

For all tests with particles present in the contact, 0.025 g of material was used. This amount was selected as the sand concentration in the contact would be equal to 0.15 kg/m^2, or the maximum allowable sand concentration for British railways [10], [53].

For tests conducted under wet conditions, 20 µl of distilled water was pipetted into the contact with care taken to ensure an even spread in the contact. When both water and particles were applied, the particles were applied first in the manner shown in Figure 5.12 and the water applied afterwards.

For tests conducted with a leaf layer present, 0.025 g of sycamore leaf powder was applied to the contact, ensuring an even spread. This powder was then wetted with 20 µl of distilled water using a pipette. One test run was then performed to condition the layer. After this conditioning run another 20 µl of distilled water was pipetted onto the contact. For leaf tests with particles present, the particles were applied after the conditioning run and before the second application of 20 µl of distilled water.

5.2.5 HPT Test Parameters

The parameters used for run-in sequences have been included in Table 5.1. Tests were performed at 0°, 30°, & -30°, with two oscillations at each angle. A “loose” PID tuning was incorporated here because this has previously been shown to effectively condition the surfaces and it was much quicker than using “tight” PID tuning.

Table 5.1. Run-in Parameters.

Parameters		Value
Contact Pressure (MPa)		900
Sweep Rate (°/s)		0.1
Oscillation End Conditions	Max Sweep Length (mm)	0.2
	Max Torque (Nm)	950
	Slip Detected	N/A
PID Loop	Proportional Term	0
	Integral Term	0.1
	Derivative Term	0

The parameters used for HPT test runs have been included in Table 5.2. Unless otherwise stated, these parameters were used for all tests. Here the PID loop is tuned for the revised test method discussed in sub-chapter 5.2.2.

Table 5.2. HPT Test Parameters.

Parameter		Value
Contact Pressure		900 MPa
Sweep Length		0.4 mm
Sweep Rate		0.02 °/s
Test Progression		10°
PID Loop	Proportional Term	5
	Integral Term	0.3
	Derivative Term	0

5.2.6 Post-Processing of HPT Data

The HPT data included in this chapter was post-processed, firstly by isolating each test run i.e. from test start point to reaching test finish point. Coefficient of traction was then calculated from dividing the tangential force (torque at the effective radius of friction(see Evans et al. [145])) by the axial force. Displacement was adjusted to account for a rig stiffness of 0.0005 °/Nm (see Evans for calculation [144]).

For the sake of clarity runs under the same conditions were averaged; where further analysis was undertaken each individual run was used instead. The traction data includes two or three runs for each condition which have been interpolated and averaged for every 0.0001 mm, and the data has been plotted with error bars denoting one standard deviation above and below every 200th data point for the sake of clarity. Unless otherwise stated the runs that are being plotted are the initial test run after surface conditioning/material application.

5.2.7 Post-Test Surface Analysis

Roughness measurements of the tested surfaces were taken using the Alicona InfiniteFocusSL 3D optical profilometer and analysed using built-in software. Two scans were taken for each tested wheel and rail specimen at the end of all test runs. Each 3D scan was taken over a 3.66 × 3.66 mm^2 area with a vertical resolution of 500 nm, though it should be noted that when this was not possible (e.g. due to immovable contamination), a smaller area was used to obtain measurements. The measure of roughness used in this paper was the RMS height, S_q, from a reference plane (calculated from a default function of the software). The roughnesses (S_q) of the pre-test specimens were 2.57 ± 0.20 µm for the wheel specimen and 2.43 ± 0.13 µm for the rail specimen.

For presentation purposes, RMS height, S_q, was calculated for each set of test specimens and averaged over repeat runs, with the standard deviation included as

an error bar. Where further analysis is undertaken individual measurements were used.

5.3 Results

The HPT results included in this sub-chapter are organised into five categories, that each review the test results for when the following particles were applied into three contact conditions (dry, wet, leaf powder):

- No particles;
- Rail sand particles;
- Other particles;
- Glass Beads of varying sizes;
- LB rail sand with varying contact pressures.

For each, the traction data and the post-test surface analysis is included.

5.3.1 Unsanded[4] Tests

The following section includes traction data and surface analysis for the case where no particles were applied to the contact and three different contact conditions were analysed:

- Dry, no material applied;
- Wet, 20 µl of distilled water applied;
- Leaf powder, 0.025 g of sycamore leaf powder with 20 µl of distilled water applied twice, before and after one further conditioning run.

5.3.1.1 Traction Data

The traction data for conditions where no adhesion materials are present in the HPT contact ("Unsanded") is included in Figure 5.13, where error bars denoting one standard deviation either side are plotted for every 200 points for the purposes of clarity. This style of plotting HPT data is used throughout the chapter.

[4] Throughout this thesis the term "unsanded" refers to a contact with no adhesion materials applied i.e. dry, wet, or leaf contaminated contacts. As the process of applying dry particles to the wheel/rail contact is commonly referred to as "sanding" regardless of the exact material being applied.

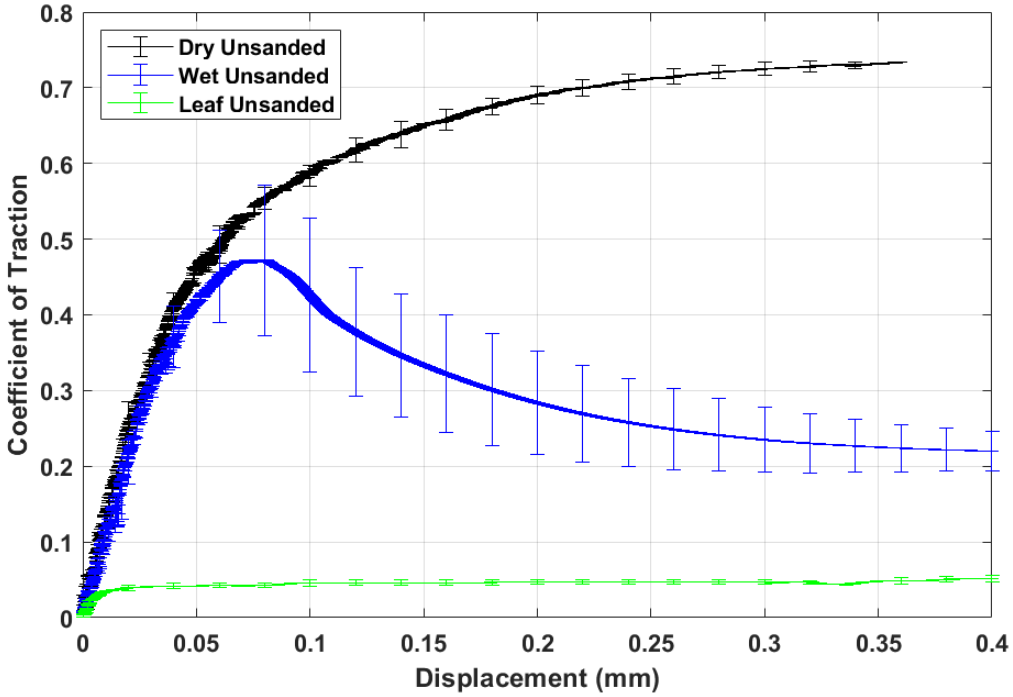

Figure 5.13. HPT Data for Unsanded Contacts with Dry, Wet, and Leaf Contaminated Conditions.

The dry, unsanded coefficient of traction peaked at just above 0.7 and showed relatively little variation across runs. The wet unsanded data shows a similar initial stiffness to the dry unsanded data and its coefficient of traction peaks at just below 0.5 before a gross slip occurs in the contact, reducing shear stress and bringing the coefficient of traction down to just above 0.2; upon gross stick-slip occurring, the variation in measured coefficient of traction for wet unsanded data also increases substantially. The leaf contaminated, unsanded condition exhibited a much lower coefficient of traction peaking at ~0.05, with very little variation in measured data; the initial gradient also appears to be slightly less than the previous unsanded cases.

5.3.1.2 Post-Test Surface Analysis

Photos of select, post-test specimens have been included in Figure 5.14. The dry specimens appear to be shinier than the wet specimens, possibly due to the distilled water present in the latter case more easily retaining wear debris. As previously noted, there is a black layer present in the leaf contaminated condition, though the visible steel underneath seems to be shinier than in the wet case.

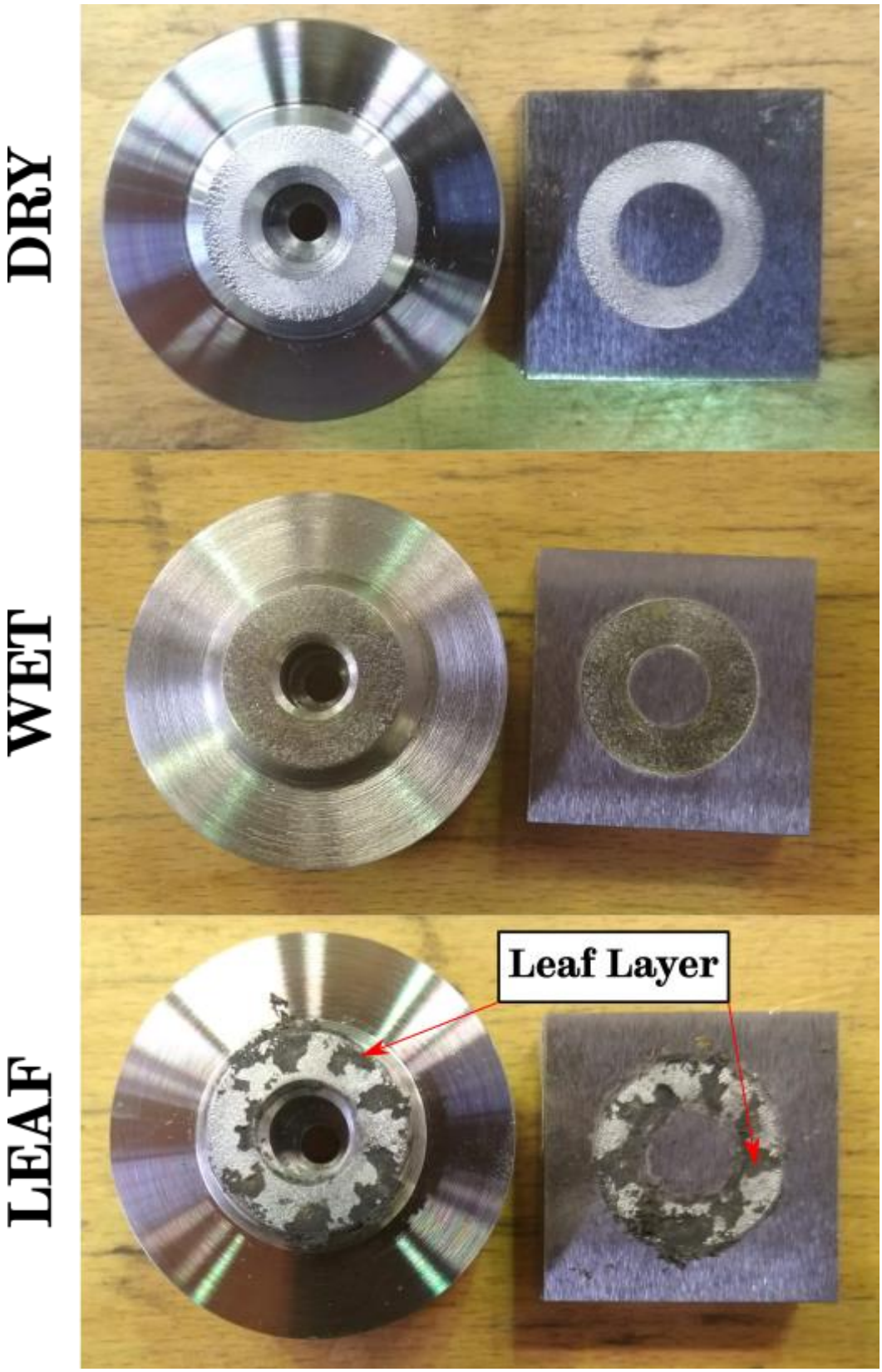

Figure 5.14. Post-test, Unsanded Specimens.

The RMS height, S_q, for each unsanded condition has been included in Figure 5.15, where the error bars represent one standard deviation above and below. For all conditions, S_q was higher on the wheel surface compared to the rail surface. The

measured S_q was highest for the dry unsanded case, being ~8 µm and ~10 µm for the rail and wheel specimen respectively. The wet unsanded case saw both rail and wheel S_q measured at between 3-4 µm, less than half the measured roughness in the dry unsanded case. Lastly, the leaf contaminated case was somewhere in between, with a measured S_q between 5.5-6.5 µm for both rail and wheel specimens.

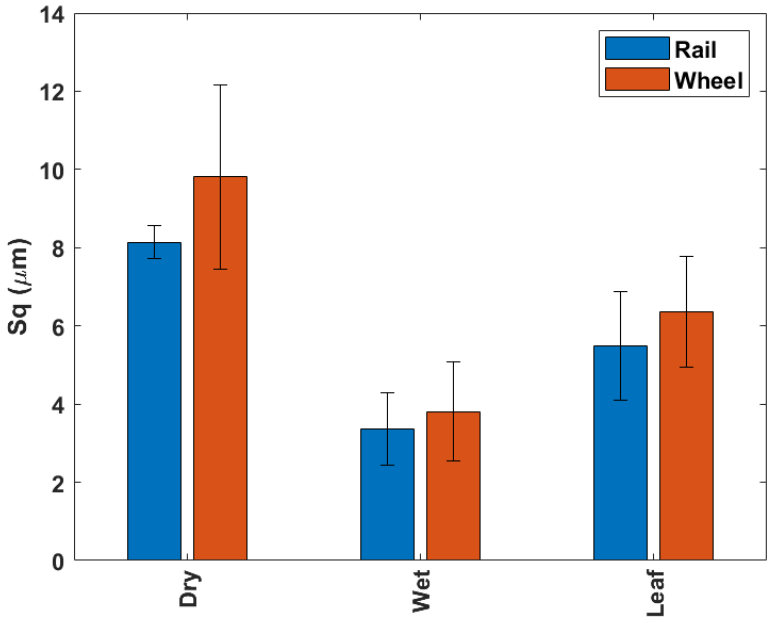

Figure 5.15. Post-Test Surface Roughness Measurements for Unsanded Test Contacts.

Example surface scans for all three unsanded conditions have been included in Figure 5.16. The scans corroborate the measurements presented in Figure 5.15, with the dry scans showing greater changes in height than both wet and leaf contaminated scans. In the leaf contaminated scans the areas where a leaf layer was still present are noticeable due to their pronounced height.

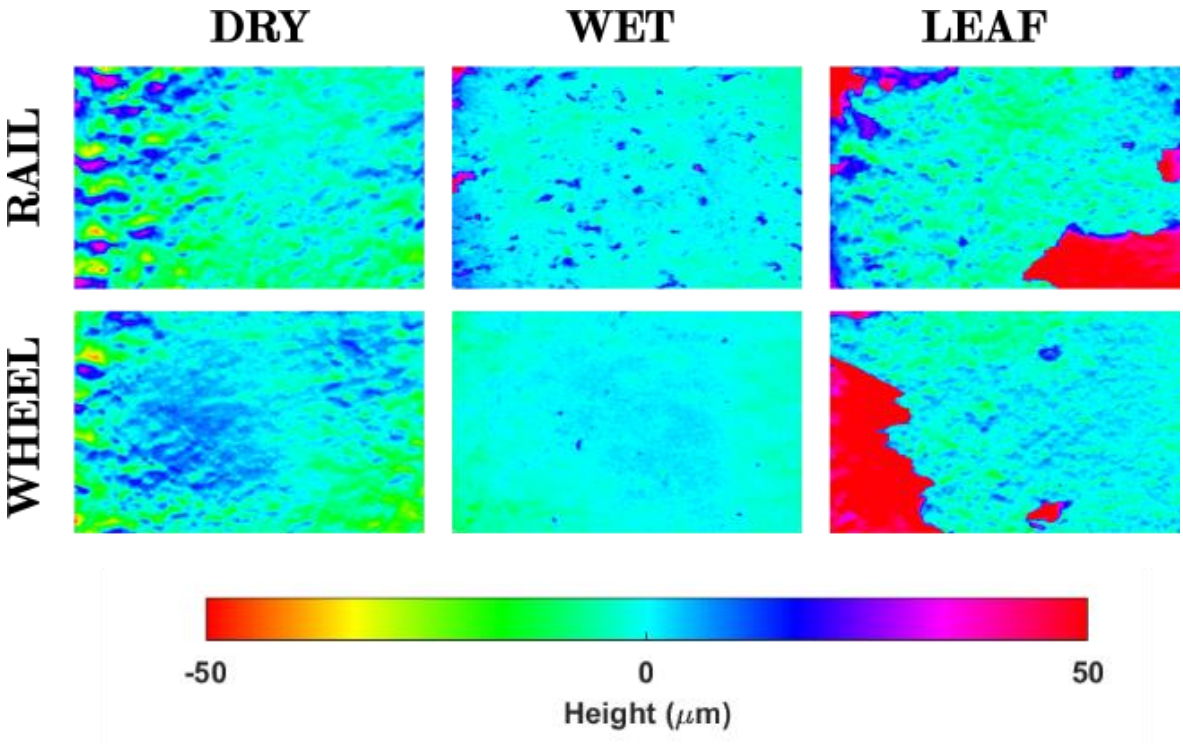

Figure 5.16. Post-test Surface Scans of Unsanded Surfaces.

5.3.2 Rail Sand Tests

The following section includes traction data and post-test surface analysis for the various rail sands outlined in sub-chapter 4.1.3. All rail sands were tested in dry, wet and leaf contaminated conditions in accordance with the application methods set out in sub-chapter 5.2.4. Two or three tests were run for each contact condition to assess result variance.

5.3.2.1 Dry Conditions

5.3.2.1.1 Traction Data

Traction data for all rail sands in dry conditions has been included in Figure 5.17. All sands recorded a peak coefficient of traction between 0.59-0.76, well above the threshold for low adhesion (<0.2). Most sands acted similarly to the dry unsanded case, with similar initial stiffnesses, reaching a coefficient of traction ~0.7, and showing little variance, though there were some exceptions. The initial gradient of FI was similar to most other rail sands, but behaved differently after entering the PPR, the coefficient of traction was relatively lower at this point and the variance increased. AT also acted differently, exhibiting a lower initial gradient, reaching a much lower peak CoT of 0.59, and showing a greater variance.

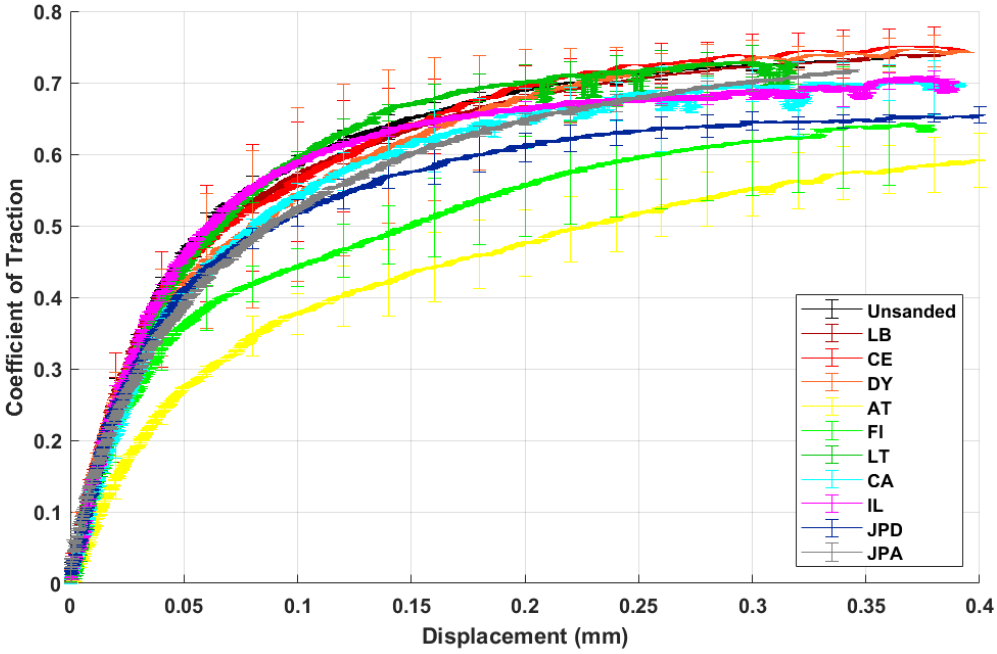

Figure 5.17. HPT Traction Data for Dry Conditions with Rail Sands applied.

5.3.2.1.2 Post-Test Surface Analysis

Photos of some of the specimen surfaces post-test have been included in Figure 5.18. Most specimens appear to have very little material remaining in the contact as the grains were expelled out of the contact upon crushing; what does remain appears to be spread out throughout the contact. However, AT, FI, and JPA all show remaining material after the test; the remaining material appears to have remained in a clump of material. These sands also tended to show lower coefficients of traction, as seen in Figure 5.17.

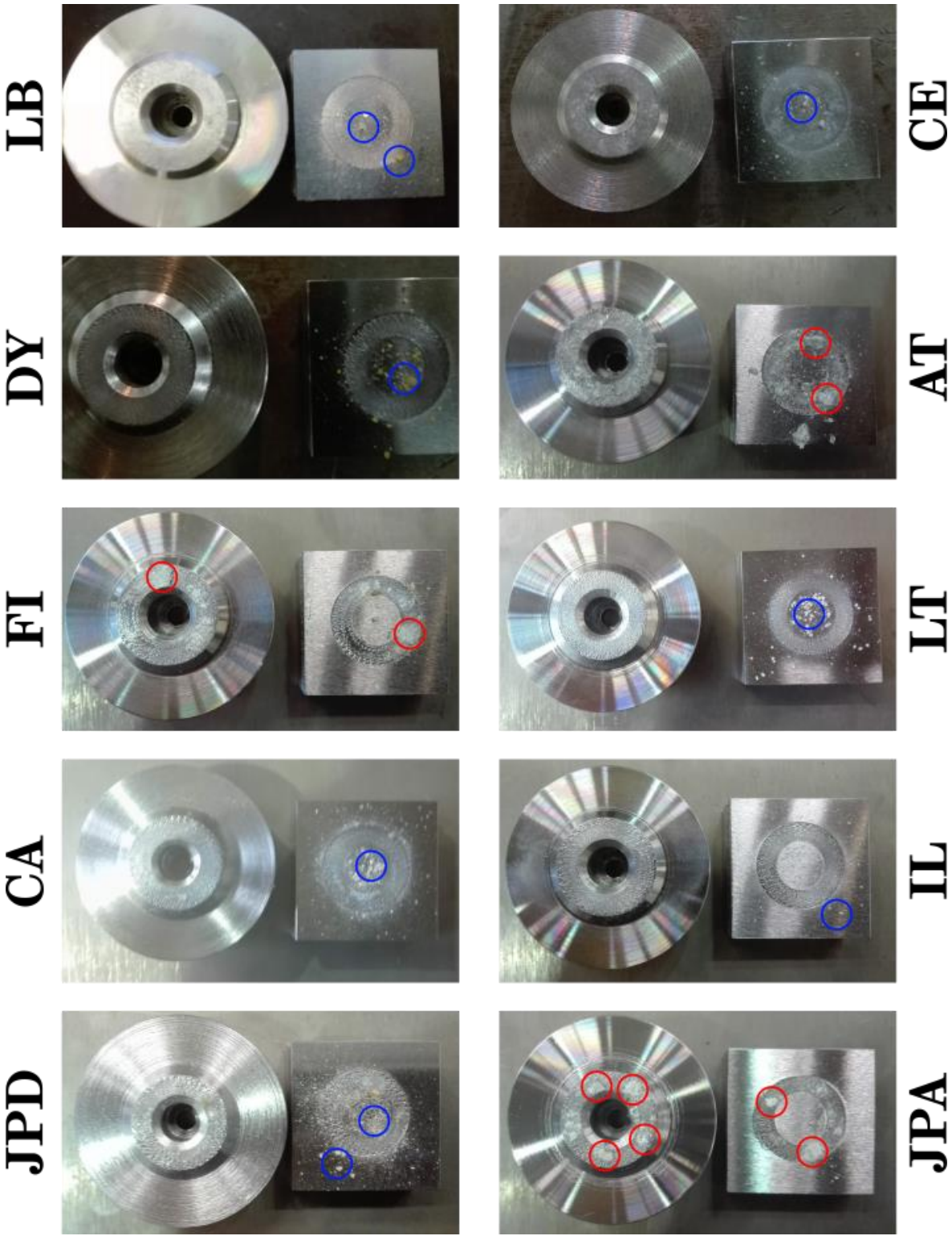

Figure 5.18. Post-test Specimens with Rail Sands applied in Dry Conditions. Red Circles denote Areas with Clumps of Material Remaining in the Contact, Blue Circles denote Areas with Scattered Material expelled from the Contact.

Measurements of S_q from all aforementioned tests have been included in Figure 5.19. In most cases the average roughness of the wheel was greater than for the rail, though this was the opposite for IL and JPD, though in the case of the former there was only a marginal difference; a similar trend will be commonly observed

throughout this chapter and can be attributed to the wheel surface being softer (1.9 GPa) than the rail surface (2.9 GPa) [22]. All sanded contacts showed greater or similar average roughness values compared to the unsanded contact. Sanded cases also seemed to exhibit a much greater variance in measured roughness values compared to the unsanded case.

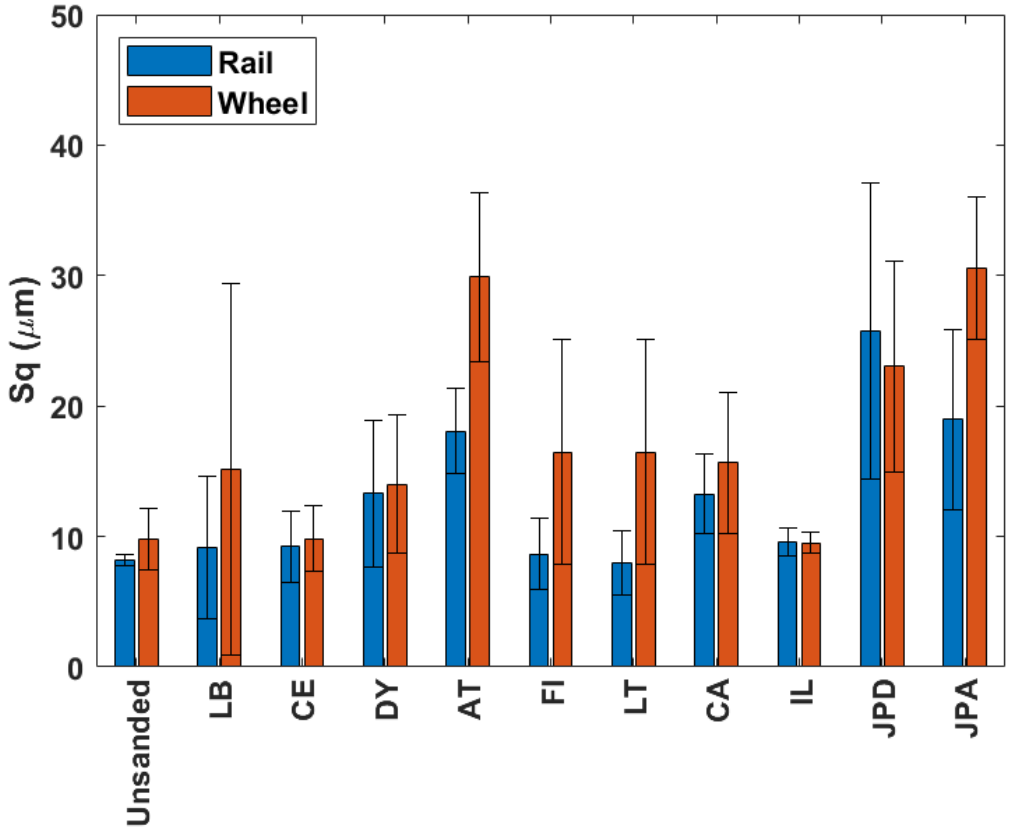

Figure 5.19. Post-Test Surface Roughness Measurements for Test Contacts with Rail Sands applied in Dry Conditions.

Some scans of the specimen surfaces have been included in Figure 5.20. For some rail sands large indentations can be seen, especially AT and JPD; these sands also retained a lot more material in the contact and showed a high post-test roughness. In comparison, IL exhibited a similar wear pattern and average roughness to the unsanded case and retained little to no material post-test.

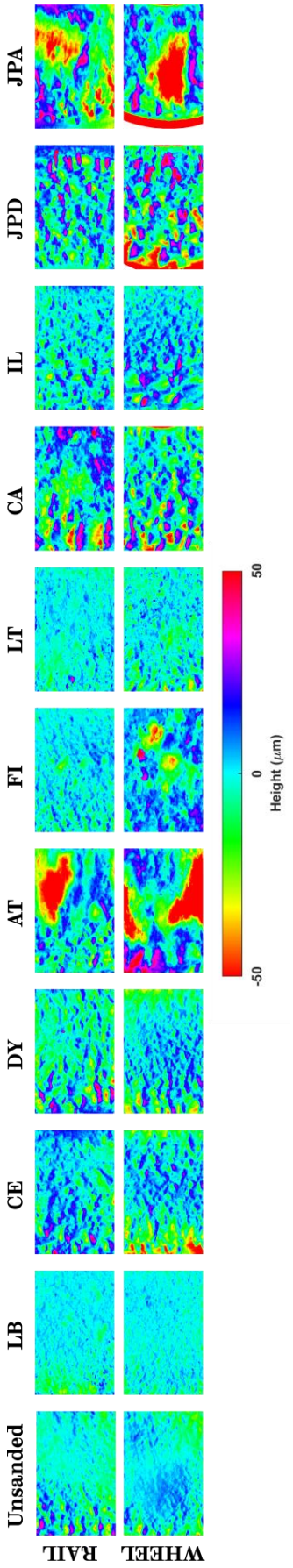

Figure 5.20. Post-test Surface Scans of Dry Contacts with Rail Sands applied.

5.3.2.2 Wet Conditions

5.3.2.2.1 Traction Data

Traction data for all rail sands in wet conditions has been included in Figure 5.21. All sands produced a greater peak CoT compared to the unsanded case, ranging from 0.5-0.64, all well above the minimum permissible threshold for adhesion level. The rail sands also did not exhibit the sudden drop in CoT that the unsanded case undergoes, inferring that a gross stick-slip event did not occur. There was a greater variance in initial stiffnesses of the ER for the rail sands when compared to dry conditions. As for the dry case, AT returned the lowest peak CoT and showed lower stiffness and greater relative variance in the PPR compared to other rail sands.

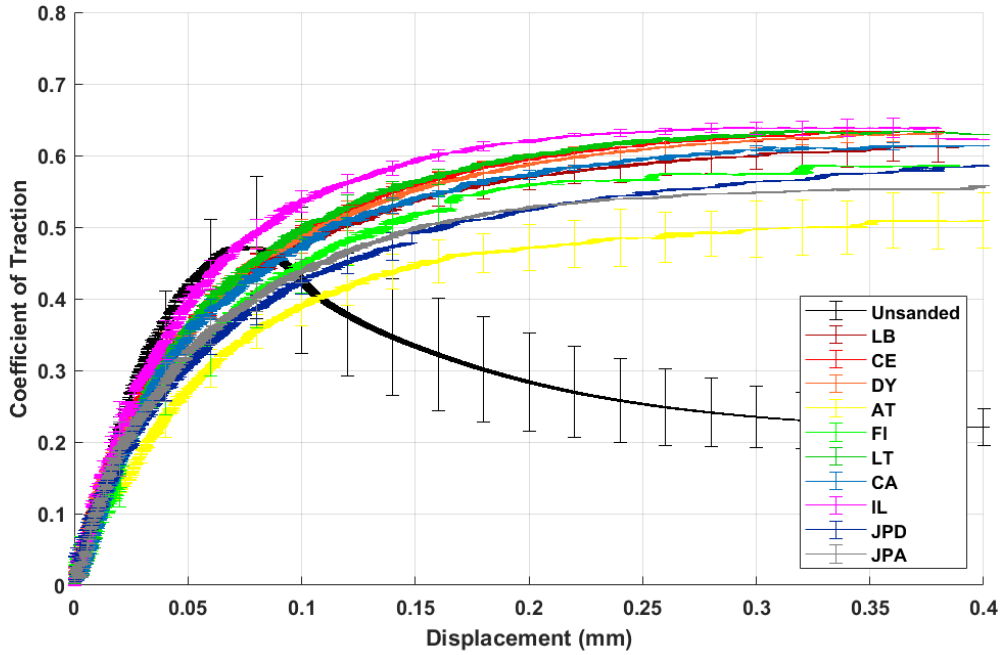

Figure 5.21. HPT Traction Data for Wet Conditions with Rail Sands applied.

5.3.2.2.2 Post-Test Surface Analysis

Some pictures of post-test wheel and rail specimens have been included in Figure 5.22. For all rail sands there appears to be a visible amount of material remaining in the contact, unlike the dry conditions; the remaining material appears to form clumps of crushed particles within the contact.

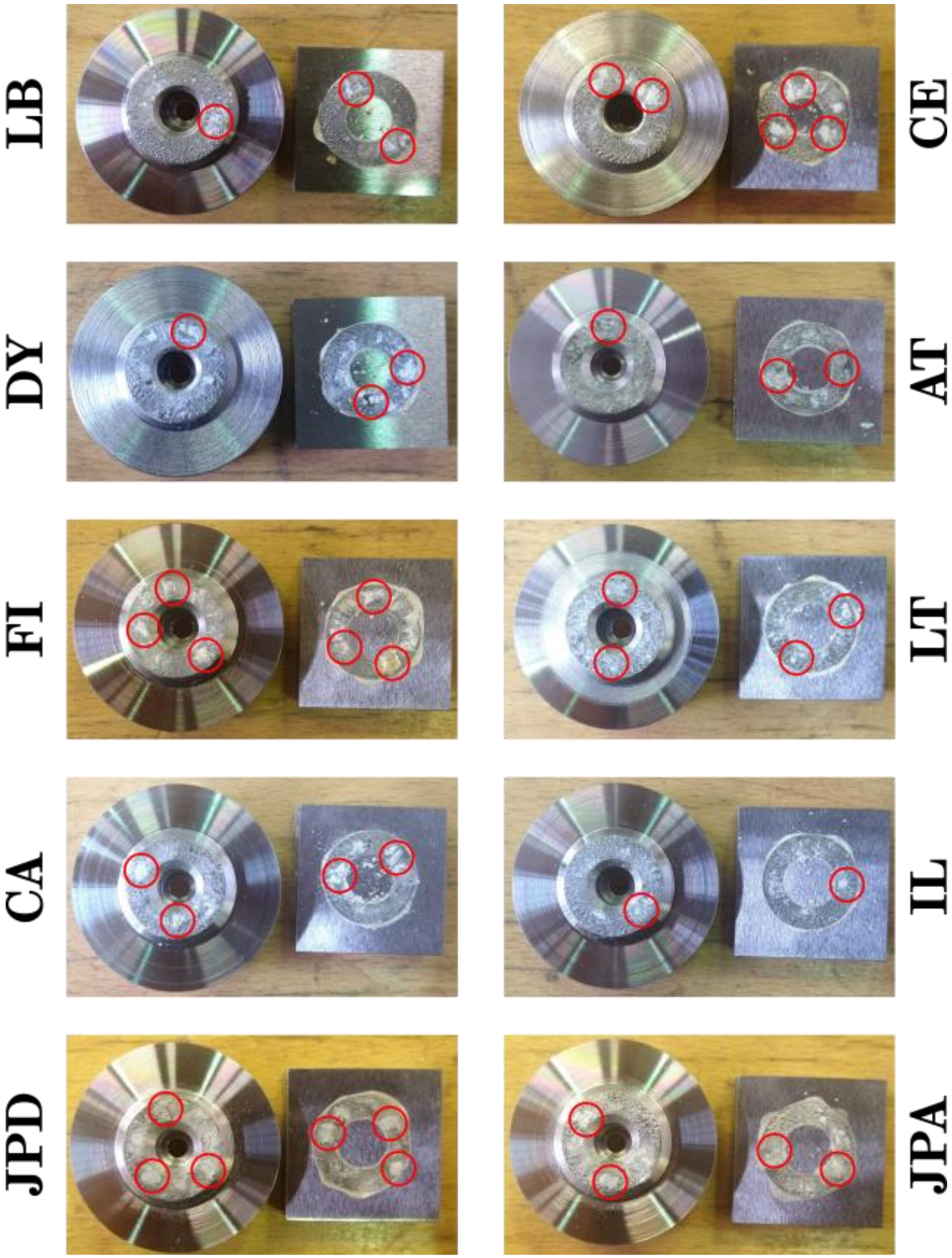

Figure 5.22. Post-test Specimens with Rail Sands applied in Wet Conditions with Remaining Material encircled.

Post-test measurements of surface roughness have been included in Figure 5.23. In all cases, unsanded and sanded, the wheel specimen was rougher than the rail specimen. All sanded cases showed considerably greater roughness compared to the sanded case.

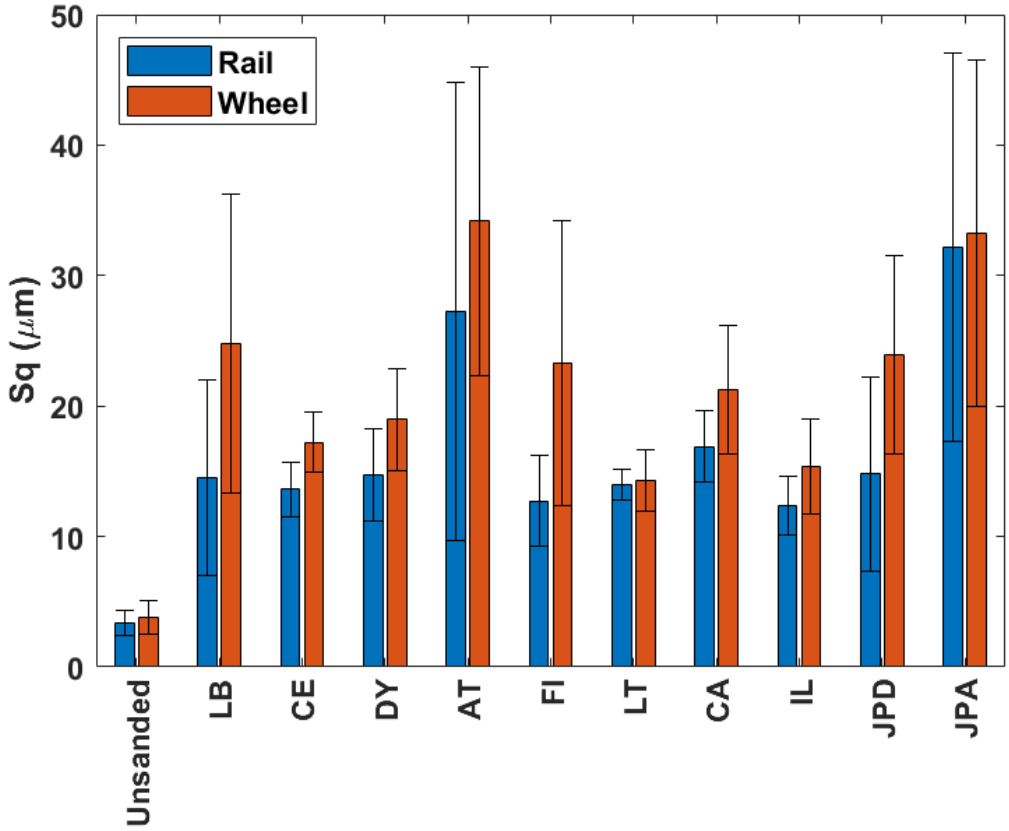

Figure 5.23. Post-Test Surface Roughness Measurements for Test Contacts with Rail Sands applied in Wet Conditions.

Post-test surface scans of both wheel and rail specimens have been included in Figure 5.24. All sanded cases appear to have much greater variations in height compared to the unsanded case. The sands with the largest indentations appear to be AT & JPA, this was the case for the dry contact also.

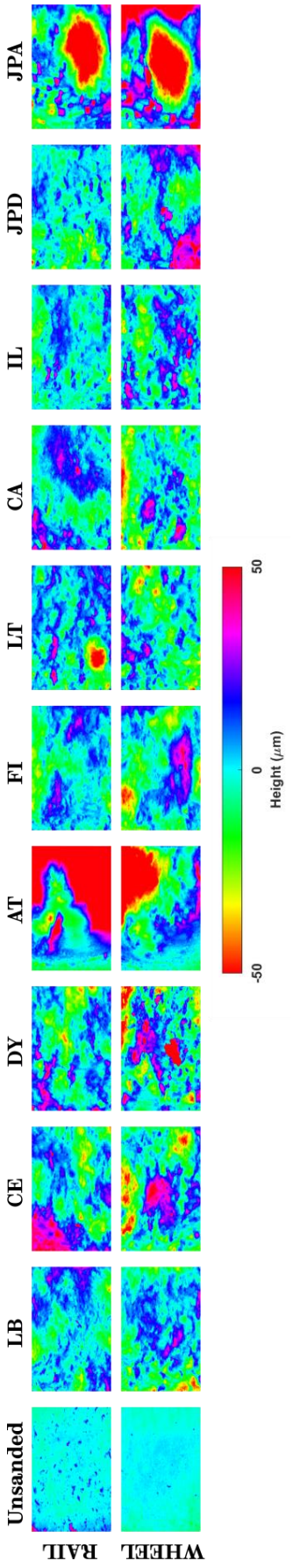

Figure 5.24. Post-test Surface Scans of Wet Contacts with Rail Sands applied.

5.3.2.3 Leaf Contaminated Conditions

5.3.2.3.1 Traction Data

The traction data for all rail sands in leaf contaminated conditions has been included in Figure 5.25. All rail sands increased the CoT in the contact compared to the unsanded case, with the increase being sufficient to get above the minimum level of adhesion needed for braking (0.09). though the CoT did not get above 0.2 for any rail sand, the minimum adhesion level needed for acceleration [2]. For all rail sands peak CoT ranged between 0.11-0.17. Unlike the previous dry and wet conditions, AT did not exhibit the lowest CoT, instead JPA gave the lowest peak CoT.

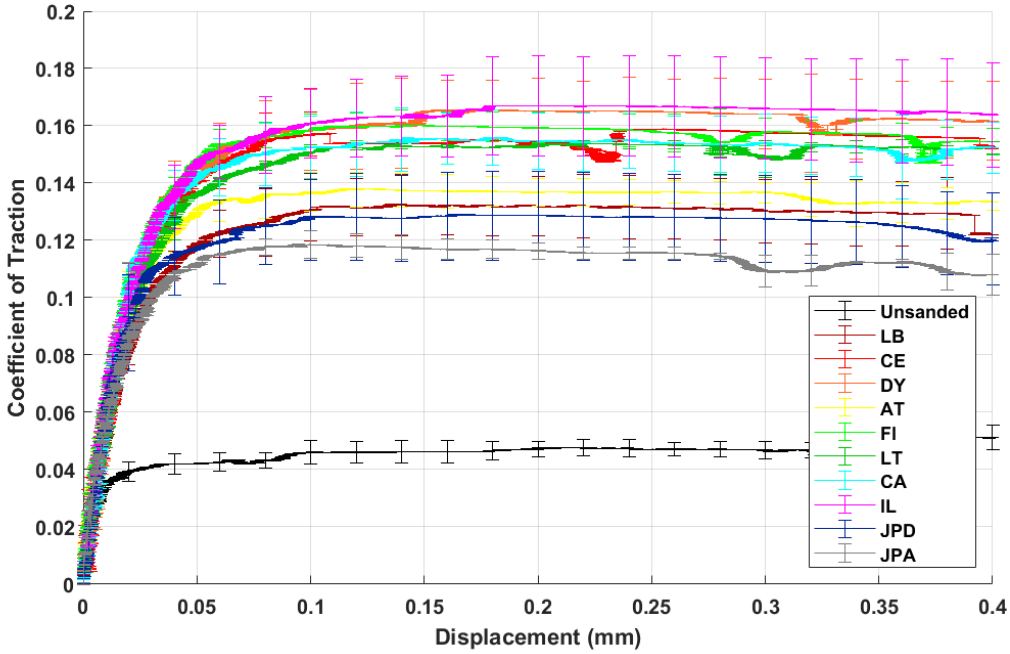

Figure 5.25. HPT Traction Data for Leaf Contaminated Conditions with Rail Sands applied.

5.3.2.3.2 Post-Test Surface Analysis

Some pictures of specimen surfaces have been included in Figure 5.26. In all cases some amount of black leaf layer remains, though there is also remaining sand material. In some cases, the remaining sand has been embedded into the leaf layer. These areas are marked in Figure 5.26 for clarity, where specks of white can be seen amongst the leaf layer.

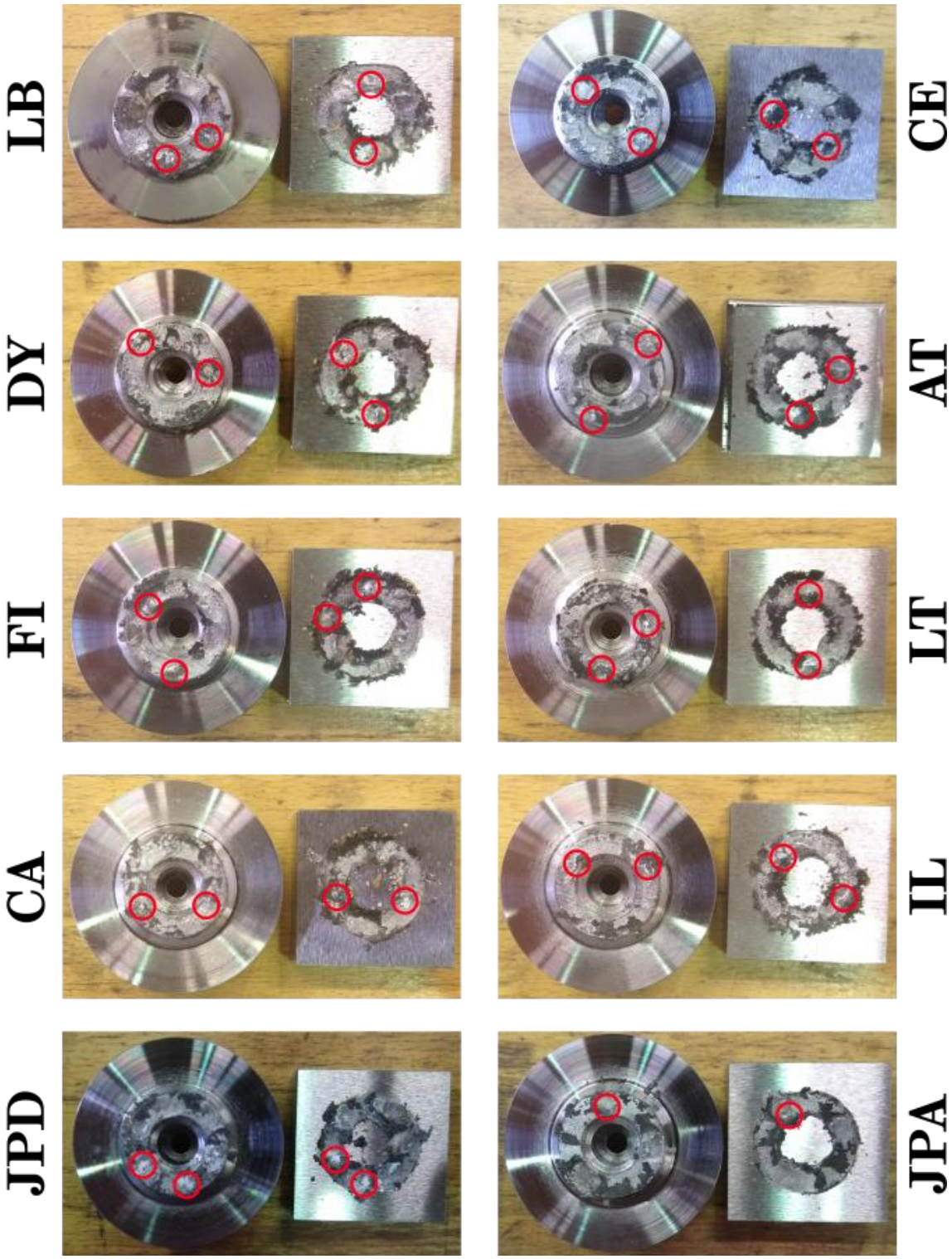

Figure 5.26. Post-test Specimens with Rail Sands applied in Leaf Contaminated Conditions with Remaining Material encircled.

Roughness measurements, featured in Figure 5.27, show that roughness was significantly higher for the sanded contacts compared to the unsanded contact. As for dry and wet conditions, the wheel specimens are mostly rougher than the rail specimens, CE and IL are the opposite, but are still relatively close.

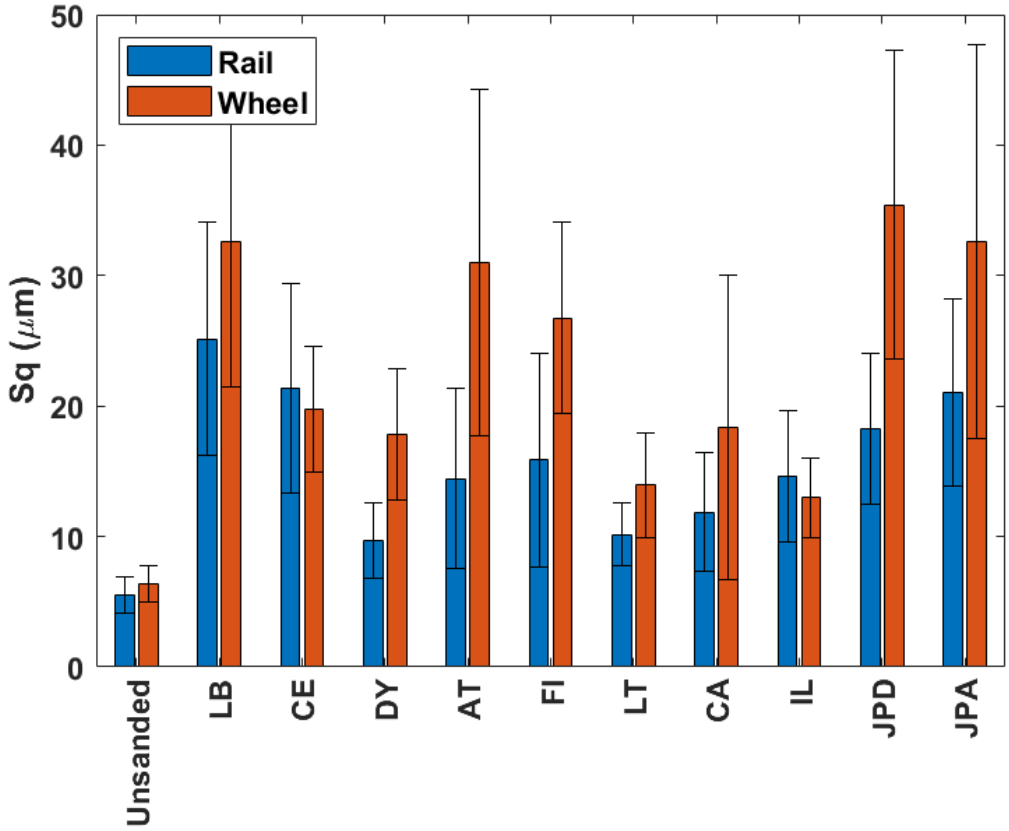

Figure 5.27. Post-Test Surface Roughness Measurements for Test Contacts with Rail Sands applied in Leaf Contaminated Conditions.

Surface scans of the unsanded and sanded contacts have been included in Figure 5.28, remaining leaf layer is distinguishable from the specimen surface as it exhibits a steep jump in measured surface height. All sanded scans show a greater variation in height compared to the unsanded scan, with many sands exhibiting large indentations on their surfaces.

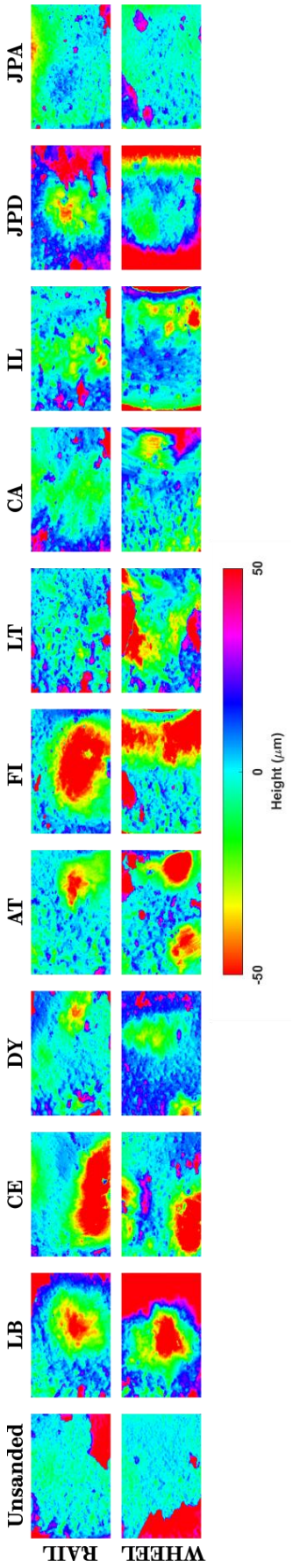

Figure 5.28. Post-test Surface Scans of Leaf Contaminated Contacts with Rail Sands applied.

5.3.2.4 Discussion

For all conditions, there was not a large amount of variance between the traction restoring performance of the different rail sands. However, in dry and wet conditions, AT stood out as producing the lowest peak CoT; in leaf contaminated contacts this was not apparent though some particles produced notably lower adhesion than others. This range of rail sand performances suggests that differences between the characteristics of the rail sand may impact their efficacy at increasing traction in the HPT contact.

Testing with rail sands, has shown that a link between particle characteristics, traction performance, and surface damage is extant. This link will be need to be investigated across all tested particles.

5.3.2.4.1 Particle Retention

In dry conditions, the amount of remaining sand seemed to play a large part in both the traction performance and the post-test surface. There did appear to be less remaining material, when compared to wet and leaf contaminated conditions, possibly due to crushed material being free to be expelled from the contact, as demonstrated in Figure 5.29.

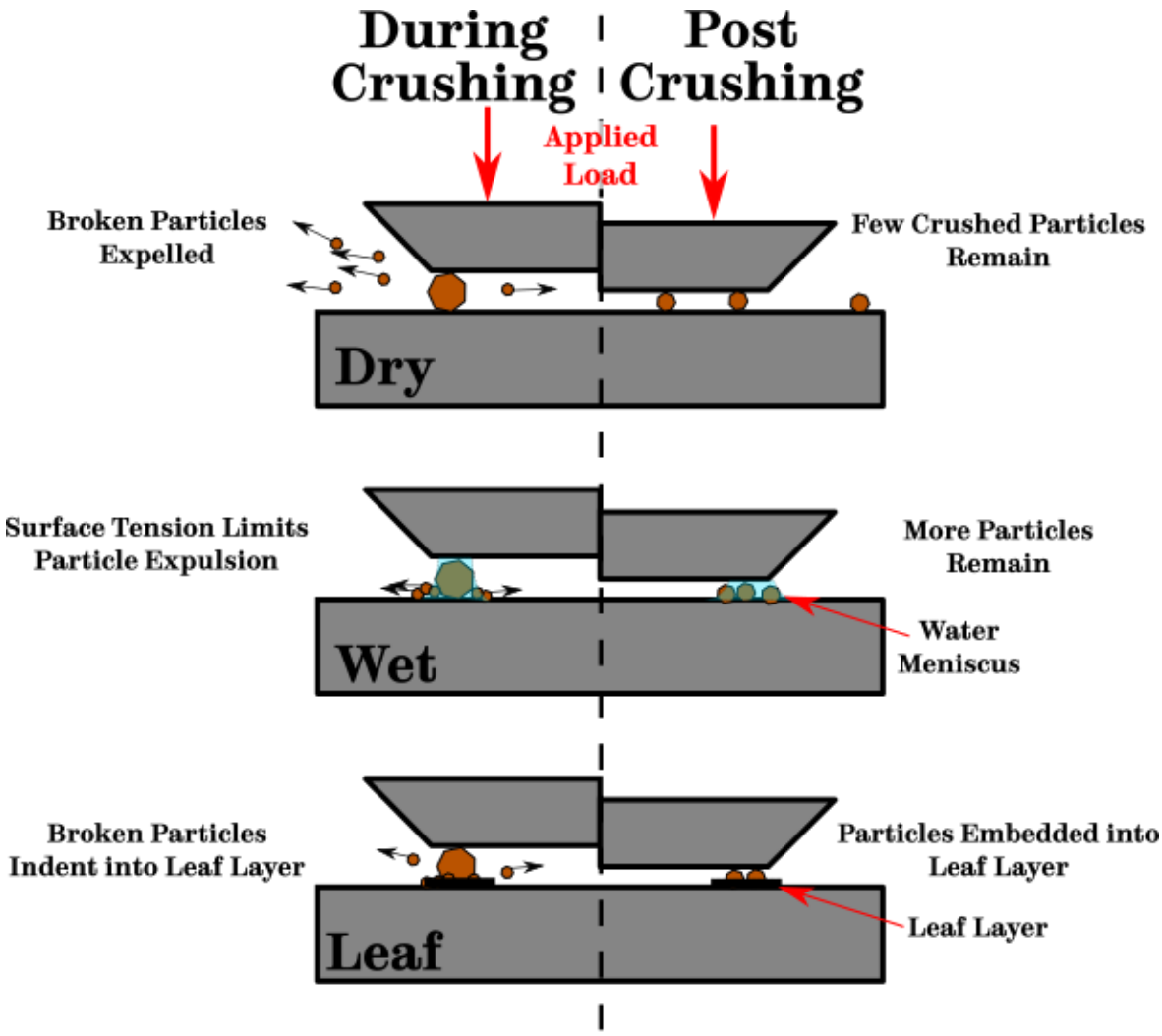

Figure 5.29. Schematic of Particle Entrainment upon Crushing.

Those sands where noticeable amounts material of material remained at the end of the test, also tended to exhibit lower traction data and greater surface damage. This indicates that in dry conditions remaining sand particles have the capacity to act as a dry lubricant layer, similar conclusions were arrived at in twin-disc work by Arias-Cuevas et al. [20].

In wet conditions, all sands appeared to have an amount of material remaining in the contact post-test, due to the surface tension of the water retaining particles, as represented in Figure 5.29. Therefore, any differences in traction performance and surface characteristics cannot be attributed to the mere presence of rail sand alone and must be dependent on the effect of the particles when in the contact.

When material was retained in the contact, it tended to clump together; this was especially noticeable in wet conditions. This clumping in wet conditions may be due to the surface tension of the water keeping the particles more cohesive as they

crush down. The inference of this is that the crushed particles retain some of their initial size, such as shown in Figure 5.30.

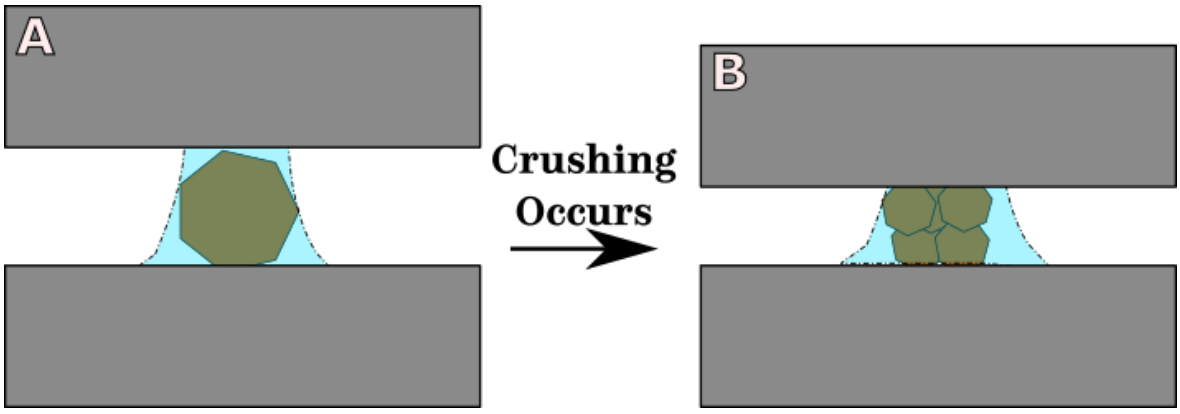

Figure 5.30. Clumping of Particles in Wet Conditions: *(a)* Pre-Crushing; *(b)* Post-Crushing.

5.3.2.4.2 Quartz vs Non-Quartz Particles in Dry & Wet Conditions

In both dry and wet conditions, those particles which were non-pure quartz seemed to produce lower traction, with damage appearing more severe with non-pure quartz sand particles. These particles were generally softer, suggesting this property has a strong effect on particle efficacy.

This could be due to harder particles creating deeper indents between the two surfaces, transferring tractive force more effectively and creating greater surface damage. A schematic of how a harder particle may behave in comparison to a softer particle has been included in Figure 5.31. The harder particle (Figure 5.31*(a)*) is able to indent into the specimen surfaces, creating large areas against which the applied force (F_A) acts, creating a couple force (F_P) on the particle, which is then transferred in turn to create a reactive force (F_R). This mechanism can still take place for the softer particle (Figure 5.31*(b)*), however as the particle has indented less into the surfaces, it cannot transfer as much tractive force as the harder particle.

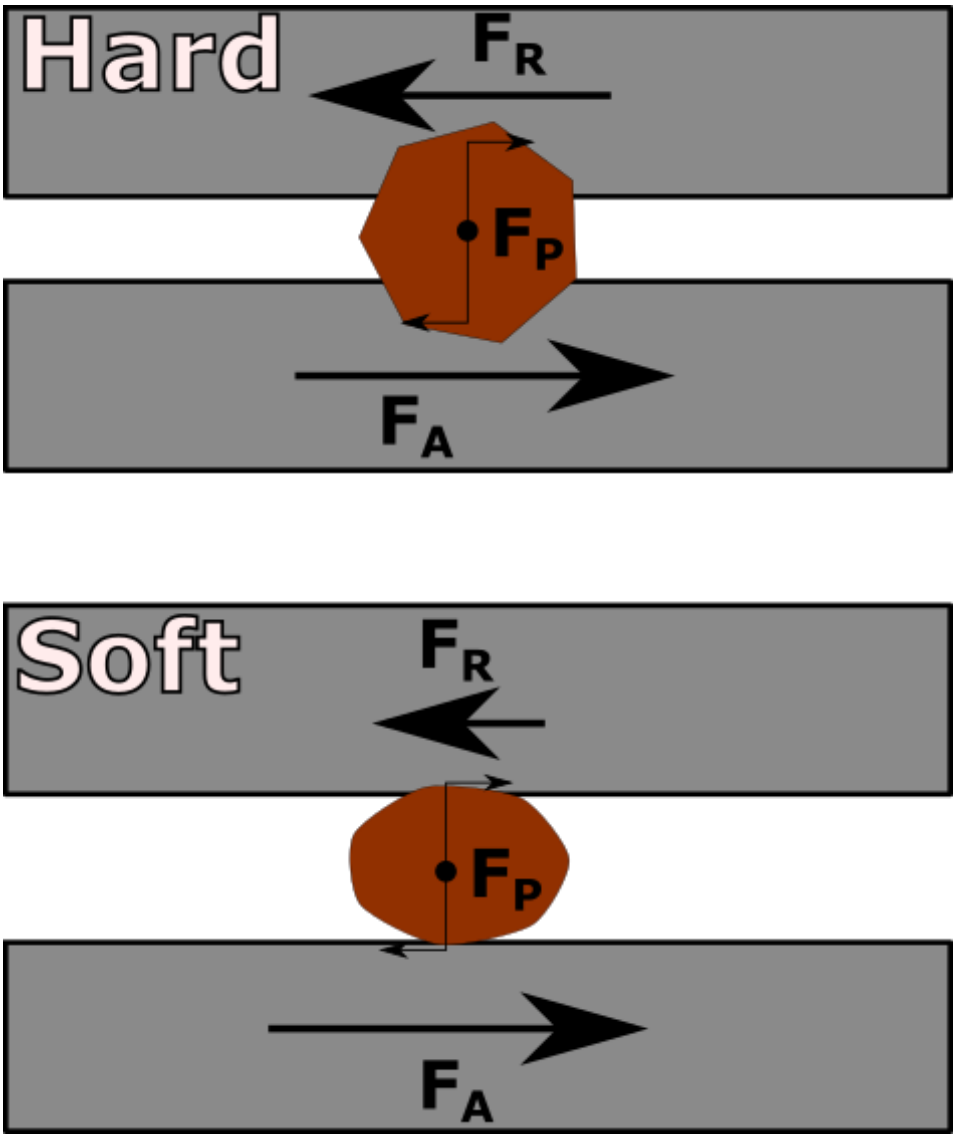

Figure 5.31. Schematic of Two Particle Types in the HPT Contact: *(Top)* Harder Particle; *(Bottom)* Softer Particle.

In dry conditions, these softer particles were seen to reduce traction. In wet conditions. In wet conditions, all particles increased traction compared to the unsanded case as all particles were able to break up the liquid lubricating layer.

5.3.2.4.3 Rail Sands in Leaf Contaminated Contact

In leaf contaminated conditions, material is retained within the contact, with some material indented into the leaf layer itself, in a manner similar to that presented in Figure 5.29. The rail sands producing lower traction data also appeared to cause more surface damage generally, whilst no immediately obvious link between particle characteristics and traction performance and surface damage exists.

The mechanism for how a particle restores traction in a leaf contaminated contact may also be subtly different to the example shown in Figure 5.31*(Top)*. Before the

particle starts to break up under crushing and before it indents into the wheel/rail surfaces, it will indent into the soft leaf layer producing something similar to the examples seen in Figure 5.26.

5.3.3 Tests with Other Particles

The following section includes traction data and post-test surface analysis for the various particles outlined in sub-chapter 4.1.3. These other particles were tested in dry, wet and leaf contaminated conditions in accordance with the application methods set out in sub-chapter 5.2.4. Two or three tests were run for each contact condition to assess result variance.

These other particles have been grouped together as miscellaneous particles not suitable to be grouped among other categories i.e. rail sand. Thus direct comparison is not as appropriate for this category of particles and discussion on these particles will be included only when comparing all tested particles.

5.3.3.1 Dry Conditions

5.3.3.1.1 Traction Data

In Figure 5.32 the traction data for other particles has been presented. Unlike the rail sands, there is a wide range of different behaviours being shown by different particles. AL eventually reaches a similar peak CoT as the unsanded case, but due to a lower initial gradient, it took longer for AL to reach a peak CoT of 0.73. NSS had a similar initial gradient to the unsanded case, but failed to reach a similar peak CoT as the unsanded case, instead peaking at 0.63. DE and ZL behaved very similarly, exhibiting similar initial stiffnesses to one another, though slightly lower stiffness when compared to the unsanded case; they peaked at similar CoTs also, 0.59 and 0.56 respectively. AC and NA also acted fairly similarly, with a much lower gradient and peak CoT compared to the unsanded case, AC peaked at 0.08 and NA at 0.13; both of which can be considered to have caused low adhesion within the contact, in the case of the latter, very low adhesion.

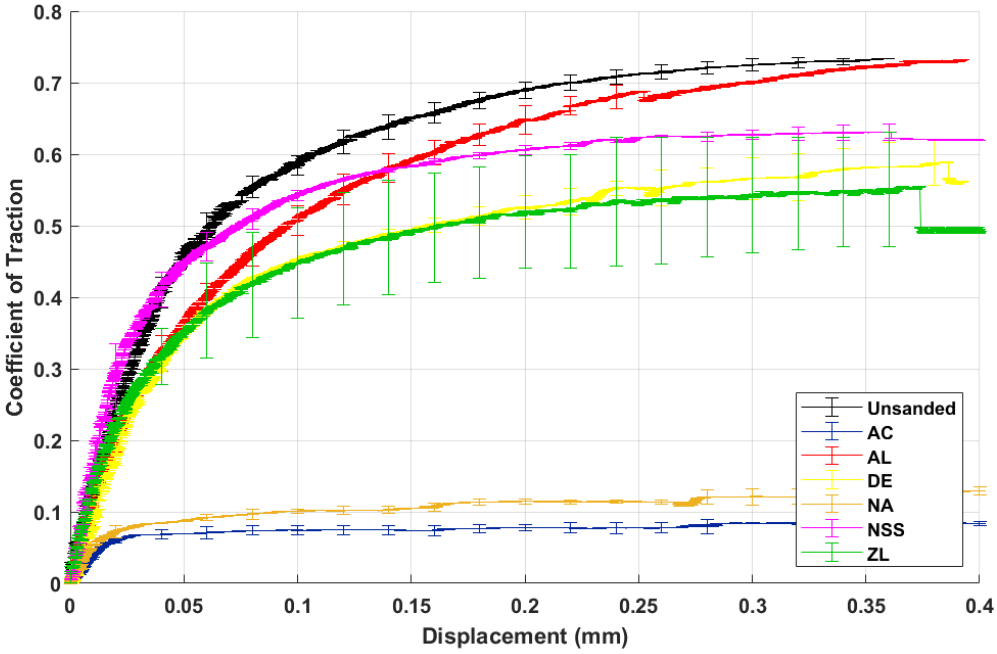

Figure 5.32. HPT Traction Data for Dry Conditions with Other Particles applied.

5.3.3.1.2 Post-Test Surface Analysis

The photos of specimens post-test, included in Figure 5.33 also show how varied the behaviour of the other particles were. AC seems to bunch up together whilst not adhering to the surface. AL was retained in the contact, but compared to sand particles has not clumped up, but spread relatively evenly across the contact. DE and ZI remained in the contact, but in clumps, in a similar way that some rail sands would remain in the contact. NA appears to have been crushed down into a continuous layer around the contact, with the majority of the material being present on the wheel specimen. Some NSS material is visible after the test, it appears to have spread relatively evenly around the contact.

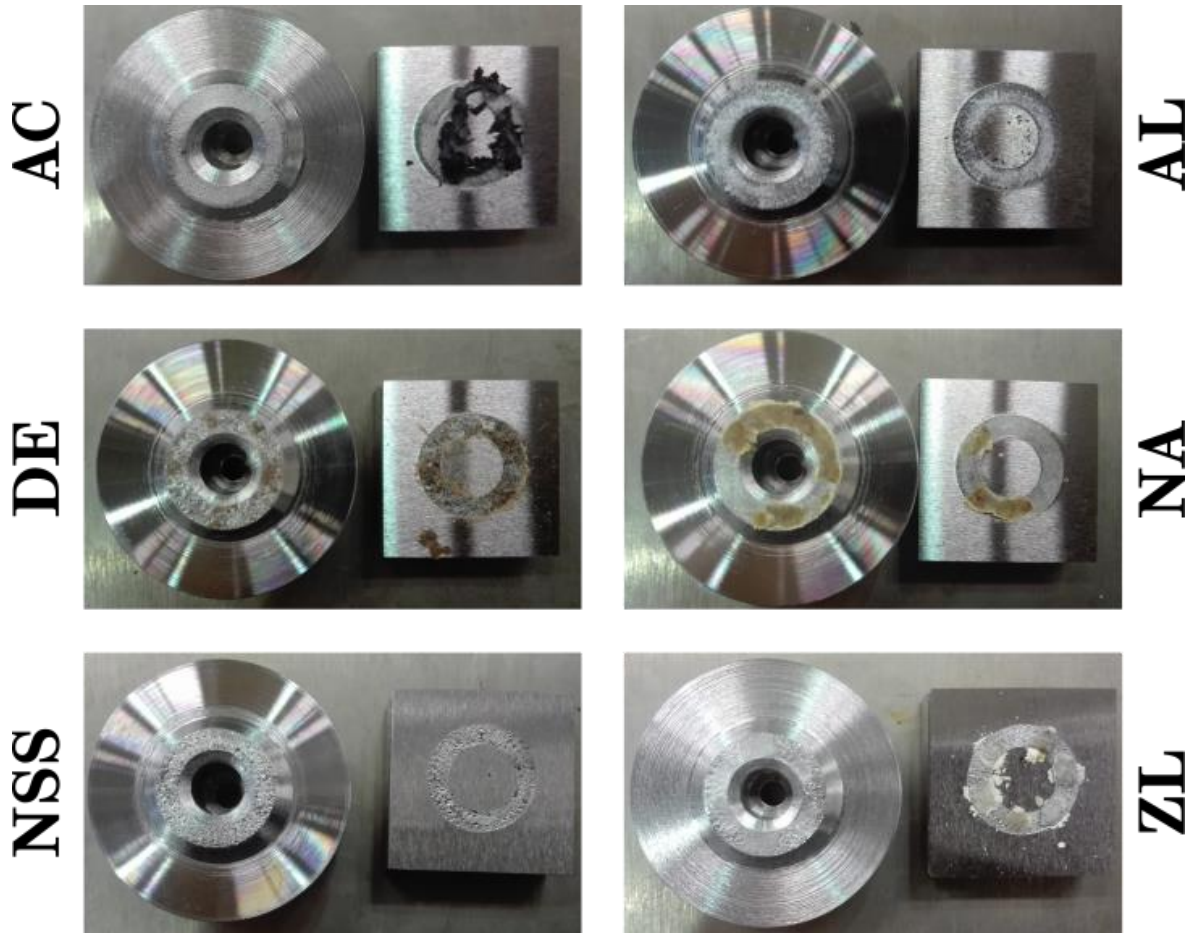

Figure 5.33. Post-test Specimens with Other Particles applied in Dry Conditions.

The S_q measurements have been included in Figure 5.34. In most cases, wheel specimen roughness was higher than rail specimen roughness, DE marginally excepted. AC and NA showed similar surface roughness to the unsanded case, whereas AL, DE, and NSS showed slightly higher roughness values. ZL showed significantly higher roughness than the unsanded case, though the variation in measurement was especially large.

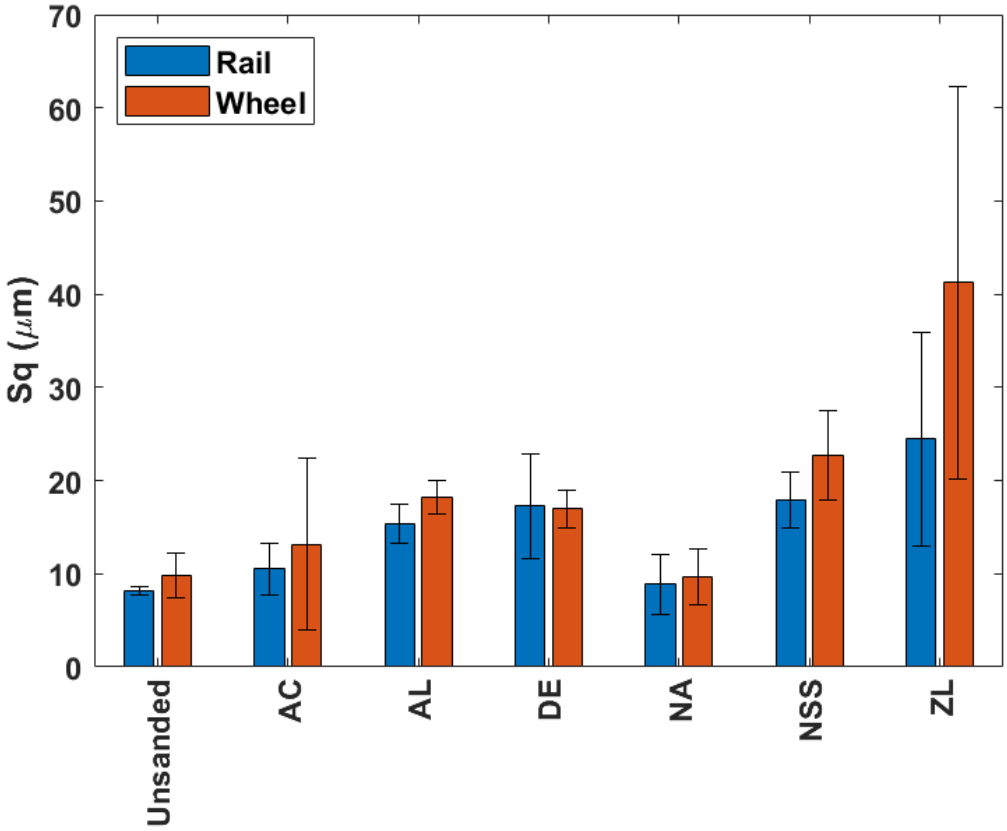

Figure 5.34. Post-Test Surface Roughness Measurements for Test Contacts with Other Particles applied in Dry Conditions.

The post-test surface scans, included in Figure 5.35, show how scans from AC and NA tests compare similarly to the unsanded case. AL and NSS, show a marked difference between the unsanded case, with small indentations and disturbances on their surfaces. DE and ZL include large indentations on the surface.

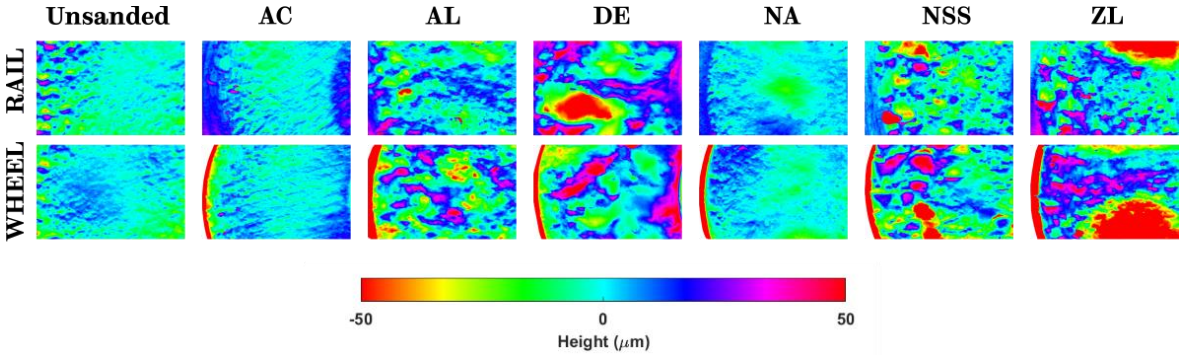

Figure 5.35. Post-test Surface Scans of Dry Contacts with Other Particles applied.

Though all these particles have very different characteristics, they are all similar in one respect: all particle types were retained within the contact during the test, unlike rail sand in dry conditions. The low adhesion particles (AC and NA) did not appear to affect the surface roughness or appearance, though both were present in

the contact. DE and ZL both acted similarly, in that they clumped together in the contact creating higher roughness and large indentations compared to an unsanded case, this was more severe for ZL. AL and ZL, though being very different types of particles, both acted similarly, spreading relatively evenly throughout the contact and roughening the surface without creating the large indents that DE and ZL created.

5.3.3.2 Wet Conditions

5.3.3.2.1 Traction Data

The traction data concerning other particles in wet conditions has been included in Figure 5.36. Both AC and NA act similarly to how they acted in dry conditions, though their CoTs are slightly lower, at 0.07 and 0.09 respectively. Only NSS matched the initial stiffness of the unsanded case, though gross stick-slip happened at a lower CoT, occurring at 0.42, though it did not drop as low as the unsanded case. Gross stick-slip also occurred with DE, though not till much later and much less grossly than the gross stick-slip event for the unsanded case, DE had a peak CoT of 0.51. Both AL and ZL, did not undergo gross stick-slip events, though there was a relatively large difference in their peak CoTs, 0.65 for the former and 0.43 for the former. All particles returned lower peak values of CoT compared to dry conditions.

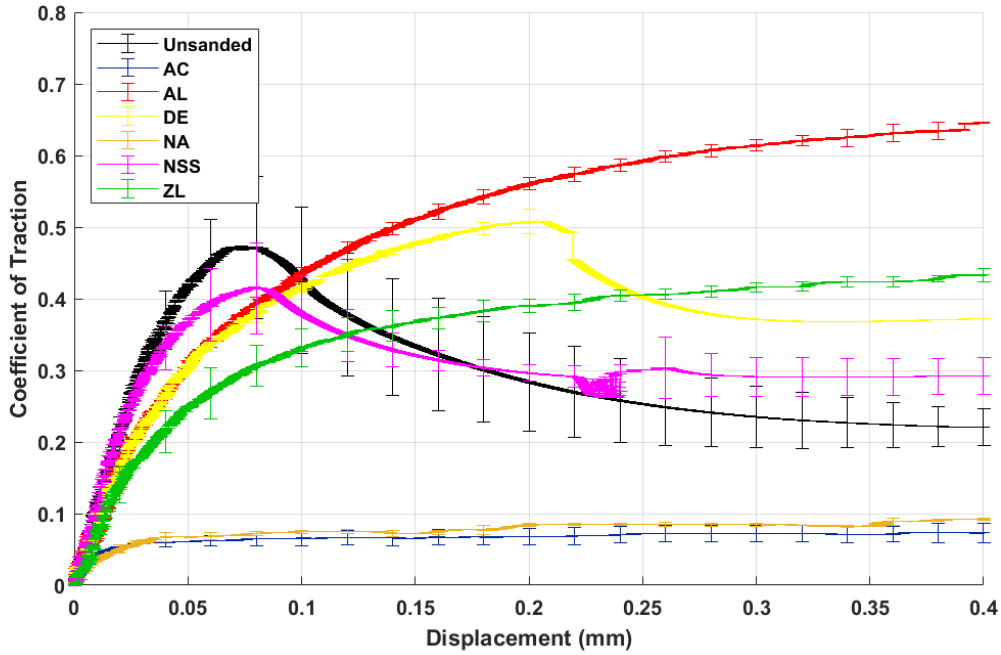

Figure 5.36. HPT Traction Data for Wet Conditions with Other Particles applied.

5.3.3.2.2 Post-Test Surface Analysis

The pictures of the post-test wheel and rail specimens have been included in Figure 5.37. As for dry conditions, AC has not adhered to the surface and has bunched together during the test. Similarly, AL, NSS, and ZL have also acted similarly to the dry contact, the former two spreading relatively evenly around the contact and the latter clumping up. Conversely, DE has not acted as it did in dry conditions, spreading around the surface more evenly in this instance. Whilst the spread of NA is similar to what was observed in dry conditions, there are differences in its appearance, being less brown and appearing flakier after undergoing wet conditions.

Figure 5.37. Post-test Specimens with Other Particles applied in Wet Conditions.

The post-test surface roughness measurements, included in Figure 5.38, show how roughness was increased in the presence of all other particles in wet conditions. In the cases of AC and NA, the increase in roughness brings measurement up to a similar level as was seen for dry unsanded conditions. All remaining particles exhibited a relatively similar increase in roughness.

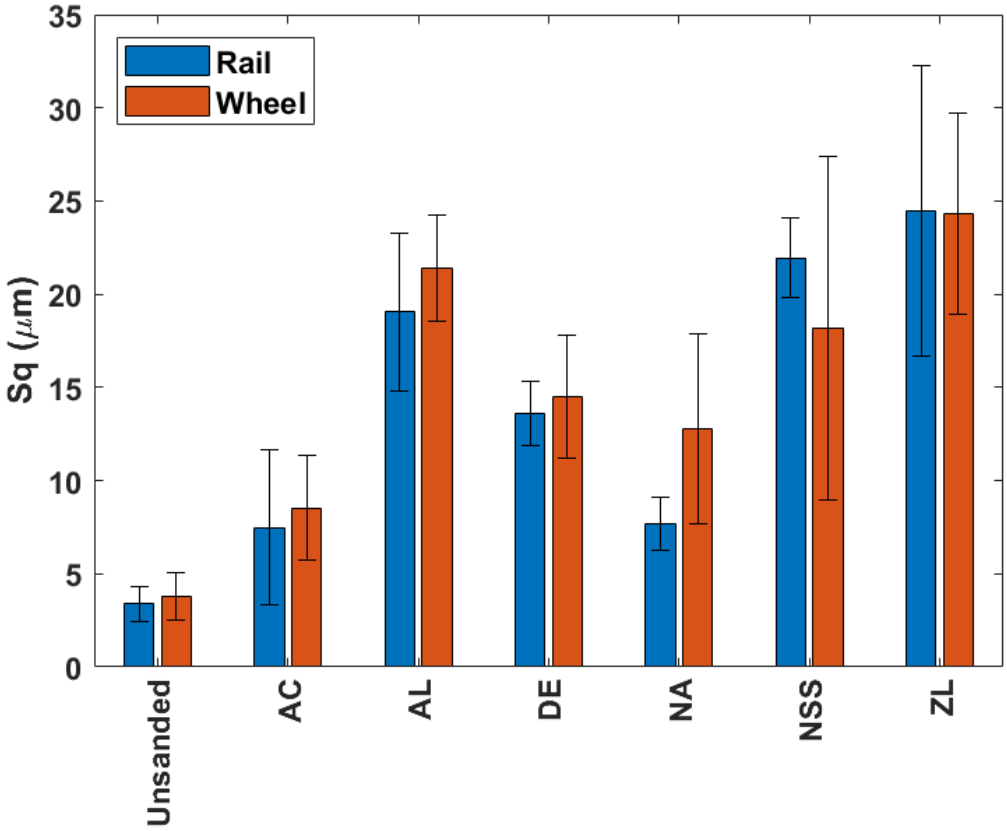

Figure 5.38. Post-Test Surface Roughness Measurements for Test Contacts with Other Particles applied in Wet Conditions.

The surface scans for AC, shown in Figure 5.39, show how relatively similar the surfaces are to the unsanded case. NA, shows some surface wear, including a shallow broad scar. The remaining particles all exhibit areas of indentation, NSS having the highest number of indentations but ZL showing the largest indents.

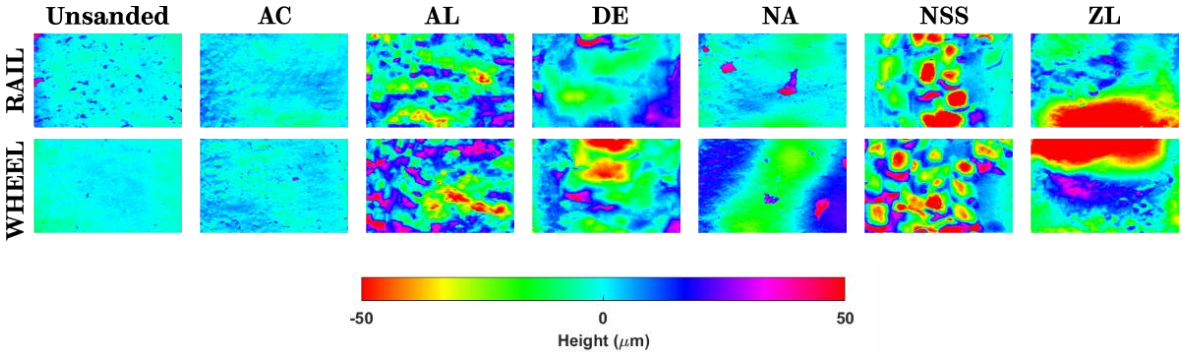

Figure 5.39. Post-test Surface Scans of Wet Contacts with Other Particles applied.

All particles remained within the contact to some extent during wet conditions, and all had a marked effect on the surface characteristics post-test. AC and NA appeared to have a lesser effect than the other particles, whereas AL, NSS, and ZL all produced

a rougher, more indented surface. DE produced indents and roughness, but not to the same extent as these other particles.

5.3.3.3 Leaf Contaminated Conditions

5.3.3.3.1 Traction Data

The traction data from HPT tests for other particles in a leaf contaminated contact has been presented in Figure 5.40. AC makes very little difference upon its application when compared to the unsanded case, with a peak CoT of 0.05. DE, NA, NSS, and ZL all increase the level of traction, with peaks of 0.08, 0.07, 0.08, and 0.09 respectively; in the case of ZL there also appears to be a greater variance in traction data. AL was the only particle to increase traction above minimum required levels, peaking at 0.17, AL also showed some variance in traction results.

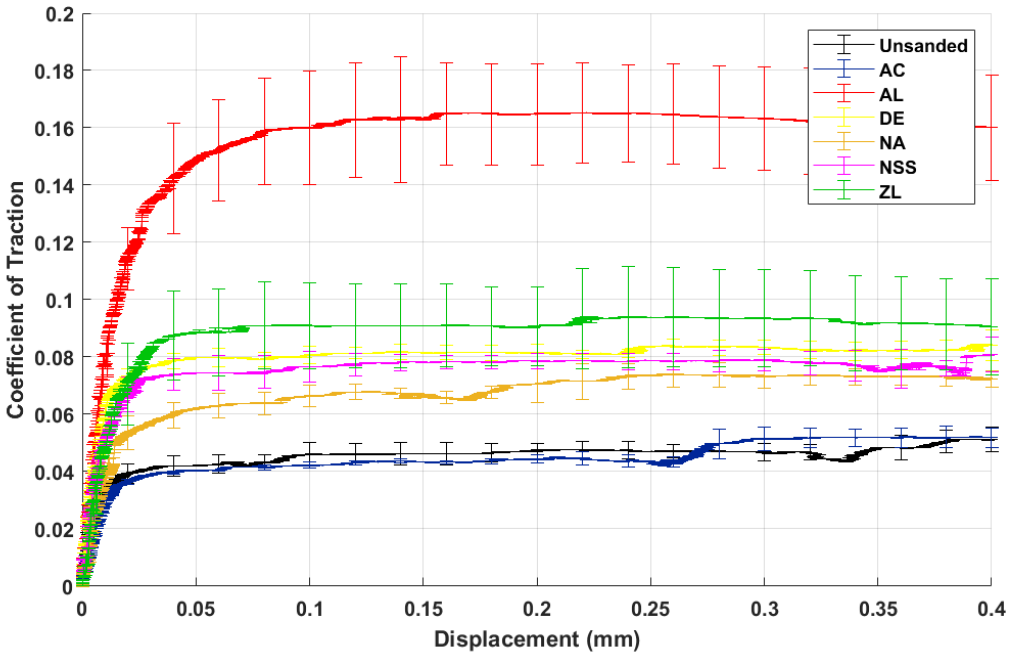

Figure 5.40. HPT Traction Data for Leaf Contaminated Conditions with Other Particles applied.

5.3.3.3.2 Post-Test Surface Analysis

Pictures of wheel and rail specimens post-test have been included in Figure 5.41. As for other particles in dry and wet conditions, all particles remained in the contact at the end of the test. AC, acted similarly to dry and wet conditions, not adhering to the surface and bunching up. All other particles became embedded into the leaf layer surface, DE, NA, and ZL doing so in clumps.

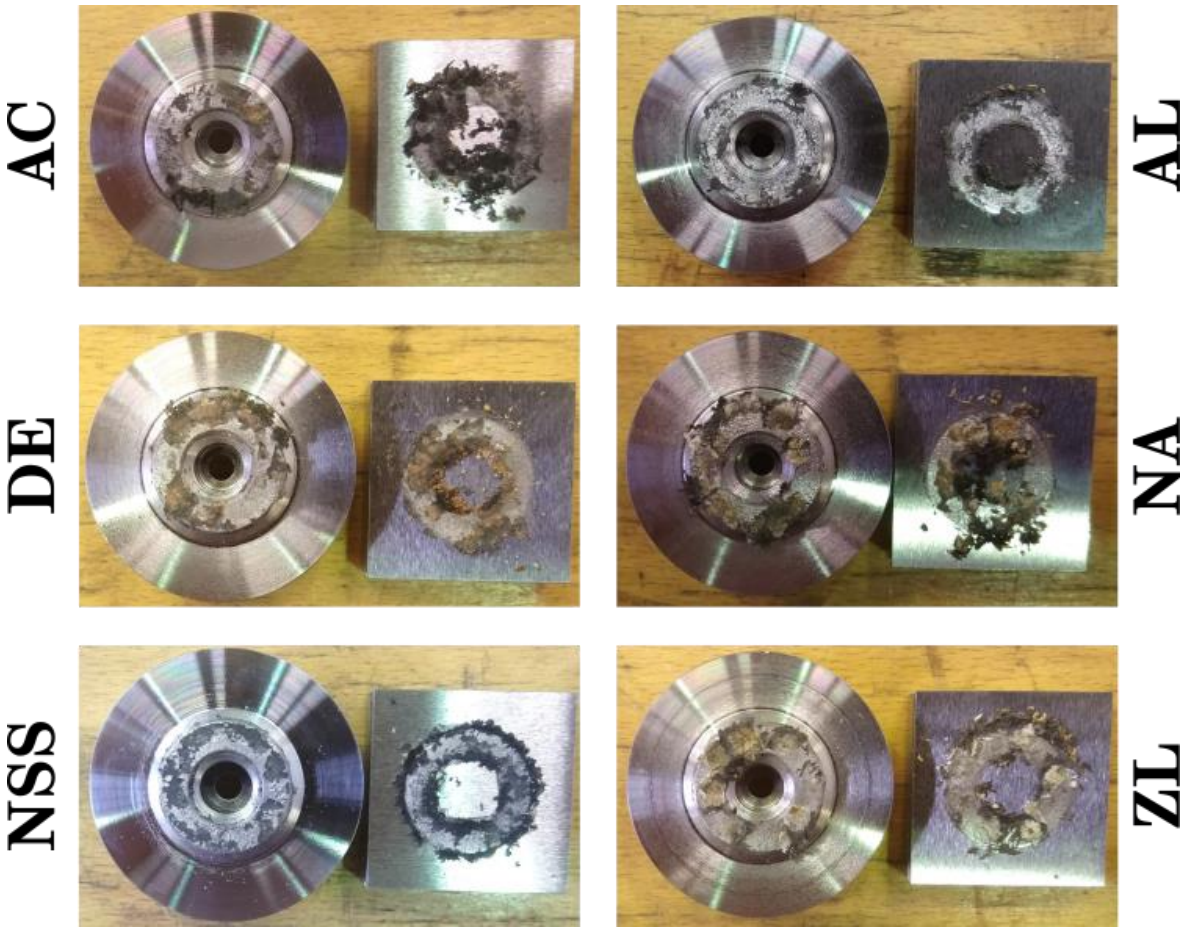

Figure 5.41. Post-test Specimens with Other Particles applied in Leaf Contaminated Conditions.

Measurements of post-test surface roughness have been included in Figure 5.42. ZI had the largest impact on surface roughness post-test, though with a large variance in roughness values. AC and AL both seemed to have little effect on roughness, whilst DE, NA, and NSS seemed to have slightly more effect.

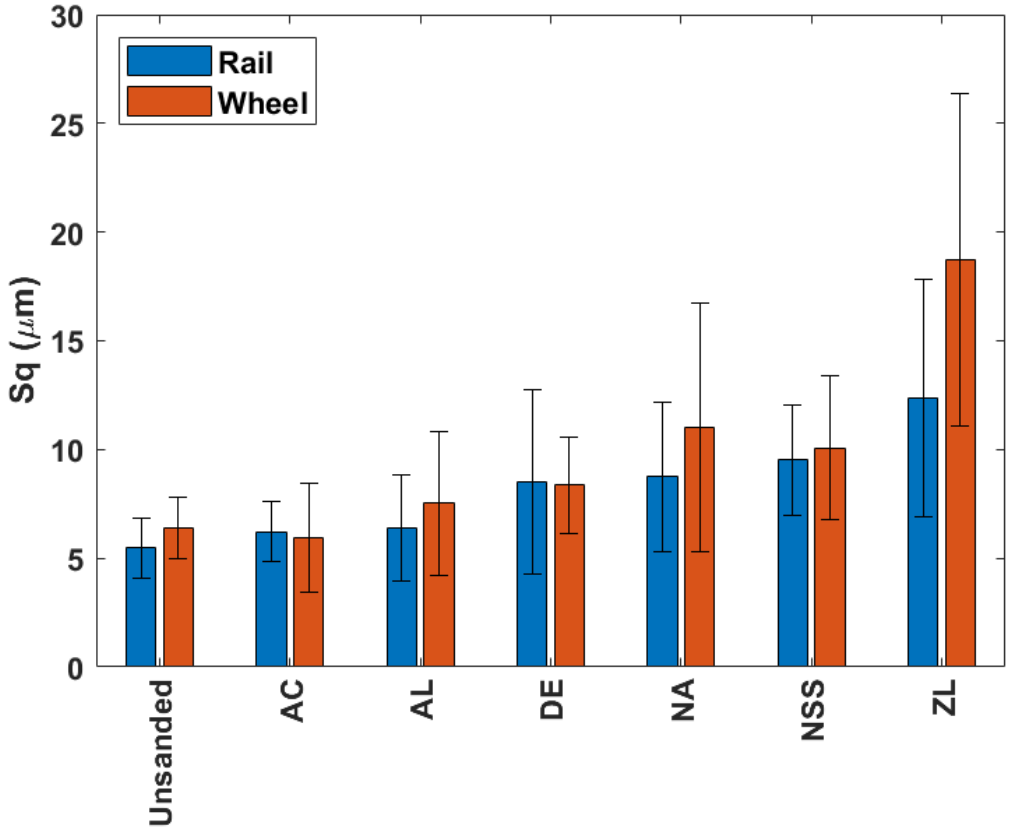

Figure 5.42. Post-Test Surface Roughness Measurements for Test Contacts with Other Particles applied in Leaf Contaminated Conditions.

The post-test surface scans of other particles in a leaf contaminated contact has been included in Figure 5.43. Only in ZL were large indentations noticeable, with NSS appearing to have smaller indentations. All other particles showed only shallow disturbances on the surface.

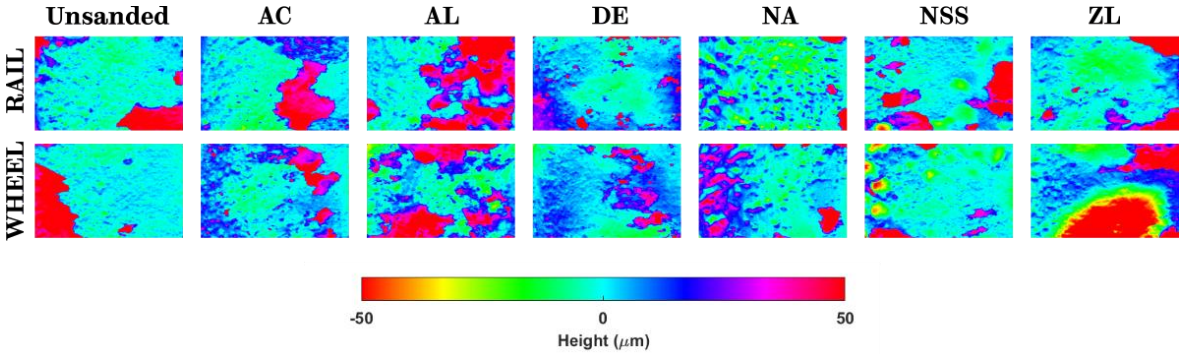

Figure 5.43. Post-test Surface Scans of Leaf Contaminated Contacts with Other Particles applied.

ZL was the only particle to demonstrate a marked difference in surface condition post-test when compared with the unsanded case. All other particles only showed a slight roughening of the surface with little indentation present. This relatively small change may be due to particles embedding into the leaf layer, thereby not affecting

the steel surfaces of the wheel and rail specimens as greatly as was seen for dry and wet conditions.

5.3.4 Glass Bead Tests

The following section includes traction data and post-test surface analysis from tests in dry, wet and leaf contaminated conditions with various glass bead types, outlined in sub-chapter 4.1.3, applied to the contact in the manner described in sub-chapter 5.2.4.

5.3.4.1 Dry Conditions

5.3.4.1.1 Traction Data

The traction data from tests conducted in dry conditions with glass beads has been included in Figure 5.44. There is some spread between the non-pre-crushed particles, but crushed glass beads (GBC) were noticeably lower than all these and the unsanded case, peaking at 0.67. Large glass beads (GBL) gave the highest peak CoT, 0.77, though there was a relatively large amount of variance compared to the unsanded case. Small glass beads (GBS) were lower than the unsanded case, peaking at 0.75, whilst medium glass beads (GBM) peaked at 0.71.

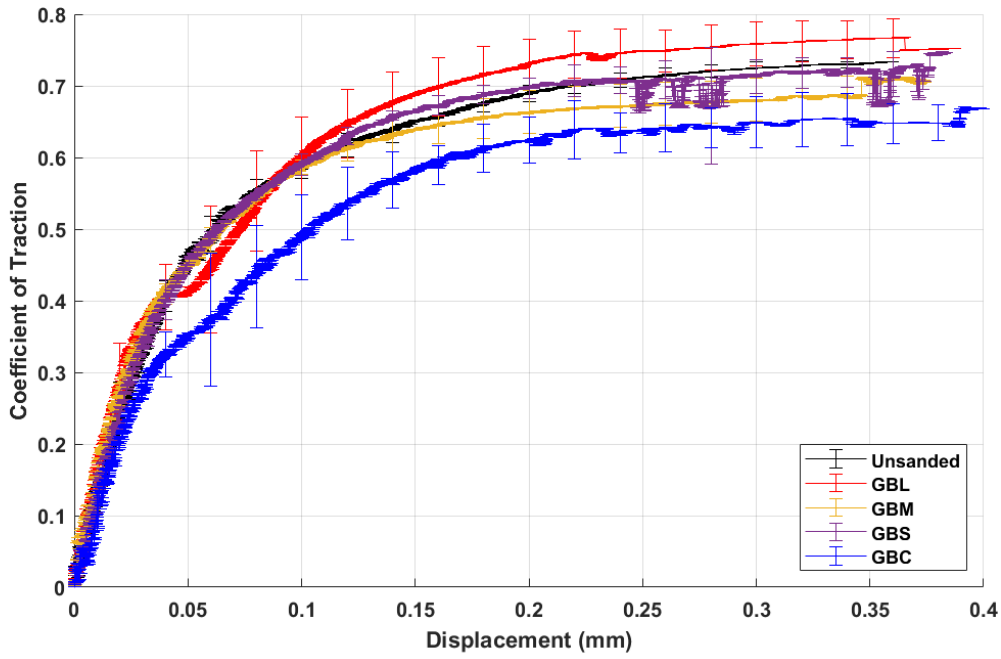

Figure 5.44. HPT Traction Data for Dry Conditions with Glass Beads applied.

5.3.4.1.2 Post-Test Surface Analysis

Pictures of the wheel and rail specimens post-test have been included in Figure 5.45. Within the non-pre-crushed glass bead contacts, no visible material remains. In the

GBC contact there does appear to be some material remaining, though this is very spread out.

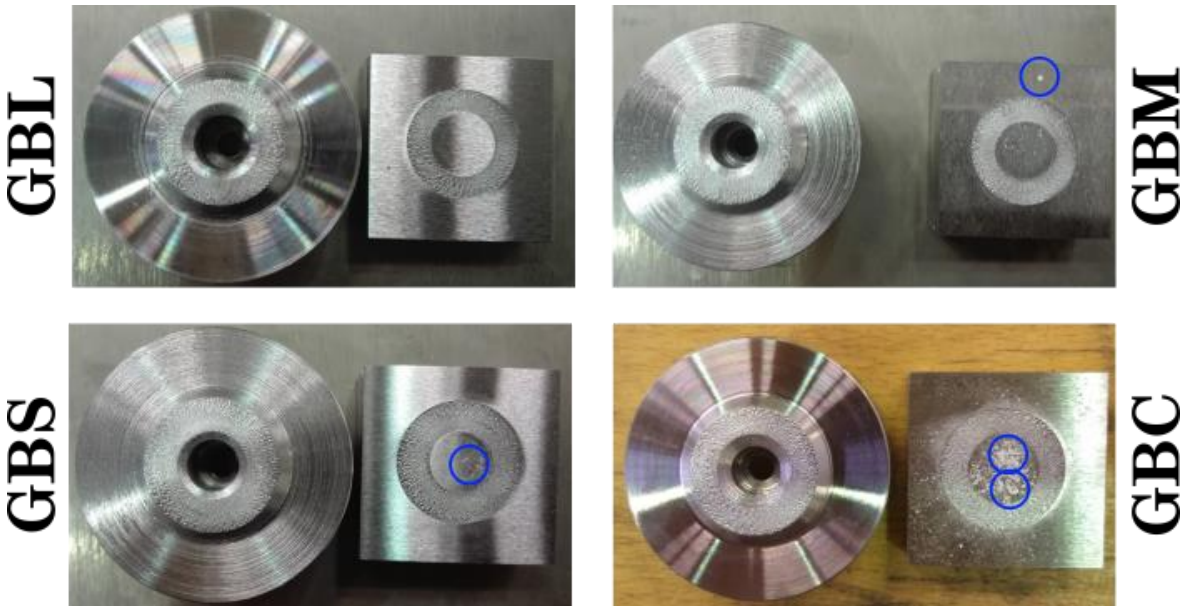

Figure 5.45. Post-test Specimens with Glass Beads applied in Dry Conditions with Expelled Material encircled.

Surface roughness measurements have been presented in Figure 5.46. GBL, GBM, and GBC measured greater roughness in the contact than the unsanded case, whilst GBS gave similar roughness values.

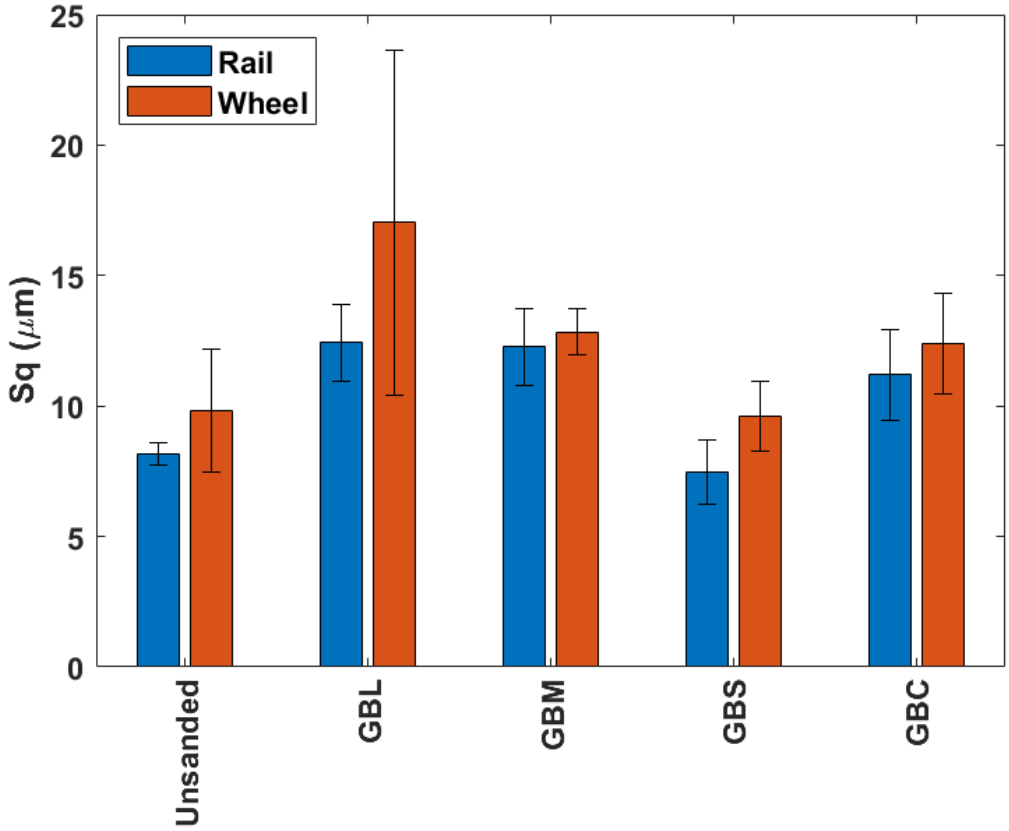

Figure 5.46. Post-Test Surface Roughness Measurements for Test Contacts with Glass Beads applied in Dry Conditions.

The surface scans, shown in Figure 5.47, indicate that there was not a large difference between the unsanded contact and the contact with any glass bead type. Though there were small indents apparent when GBC was applied.

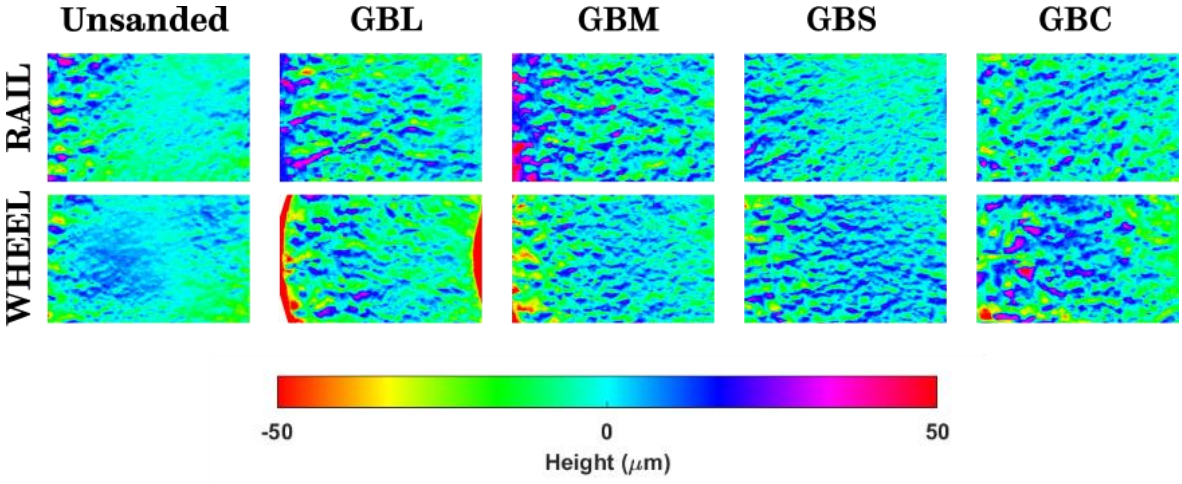

Figure 5.47. Post-test Surface Scans of Dry Contacts with Glass Beads applied.

5.3.4.2 Wet Conditions

5.3.4.2.1 Traction Data

The traction data from tests conducted with glass beads in wet conditions has been included in Figure 5.48. For all cases gross stick-slip events occurred though glass beads produced greater and later CoT peaks than the unsanded case. GBL and GBM both peaked at similar times, with peaks of 0.58 and 0.55 respectively. GBS peaked later, but had a similar peak CoT at 0.58. Lastly, GBC peaked later with a slightly higher peak CoT of 0.61. All cases exhibited similar initial stiffnesses.

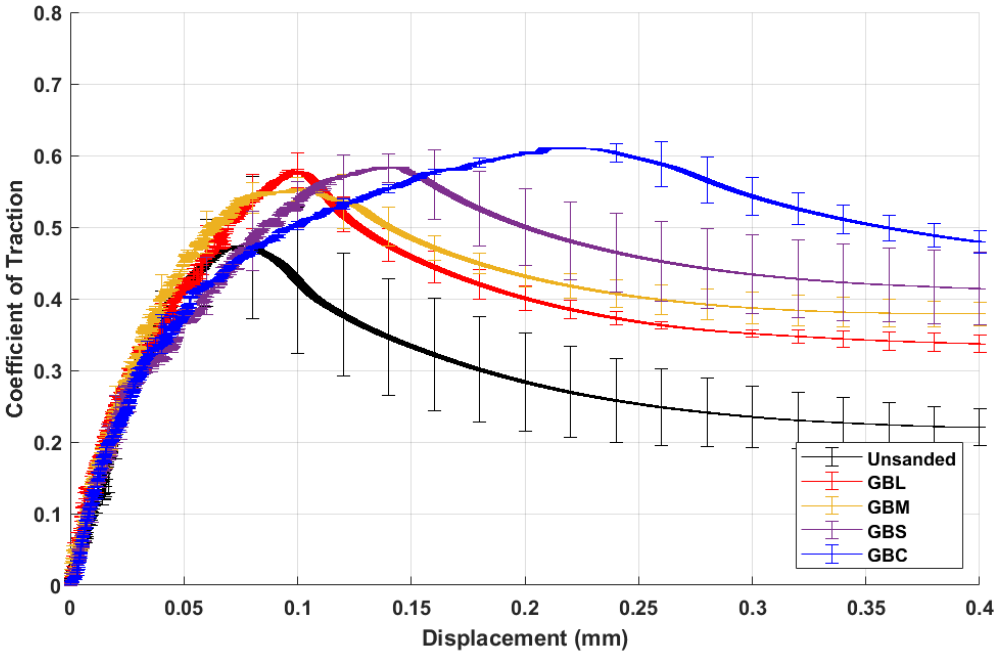

Figure 5.48. HPT Traction Data for Wet Conditions with Glass Beads applied.

5.3.4.2.2 Post-Test Surface Analysis

Pictures of the wheel and rail specimens after testing have been included in Figure 5.49. Some material remains in all the contacts though all are spread out throughout the contact and have not clumped together.

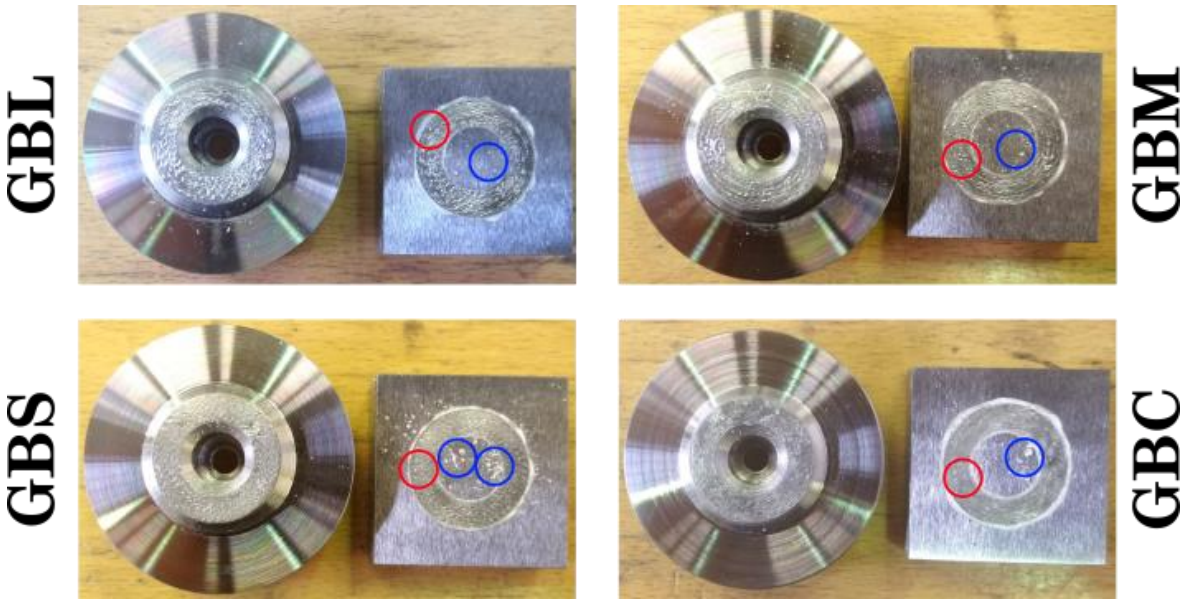

Figure 5.49. Post-test Specimens with Glass Beads applied in Wet Conditions. Red Circles denote Areas with Material Remaining in the Contact, Blue Circles denote Areas with Material expelled from the Contact.

Roughness measurements of test surfaces after tests with glass beads in wet conditions have been included in Figure 5.50. All glass beads produced rougher surfaces than the unsanded case, with GBM producing the greatest roughness of the non-pre-crushed particles; GBM also produced the largest variance in test results. GBC produced much higher roughness on the wheel specimen surface than the rail specimen surface, the latter being in line with the non-pre-crushed particles.

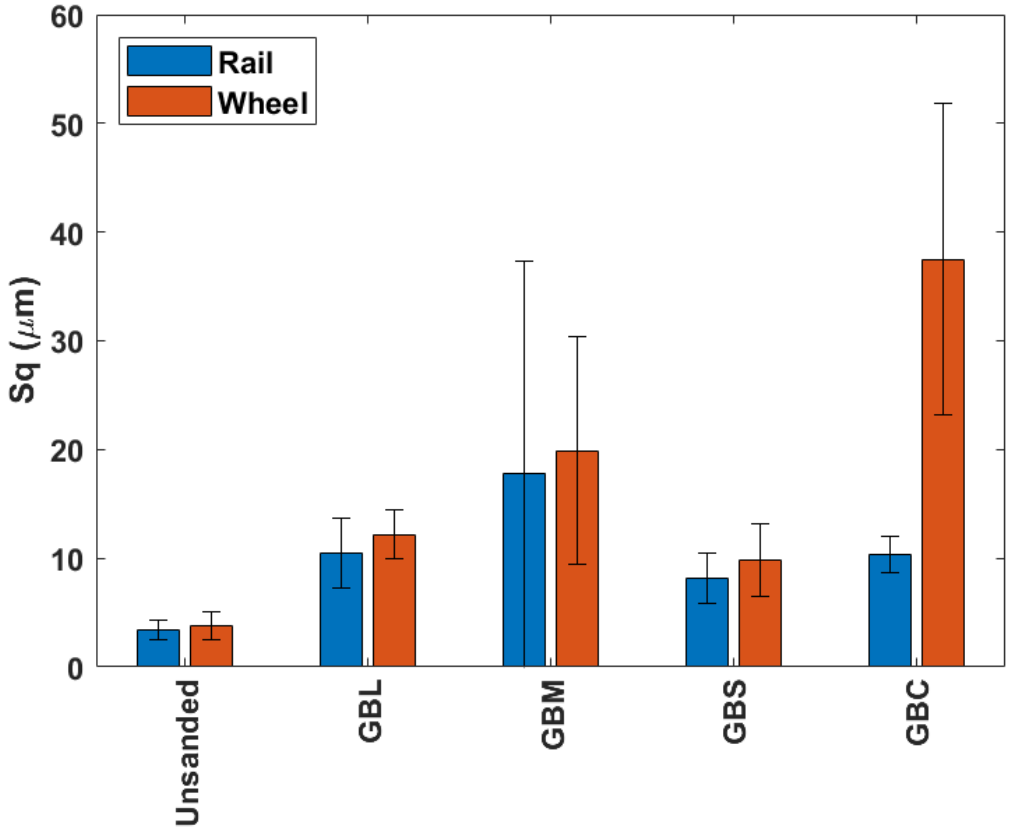

Figure 5.50. Post-Test Surface Roughness Measurements for Test Contacts with Glass Beads applied in Wet Conditions.

Scans of the post-test surfaces have been included in Figure 5.51. All surfaces with glass beads applied appear different than the unsanded case. GBS appears to have many, shallow indents, whereas GBL and GBM have many, deeper indents. GBC shows some indentation, but most surface damage appears to be large areas of possible delamination.

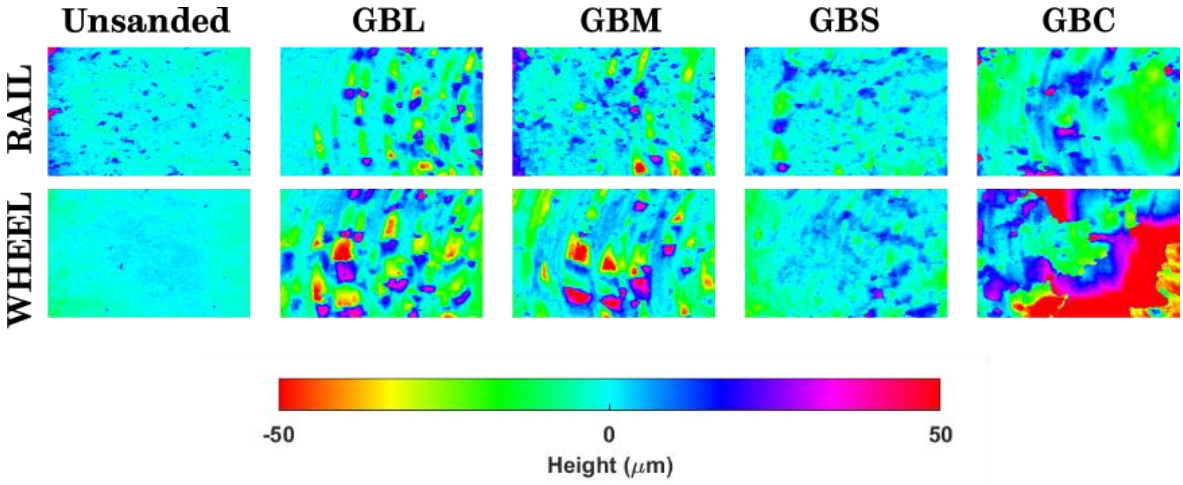

Figure 5.51. Post-test Surface Scans of Wet Contacts with Glass Beads applied.

5.3.4.3 Leaf Contaminated Conditions

5.3.4.3.1 Traction Data

Traction data from tests conducted with glass beads in leaf contaminated conditions have been included in Figure 5.52. All glass beads produced higher peak CoTs than the unsanded case, though GBC produced the largest change in traction, reaching a peak CoT of 0.13. Both GBM and GBS produced similar CoT peaks to one another, both peaking at 0.09. GBL only reached a peak CoT of 0.07, making it the least effective at restoring traction in a leaf contaminated contact.

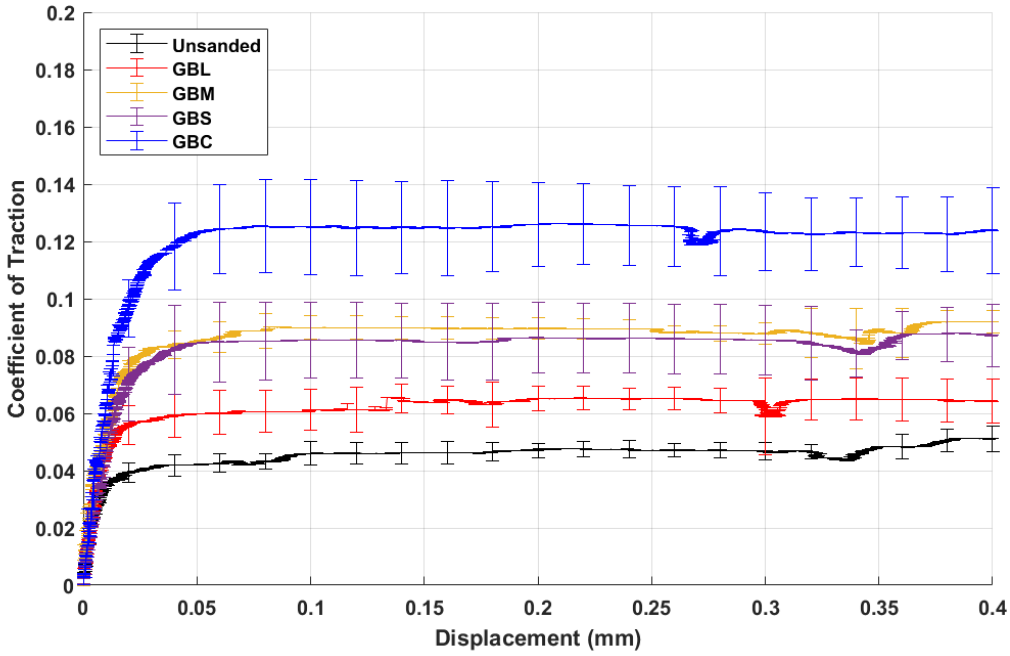

Figure 5.52. HPT Traction Data for Leaf Contaminated Conditions with Glass Beads applied.

5.3.4.3.2 Post-Test Surface Analysis

Pictures of leaf contaminated contacts after the application of glass beads have been included in Figure 5.53, areas with remaining material have been marked for clarity. Very little material is remaining in the GBL case, with more material being apparent in the GBM and GBS cases, where areas of the leaf layer have been indented into. The most material remaining appears to be the GBC case where very little of the leaf layer has not been indented into.

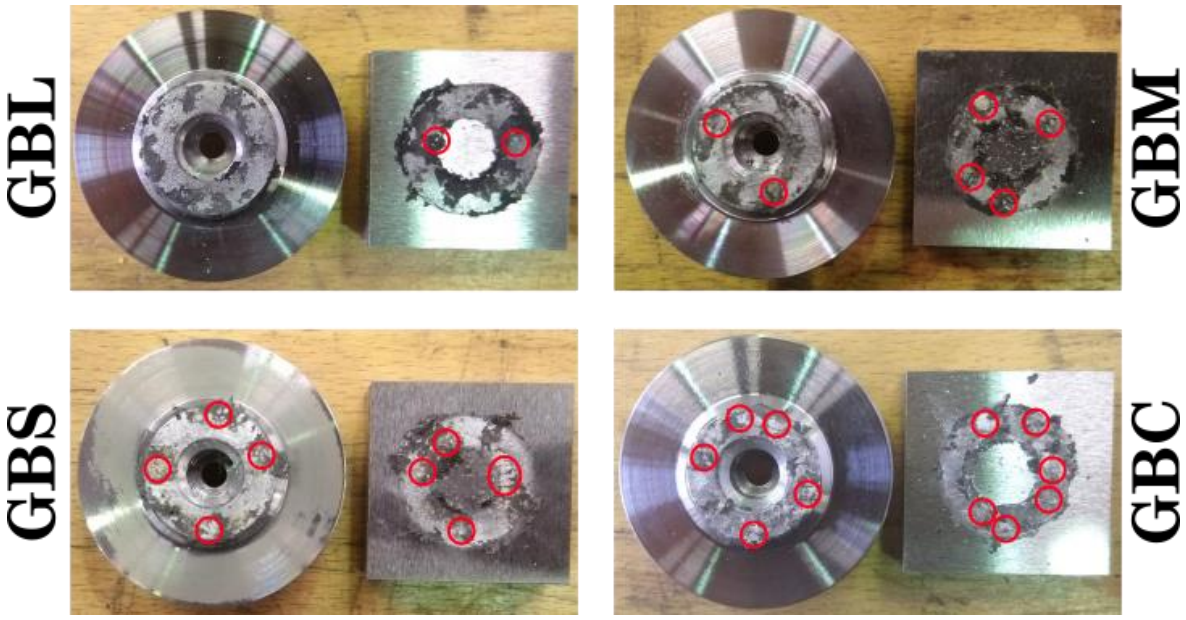

Figure 5.53. Post-test Specimens with Glass Beads applied in Leaf Contaminated Conditions with Remaining Material encircled.

Roughness data from after the tests have been included in Figure 5.54. GBL shows very similar roughness values to the unsanded case, with GBM showing a marginal increase in roughness. GBS presents higher roughness measurements than all other non-pre-crushed sands. Similar to wet conditions, the roughness of the rail specimen with GBC applied is similar to non-pre-crushed particles and the roughness of the wheel specimen is much greater with a large variance in measured values.

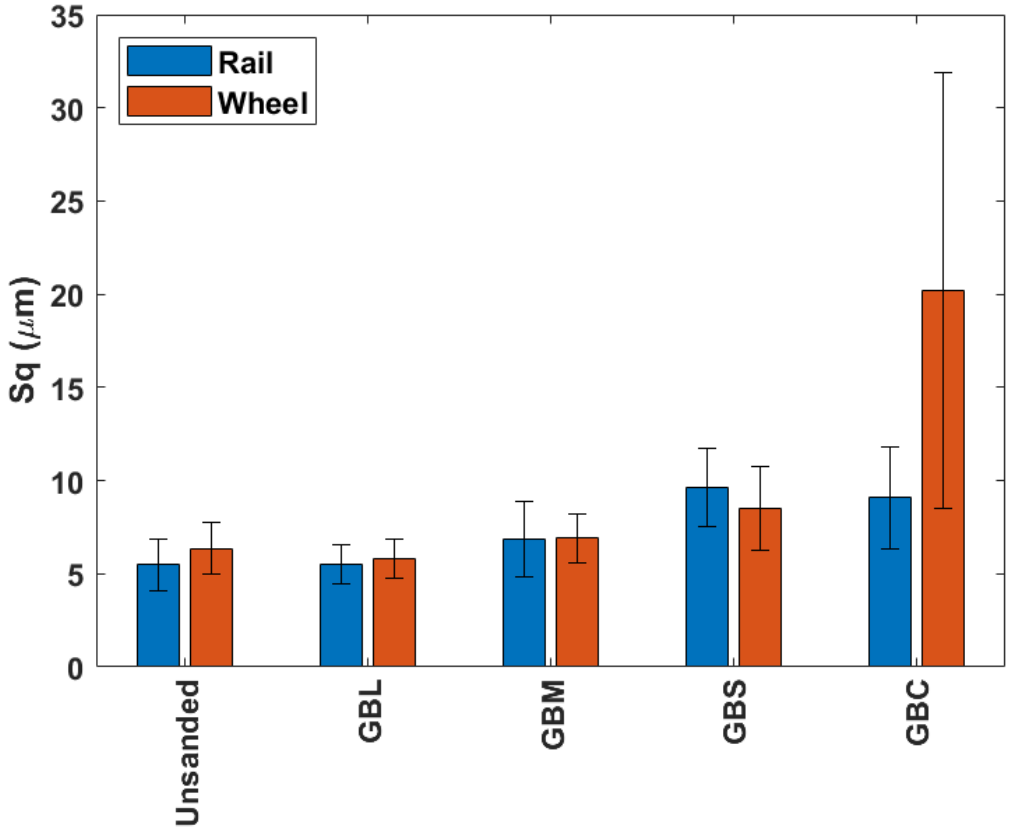

Figure 5.54. Post-Test Surface Roughness Measurements for Test Contacts with Glass Beads applied in Leaf Contaminated Conditions.

Post-test surface scans have been included in Figure 5.55, where the surfaces of both GBL and GBM appear to be very similar to the unsanded case. There appears to wide, shallow damage occurring in the GBS case. In the Contact with GBC applied, there appears to be the same wide, relatively shallow scars, as well as, some areas of indentation.

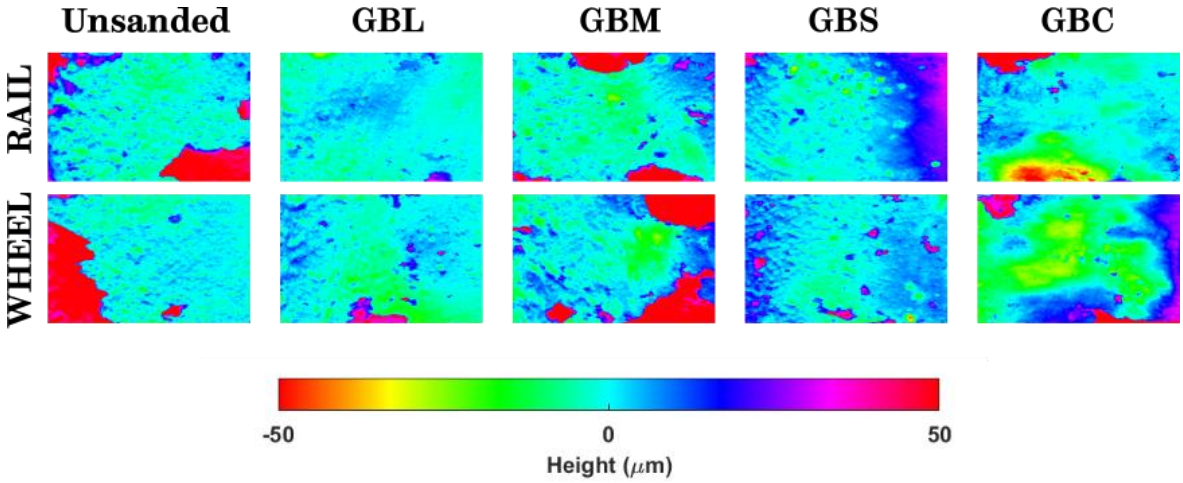

Figure 5.55. Post-test Surface Scans of Leaf Contaminated Contacts with Glass Beads applied.

5.3.4.4 Discussion

A summary of the peak CoTs reached for each glass bead type have been included in Figure 5.56. When looking at the effect of different glass beads that were initially circular in shape (GBS, GBM, GBL) all produce peak CoTs, within their respective error margins, that are very similar in dry and wet conditions, regardless of the difference in particle size. These initially circular glass beads did seem to show differences in leaf contaminated conditions, GBM and GBS produced similar peak CoTs, but GBL seemed to produce a lower peak CoT. These results suggest particle size may only have a significant effect in leaf contaminated conditions.

When comparing the pre-crushed GBC to the initially circular particles, the peak CoT is significantly lower in dry conditions, and marginally higher in wet conditions, and markedly higher leaf contaminated conditions. These results suggest particle shape may be an important characteristic in all conditions.

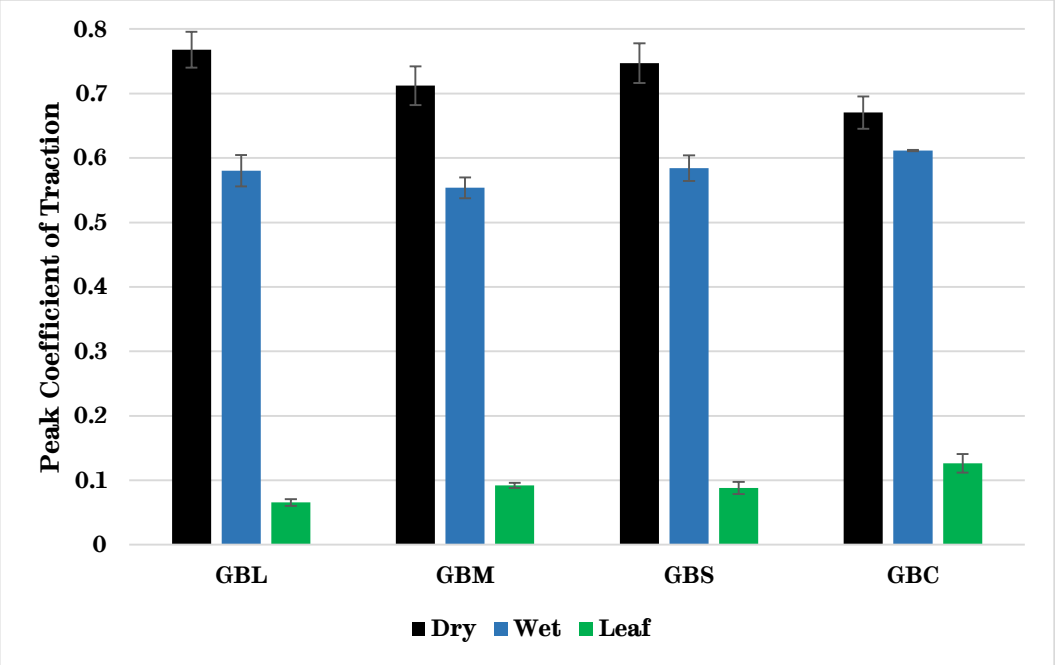

Figure 5.56. Comparison of Peak Coefficients of Traction for Glass Beads.

5.3.4.4.1 Glass Bead Shape Effects in Dry & Wet Conditions

In Figure 5.45, it was observed that there was more GBC material remaining in the contact compared to the circular beads in dry conditions. This material may have acted as a dry lubricant (in a similar manner to some of the rail sands mentioned in sub-chapter 5.3.2.4.1) and created lower peak CoTs than the other glass beads. As GBC had already been crushed, it may have resulted in a less violent expulsion of material upon crushing in the HPT.

In wet conditions, the reverse of this is true, though only marginally and as seen in Figure 5.48 has a larger effect on the shape of the traction curve as opposed to its peak. These differences may also be due to less of the material being expelled due to GBC being crushed prior to testing; in wet conditions it being more of an advantage to retain material that can provide traction by breaking up the liquid lubricant layer.

5.3.4.4.2 Glass Bead Shape Effects in Leaf Contaminated Conditions

In leaf contaminated conditions, GBC produced a markedly higher peak CoT. A possible explanation for this could be that as GBC will be more angular than the other spherical particles, it was able to cut into the leaf layer more effectively, thus creating more contact with the surface below the leaf layer and transferring traction in a similar manner to that shown in Figure 5.31(A).

5.3.4.4.3 Glass Bead Size Effects in Leaf Contaminated Conditions

GBL produced a notably lower peak CoT compared to both GBM and GBS. As the only differences between the particles are in their sizes, this can be the only reason for this difference. Figure 5.57 illustrates how a large particle may act upon being crushed in a leaf contaminated HPT contact; after the particle has embedded into the leaf layer it will begin to break apart. The particle breakages occurring above the leaf layer would expel particles in a similar manner to what is seen in a dry contact, whereas breakages below the leaf layer would retain the ejected particles within the leaf layer itself. Thus, the larger the particle, the more of it will be above the leaf layer and be expelled from the contact.

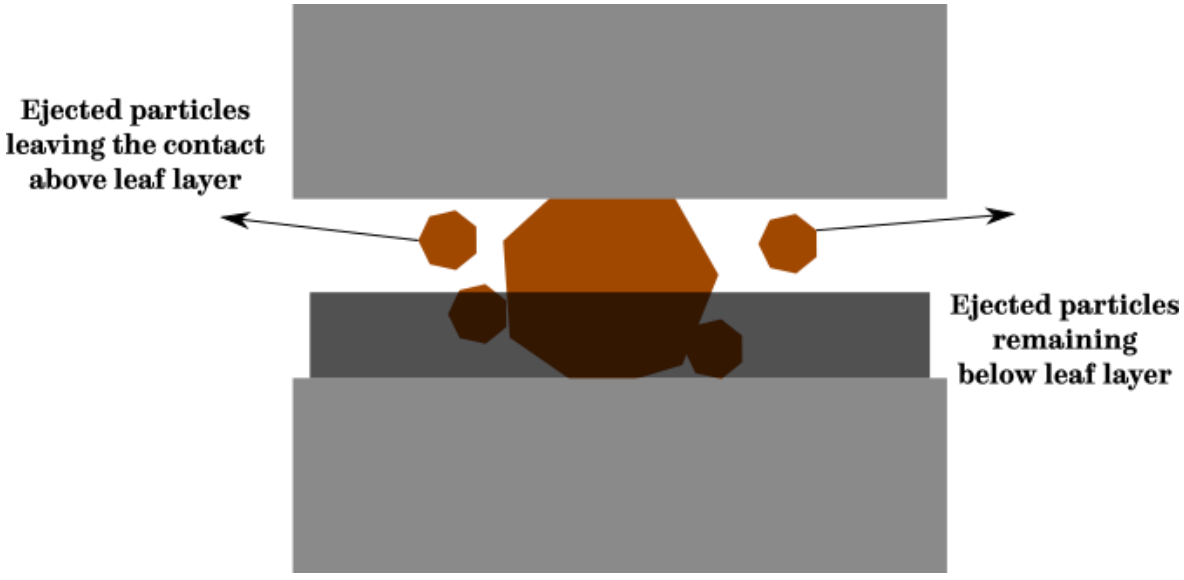

Figure 5.57. Larger Particle in a Leaf Contaminated HPT Contact.

5.3.5 Effect of Multiple Passes

In this sub-chapter the effect of multiple passes on traction data will be presented for both unsanded and sanded contacts. Here, only LB was used to present the sanded case. Dry, wet, and leaf contaminated contacts were used.

In this sub-chapter, the 1st pass refers to the 1st test run and so on for the 2nd and 3rd passes.

5.3.5.1 Unsanded

From the data presented in Figure 5.58, there appears to be very little difference between passes. All passes had a very similar shape and peaked between 0.73-0.75.

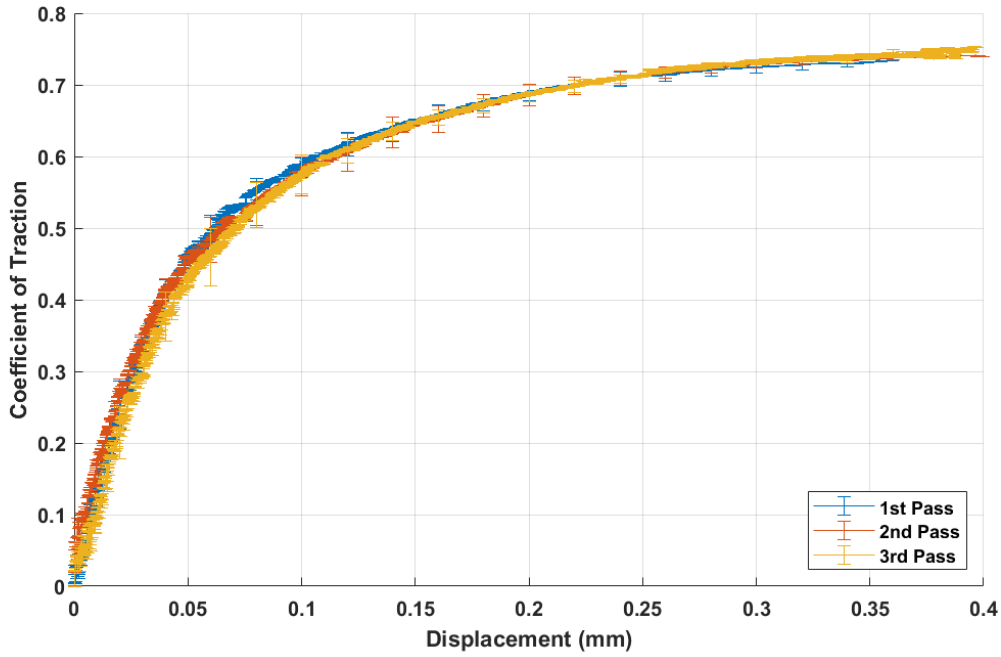

Figure 5.58. Effect of Multiple Passes in a Dry, Unsanded Contact.

The effect of multiple passes is more apparent in wet conditions shown in Figure 5.59, where the 1st pass shows the highest CoT peak, 0.47, and after gross stick-slip reduces to below the 2nd and 3rd pass at the same point. The 2nd and 3rd pass act very similarly, peaking at 0.35 and 0.37 respectively, and not undergoing as gross a stick-slip event as seen in the 1st pass.

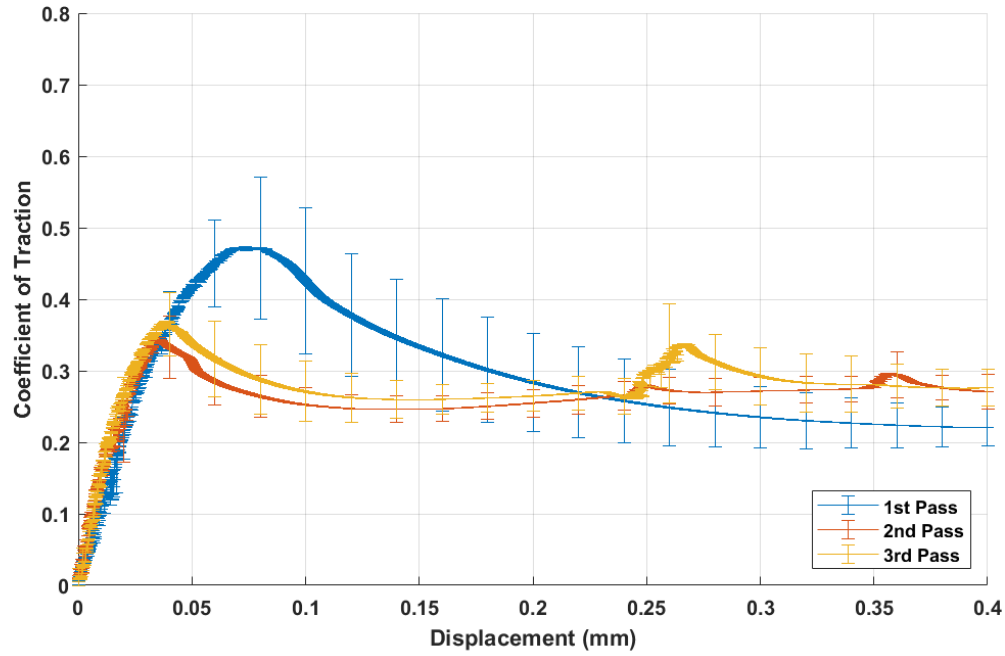

Figure 5.59. Effect of Multiple Passes in a Wet, Unsanded Contact.

The effect of multiple passes was also apparent for leaf contaminated contact, shown in Figure 5.60. The 2nd pass produced marginally greater traction than the 1st pass, both being ~0.05, however the variance in data was also greater for the 2nd pass compared to the 1st pass. The 3rd pass produced higher traction, peaking at 0.08, and greater variance than either the 1st or 2nd pass.

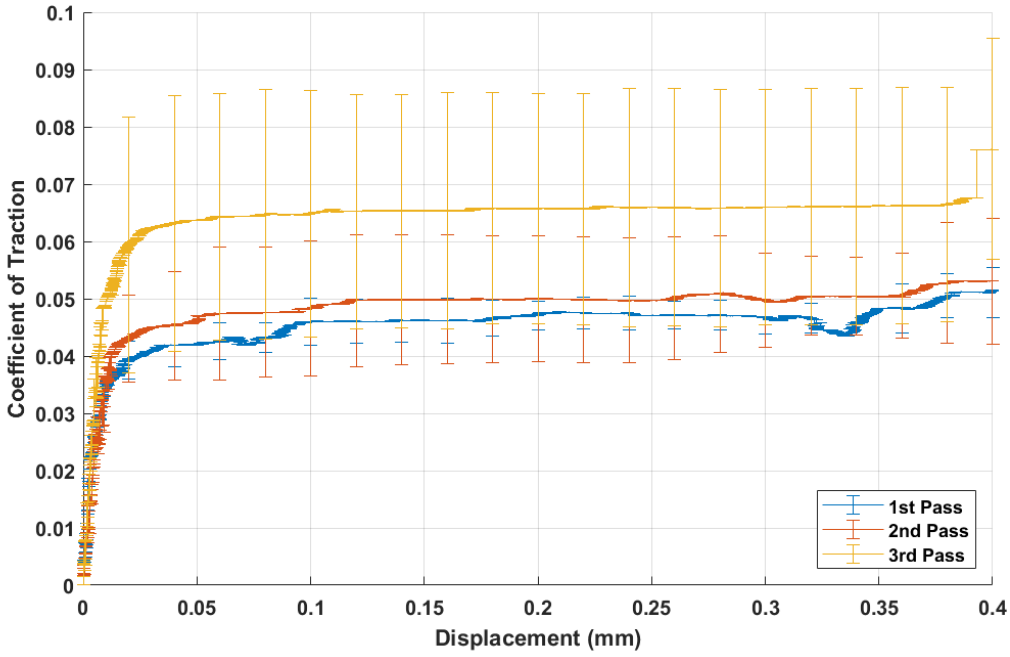

Figure 5.60. Effect of Multiple Passes in a Leaf Contaminated, Unsanded Contact.

5.3.5.2 Sanded

When LB was applied in dry conditions, there was very little difference in traction data, as seen in Figure 5.61. All tests reached a peak CoT of between 0.73-0.75. The only slight difference between the passes was the shape of the traction data for the 1st pass, where it took slightly longer to get up to its peak and had a shallower transition between the ER and the PPR of the curve.

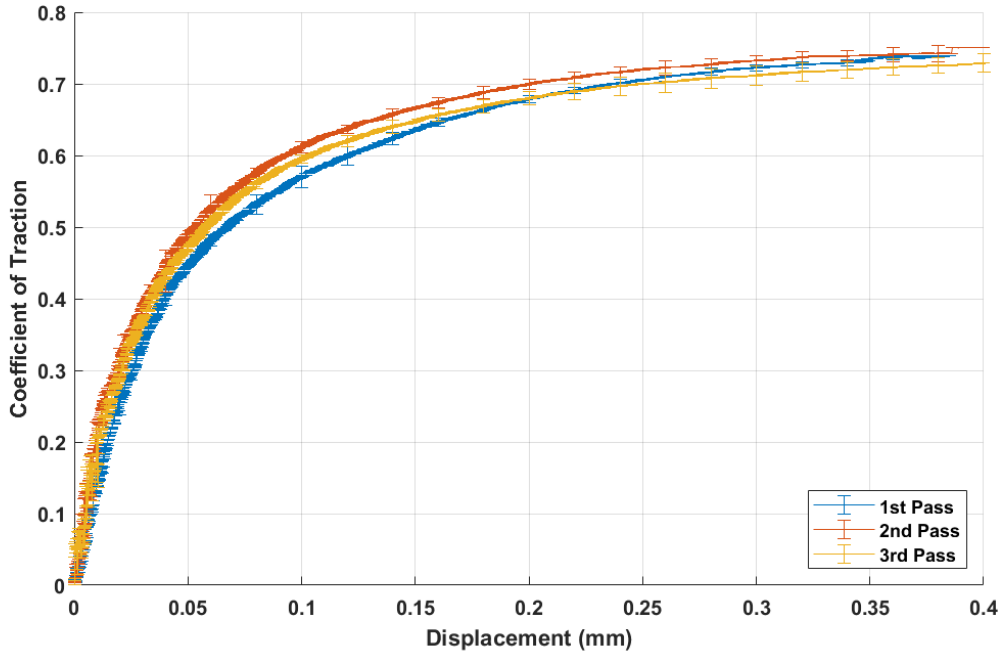

Figure 5.61. Effect of Multiple Passes with LB in a Dry Contact.

Similar trends were apparent for wet conditions, presented in Figure 5.62. All passes reached similar CoT peaks, between 0.61-0.63, though the shape of the 1st pass was different. Similar to dry conditions, it took longer to reach a peak CoT and exhibited a shallower transition between the ER and the PPR of the curve.

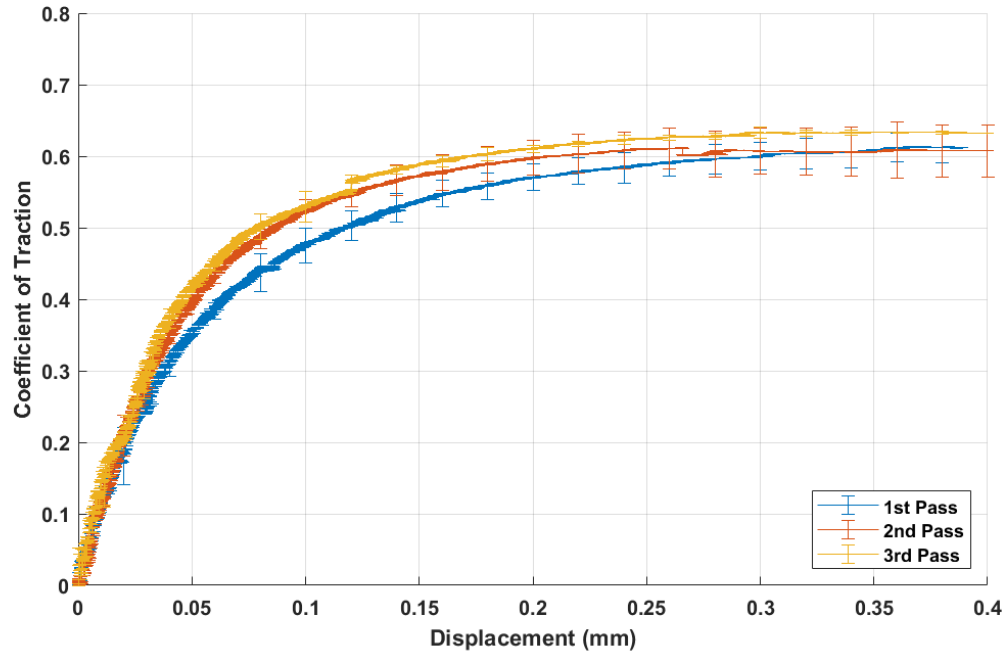

Figure 5.62. Effect of Multiple Passes with LB in a Wet Contact.

Converse to the unsanded, leaf contaminated contact, the 1st pass produced a slightly greater maximum CoT of 0.13 than the 2nd and 3rd passes, as can be seen in Figure 5.63. The 2nd and 3rd passes produced similar peak CoTs, with the 3rd pass being slightly greater, though both were around 0.12.

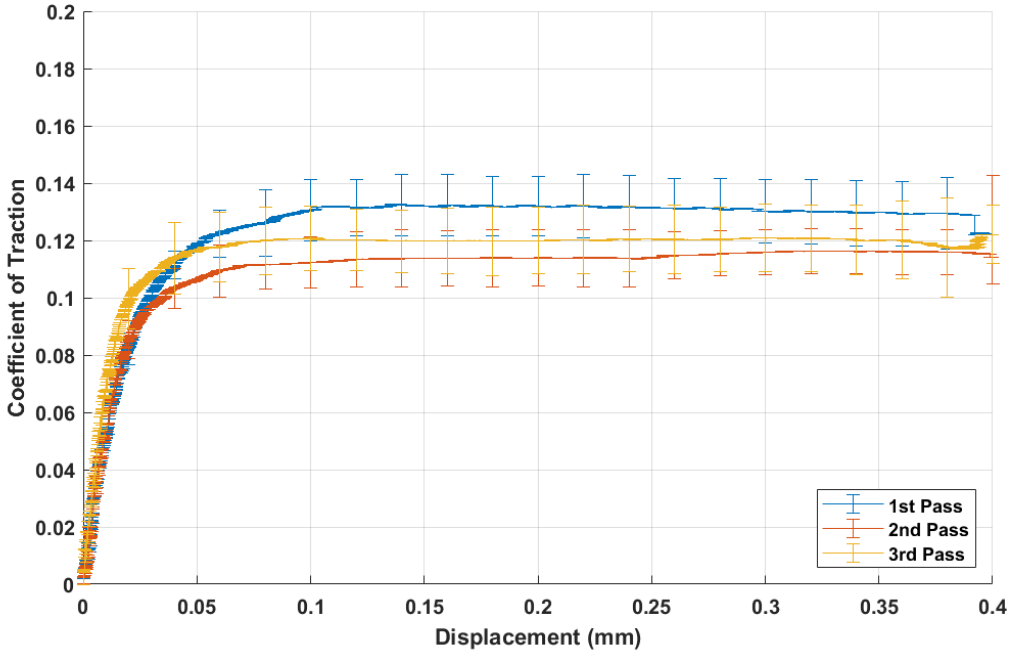

Figure 5.63. Effect of Multiple Passes with LB in a Leaf Contaminated Contact.

5.3.5.3 Discussion

In dry conditions, there was very little variation in both an unsanded and sanded contact, with only the shape of the 1st sanded pass showing a slight variation in the shape of the traction curve. As previously shown, LB rail sand has very little effect in dry conditions, thus as the wheel/rail surfaces have already been work hardened from the run-in process, very little change will occur between passes.

In wet conditions, the sanded contact shows little variation in passes, unlike the unsanded contact. Indicating that the application of sand has an enduring effect on the passes coming after it. Rail sand was previously seen to clump up in the presence of moisture, thus it persists in the contact and keeps adhesion at a steady level.

In leaf contaminated conditions, the unsanded contact exhibited increasing traction over multiple passes, whereas traction marginally decreased after initial application of LB in the sanded contact. In the unsanded case, this may be due to the leaf layer drying out and breaking up over runs; the amount this happens does not appear to be consistent as indicated by the increasing error bars. The efficacy of sand in a leaf contaminated contact is most pronounced on the first pass, possibly due to the initial indentation of the sand into the leaf layer upon first crushing.

5.3.6 Pressure Dependency

The following sub-chapter presents the results of varying pressure with dry, wet, and leaf contaminated contacts where LB has been applied. The contact pressures investigated included: 300 MPa, 600 MPa, and 900 MPa.

In addition, the results of varying pressure with an unsanded, leaf contaminated contact are also covered. The effects of varying pressure in unsanded dry and wet contacts have not been included, as this has been previously covered by Evans [144].

5.3.6.1 Dry Conditions

5.3.6.1.1 Traction Data

The effects of varying pressure in a dry sanded contact have been presented in Figure 5.64. The effect of increasing pressure also appears to increase the peak CoT reached. At a contact pressure of 300 MPa, a maximum CoT of 0.61 was reached, whereas for 600 MPa this peak reached 0.66, and 900 MPA peaked even higher at 0.76. The initial stiffnesses of the curves were very similar, though there is noticeably more variance in test data at 300 MPa and 600 MPa.

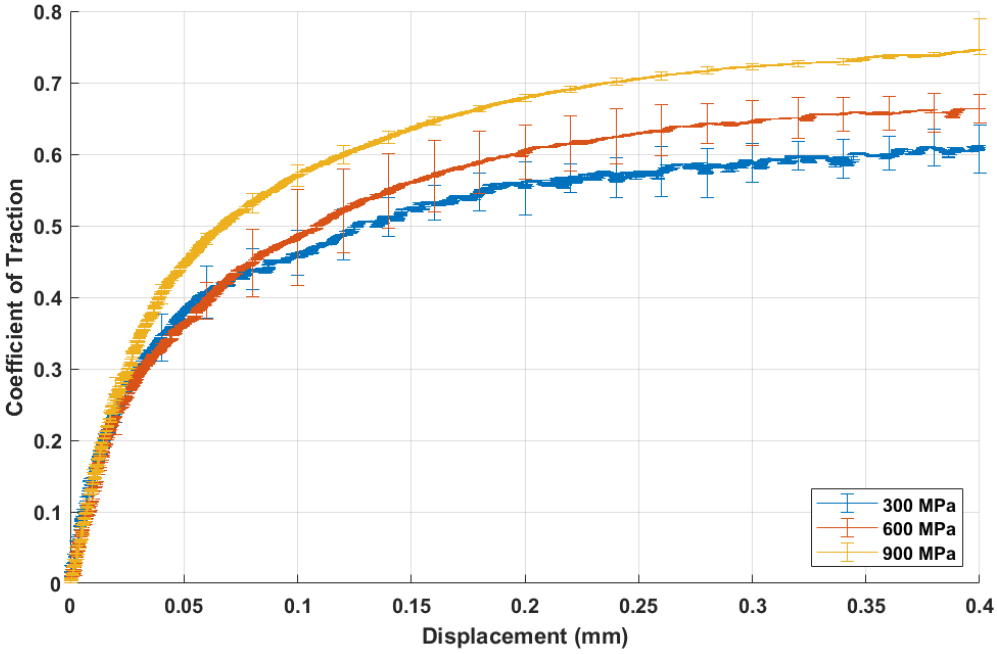

Figure 5.64. Effect of Varying Pressure with LB in a Dry Contact.

5.3.6.1.2 Post-Test Surface Analysis

Example pictures of post-test surfaces from all three contact pressures have been included in Figure 5.65. It appears that, as the pressure increases the amount of material remaining in the contact decreases, with more material remaining at 300 MPa than 600 MPa, and at 600 MPa compared to 900 MPa. What remains in the contact at lower pressures appears to have clumped together.

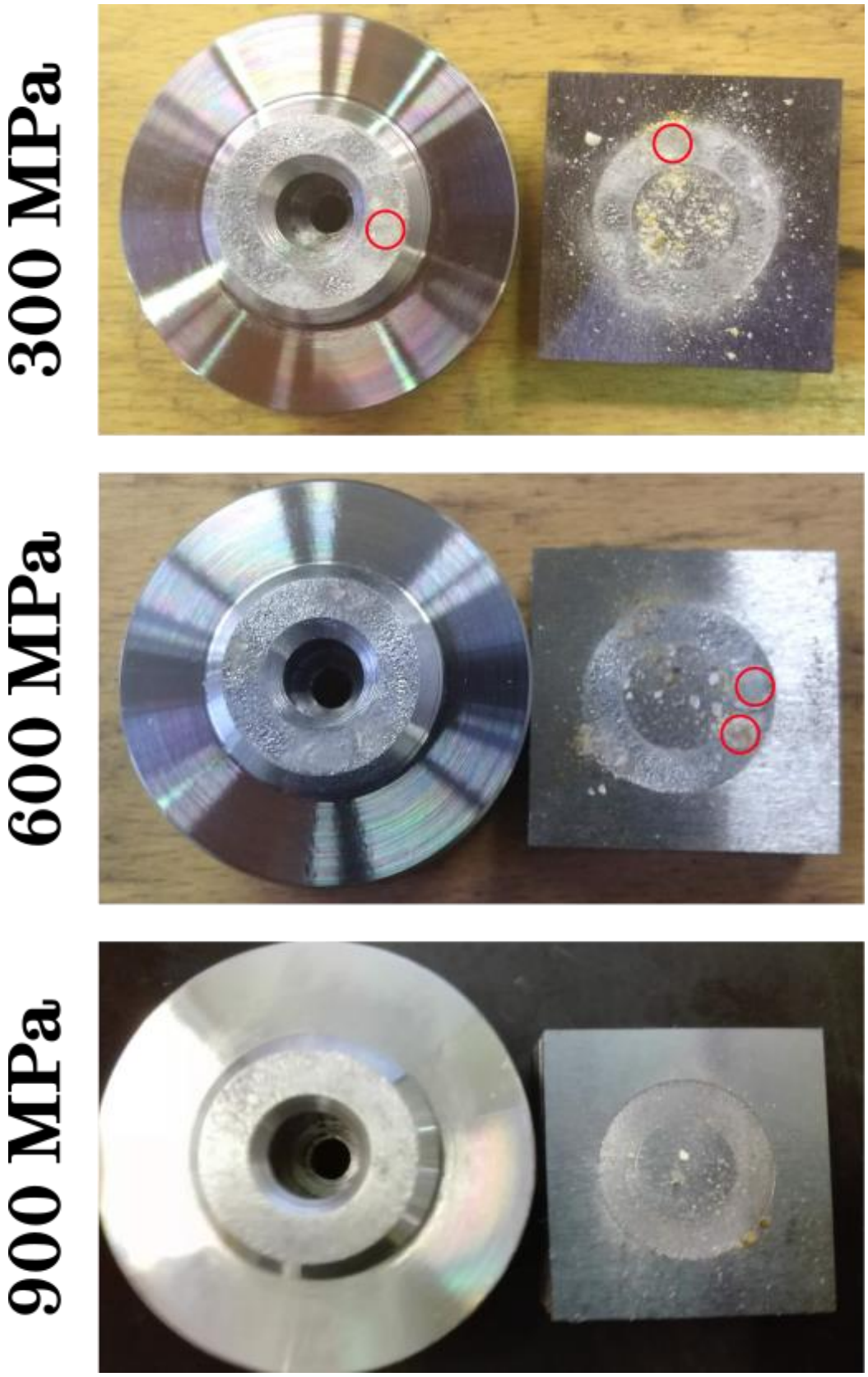

Figure 5.65. Post-test Specimens with LB applied in Dry Conditions with Varying Contact Pressure with Remaining Material encircled.

Surface roughness data for all three pressures have been included in Figure 5.66. There appears to be slightly greater roughness for 600 MPa compared to 300 MPa.

The roughness measurements from the rail specimen at 900 MPa seem to indicate that the roughness of the surface reduces at 900 MPa, however for the wheel specimen, the level of roughness is similar to at other pressures. The amount of variance in the wheel specimen roughness at 900 MPa is, however, relatively high.

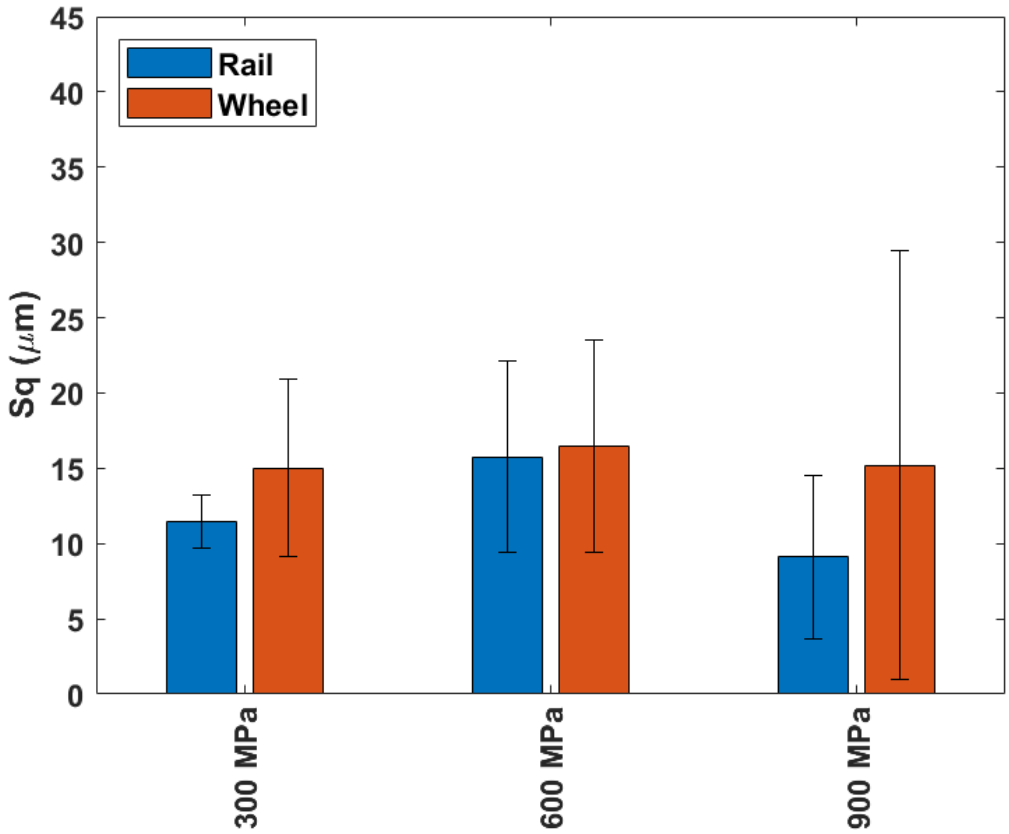

Figure 5.66. Post-Test Surface Roughness Measurements for LB in a Dry Contact with Varying Contact Pressure.

Surface scans from all three pressures have been included in Figure 5.67. Both 300 MPa and 600 MPa seem to show greater variance in height than at 900 MPa, with noticeable ridges perpendicular to the direction of motion. There appears to be little surface disturbance in the 900 MPa contact.

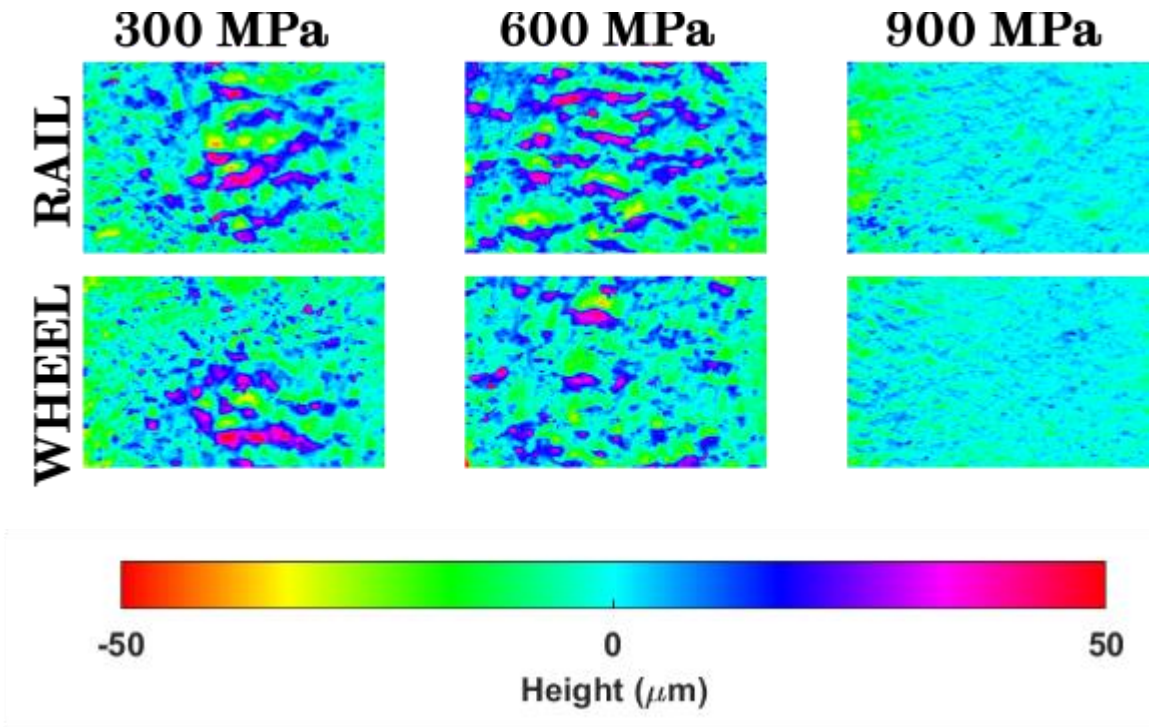

Figure 5.67. Post-test Surface Scans of Dry Contacts with LB applied with Varying Contact Pressure.

5.3.6.2 Wet Conditions

5.3.6.2.1 Traction Data

Traction data for wet tests with varying pressure, seen in Figure 5.68, show a similar trend to dry tests; as contact pressure increases, so does peak CoT. 300 MPa produced a peak CoT of 0.48, 600 MPa produced 0.54, and 900 MPa produced 0.61. In addition, the curves present a similar trend to dry conditions as the initial gradients are similar, whilst the variance in data appears to grow with decreasing pressure.

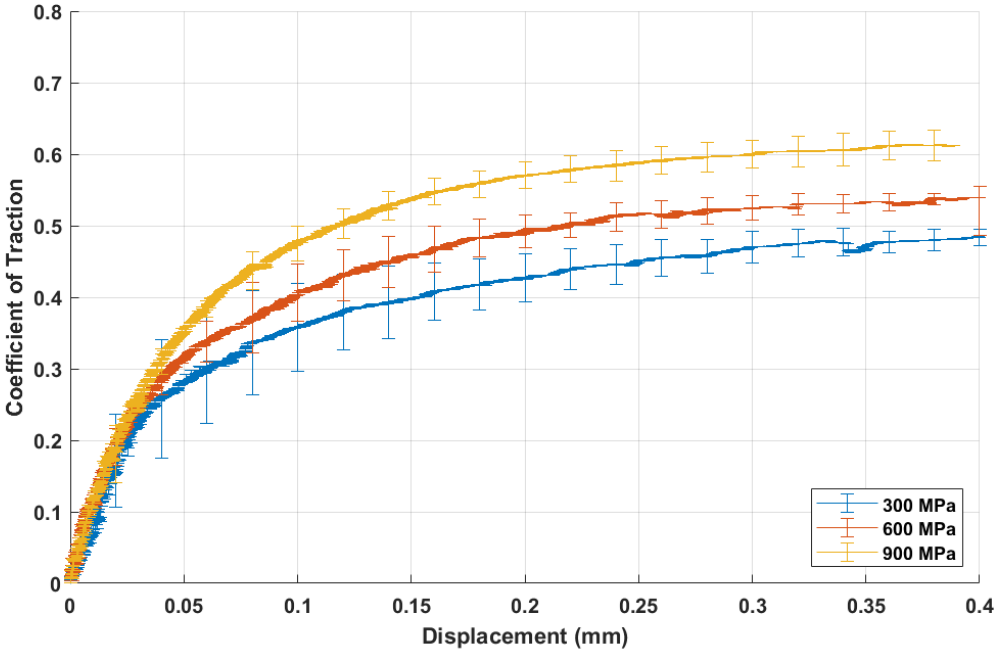

Figure 5.68. Effect of Varying Pressure with LB in a Wet Contact.

5.3.6.2.2 Post-Test Surface Analysis

Pictures from wet tests at varying pressures, included in Figure 5.69, again show similar trends to those tests in dry conditions. More material remains at lower pressures compared to higher pressures. It all appears that the clumps of particles are larger at lower pressures, the rail specimen is almost completely covered by remaining LB.

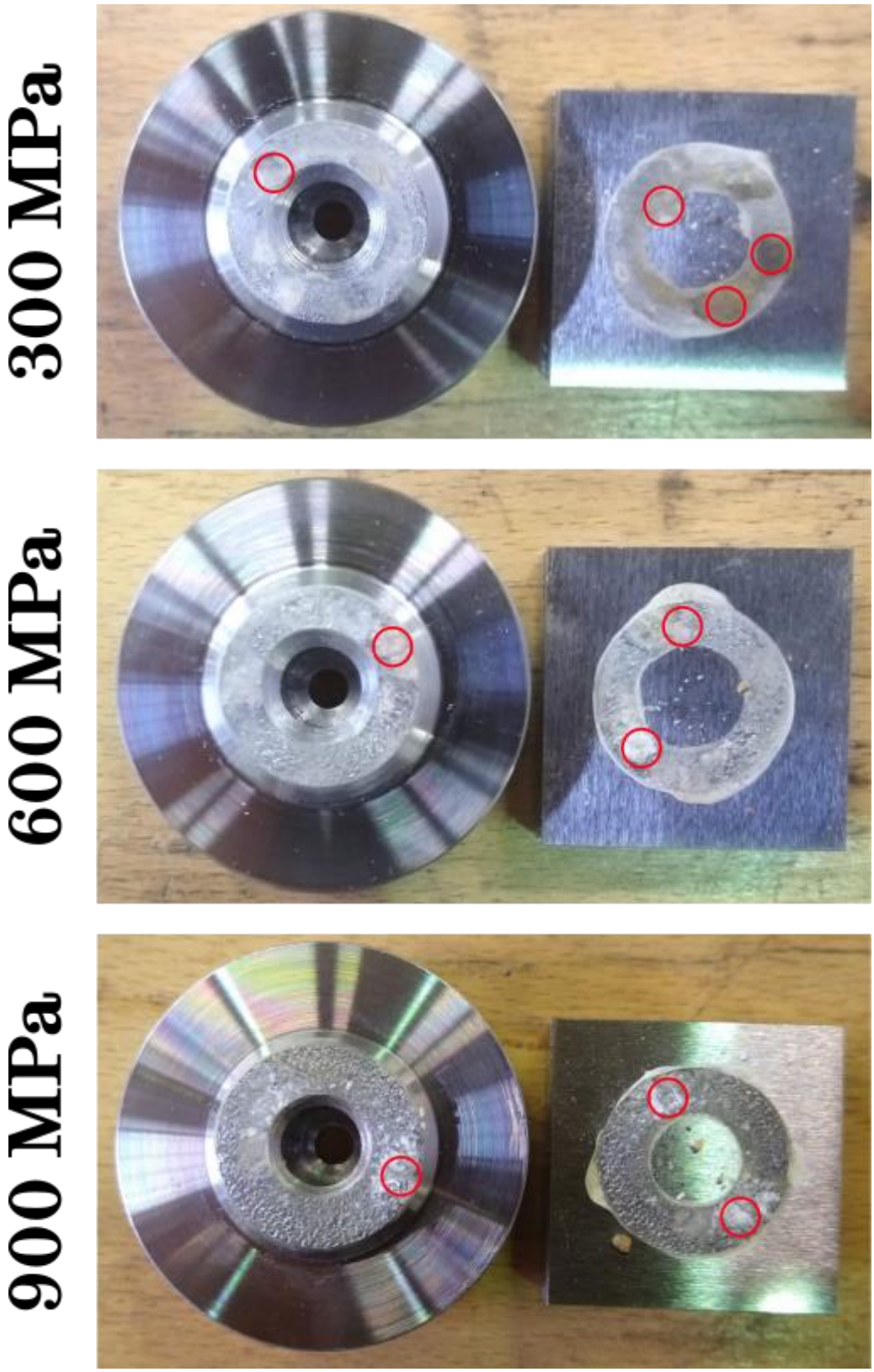

Figure 5.69. Post-test Specimens with LB applied in Wet Conditions with Varying Contact Pressure with Remaining Material encircled.

Roughness measurements presented in Figure 5.70 are, again, similar in trend to those measured in dry conditions. The surface roughnesses at 300 MPa and

600 MPa are fairly similar, whereas at 900 MPa the rail specimen is similar, but not the wheel specimen.

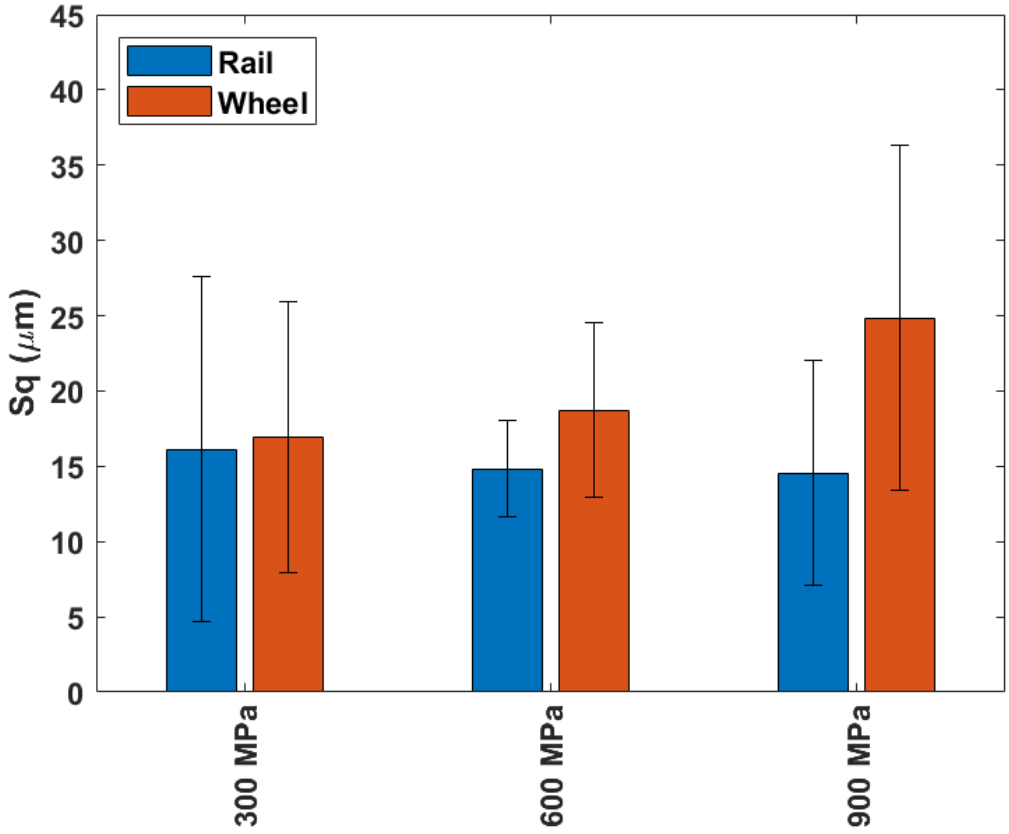

Figure 5.70. Post-Test Surface Roughness Measurements for LB in a Wet Contact with Varying Contact Pressure.

Surface scans have been included in Figure 5.71, unlike other surface characteristics a difference is apparent between trends in wet conditions and in dry conditions. Both 600 MPa and 900 MPa appear broadly similar, with ridges on their surfaces, though the former appears to have smaller, more numerous ridges compared to the latter. At 300 MPa these ridges are not apparent and instead large indentations can be seen.

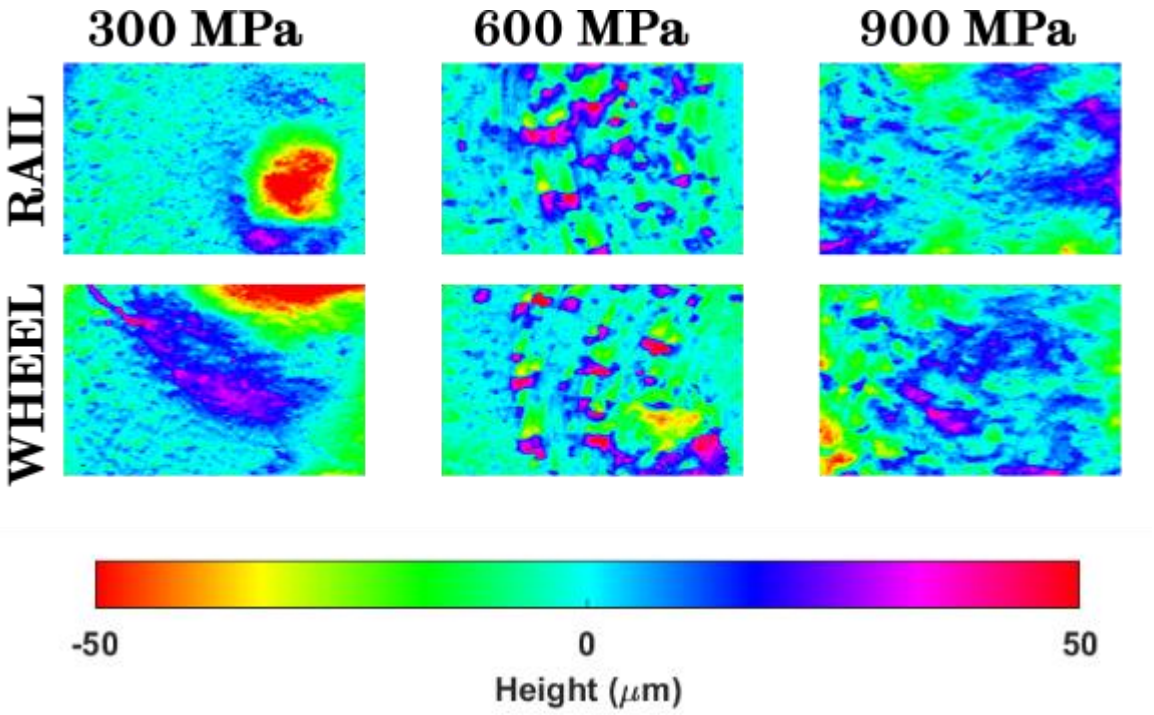

Figure 5.71. Post-test Surface Scans of Wet Contacts with LB applied with Varying Contact Pressure.

5.3.6.3 Leaf Contaminated Conditions

5.3.6.3.1 Traction Data

The effect of varying pressure when LB is applied to a leaf contaminated contact can be seen in Figure 5.72. Unlike dry and wet conditions, as the contact pressure decreases the peak CoT increases. At 300 MPa, a peak CoT of 0.22 can be observed, at 600 MPa the peak is at 0.20 and at 900 MPa the CoT peaks at 0.13.

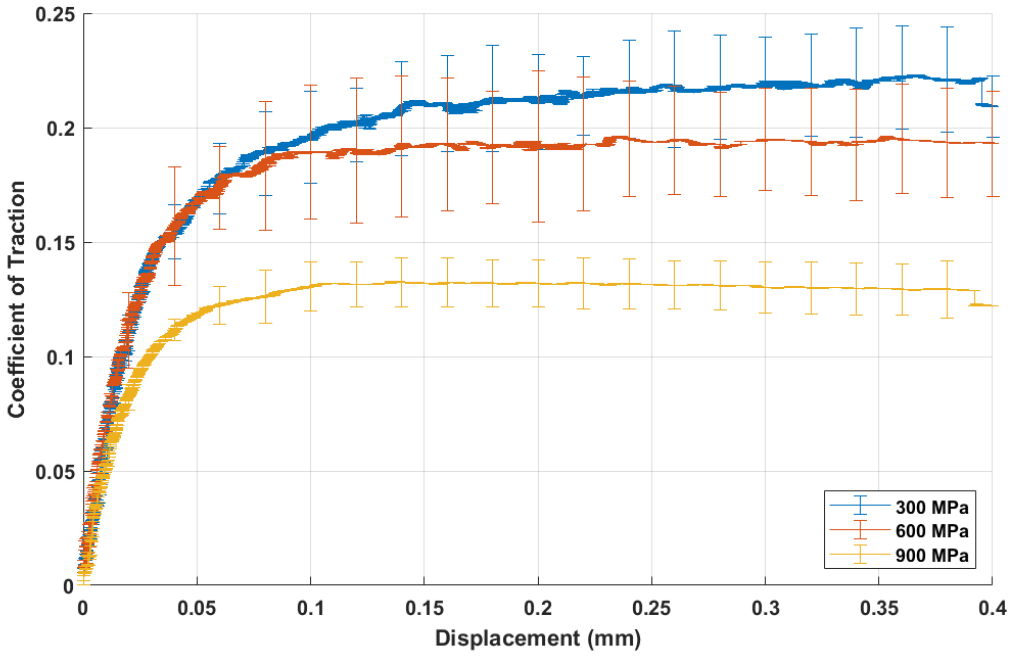

Figure 5.72. Effect of Varying Pressure with LB in a Leaf Contaminated Contact.

As Figure 5.73 shows, this rise in traction with decreasing pressure cannot be attributed to the effect of varying pressure on the leaf layer alone. For this unsanded data all peak CoTs are very similar, being between 0.05-0.06.

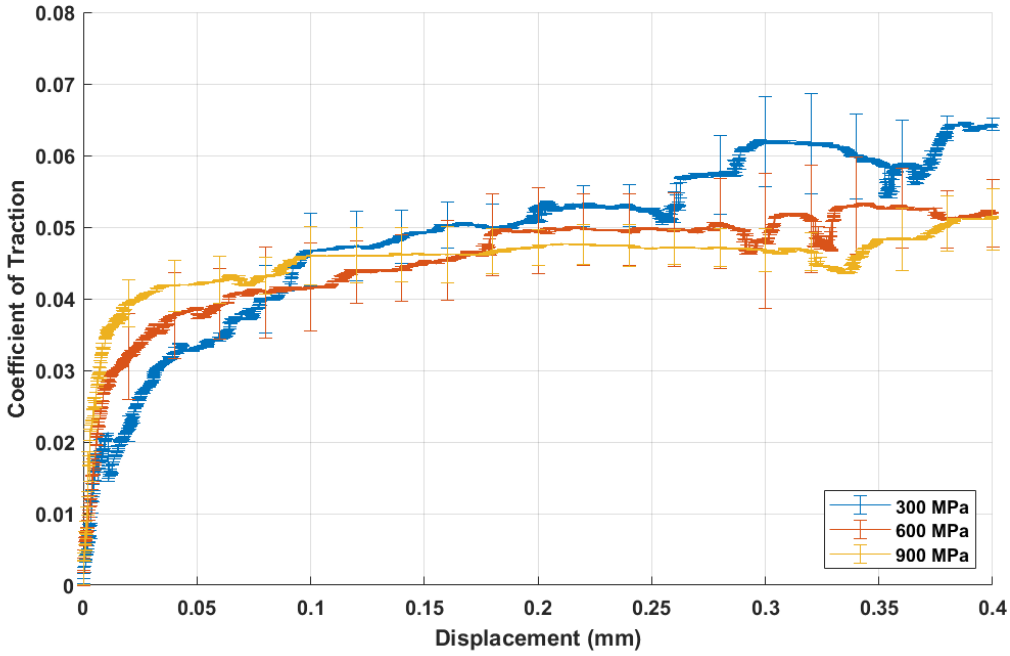

Figure 5.73. Effect of Varying Pressure in an Unsanded, Leaf Contaminated Contact.

5.3.6.3.2 Post-Test Surface Analysis

Pictures of the specimens, post-testing with LB applied, are shown in Figure 5.74. LB remains within the contact at all three pressures, the size of the clumps appears to be larger at lower pressures.

Figure 5.74. Post-test Specimens with LB applied in Leaf Contaminated Conditions with Varying Contact Pressure.

Figure 5.75 includes pictures from the unsanded tests. The leaf layer in each picture appears to be very similar.

Figure 5.75. Post-test Specimens in Unsanded, Leaf Contaminated Conditions with Varying Contact Pressure.

Surface roughness measurements when LB was applied are shown in Figure 5.76. The amount of roughness in the contact appears to increase with increasing pressure.

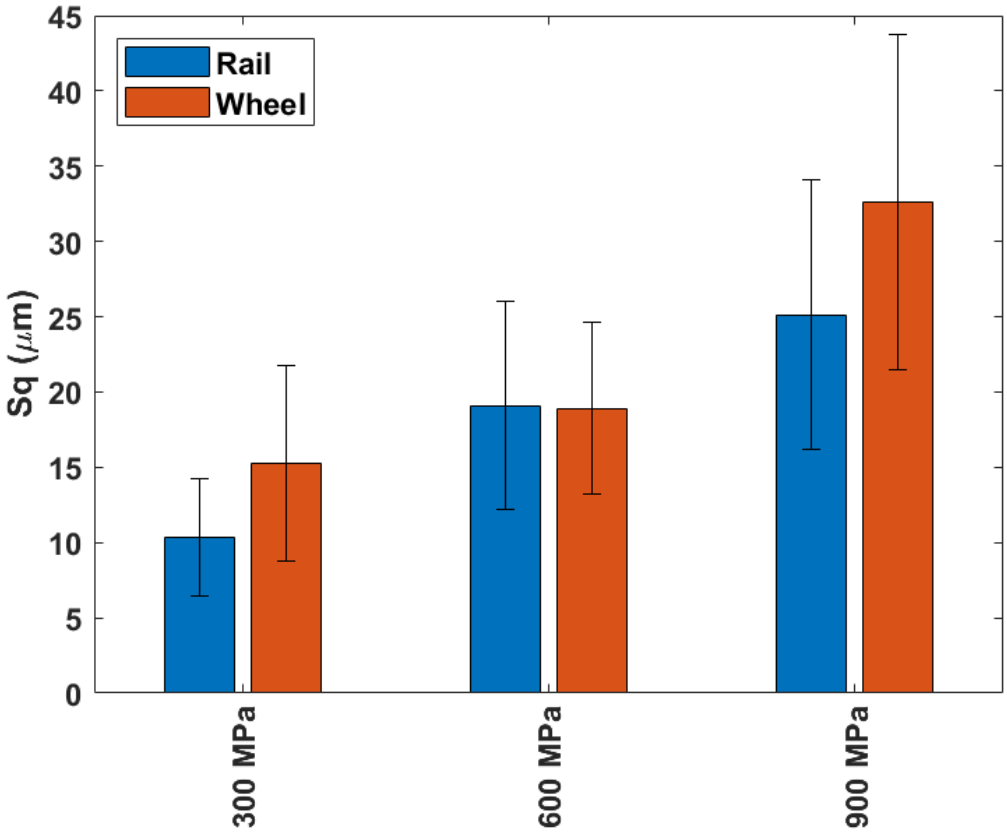

Figure 5.76. Post-Test Surface Roughness Measurements for LB in a Leaf Contaminated Contact with Varying Contact Pressure.

The increase in roughness with pressure is not apparent when sand is not applied. In Figure 5.77, the surface roughness remains constant with varying contact pressure.

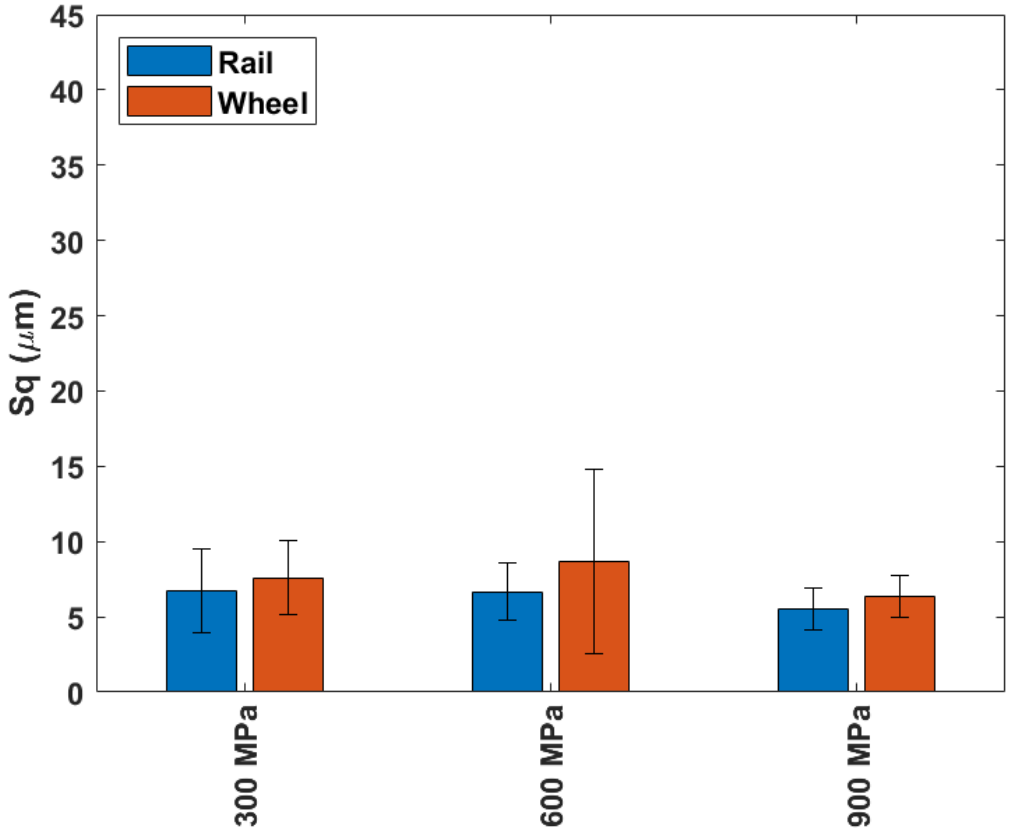

Figure 5.77. Post-Test Surface Roughness Measurements for an Unsanded, Leaf Contaminated Contact with Varying Contact Pressure.

Surface scans when LB was applied are included in Figure 5.78. All surfaces show evidence of indentation; however, the indentation area appears to grow with increasing pressure.

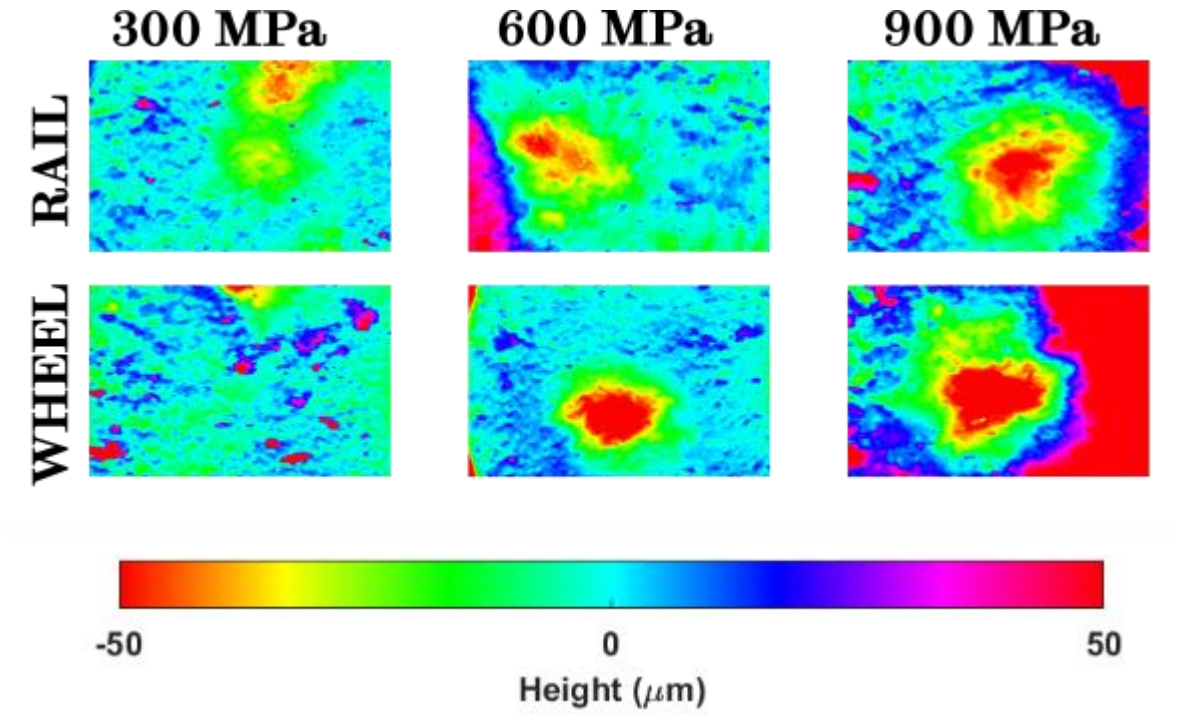

Figure 5.78. Post-test Surface Scans of Leaf Contaminated Contacts with LB applied with Varying Contact Pressure.

When sand was not applied the surfaces remained broadly the same. Surface scans from these unsanded cases are included in Figure 5.79.

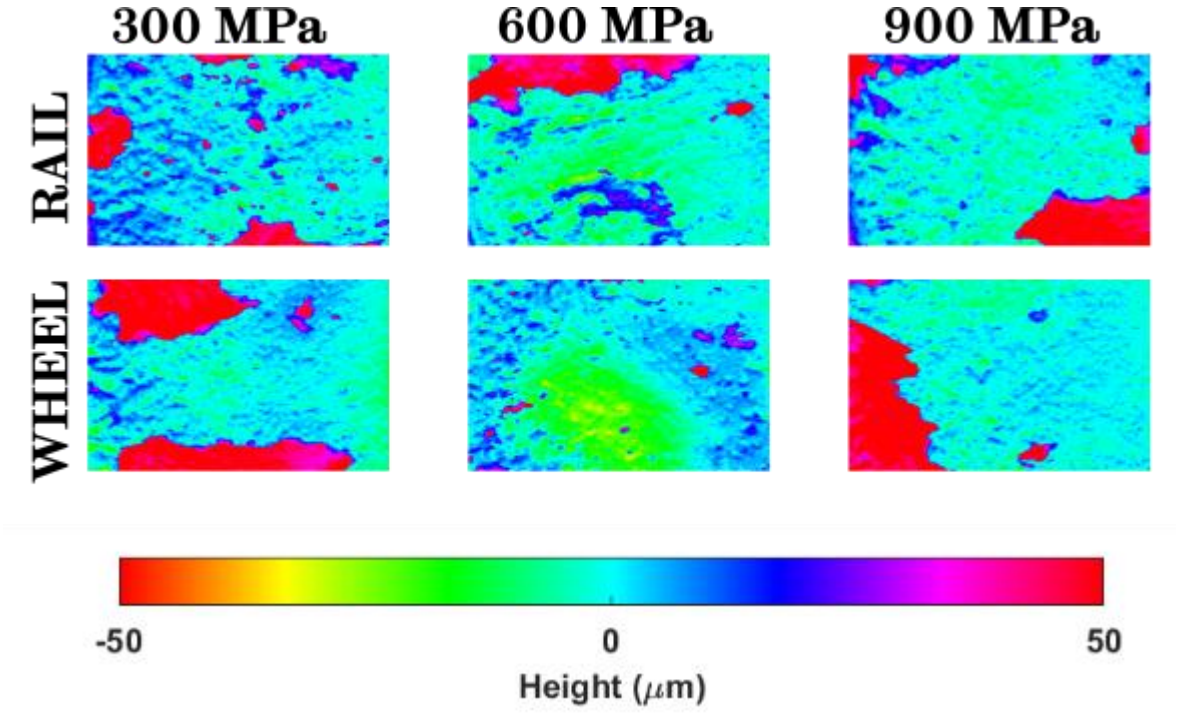

Figure 5.79. Post-test Surface Scans of Unsanded, Leaf Contaminated Contacts with Varying Contact Pressure.

5.3.6.4 Discussion

From all conditions, it can be seen that the contact is pressure agnostic when no sand is applied, however sand has a marked effect on pressure dependency in all conditions, though with varying consequences.

5.3.6.4.1 Dry & Wet Conditions

In both dry and wet, sanded conditions, increasing contact pressure created higher traction with similar or less surface damage compared to lower pressures. However, in a leaf contaminated contact, the contact pressure versus traction relationship was inverse and higher pressure created greater surface damage.

In dry conditions, the direct relationship between increasing pressure and traction for the sanded contact was unlike that observed by Evans [144] in dry, unsanded conditions, where there seemed to be no clear relationship between pressure and traction. In the sanded contact, more sand remained at lower pressures as less was forced out of the contact. As previously observed, in dry conditions remaining sand can act as a lubricant, this perhaps being the reason for lower traction with lower pressure in the sanded contact.

In wet conditions, the direct relationship between pressure and traction was maintained. In wet, unsanded tests conducted by Evans [144], there was no clear relationship between pressure and traction. There appeared to be little difference in post-test surface characteristics, though the size of the remaining material clumps and surface indents appeared to be largest at 300 MPa.

This trend of decreasing traction with decreasing normal pressure, apparent in both dry and wet conditions, may be due to the decreasing indentation depth of the particles as less pressure is applied and the amount of particle transferring tractive force in a manner similar to that in Figure 5.31(A) is reduced. The amount of material remaining in the contact may also play an important part in determining the effect of the particles; in dry conditions, where less material was retained at higher pressures, the lack of particles acting as a dry lubricant at higher pressures may also contribute to greater traction. Similar findings relating lower normal loads, with lower friction due to less indentation were observed by Bhusan and Kulkarni [148]; they summarised that lower normal loads lead to less indentation depth, thus a lower contact area and the coefficient of friction being lower as less ploughing occurred.

5.3.6.4.2 Leaf Contaminated Conditions

In leaf contaminated conditions, as contact pressure increased the traction decreased; this was not apparent in the unsanded case. In the unsanded contact there was also little effect of pressure on surface conditions, whereas increasing pressure saw greater surface damage in the sanded cases.

One explanation for this may be that as normal pressure increased, the particles indented further into the steel surface of the wheel and rail specimens, as posited for the wet case. However, as more the particle is indented into the wheel/rail surface there is less of the particle acting on the leaf layer itself, thus there is less material to remove the leaf layer, see Figure 5.80 for a schematic representation. This would explain the lower normal pressure post-test surfaces having less of a leaf layer in Figure 5.74 and is corroborated by the greater roughness and indentations seen in Figure 5.76 and Figure 5.78 respectively.

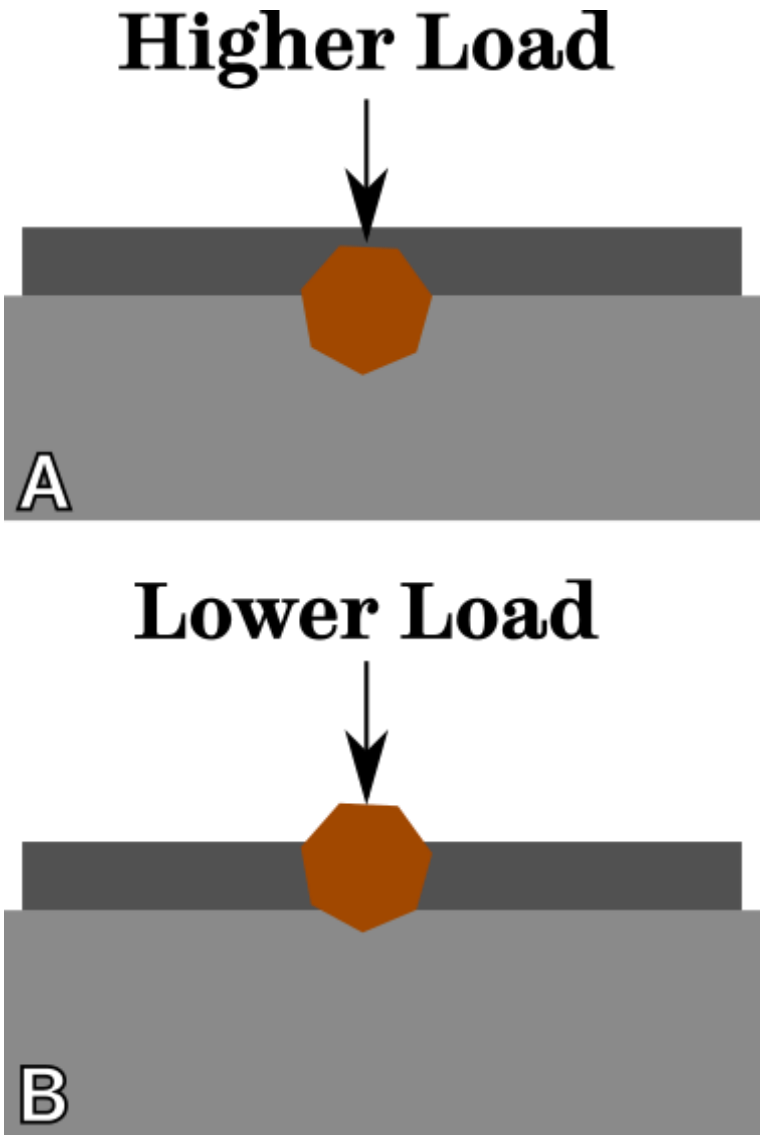

Figure 5.80. Difference in Particle Indentation under: *(a)* Higher Contact Pressures; *(b)* Lower Contact Pressures.

5.4 Discussion

The following sub-chapter will draw relationships between different particle characteristics (see Chapter 4) and their effect on the traction and surface damage present in the HPT contact.

Initially, potential relationships will be drawn out from examining simple plots to identify any potentially important particle characteristics; this will be determined from the calculated R^2 value, where the R^2 value denotes the variance in test measurements from a linear line of best fit and ranges from 0-1, with higher values meaning a stronger relationship. These characteristics will then be analysed using an ordinary least squares model to quantify how important these characteristics are for determining their effect in the HPT contact.

5.4.1 Effect of Particle Size in the HPT Contact

When initially comparing the effect of particle size to the coefficient of traction, there is no obvious trend. Generally, dry conditions produced higher traction, with the presence of water reducing this; leaf contaminated contacts were much lower. When all particles are plotted there appears to be very little relationship between particle size and traction in any third body condition, however there are large outliers present, especially in dry and wet conditions. These outliers were generally from non-sand particles and non-pure quartz particles, i.e. softer particles.

When only quartz particles are included in Figure 5.81, clearer relationships emerge. In dry conditions, a relatively weak relationship (indicated by the low R^2 value) between particle size and traction is indicated. In both wet and leaf contaminated conditions, there is a stronger relationship between decreasing particle size and increasing peak traction.

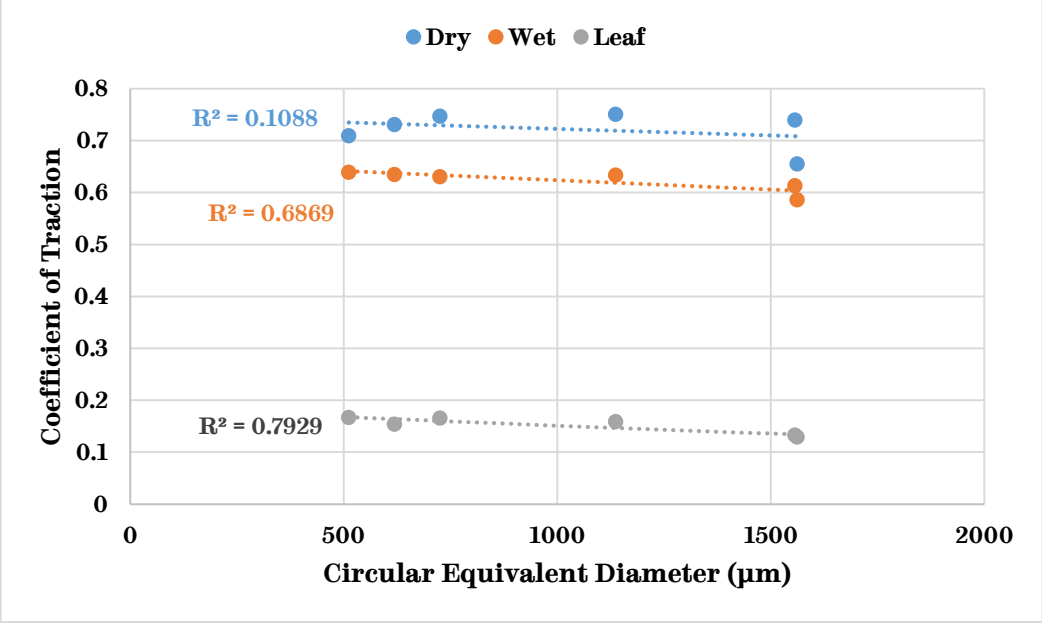

Figure 5.81. Relationship between Particle Size and Coefficient of Traction for Quartz Particles.

Comparing the effect of differing particle sizes on surface roughness, produces no strong relationships when all particles are considered. There also appears there is no strong difference between the third body conditions. There does, however, appear to be more variation in surface roughness measurements with higher particle sizes, possibly due the larger variation in whether a particle will remain in the contact at larger sizes.

When quartz particles alone are considered, stronger trends once again become apparent, as seen in Figure 5.82. The relationship between particle size and roughness is fairly weak, but seems to indicate there is an increase in surface

damage when tending towards larger particles; a similar, though, much stronger relationship is seen in wet conditions. There is a strong relationship between particle size and surface damage in leaf contaminated conditions, larger quartz particles produce significantly higher damage than smaller particles.

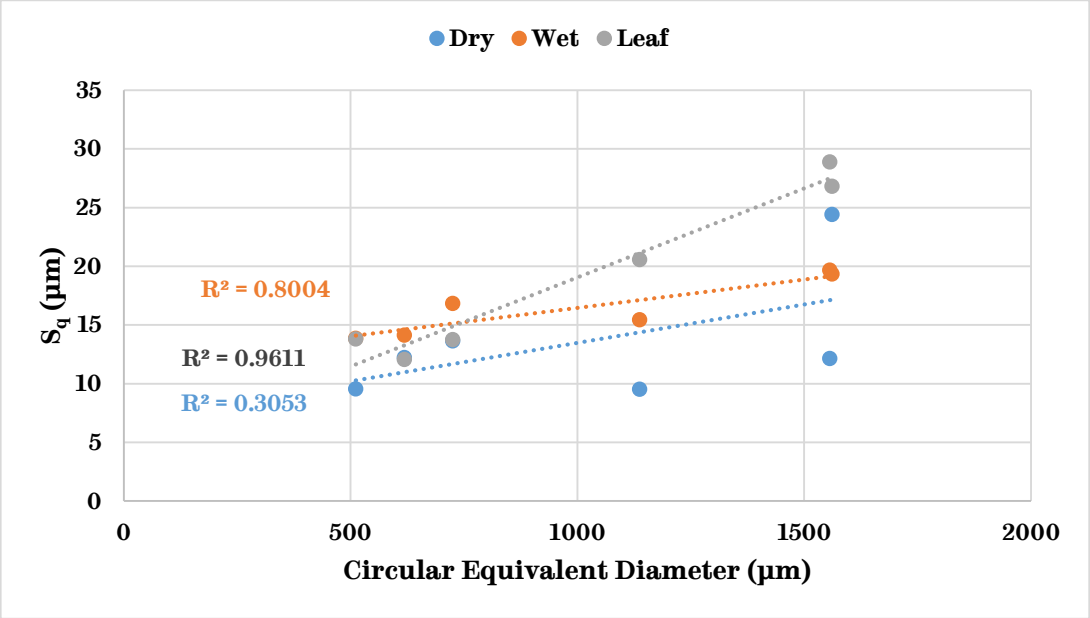

Figure 5.82. Relationship between Particle Size and Surface Roughness for Quartz Particles.

These analyses suggest size has an impact on both the peak coefficient of traction and surface roughness. Further analysis will be needed to ascertain the exact nature of this relationship, though from studying just quartz particles, it appears increasing particle size decreases peak CoT and increases surface roughness.

5.4.2 Effect of Particle Shape in the HPT Contact

When considering shape, particularly shape, against traction for all particles there was no apparent link between particle shape and traction. When only mineral particles are plotted, in Figure 5.83, a clearer relationship can be seen in all conditions. There is a very weak positive correlation apparent in dry and wet conditions, though the opposite is true for the leaf contaminated contact.

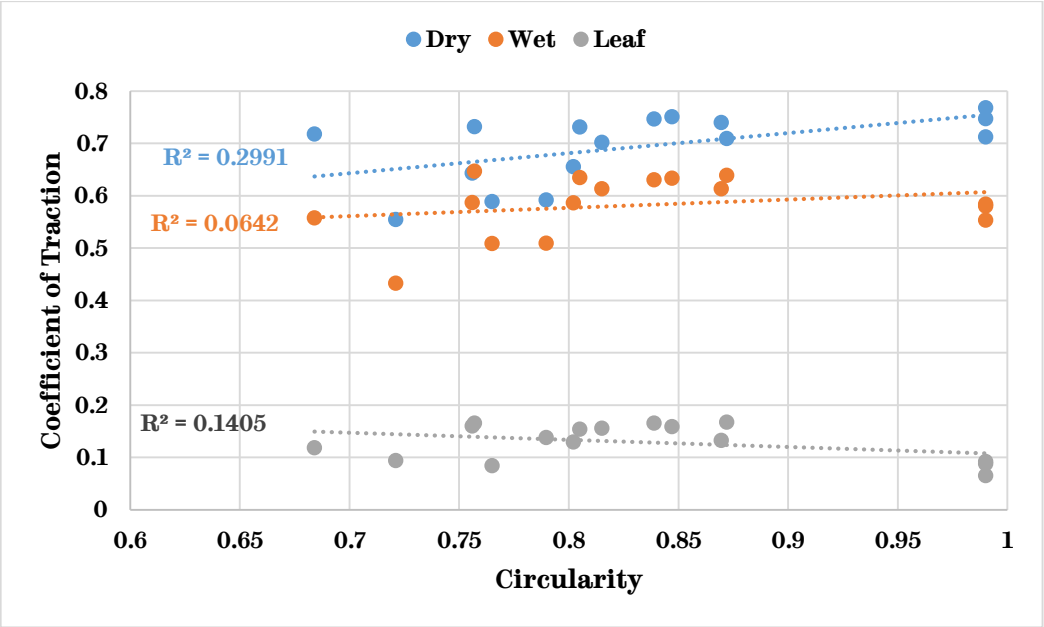

Figure 5.83. Relationship between Particle Shape and Coefficient of Traction for Mineral Particles.

When considering particle circularity against surface roughness, no apparent relationships are apparent when all particles are considered. In Figure 5.84, only mineral particles are plotted. In general, as circularity increased, roughness decreased.

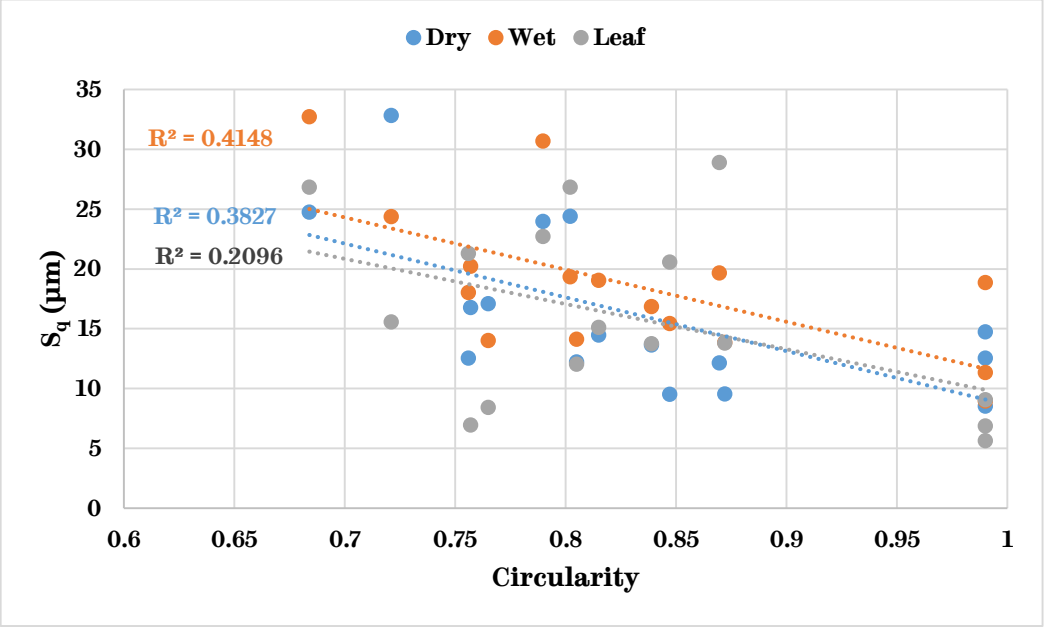

Figure 5.84. Relationship between Particle Shape and Surface Roughness for Mineral Particles.

There is some evidence to suggest shape has some effect on peak CoT, and acts differently when leaf contamination is present, and stronger evidence to suggest it has an increasing circularity has a reductive effect on surface roughness.

5.4.3 Effect of Particle Hardness in the HPT Contact

In Figure 5.85, particle hardness has been plotted against traction for all particles. Both dry and wet conditions show a similar trend: traction increases with particle hardness, with this change plateauing with increasing particle hardness. In leaf contaminated conditions, the relationship is the same though linear.

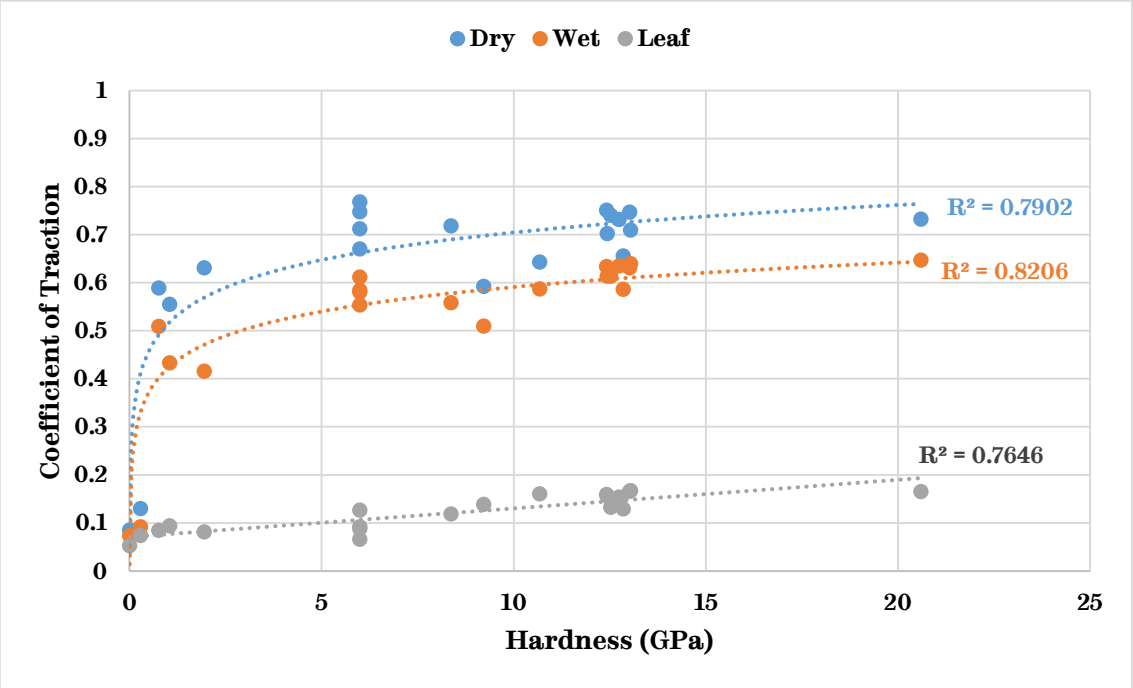

Figure 5.85. Relationship between Particle Hardness and Coefficient of Traction for All Particles.

A similar relationship between particle hardness and coefficient of traction in dry conditions was observed by Zobel [47], who also observed this relationship was non-linear.

Converse to particle hardness' effect on traction, there appears to be no obvious relationship with surface roughness.

The results assessed in the sub-chapter strongly suggest hardness has an effect on the peak coefficient of traction in all conditions. There is also evidence that the effect of hardness is non-linear in dry and wet conditions.

5.4.4 Effect of Particle Fracture Toughness in the HPT Contact

The effect of fracture toughness on traction has been plotted in Figure 5.86. No relationship is apparent in leaf contaminated conditions. Both dry and wet conditions exhibit a similar relationship, with a possible positive correlation between fracture toughness and peak CoT

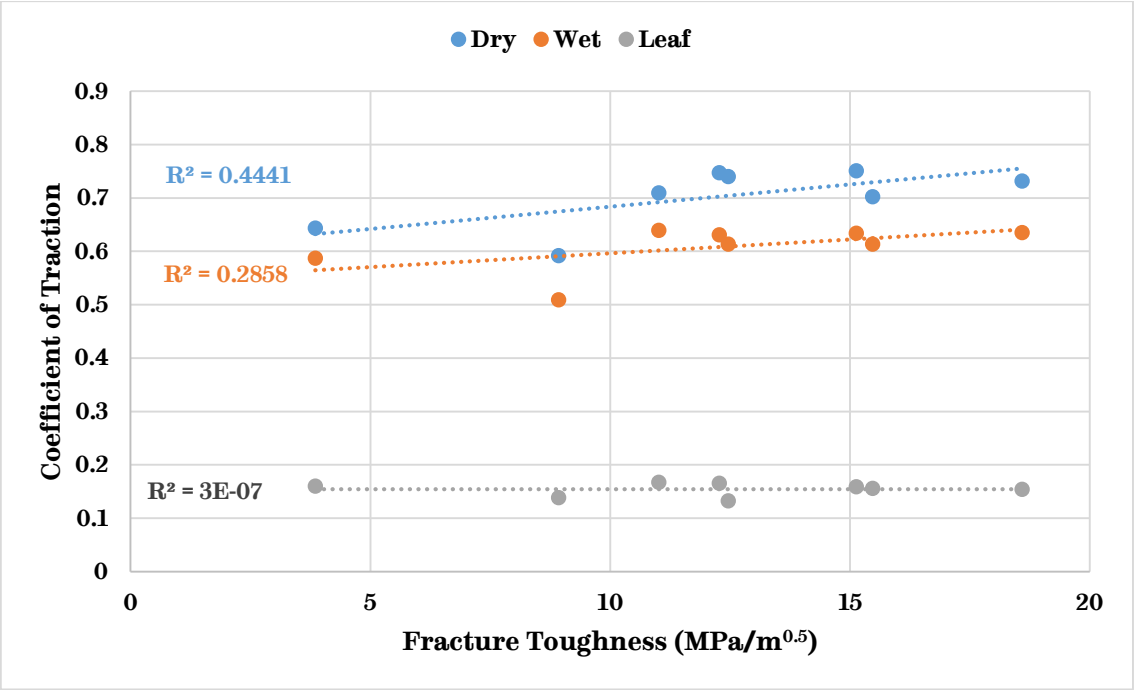

Figure 5.86. Relationship between Particle Fracture Toughness and Coefficient of Traction for Applicable Particles.

The relationships between fracture toughness and surface roughness are weaker. There is some evidence that surface roughness decreases with increasing fracture toughness, though the trends have been deemed too weak to merit further comment.

5.4.5 Relationship between Post-test Surface Roughness and Traction Performance

As opposed to previous comparisons, this comparison is between two dependent variables. Thus, it is harder to draw conclusions about one variable's effect on the other, but correlations between the two may help to suggest certain mechanisms occurring in the contact.

The relationships between surface roughness and traction in dry, wet, and leaf contaminated contacts have been illustrated in Figure 5.87. There is no link in dry conditions and wet conditions. There is a stronger link in leaf contaminated conditions, with the inference being that when surface roughness is higher, so is the peak coefficient of traction. This may be due to the particles fully indenting the leaf layer through to the surface, if this happens it will roughen up the surface and increase traction simultaneously. Overall though, there appears to be no strong correlation between surface roughness and the peak coefficient of traction.

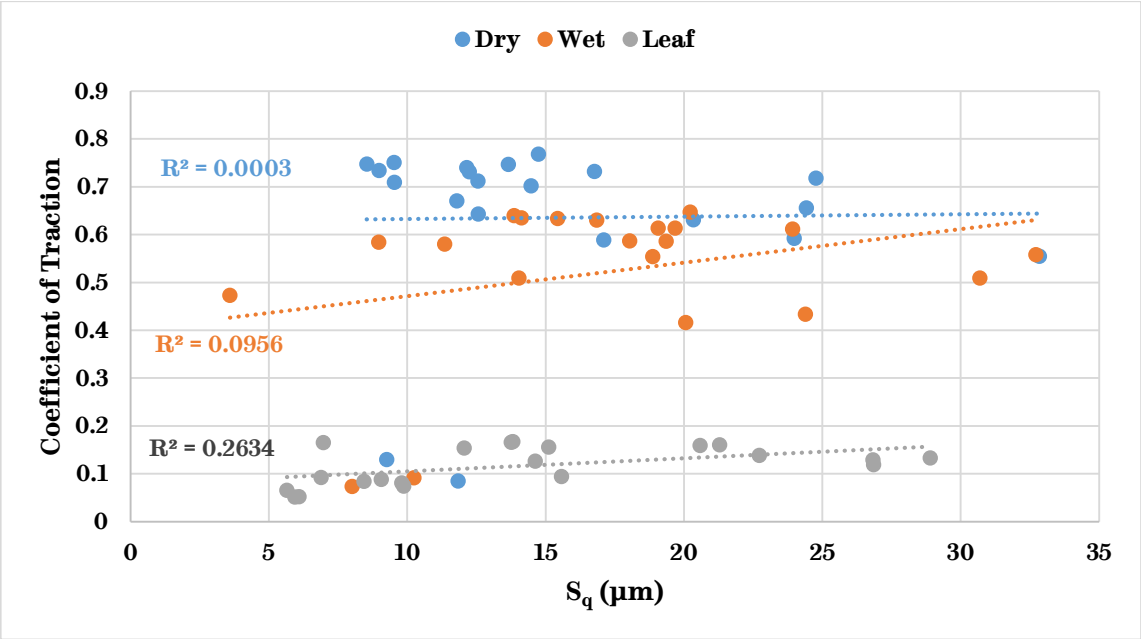

Figure 5.87. Relationship between Surface Roughness and Coefficient of Traction for All Particles.

5.4.6 Ordinary Least Squares Model

An ordinary least squares model was created taking potential relationships identified previously into account. Separate models were generated for dry, wet, and leaf contaminated conditions with regards to analysing the effect of particle characteristics on the peak coefficient of traction (CoT) as they presented stark differences. With regards to roughness, one model was generated for wheel and rail roughness respectively, where all conditions were included. All relationships discussed in this sub-chapter have very strong statistical significance ($p<0.001$).

Before data were modelled, they were scaled according to a normal distribution, where the mean was equal to zero and unit standard deviation was used. In this way, coefficients could be more easily comparable.

Summaries of the statistically significant coefficients of particle characteristics vs peak coefficient of traction and wheel and rail roughness have been included in Table 5.3 and Table 5.4 respectively. Where depth and size^2 represent non-linear terms for particle hardness and particle size respectively. The rest of this sub-chapter will further discuss these trends.

Table 5.3. Summary of Variable Coefficients with respect to Peak Coefficient of Traction.

	All Particles	**Hard Particles**
Dry	Hardness: -0.77 Depth: 1.35	Hardness: 0.54 Circularity: 0.46
Wet	Hardness: -0.44 Depth: 0.96	Hardness: 0.81 Circularity: 0.33
Leaf	Hardness: 0.13 Size: 0.18 Size^2: -0.20	Hardness: 0.69 Circularity: -0.24 Size: 1.47 Size^2: -1.65

Table 5.4. Summary of Variable Coefficients with respect to Surface Roughness.

	All Particles
Wheel S_q	Circularity: -0.59 Size: 0.31
Rail S_q	Circularity: -0.56

5.4.6.1 Peak Coefficient of Traction in Dry Conditions

When all particles were included in the dry model the only significant trend was the non-linear effect of hardness on peak CoT, this was also observed when simply plotting hardness against peak CoT in sub-chapter 5.4.3. However, further analysis showed that the very soft particles (AC, NA) were over-leveraged i.e. the model was too dependent on these data points. When these particles were removed from the fitting process, increasing hardness was positively correlated to peak coefficient of traction (coefficient=0.54), but higher order terms were no longer statistically significant. In addition, increasing particle circularity was also found to have a positive, albeit lesser, effect on peak CoT (coefficient=0.46).

The effect of hardness in dry conditions has also been seen when testing rail sands and was a strong trend identified in Figure 5.85; in addition, work by Zobel [47] also identified a link between hardness and traction. The mechanism for this was previously identified and outlined in Figure 5.31, where harder particles were able to

indent into the surface and transfer traction more effectively. Further analysing Figure 5.85, the point at which the gradient begins to lessen is around the same hardness as rail and wheel steel i.e. 1.9 GPa and 2.9 GPa [22] respectively. From this it can be concluded that a prospective adhesion material should have a hardness greater than the wheel/rail surfaces and after this point the increase in traction is relatively minor.

The effect of shape was not immediately obvious from initial plots of circularity vs peak CoT in sub-chapter 5.4.2, demonstrating the value of using the ordinary least squares model. Previous work from Nakata et al. [149] found that more circular particles had higher initial crushing stress than more angular particles. This greater initial crushing stress may result in greater stored elastic energy, thereby resulting in a more explosive initial fracturing of the particle, leaving less material in the contact to act as a dry lubricant, as previously discussed in this chapter.

One notable characteristic that did not have a statistically significant link with peak coefficient of traction was particle size; it should be stressed that this does not mean that particle size had no effect on traction in the HPT contact, rather no statistically significant link was observed. Previous work by Arias-Cuevas et al. [20] found there was a link between particle size and traction in dry conditions when twin-disc tests were conducted, with larger particles seeing higher traction. The proposed explanation of this was that larger particles were less easily entrained into the contact; therefore, less material was present to act as a dry lubricant.

Due to the nature of the HPT contact, the entrainment mechanism was different to a twin-disc test, this may explain the lack of a statistically significant link across all tested particles. In addition, the two test methodologies were rather different, with these twin-disc tests using a continual application of sand over many cycles. This could have led to a build-up of material on the surfaces of the discs as more material was being applied over recycled material, thus exaggerating the lubricating effect of sand application. There was, however, some evidence from glass bead tests that the largest bead size produced the highest traction.

5.4.6.2 Peak Coefficient of Traction in Wet Conditions

These trends were similarly present in wet conditions. Hardness being having significant second order terms when soft particles were included, and hardness and circularity becoming significant trends when only harder particles were considered. There was a stronger relationship between hardness and peak CoT in wet conditions (coefficient =0.81), with circularity being relatively less effective (coefficient=0.33). Contrary to the trends seen in dry conditions, the effect of

hardness is even more important and the effect of shape less important in wet conditions.

Whilst the mechanism by which particle hardness affects the HPT contact in dry conditions has previously been discussed, the mechanism by which particle shape affects the HPT contact in wet conditions does not hold true here. The presence of remaining material helps to provide break up the liquid lubricating layer, thus it is better for more material to be retained upon crushing. A more angular particle may break up the attractive meniscus formed by the water (see Figure 5.29 and Figure 5.30), leading to more material being expelled, thereby making more angular particles less effective at increasing traction in wet conditions than more circular particles.

As in dry conditions, particle size did not possess a statistically significant link with coefficient of traction. Twin-disc tests performed by Huang et al. [44] did see a link between particle size and traction in wet conditions, though the methodology differed from HPT testing, as particles were continuously applied over thousands of cycles. As noted when discussing the link between particle size and traction in dry conditions, this may have resulted in a build-up of material in the contact and a change in effect vs application at representative amounts. In addition, in their discussion of the results, it is mentioned that for the "early period" (when sand first begins to be applied) "adhesion coefficient fluctuates intensely" and only after many cycles does it then become stable, suggesting the effect of particle size is not as clear when sand is being initially applied (similar to HPT testing).

5.4.6.3 Peak Coefficient of Traction in Leaf Contaminated Conditions

Conversely, when analysing leaf contaminated conditions different trends were apparent. With and without soft particles being included, hardness was positively correlated with peak CoT and size had significant first order and second order terms. When only hard particles were included these trends became stronger, and shape also became a significant factor. In this leaf contaminated case, size was the most important factor, with correlations of first order and second order terms (linear coefficient=1.47; quadratic coefficient=-1.65) inferring the existence of an optimum particle size for increasing traction in leaf contaminated contacts. Particle hardness is still of import, a positive correlation exists between this and peak CoT (coefficient=0.69). As opposed to dry and wet conditions, in leaf contaminated contacts show decreasing peak CoT with increasing circularity (coefficient=-0.24).

The existence of an optimum particle size for restoring traction in leaf contaminated contacts was also observed in twin-disc and field trials conducted by Arias-Cuevas et al. [39], [43]. The drop in traction with larger sizes was previously

discussed in sub-chapter 5.3.4.4.3. The drop with smaller sizes has been incorporated into the previously used schematic and presented in Figure 5.88. As previously discussed, a larger particle will result in more material being expelled from the contact; a smaller particle however, will not have as large an effect on the leaf layer as it is not acting over as large an area of the leaf layer.

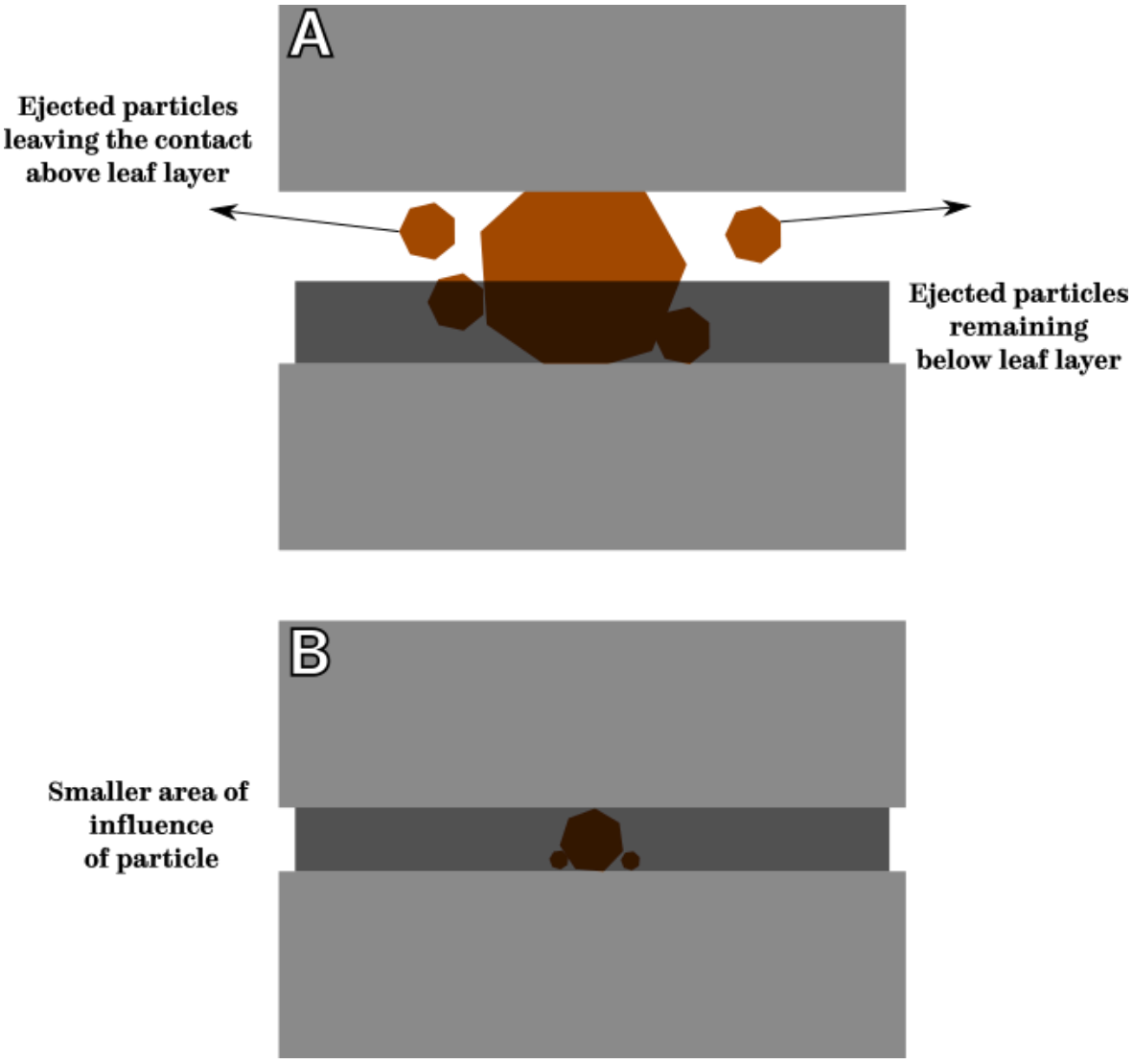

Figure 5.88. Influence of Particle Size in Leaf Contaminated Contact: *(a)* Larger Particle; *(b)* Smaller Particle.

The link between decreasing particle shape and increasing traction was also identified in sub-chapter 5.3.4.4.2, where this link was explained by the more angular particle being more effective at cutting through the leaf layer. The link with hardness is probably the same mechanism as previously discussed, though in this case the particles' effect on the leaf layer is more important than the wheel/rail surfaces below, thus making particle hardness less important than for dry and wet conditions.

5.4.6.4 Surface Roughness

With regards to the effect of particle characteristics on surface roughness, both the wheel and rail roughness were negatively correlated to particle circularity, the former showing a slightly stronger correlation (coefficient=-0.59) than the latter (coefficient=-0.56). In addition, when analysing wheel data, it is apparent that increasing particle size increases wheel roughness (coefficient=0.31); this was not the case when looking at rail roughness.

The effect of increasing particle size increasing surface roughness was also observed in work undertaken by Huang et al. [44].

Notably, there was no statistically significant link observed between particle hardness and surface roughness (though this does not mean no link between the two exists). Work undertaken by Wang et al. [51] did find a link between increasing particle hardness and increasing wheel/rail damage using a twin-disc set-up over thousands of cycles. The inability to see how damage progresses over many cycles is a limitation of the HPT rig, with inferences made about the effect of damage from the initial few cycles of the application of sand only. This may explain why no significant trend was observed between hardness and roughness during HPT testing.

5.5 Summary

In this chapter, the high pressure torsion (HPT) rig was adapted for testing granular material in low adhesion conditions. The HPT rig simulates the wheel/rail interface through high contact pressures and the stick-slip nature present in the contact.

Numerous particle types were applied to the HPT contact in dry, wet, and leaf contaminated conditions; the latter third body condition being developed as part of this work and returning extremely low traction (<0.05). Dry conditions generally gave the highest traction, with the presence of water reducing available traction, and the leaf contaminated test returning the lowest traction.

For both dry and wet conditions, increasing particle hardness and circularity increase the measured peak coefficient of traction, with hardness being the stronger of the two trends. When analysing all particles, using both simple logarithmic models and the ordinary least squares model, the effect of hardness appears to be non-linear, where a hardness value exists below which efficacy rapidly decreases and above which efficacy is only marginally increased.

Hardness also appears to have a positive linear effect on peak CoT in leaf contaminated conditions, though the effect of increasing particle size is much

stronger. This relationship between particle size and peak CoT is non-linear and suggests the existence of an optimum particle size for mitigating against leaf layers. Particle circularity is negatively correlated with peak CoT when leaf layers are present.

Post-test roughness increased with decreasing particle circularity and in the case of wheel roughness, increasing particle size increased measured roughness. Hardness had no discernible effect.

In sanded contacts, the effect of multiple passes had little effect on traction in dry and wet conditions, though traction decreased with an increasing number of passes in a leaf contaminated contact.

There was an apparent pressure dependency in the sanded contact, which was not apparent when observing the effect of pressure on an unsanded contact. In dry and wet, sanded contacts traction increased with contact pressure, the inverse was true for the leaf contaminated contact.

6 SCALED-WHEEL RIG TESTING

6.1 Introduction

The scaled-wheel rig (SWR) was initially designed for assessing the optimisation of grease pick-up and carry down [150], [151]. In this work it was used for assessing the entrainment of sand particles into the nip of the wheel/rail contact.

Using the SWR in conjunction with high speed videography (HSV) certain hypotheses, about the behaviour of sand particles upon crushing in the wheel/rail contact, that were formulated from the previous sub-chapter 4.9 and chapter 5 could be validated. Namely, that sand particles crush at a fraction of the full wheel/rail load and much of the material is expelled from the contact, especially in dry conditions.

6.2 Methodology

The set-up used for testing with the SWR is shown in Figure 6.1. The scaled-wheel rests on an axle which in turn is connected to a trolley, this allows the wheel to freely rotate. The scaled-wheel has a diameter of 180 mm, roughly equating to a 1:5 scale compared to a full-scale wheel; the scaled-wheel has a P8 profile. The trolley allows linear motion in the direction of the length of the rail as it runs on a guiding rail parallel to the rail. Particles are applied to the rail head manually, with the wheel subsequently running over them. Whilst in reality sand particles are directed to the wheel/rail nip by the use of sanding equipment, this set-up simplifies this process by using only stationary particles allowing inferences about how the particles crush in a wheel/rail interface.

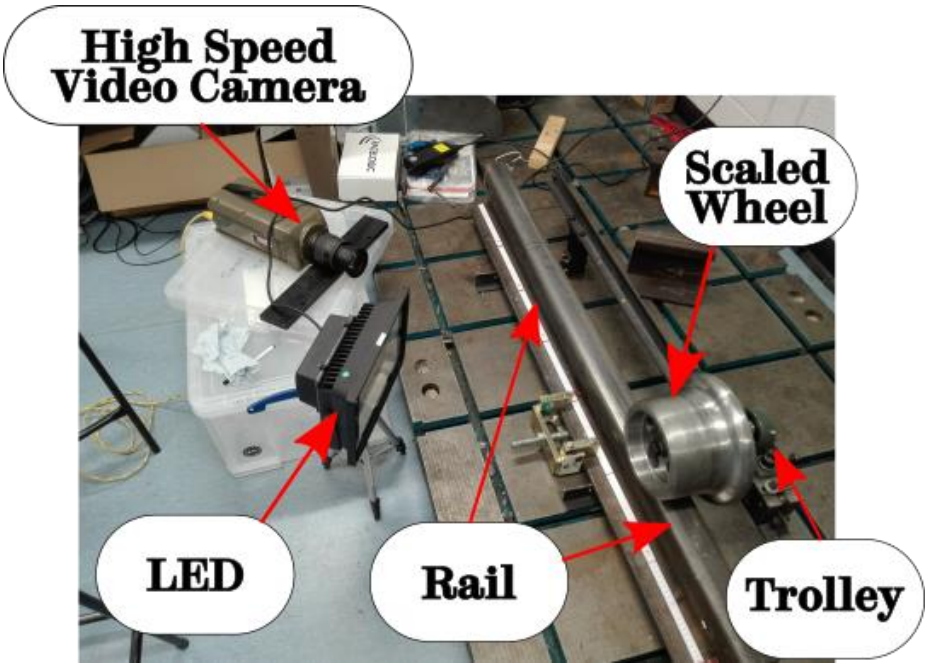

Figure 6.1. Scaled-Wheel Rig Set-up.

The HSV camera is a Phantom V210 set up to record at 750 fps at a resolution of 1280×800 pixels. Extra light is supplied by an LED light set up to illuminate the wheel/rail contact and allow higher frame rates to be used than would be otherwise.

Pictures were taken of the wheel and rail surfaces post-test to assess what material remained in the contact. Tests were conducted with LB, CE, and DY particles.

6.3 Results

High speed video stills from testing a single LB particle are included in Figure 6.2, where the particle is shown before the wheel passes over it in Figure 6.2*(a)* and as some of it is ejected from the wheel/rail contact as the wheel passes over it in Figure 6.2*(b)*.

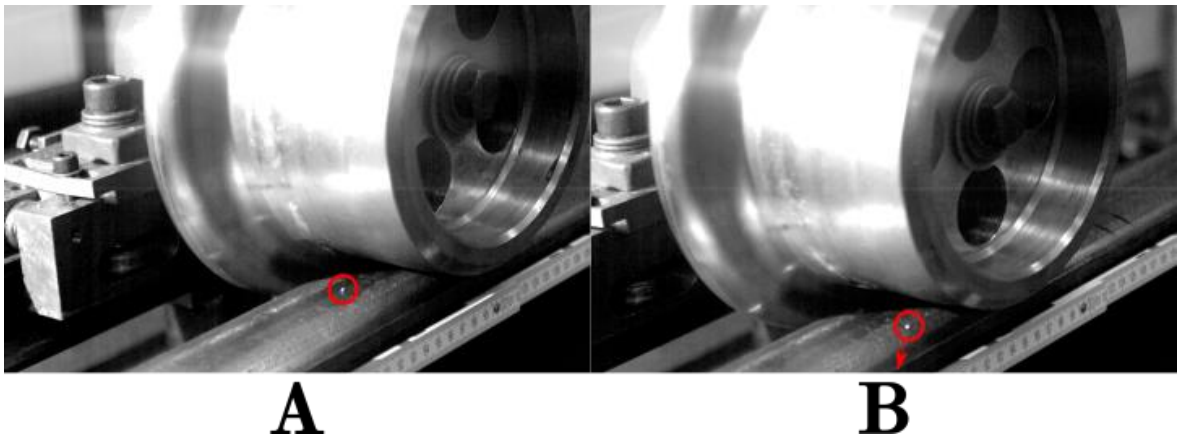

Figure 6.2. Single Particle of LB: *(a)* Pre-Wheel Pass with Resting Particle Encircled, *(b)* Post-Wheel Pass with Moving Particle Encircled with Arrow Indicating Direction of Motion.

The way a lot of the particle is expelled from the contact is similar to how many particles acted in the dry high pressure torsion (HPT) contact, where little remaining material was observed for many particles upon crushing as they were expelled from the contact. Figure 6.3 shows how little material remains on the rail head, with what is remaining being relatively spread out compared to the initial particle size.

Figure 6.3. Rail Head Post-Wheel Pass over a Single LB Particle with Remaining Material Encircled.

A single particle of CE acts similarly, as can be seen in Figure 6.4. Though in this particular instance, the CE particle has been expelled as many smaller fragments.

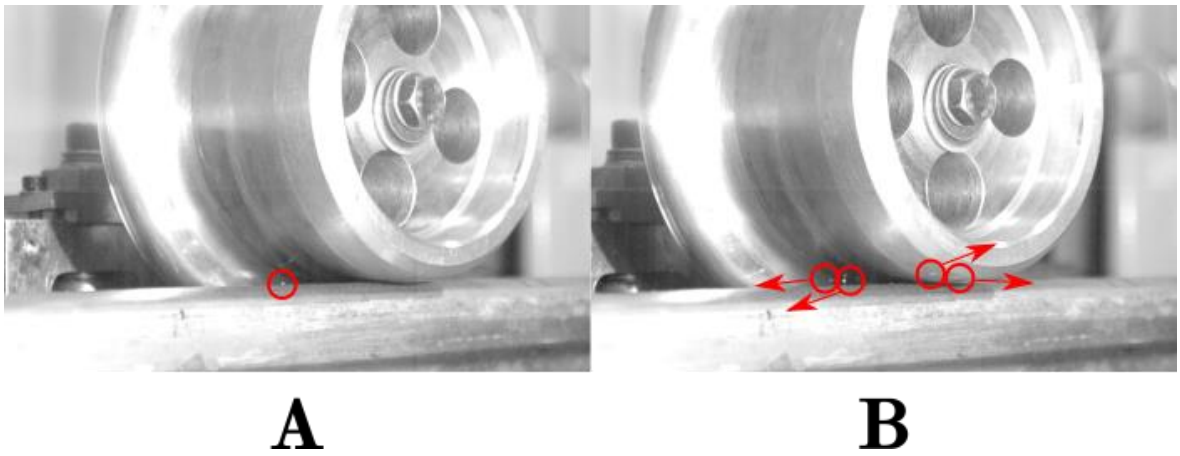

Figure 6.4. Single Particle of CE: *(a)* Pre-Wheel Pass, *(b)* Post-Wheel Pass.

There is very little material remaining in the aftermath of the wheel pass over the CE particle as can be seen on the rail head in Figure 6.5. Possibly indicating more was expelled from this pass than compared to the pass with a single particle of LB.

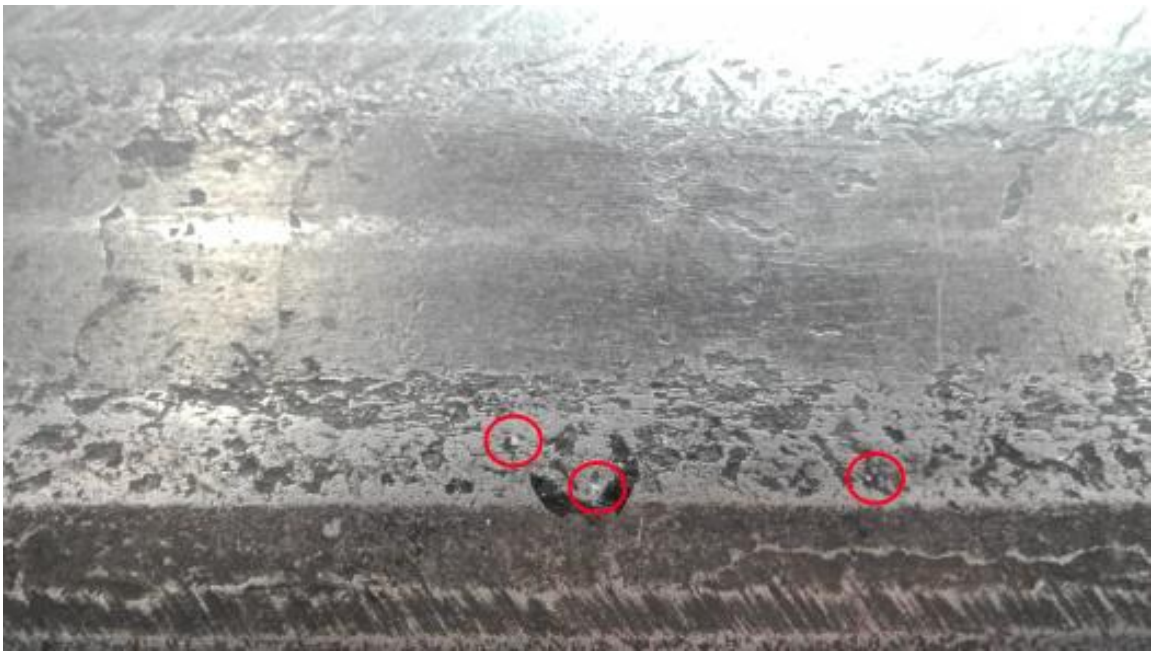

Figure 6.5. Rail Head Post-Wheel Pass over a Single CE Particle.

Finally, a single particle of DY was passed over, the stills of which are included in Figure 6.6. As previously, some material is expelled, though the fragment being expelled is very small when compared to the previous larger particles in this sub-chapter.

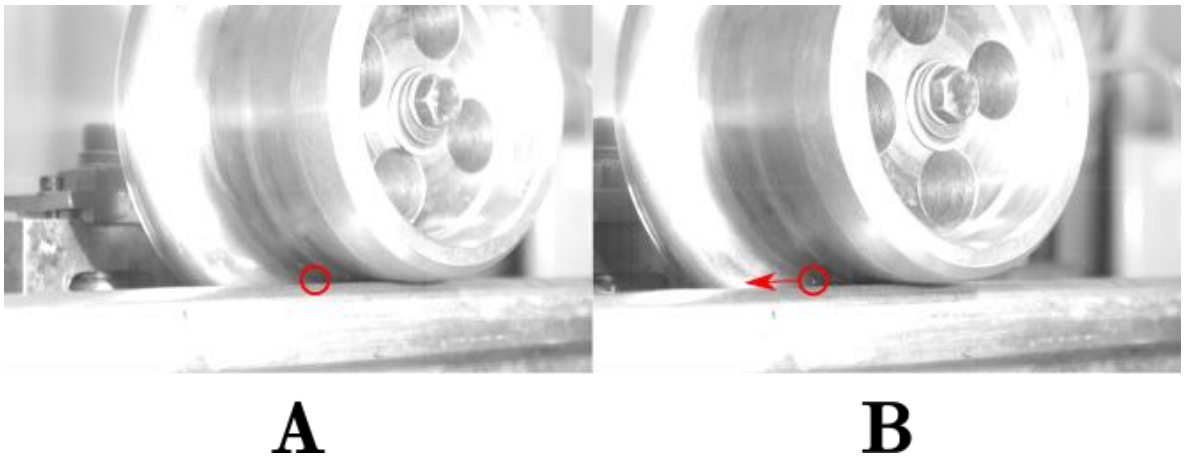

Figure 6.6. Single Particle of DY: *(a)* Pre-Wheel Pass, *(b)* Post-Wheel Pass.

There is a very small amount of material remaining after the wheel pass over the DY particle. In Figure 6.7, there is a small smudge where the particle was run over.

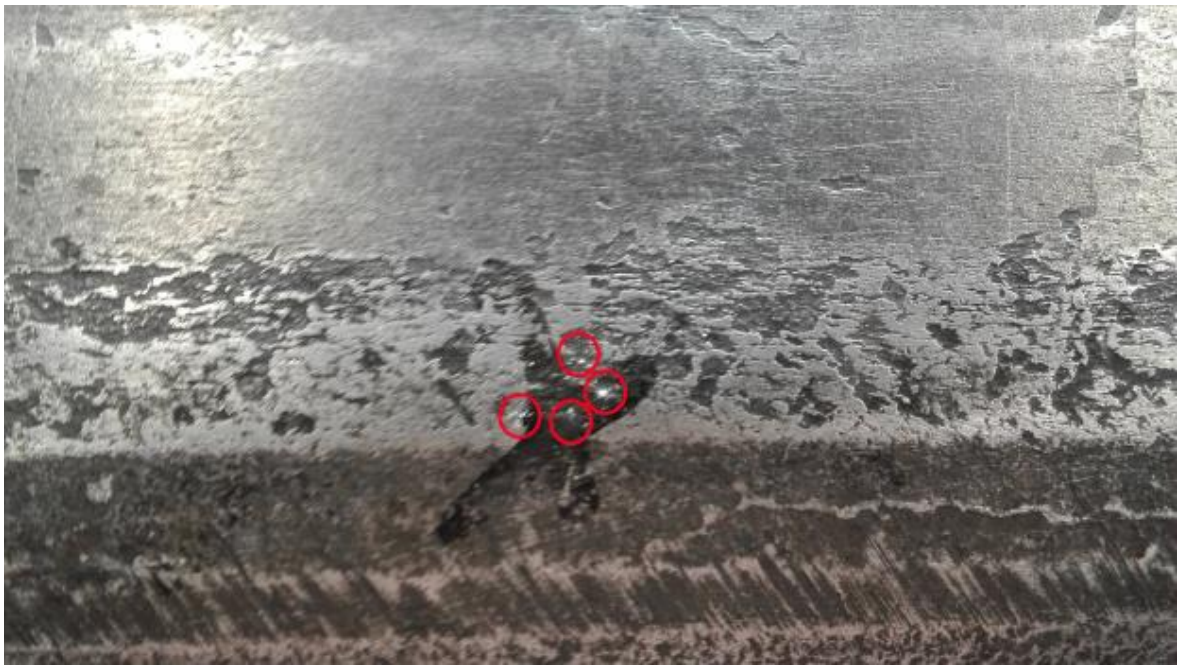

Figure 6.7. Rail Head Post-Wheel Pass over a Single DY Particle.

In addition to tests conducted with single particles, tests with multiple particles were also recorded. Figure 6.8 includes stills of the scaled-wheel passing over multiple LB particles. In these, it is apparent that material is expelled throughout the wheel pass. Material is also expelled relatively forcefully, as evidenced by the trajectory and height of some expelled fragments.

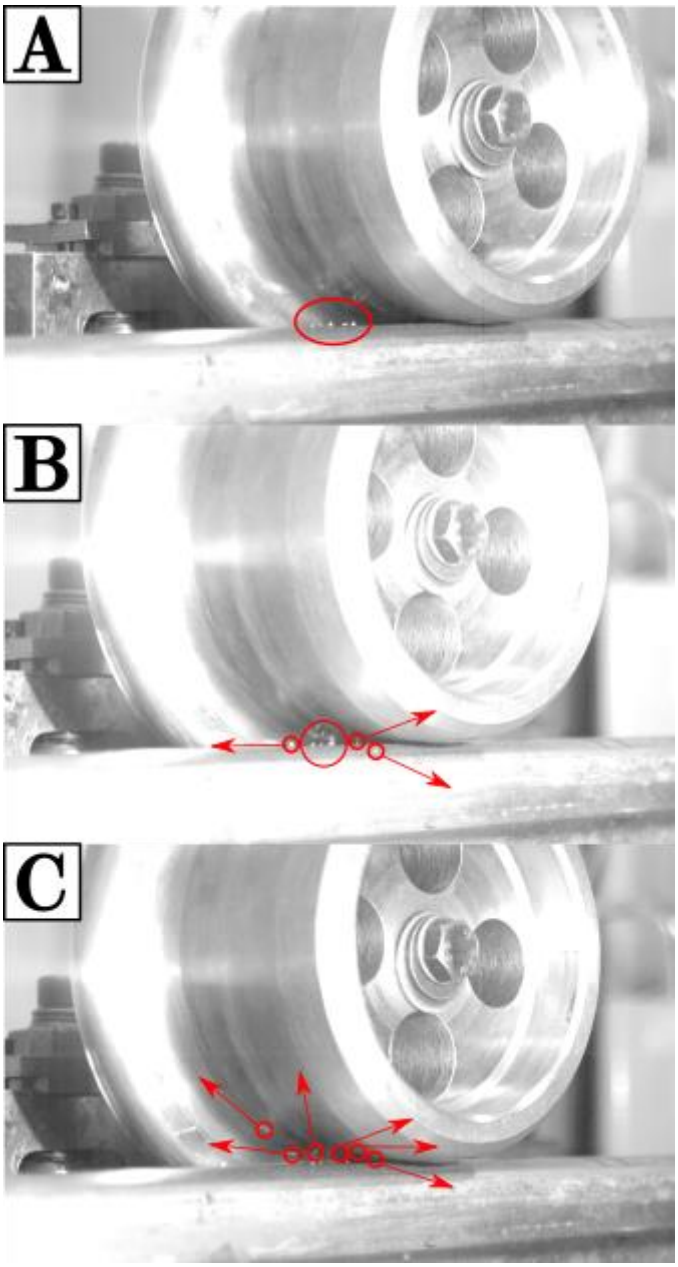

Figure 6.8. Multiple Particles of LB: *(a)* Pre-Wheel Pass, *(b)* Partial Wheel Pass, *(c)* Post-Wheel Pass.

Post-pass pictures of the rail head and wheel tread are included in Figure 6.9. Some material has remained on the rail head; most is being relatively spread out. There is however one particle, that appears to have been squashed as it has stayed relatively coherent. On the wheel tread only small dust spots are visible; indicating where the wheel has run over the particles.

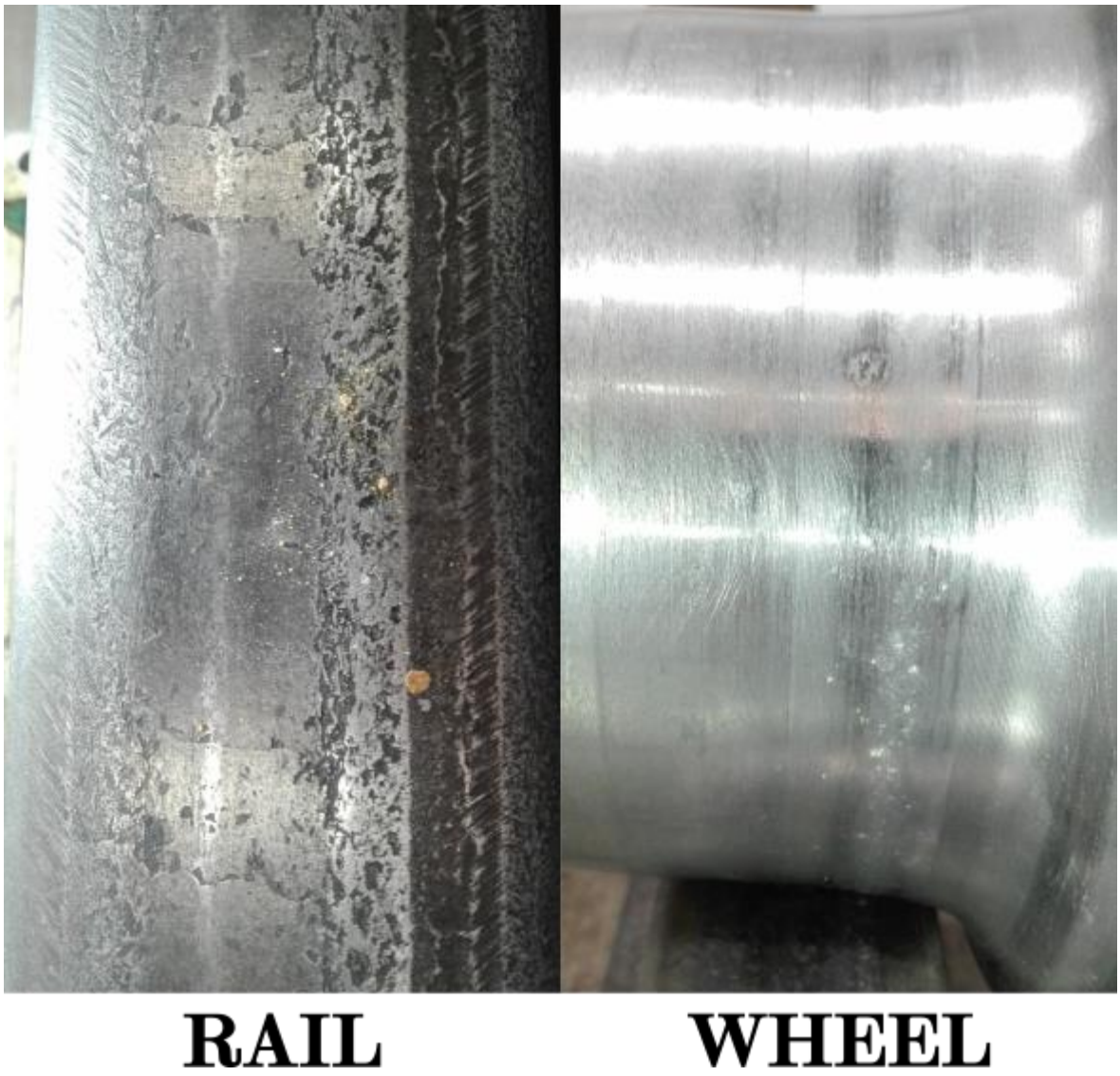

Figure 6.9. Rail Head & Wheel Tread Post-Wheel Pass over Multiple LB Particles.

Stills of a wheel pass over multiple CE particles have been included in Figure 6.10. The CE particles act very similarly to the LB particles, as numerous, violent expulsions of material occur throughout the wheel pass. Though, it is hard to appreciate from stills alone, in this test expelled particle debris came into contact with, as yet, uncrushed particles causing them to move slightly; these particles still, however, remained in the path of the wheel pass.

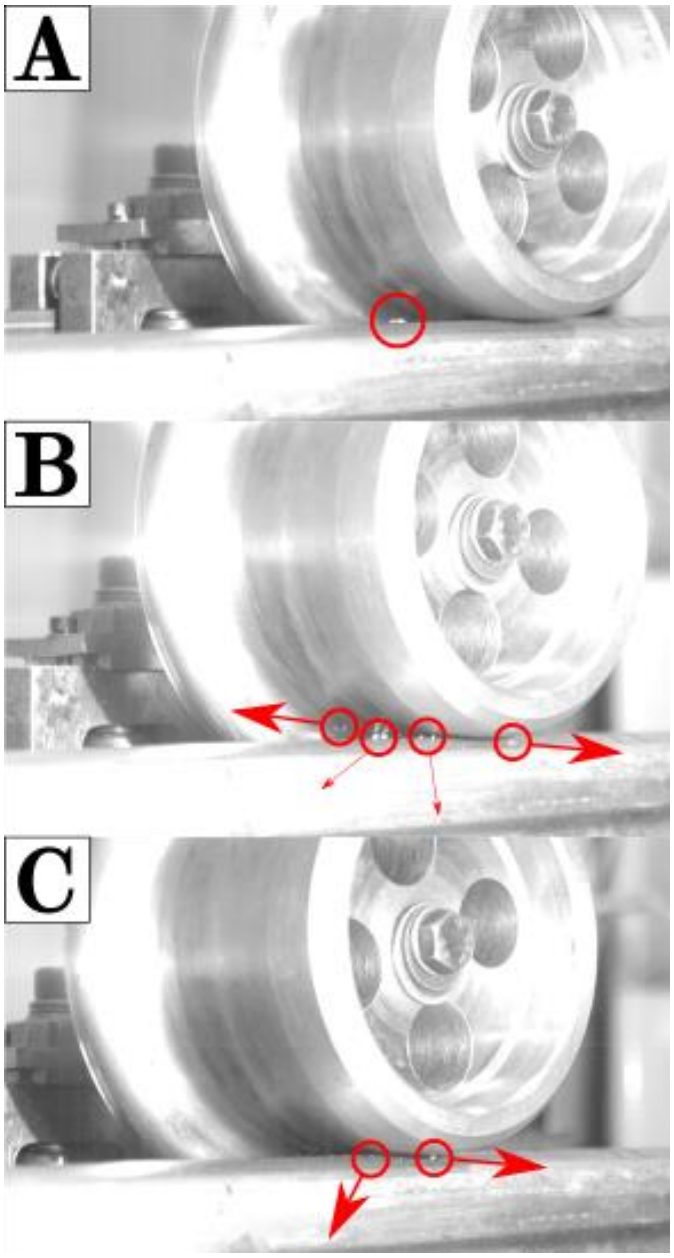

Figure 6.10. Multiple Particles of CE: *(a)* Pre-Wheel Pass, *(b)* Partial Wheel Pass, *(c)* Post-Wheel Pass.

The aftermath of this wheel pass over multiple CE particles has been included in Figure 6.11. The remaining material is very scattered, with no evidence of particles remaining coherent, as was seen for one LB particle in the aforementioned test multiple LB particles.

Figure 6.11. Rail Head Post-Wheel Pass over Multiple CE Particles.

In all previous tests, large amounts of material were expelled during the wheel pass. This expulsion of material was surmised for dry HPT tests with rail sand material also, however in wet HPT tests more material remained post-test. To better understand this video was recorded of a pass over multiple LB particles with 1 ml of water also applied, the stills of which are included in Figure 6.12. Particles are still expelled from the contact throughout the wheel pass, though there appears to be less of it when compared to dry conditions. Initially, the expulsion of particles appears less violent, with low trajectories and height of expelled fragments. This does appear to increase by the end of the wheel pass, though these particles are relatively small.

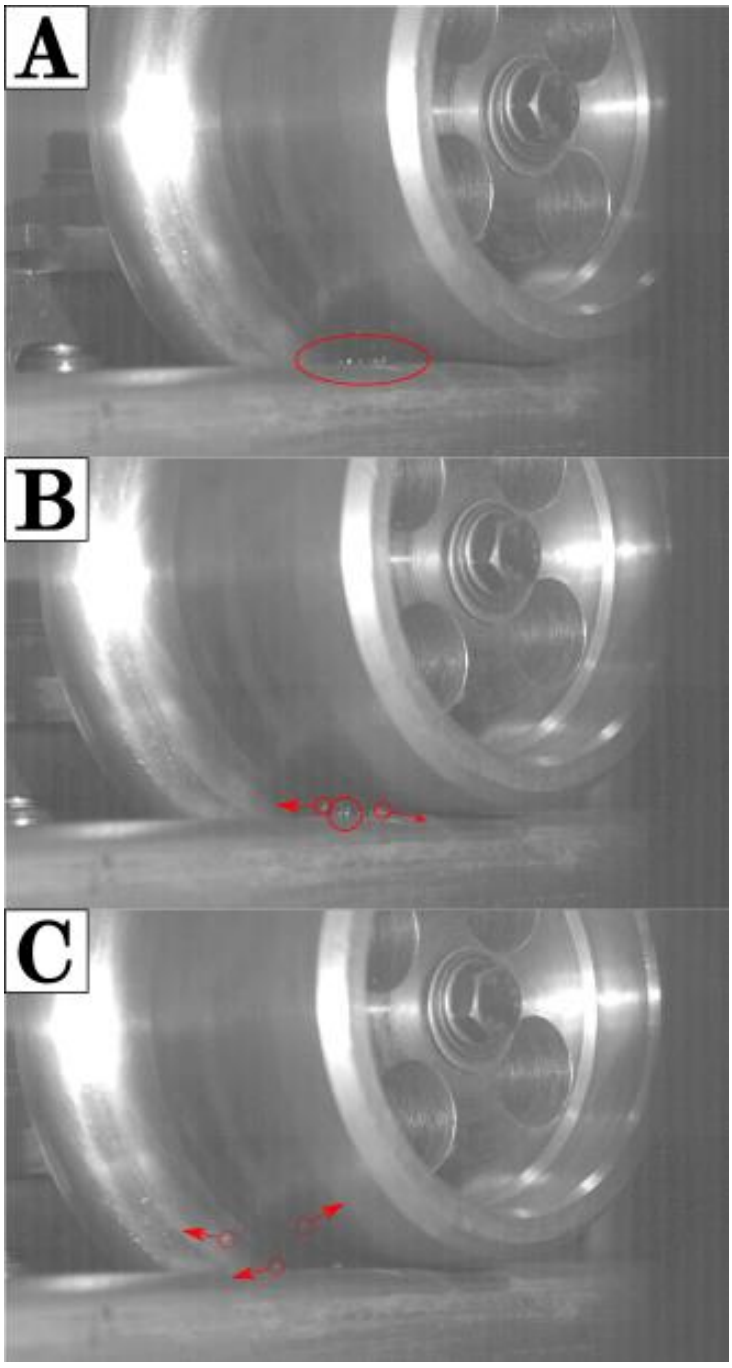

Figure 6.12. Multiple Particles of LB in Wet Conditions: *(a)* Pre-Wheel Pass, *(b)* Partial Wheel Pass, *(c)* Post-Wheel Pass.

Figure 6.13, shows pictures of both the rail head and wheel tread post-wheel pass. Noticeably more material has remained on the rail head compared to dry tests, with remaining material staying relatively condensed and particles remaining coherent post-crushing. In addition, clumps of material have adhered to the wheel tread, with no dust spots being visible.

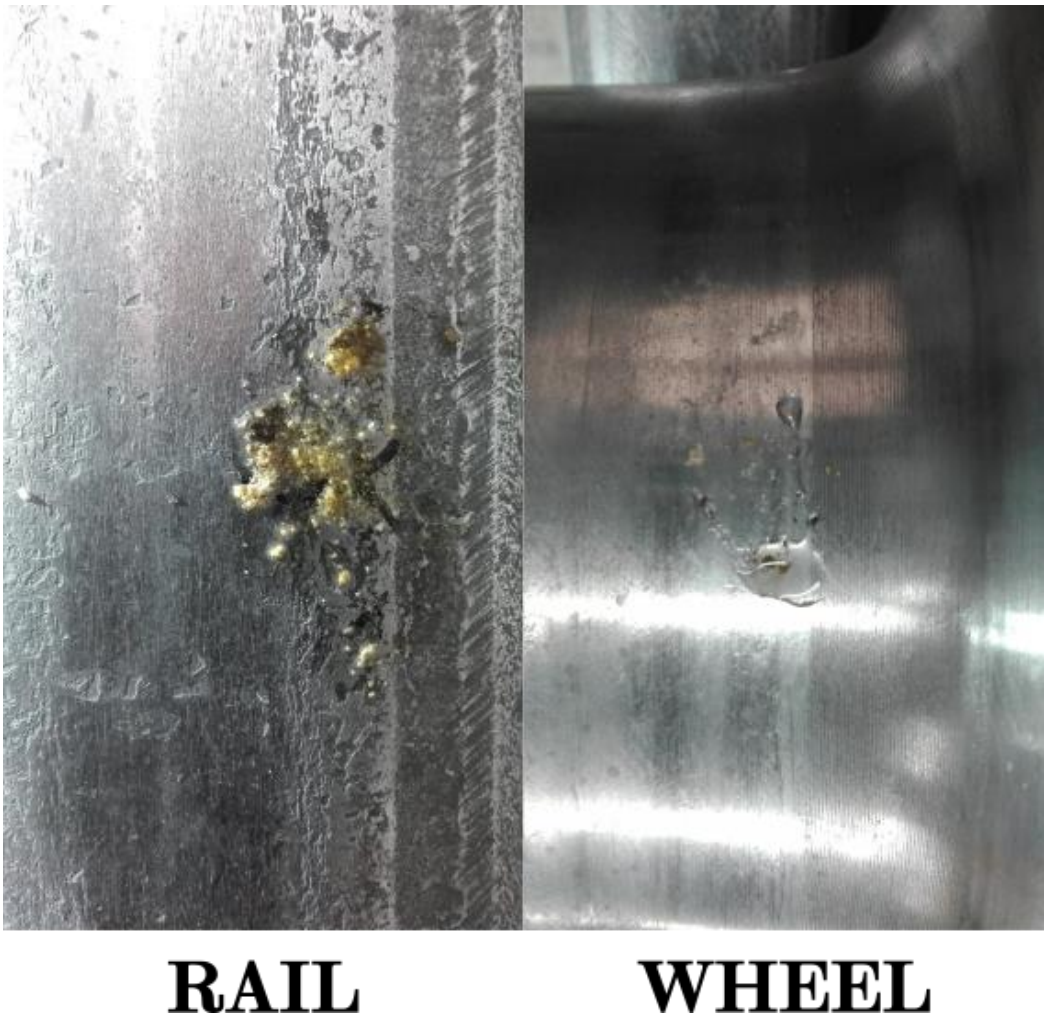

Figure 6.13. Rail Head & Wheel Tread Post-Wheel Pass over Multiple LB Particles in Wet Conditions.

From these SWR tests, it is apparent that in dry conditions very little material remains in the contact, and what does remain on the rail head are crushed down to very small particles, with larger fragments expelled from the contact entirely. As the crushing stress of quartz particles is so low compared to wheel/rail contact stresses (see sub-chapter 4.9) particles will begin to be crushed well before entering the wheel/rail contact, thus as the particle breaks much of material will expelled out of the contact as has been seen in this chapter. However, in the presence of moisture, surface tension will retain more of this material, as seen in this chapter and from HPT testing, thereby having a greater effect on the wheel/rail contact.

6.4 Summary

In this sub-chapter, high speed video footage of a scaled-wheel passing over rail sand particles was presented. From these videos, it was apparent that, in dry conditions, a significant amount of material is expelled from the rail head up entering the wheel/rail nip, thus not entering the actual wheel/rail contact. In wet conditions,

more material was retained due to surface tension, as particles were less numerously and less violently expelled from the rail head. These findings corroborate trends observed during high pressure torsion testing and single particle crushing tests strengthening hypotheses made on the effect of particle crushing on entrainment. Whilst these tests give an indication of how particles are crushing in the wheel/rail contact, direct comparison of the amount of sand being entrained into the SWR interface and the amount being entrained into an actual wheel/rail contact is not simple; as particles are stationary and not directed to the wheel/rail nip by a sanding system.

7 EXTENDED CREEP-FORCE MODEL

7.1 Model Overview & Capabilities

The extended creep-force (ECF) model was developed by Meierhofer as part of his thesis [18] and has been also been included in studies conducted by Meierhofer et al. and Six et al. [152], [153]. The ECF model assumes there are three layers of interest: the wheel and rail bulk material are assumed to be homogeneous, isotropic, and elastic; the third layer, between wheel and rail, is made up of any contaminants between the surface of the wheel and rail as well the surface and sub-layers of the wheel and rail, including asperities and micro-cracks.

This third body layer (3BL) is assumed to be homogeneous and isotropic, when considering the layer on a macroscopic scale, and can be modelled with pressure and temperature dependent elasto-plastic material properties. Normal stresses are taken as Hertzian, and local temperatures are determined according to an adapted Erzt-based sub-model; both these sub-models include time dependency, thereby allowing the reproduction of transient effects.

The 3BL can be described according to a brush model, a schematic of which is included in Figure 7.1. Two bristles of the brush (B_1 and B_2), are displaced by a distance (u) through the third body layer of height (h) with a stress of τ acting on each bristle. As each bristle travels through the contact, its respective displacement and stress increase.

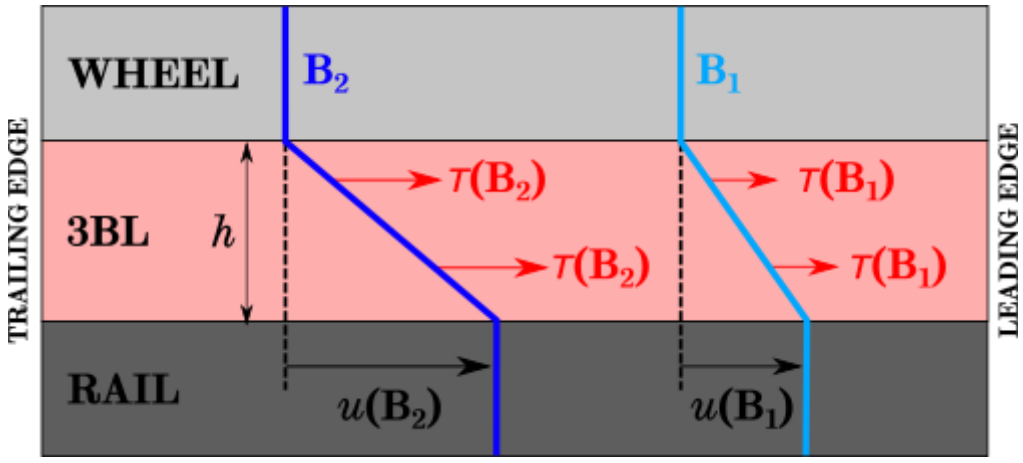

Figure 7.1. Schematic of the Principle behind the ECF Model [18].

Each bristle is considered to act elastically when the tangential stresses $\left(\underline{\tau} = (\tau_x, \tau_y)\right)$ acting upon it are below a critical limit (τ_{c1}). Under this condition, the displacement of each bristle can calculated using the inverted stiffness of the 3BL (L_e), thus:

$$\underline{\tau} = \frac{u}{L_e} \; for \; |\underline{\tau}| \leq \tau_{c1}$$

Equation 7.1

For stresses higher than τ_{c1}, but lower than a second critical shear stress (τ_{c2}), a limit that cannot be exceeded, the 3BL can be considered to act plastically. Here, Voce's strain-hardening law [130] can be used in conjunction with a "plasticity" factor (L_p):

$$|\underline{\tau}| = \tau_{c1} + (\tau_{c2} + \tau_{c1}) \left[1 - \left(\frac{-|\underline{u}| + \Delta u}{L_p} \right) \right] \; for \; \tau_{c1} < |\underline{\tau}| < \tau_{c2}$$

Equation 7.2

in this instance, $\Delta u = \tau_{c1} L_e$, thereby ensuring a continuous transition from linear, elastic behaviour, to non-linear, plastic behaviour.

From Equation 7.1 and Equation 7.2, it is apparent that the tangential stress of each bristle is influenced by four parameters: L_e, τ_{c1}, L_p, and τ_{c2}.

Their physical relation to the typical output of a high pressure torsion (HPT) test has been included schematically in Figure 7.2. The parameter L_e describes the gradient of the linear section of the graph below τ_{c1}; the parameter L_p describes the shape of the curve between τ_{c1} and τ_{c2}.

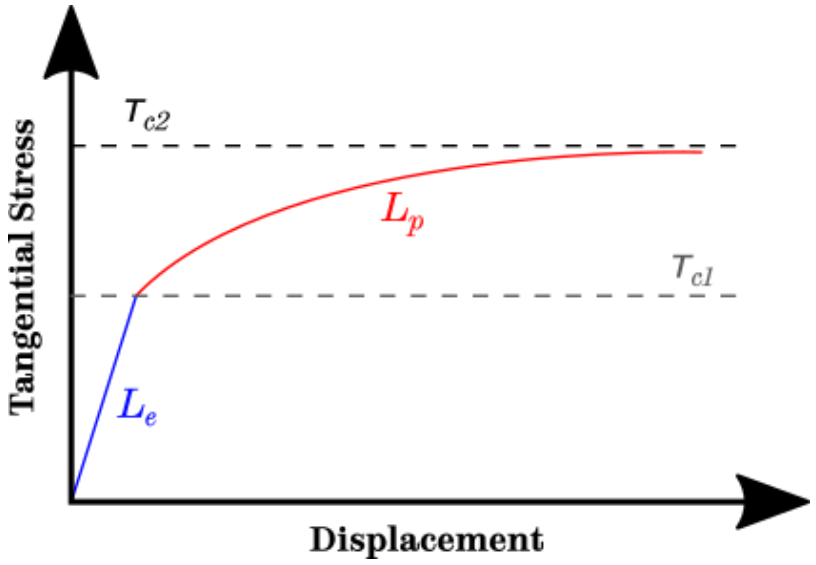

Figure 7.2. ECF Model Parameters and their Physical Relevance [18]**.**

These four parameters can then be made dependent on normal stress (p) and local temperature (T) using simple exponential laws. Both critical shear stresses are thus defined as:

$$\tau_{c1}(p,T) = \tau_{c1}^{0}\left[1 - exp\left(-p\tau_{c1}^{p}\right)\right][exp(-(T - T_0)\tau_{c1}^{T})]$$
$$\tau_{c2}(p,T) = \tau_{c2}^{0}\left[1 - exp\left(-p\tau_{c2}^{p}\right)\right][exp(-(T - T_0)\tau_{c2}^{T})]$$

Equation 7.3

where T_0 is room temperature and $\tau_{c1,c2}^{0,p,T}$ are constants. The critical shear stresses are therefore characterised by nominal values $\left(\tau_{c1,c2}^{0}\right)$, pressure dependent values $\left(\tau_{c1,c2}^{p}\right)$, and temperature dependent values $\left(\tau_{c1,c2}^{T}\right)$. The nature of these functions means critical shear stresses decrease with decreasing normal stress or increasing temperature. The yield stress and maximum shear strength of the 3BL can therefore be inferred as equivalent to $\tau_{c1,c2}^{0}$ respectively.

A similar procedure can be applied to the inverted stiffness and "plasticity" factor of the 3BL to make them dependent on normal pressure and local temperature:

$$L_e(p,T) = L_e^0\left[1 - exp\left(-pL_e^p\right)\right]^{-1}\left[exp(-(T - T_0)L_e^T)\right]^{-1}$$
$$L_p(p,T) = L_p^0\left[1 - exp\left(-pL_p^p\right)\right]^{-1}\left[exp\left(-(T - T_0)L_p^T\right)\right]^{-1}$$

Equation 7.4

where T_0 and $L_{e,p}^{0,p,T}$ have the same relative definitions as previously defined for Equation 7.3. In this case, the inverted stiffness and "plasticity" factor will increase with decreasing normal stress or increasing temperature.

The outcome of Equation 7.3 and Equation 7.4 is that there are 12 constants that can be identified using empirical methods. High pressure torsion (HPT) data can parameterise nominal and pressure dependent values, via conducting tests at three different normal pressures (see sub-chapter 5.3.6). These parameters combined with the temperature dependent values supplied by Meierhofer [18] from vehicle tests allow prediction of full-scale behaviour [145]. The HPT cannot parameterise these values as temperature remains at room temperature throughout each test.

The ECF model was selected for this project as it has the ability to describe features of real world creep curves that other models cannot, e.g. falling friction at high creep rates using temperature dependent parameters, smooth transition from low creep rates to medium creep rates.

7.2 High Pressure Torsion Results

This sub-chapter describes parameterisation of the ECF model based on HPT tests conducted in sub-chapter 5.3.6. The parameterised ECF model was then used to predict creep curves for a typical real-world wheel/rail contact.

7.2.1 Parameterisation

When parameterising the ECF model using the HPT data an extra parameter must be taken into account, the inverse shear stiffness of the test rig (L_x), as the stiffness of the rig is significant when compared to the stiffness of the 3BL. L_x is not an input into the ECF model, rather it is only used as a part of the parameterisation process. L_x was estimated by optimising this parameter during fitting the ECF model to dry sanded data and kept constant for all other models.

Initially, the value of L_e^0 calculated by Meierhofer [18] was used for dry and wet sanded contacts. This parameter was calculated using the shear modulus of steel (G_s=79.3 GPa) and an average 3BL thickness measured in [18] (h_{3BL}=20 μm) to find a value of nominal inverted stress of $L_e^0 = \frac{h_{3BL}}{G_s} = 0.252\ \frac{\mu m}{GPa}$. As the 3BL is much less stiff in leaf contaminated conditions, L_e^0 was re-parameterised for these conditions. The pressure dependent and temperature inverted stresses were fixed as $L_e^p = \infty \frac{1}{GPa}$ and $L_e^T = 0 \frac{1}{℃}$ respectively.

Parameterisation of nominal and pressure dependent values was conducted for four HPT test conditions: sand in dry, sand in wet, sand with leaf contaminant, and leaf contaminant with no sand applied. Unsanded dry and wet tests have been parameterised previously by Evans [144]. LB rail sand was the only sand with which full parameterisation of the ECF model was conducted. For each condition, 3 different normal pressures were used for parameterisation of pressure terms (300 MPa, 600 MPa, & 900 MPa) and 3 repeats were used for each normal pressure, totalling 9 test runs to parameterise each ECF model. All data were filtered before the parametrisation process to aid the optimisation algorithm in use.

7.2.1.1 LB Rail Sand in Dry Conditions

Using this dry sanded data, L_x was optimised and calculated to be 80 $\frac{\mu m}{GPa}$. This value will be used throughout the remaining parameterisation processes. The ECF model for dry, unsanded data has been included in Figure 7.3, where the overall error of the model fit was calculated as 8.4%. L_e^0 and L_e^T were not optimised remained the values calculated by Meierhofer [18]. The fit appears to fit very well at higher contact pressures, with stiffness becoming increasingly over-estimated at lower contact pressures. The critical stresses appear to fit very well to the HPT data at all normal pressures.

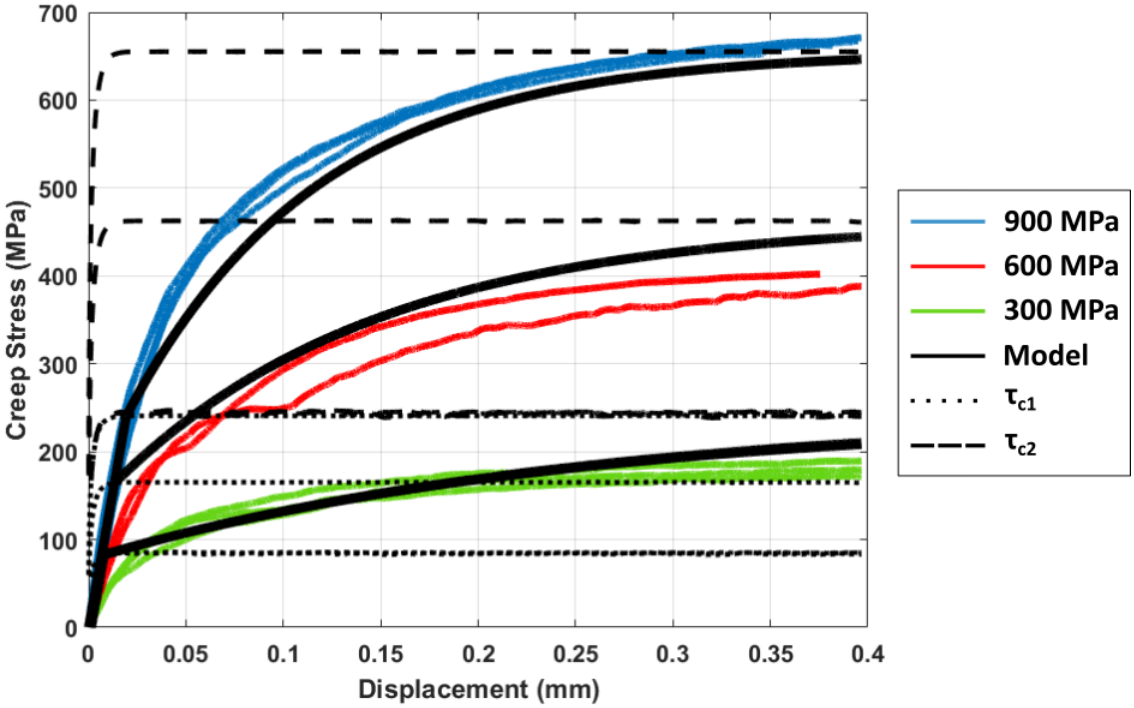

Figure 7.3. ECF Fit for Dry Tests with LB Sand.

The parameterisation of dry, sanded results produced the input parameters included in Table 7.1. These parameters are of a similar order of magnitude to previous parameterisation processes performed by Meierhofer [18] and Evans [144].

Table 7.1. ECF Input Parameters for Dry, Sanded Conditions.

Material Parameter	Nominal	Pressure Dependency
L_e	0.252 $\mu m/GPa$	∞ GPa^{-1}
L_p	0.0381 mm	0.548 GPa^{-1}
τ_{C1}	1.49 GPa	0.195 GPa^{-1}
τ_{C2}	2.16 GPa	0.401 GPa^{-1}

7.2.1.2 LB Rail Sand in Wet Conditions

The ECF model for wet, sanded HPT data has been included in Figure 7.4, where an error value of 7.6% was obtained. The rig stiffness was kept at 80 $\frac{\mu m}{GPa}$ and L_e^0 and L_e^T were also not optimised. The fit is very similar to that seen in dry, sanded conditions, with an increasingly over-estimated stiffness at lower contact pressures, but with a good fit to critical shear stresses.

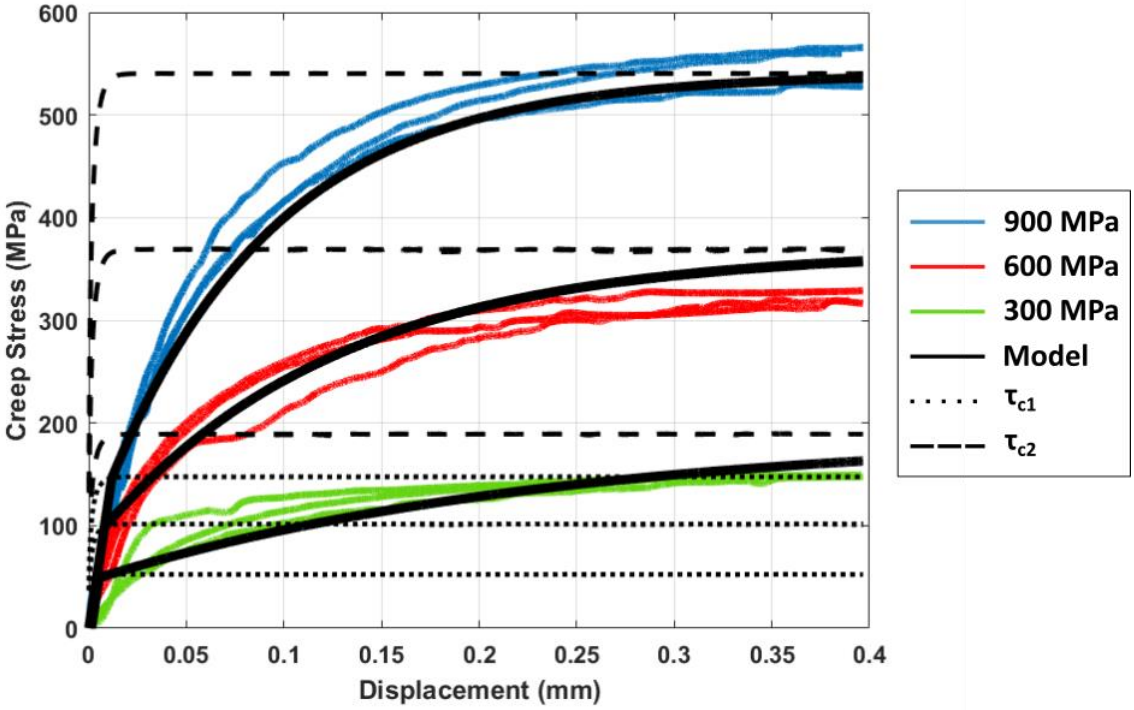

Figure 7.4. ECF Fit for Wet Tests with LB Sand.

The input parameters from wet, sanded conditions are included in Table 7.2. They remain a similar order of magnitude as the input parameters calculated from dry, sanded HPT data, unsurprising as the curves from dry and wet, sanded data appear relatively similar.

Table 7.2. ECF Input Parameters for Wet, Sanded Conditions.

Material Parameter	Nominal	Pressure Dependency
L_e	$0.252\ \mu m/GPa$	$\infty\ GPa^{-1}$
L_p	$0.0217\ mm$	$0.326\ GPa^{-1}$
τ_{C1}	$0.826\ GPa$	$0.219\ GPa^{-1}$
τ_{C2}	$3.90\ GPa$	$0.166\ GPa^{-1}$

7.2.1.3 LB Rail Sand in Leaf Contaminated Conditions

As opposed to dry and wet, sanded conditions, L_e^0 was optimised for leaf contaminated conditions, due to the large difference in stiffness in these conditions. The ECF model fitting is included in Figure 7.5, where an error value of 14.5% was calculated. Overall, the fitting is relatively accurate, though there is still some slight over-estimation of stiffness at lower contact pressures.

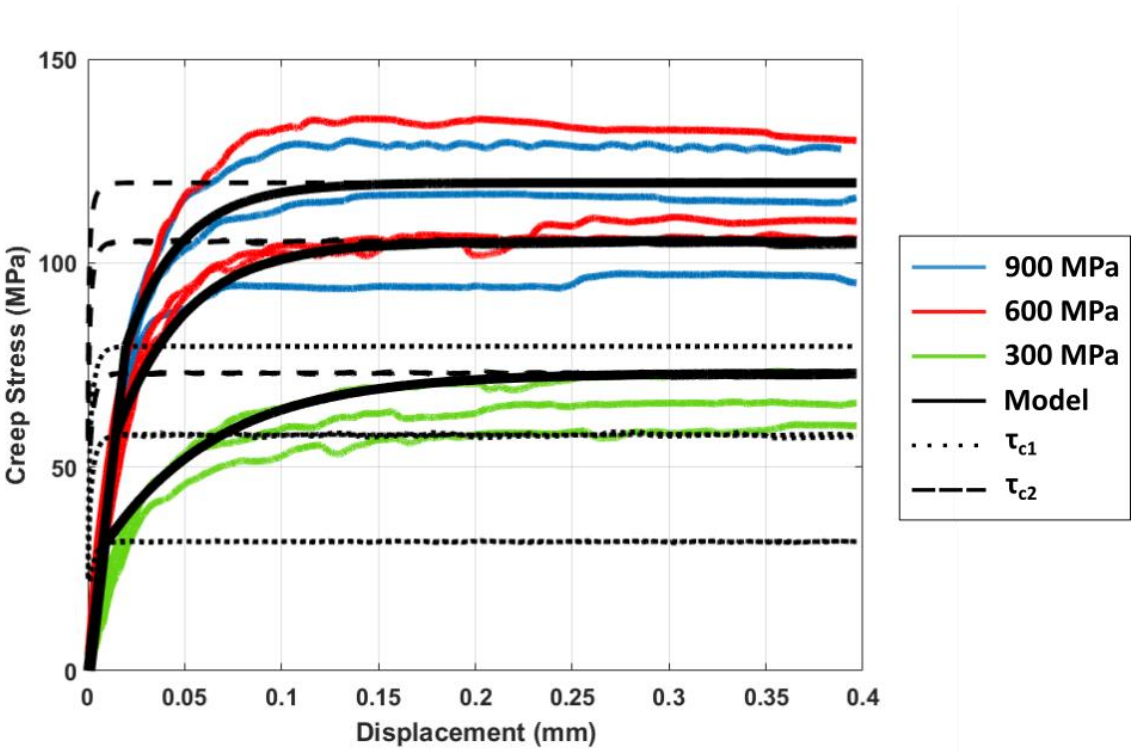

Figure 7.5. ECF Fit for Leaf Contaminated Tests with LB Sand.

The calculated input parameters have been included in Table 7.3. L_e^0 has risen by a few degrees of magnitude compared to the stiffness calculated for dry and wet conditions. Other input parameters maintain similar orders of magnitude.

Table 7.3. ECF Input Parameters for Leaf Contaminated, Sanded Conditions.

Material Parameter	Nominal	Pressure Dependency
L_e	166 $\mu m/GPa$	∞ GPa^{-1}
L_p	0.0208 mm	1.45 GPa^{-1}
τ_{C1}	0.182 GPa	0.636 GPa^{-1}
τ_{C2}	0.131 GPa	2.72 GPa^{-1}

7.2.1.4 Unsanded Leaf Contaminated Conditions

As for sanded, leaf contaminated conditions, L_e^0 was parametrised again. The results of the fitting process are included in Figure 7.6, where and error value of 11.8% was calculated. As before the stiffness at lower contact pressures is over-estimated, but the critical shear stresses are fairly accurate.

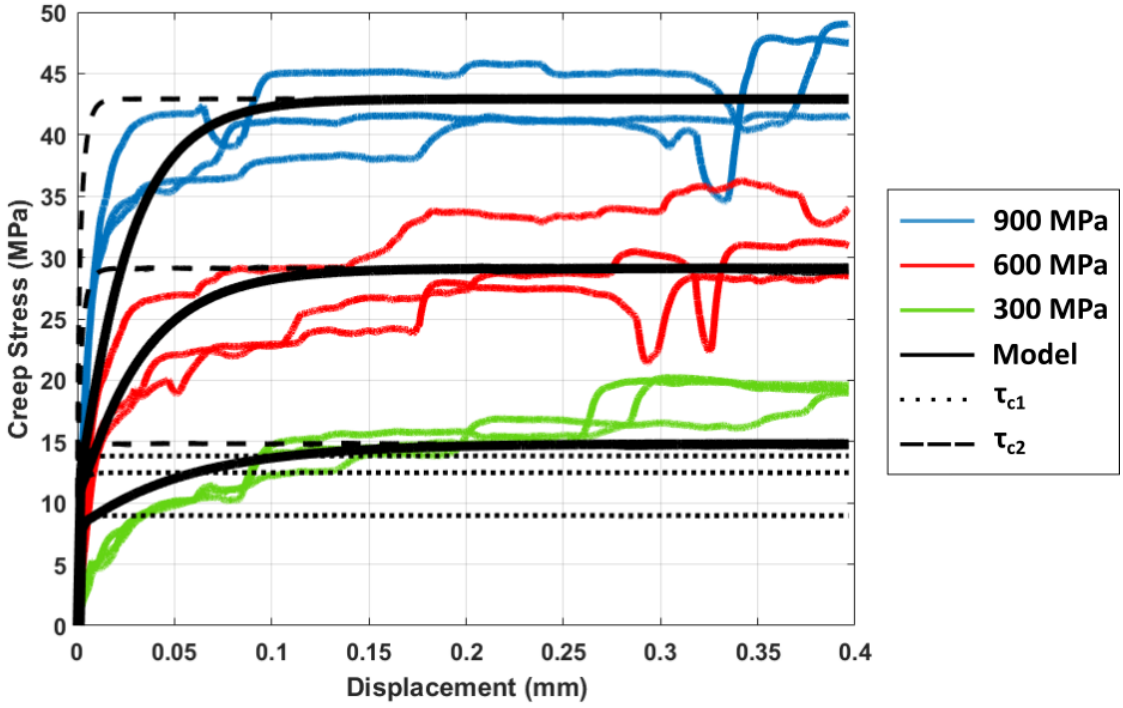

Figure 7.6. ECF Fit for Leaf Contaminated Tests with No Applied Sand.

The calculated input parameters for unsanded, leaf contaminated conditions are included in Table 7.4. As for sanded conditions, the calculated L_e^0 is much higher than for wet and dry conditions, again demonstrating the reduction in stiffness when a leaf layer is present in the contact.

Table 7.4. ECF Input Parameters for Leaf Contaminated, Unsanded Conditions.

Material Parameter	Nominal	Pressure Dependency
L_e	57.1 $\mu m/GPa$	∞ GPa^{-1}
L_p	0.0156 mm	1.09 GPa^{-1}
τ_{C1}	0.0147GPa	3.14 GPa^{-1}
τ_{C2}	0.420 GPa	0.120 GPa^{-1}

7.2.2 ECF Outputs for a Typical Train

From the input parameters calculated thus far, creep curves can be generated for all conditions. The ECF generated creep curves are included in Figure 7.7. These creep curves are based on a typical wheel/rail contact, i.e. 110 kN normal load, with a 600 mm wheel diameter, travelling at 5 m/s.

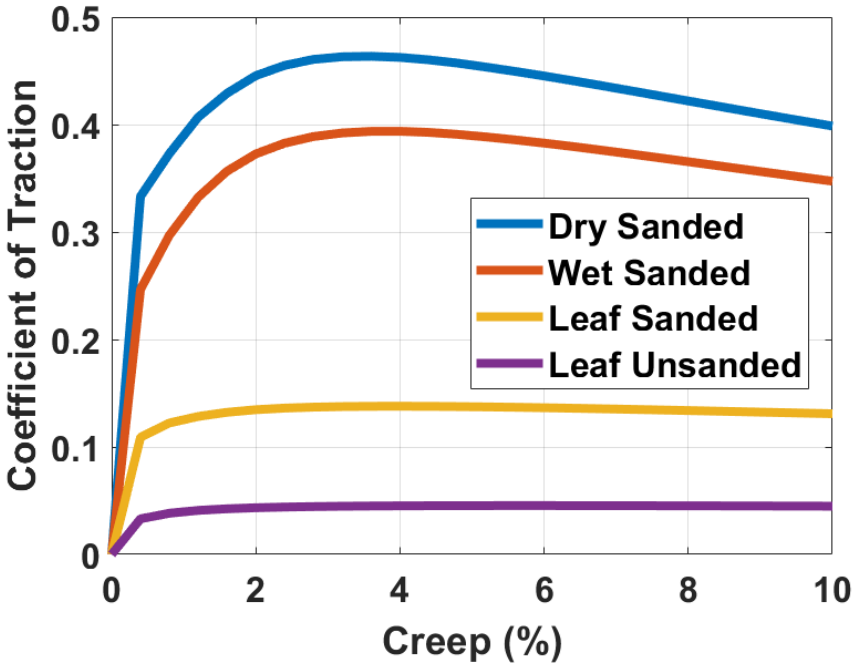

Figure 7.7. Output of ECF Model after inputting Parameters set by HPT Data Fitting.

The creep curves appear sensible and broadly follow the trends observed in HPT testing. The addition of moisture to the contact marginally reduces traction and the addition of a leaf layer drastically reduces it. The addition of sand onto a leaf contaminant increases the coefficient of traction measured.

Parameterising pressure terms means that ECF generated creep curves can be used to predict behaviour under varying normal loads. Figure 7.8 includes creep curves at 3 different normal loads in dry conditions. As the normal load increases the peak of the creep curve shifts rightwards to higher values of creep, however the peak traction is predicted to be similar for all normal loads.

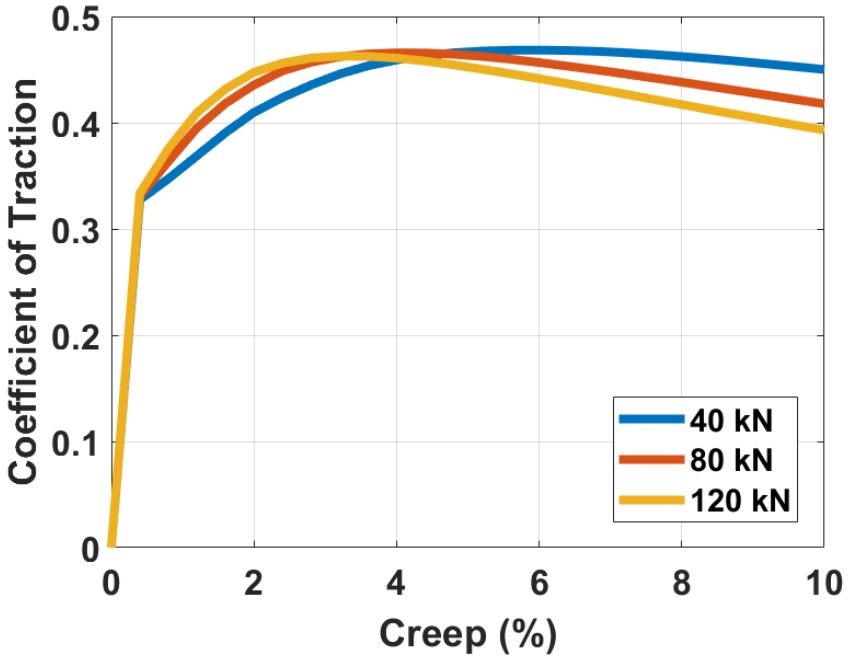

Figure 7.8. ECF Generated Creep Curves under Varying Normal Load in Dry, Sanded Conditions.

The relationship between normal load and creep curve shape holds true in wet conditions also, as can be seen in Figure 7.9. The coefficient of traction wet conditions is still generally lower than in dry conditions.

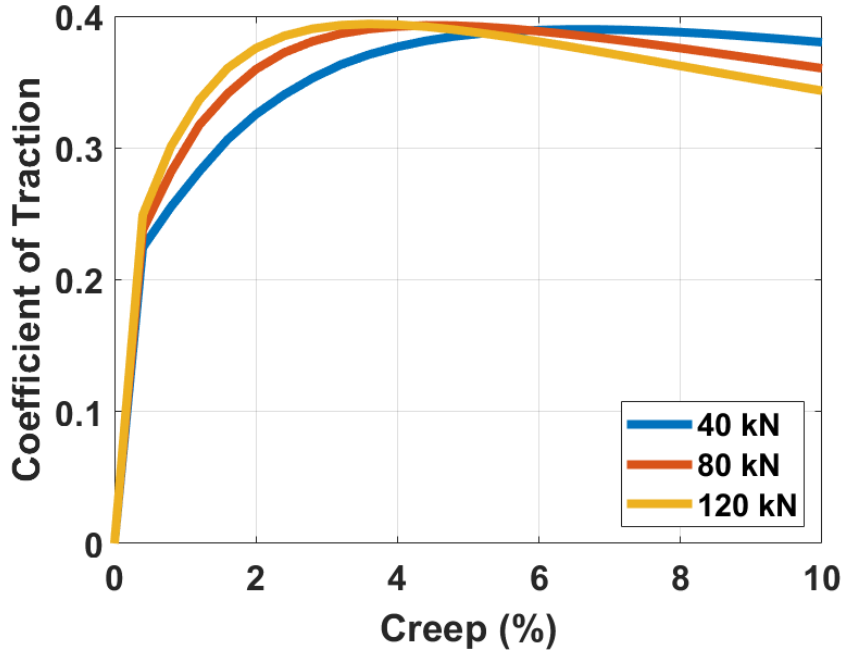

Figure 7.9. ECF Generated Creep Curves under Varying Normal Load in Wet, Sanded Conditions.

In leaf contaminated, sanded conditions the drop in traction is consistent for higher creep values, but with higher normal loads leading to this reduction, the opposite of

dry and wet conditions. Figure 7.10 shows traction dropping fairly significantly at these higher loads.

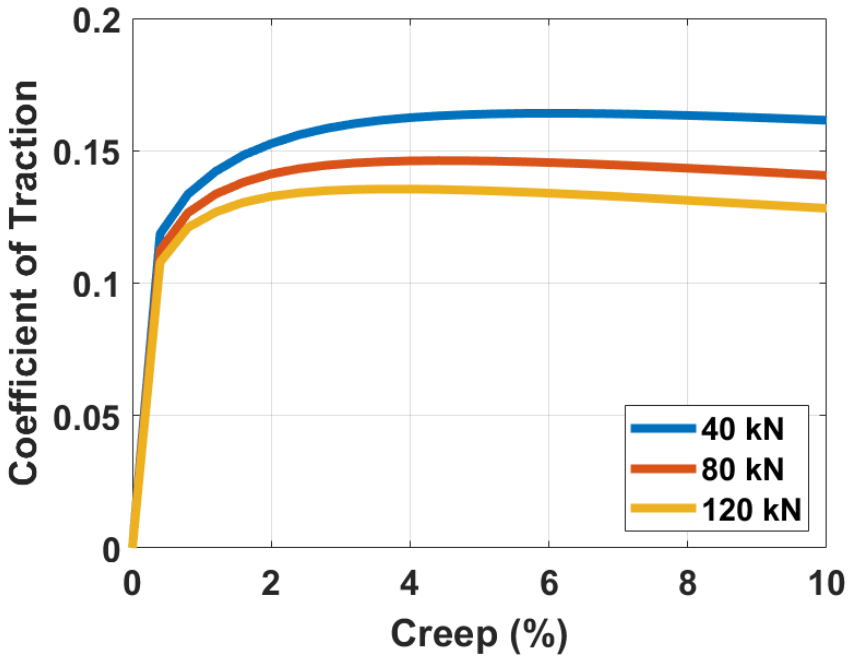

Figure 7.10. ECF Generated Creep Curves under Varying Normal Load in Leaf Contaminated, Sanded Conditions.

When sand was not applied, the ECF generated creep curves showed very little change, as is evident in Figure 7.11. The curve is slightly lower in the region of stick-slip for lower loads, but only by a small amount.

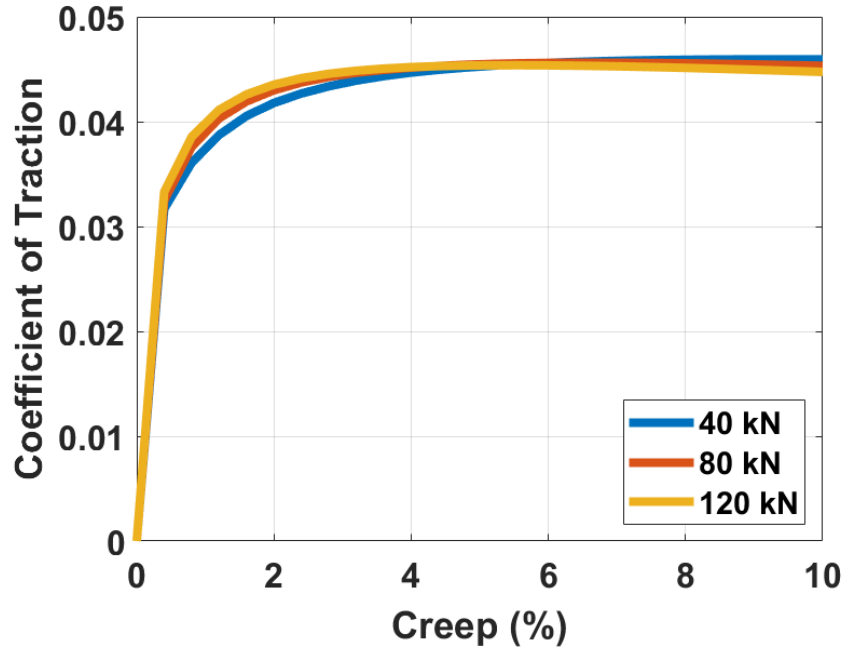

Figure 7.11. ECF Generated Creep Curves under Varying Normal Load in Leaf Contaminated, Unsanded Conditions.

7.3 Full-Scale Rig Data

In this sub-chapter, full-scale testing with LB rail sand was used to validate the predicted ECF curves produced by the parameterised ECF model. The full-scale rig (FSR) will be used with a range of normal loads and contact conditions to test how robust the ECF model is over these range of cases. In addition, data from fielding testing and literature will also be used to compare ECF predictions where appropriate.

7.3.1 FSR Methodology

7.3.1.1 Apparatus

A schematic of the FSR has been included in Figure 7.12; the wheel *(1)* is 920 mm in diameter and made of R7 steel, it is mounted upon the load frame *(2)* by an axle which can freely rotate due to journal bearings on either end. The load frame is allowed to pivot; thus the wheel can be raised or lowered as desired. The 1010 mm long rail *(3)* is made of R260 steel and is placed on a linear slider bed *(4)*, the movement of which is controlled by a horizontal actuator *(5)*, during test runs the rail is pulled back and the wheel rotates due to friction within the wheel/rail contact. During test runs, axial load is applied to the wheel via a vertical actuator *(6)*, this also controls the raising of the wheel, thereby allowing the repositioning of the rail for the start of each test run. Slip values can be modulated by a horizontal actuator *(7)*, which controls a chain and pulley system *(8)* attached to the wheel. The coefficient of traction is measured by taking the ratio between the force needed to pull the chain to achieve the desired slip value (measured by a load cell positioned near *(7)*) and the applied axial load (measured by a load cell positioned near *(6)*).

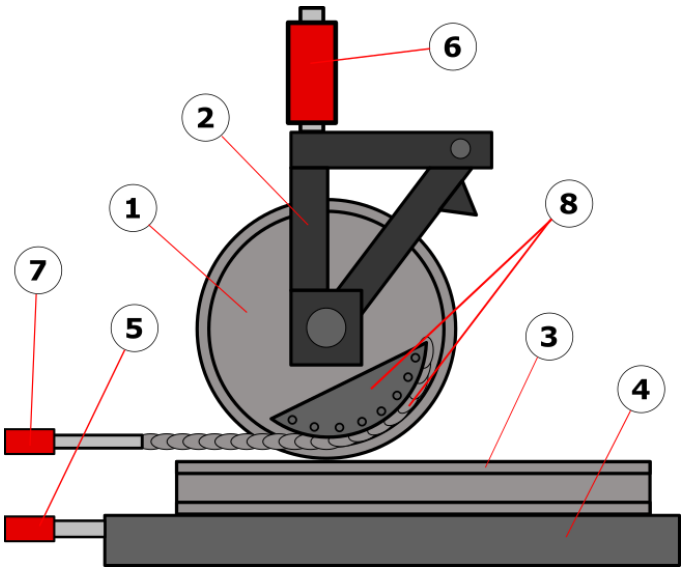

Figure 7.12. Schematic of the Full-Scale Rig.

7.3.1.2 Third Body Application

Before each set of test runs, the rail head and corresponding wheel surface were cleaned to remove unwanted contaminants. For tests conducted in wet conditions, 2 ml of distilled water was applied by pipette, this amount is approximately the same relative amount as was applied for HPT testing.

LB rail sand particles were applied to the head of the rail by hand before each set of test runs. As the test run takes place over a length calculated to achieve the necessary slip, 7.5 g/m of material was applied over this length of rail, thereby conforming to the current GB requirement of 7.5 g/m of sand on the rail head [11].

After, the set of test runs had been completed, the remaining amount was cleaned from the rail head and weighed to determine the active amount of material in the wheel/rail contact.

7.3.1.3 FSR Test Procedure

The test procedure for FSR testing is as follows:

1. Wheel and rail cleaned and a representative amount of adhesion material applied;
2. Five test runs over applied material were performed. These test runs were conducted at 5% slip and 900-1200 MPa (60-100 kN wheel load [140]). Two tests were conducted per condition;
3. Remaining material cleaned off the surface and weighed.

7.3.2 FSR Results

Full-scale tests were run in dry and wet conditions, with and without the application of LB rail sand. Due to potential issues with rig calibration, the traction values presented in this section are lower than seen in previous investigations using the full-scale rig, where traction values between 0.5-0.8 were recorded in dry conditions [37], [144], [154].

The dry traction values measured as part of this project are presented in Figure 7.13. It should be noted that due to a radius differential between the chain attachment radius and wheel radius (first observed in [144]) a creepage correction factor of 1.65% was used to adjust the raw data. Whilst the traction values are lower than can normally be expected, higher traction values at higher slip values is consistent with previous findings [37], [144], [154]. At ~3.5% slip, traction is between 0.3-0.35, the reason for these low traction values is unclear, though may be due to the FSR not undergoing calibration since it was last serviced; the data presented in this thesis can be adjusted with respect to future calibration parameters.

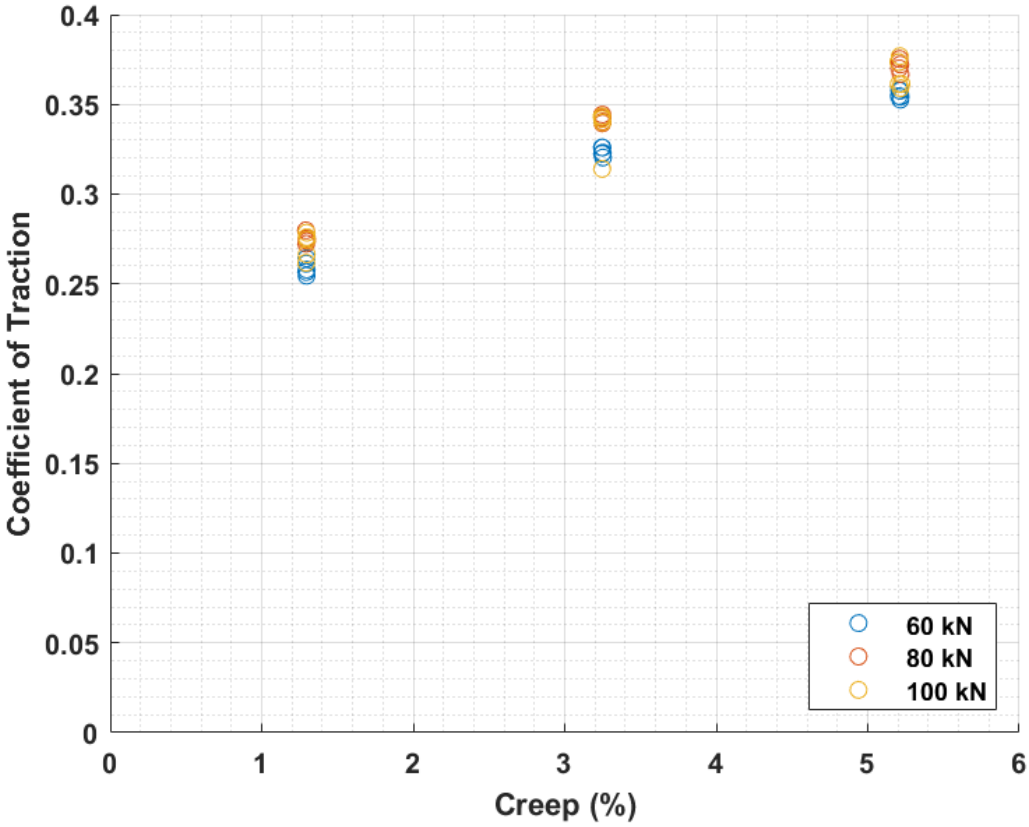

Figure 7.13. Creep Curve Produced on the FSR in Dry, Unsanded Conditions at Three Normal Loads.

The traction values measured in dry and wet conditions, with and without the application of LB rail sand and over a range of normal loads have been included in Figure 7.14. The relationship between application of sand and traction values is similar to what was observed during HPT testing; in dry conditions, there was little difference in traction when sand was applied, whereas in wet conditions, traction was increased. The relationship between contact pressure and traction values is also similar to that observed during HPT testing; in both dry and wet conditions, traction decreased with contact pressure when sand was applied.

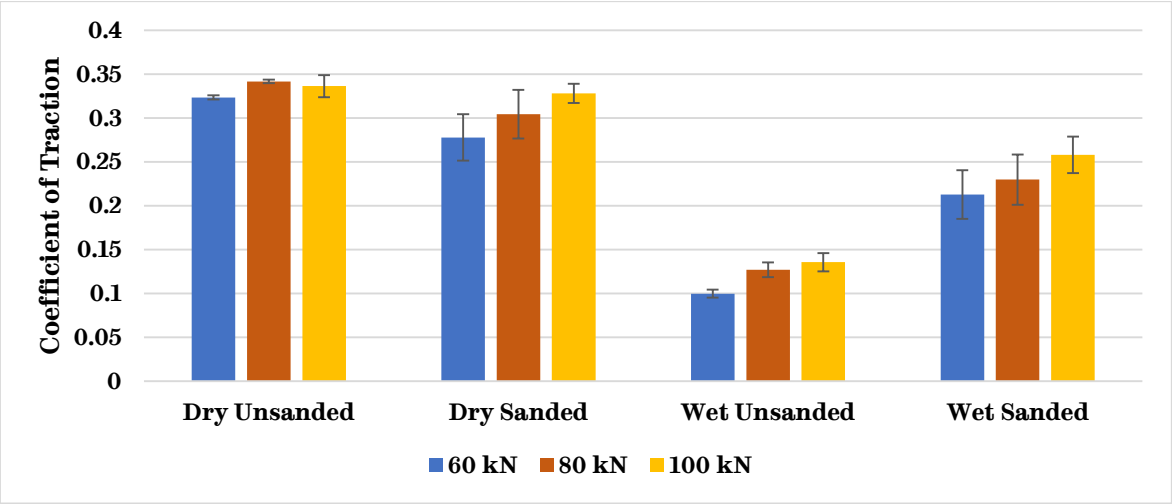

Figure 7.14. Summary of FSR Tests Conducted at a Nominal Slip Value of 5% (3.35%).

The fraction of sand remaining on the wheel and rail surface after the test runs has been included in Figure 7.15. There is more material being retained in wet conditions vs dry conditions, though the variance in the data is significant. The variance in results appears to reduce in wet conditions. This relationship between material retention and moisture is similar as to the observations made during the HPT & SWR chapters (chapter 5 & chapter 6 respectively).

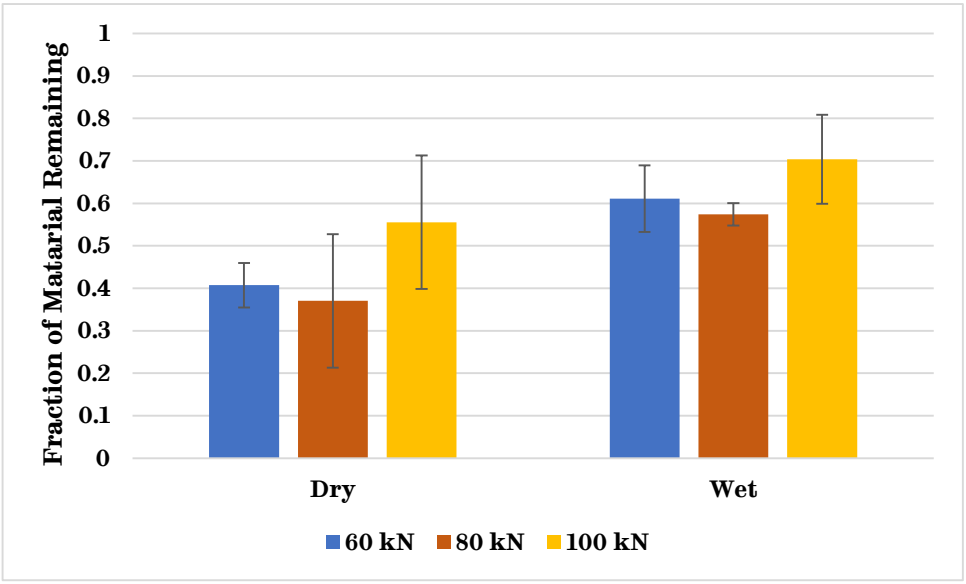

Figure 7.15. Fraction of Sand remaining on the Rail Head and Wheel Surface after 5 Test Runs.

7.4 Discussion

7.4.1 ECF Fitting Accuracy

Overall, the fitting of the ECF model to HPT data was successful, with no model showing error above 15%. A consistent trend for all the fits was the overestimation

of the stiffness of the elastic region at lower normal pressures. However, estimation of the critical shear stresses was consistently acceptable for all normal pressures.

The difference in initial stiffness accuracy with changing pressure may be abated by adjusting the pressure dependent term for inverted stiffness (L_e^p). This is not a trivial matter however, as optimising another parameter will result in difficulties with the parameter optimisation process as a whole.

The difference in nominal inverted stiffness when a leaf layer was present, unsurprisingly suggests that contact stiffness was greatly reduced when compared to the dry and wet conditions. This demonstrates how fundamentally different a HPT contact in leaf contaminated conditions behaves.

7.4.2 ECF Generated Creep Curves

The creep curves generated based on a typical wheel/rail contact produce sensible data for all conditions. It is of interest to note that for both dry and wet conditions, the peak coefficient of traction has not changed by much, rather the creep at which this peak is observed is shifted to higher creep values at lower normal loads.

For the leaf contaminated contact, with LB sand applied, there was a noticeable change in peak coefficient of traction. For both leaf contaminated contacts, sanded and unsanded, there was not as noticeable a drop in traction at higher creep values, possibly due to the lower traction values resulting in theoretically lower wheel/rail contact temperatures.

The creep curves produce predict that the presence of sand in all conditions will keep adhesion levels above the minimum specified for braking (0.09 [2]) at creep values at creep values typical of non-pure rolling, though even with sand applied the leaf contaminated contact does not produce adhesion levels above the minimum specified for acceleration (0.2 [2]). When rail sand is not applied to the leaf layer very low adhesion levels are present in the contact, corroborating their adhesion lowering effect that has been observed in the railway industry [2] and in laboratory testing [7], [147].

7.4.3 ECF Outputs vs Full-Scale Data

As previously noted, the unsanded, dry traction values measured as part of this project were much lower than previously observed, possibly due to calibration issues. Therefore, it is very difficult to use the measured traction values with much confidence, instead the relative changes in traction values in different contact conditions will be focussed on primarily.

FSR testing conducted as part of this project showed that there was little difference between sanded and unsanded traction values in dry conditions. In previous work using FSR data to validate ECF predicted creep curves, Evans found that the ECF model accurately predicted creep curves in dry, unsanded conditions [144], this comparison is included in Figure 7.16.

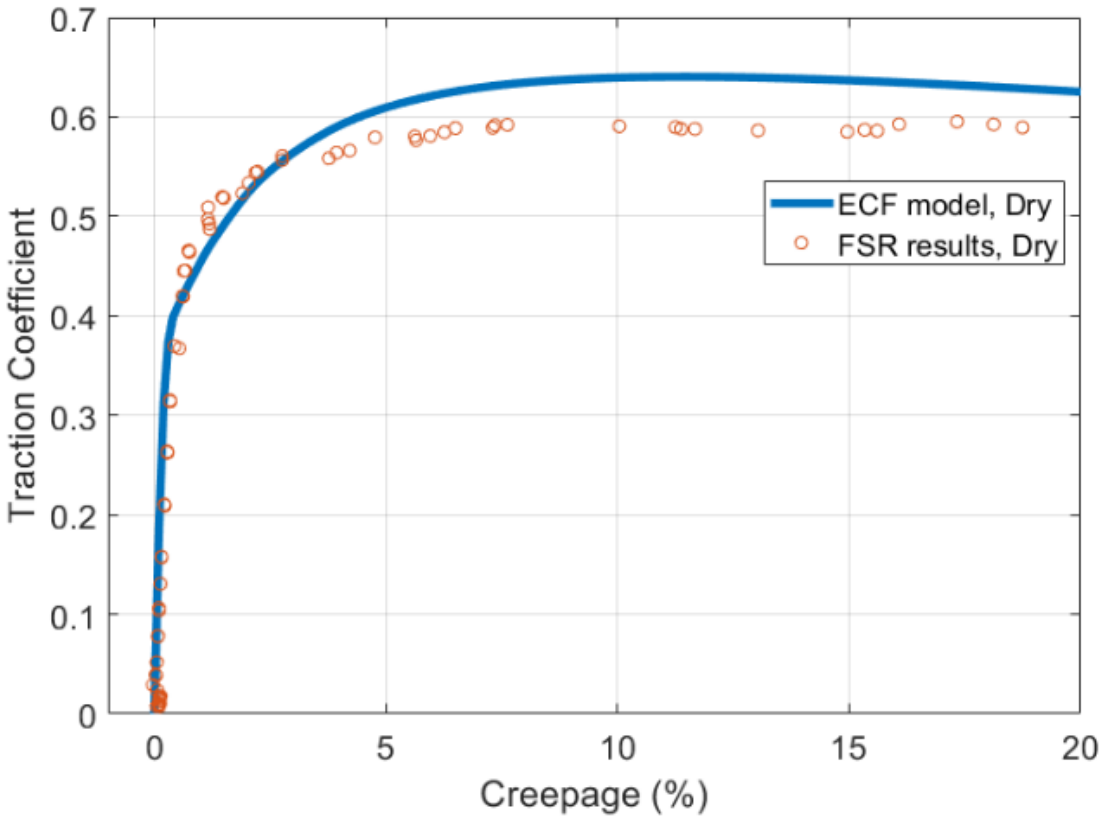

Figure 7.16. ECF Validation using FSR Results as produced by Evans [144].

Bearing this in mind, the dry, sanded ECF predicted creep curves produced from HPT data included in this project are very similar to the dry FSR data accrued by Evans, thus there is indication that the ECF has accurately predicted full-scale behaviour for these contact conditions. The ECF prediction of a dry, sanded FSR creep curve is included in Figure 7.17, the peak predicted coefficient of traction (~0.6) is very similar to the dry, unsanded FSR data observed in Figure 7.16.

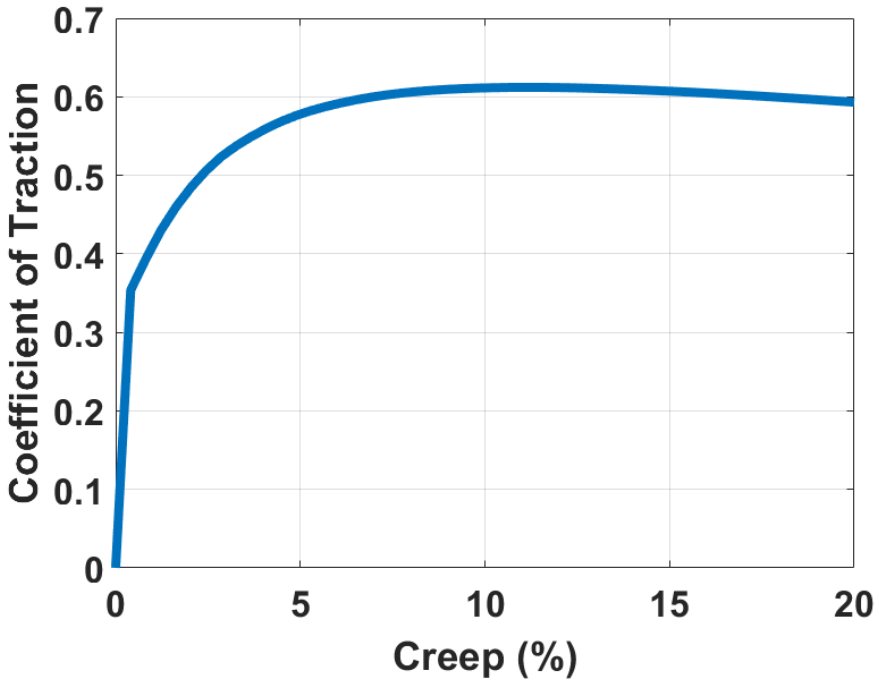

Figure 7.17. ECF Prediction of Full-Scale Rig Traction Data for Dry, Sanded Conditions.

Similarly, the ECF predicted creep curves generated from wet, sanded contact conditions are shown to exhibit lower traction values than dry creep curves; the ECF generated creep curve of wet traction data is included in Figure 7.18. This was observed in the FSR data generated as part of this project; the predicted difference between dry and wet traction is ~0.1, a similar difference can be observed in Figure 7.14, indicating the validity of the ECF predictions produced for these conditions.

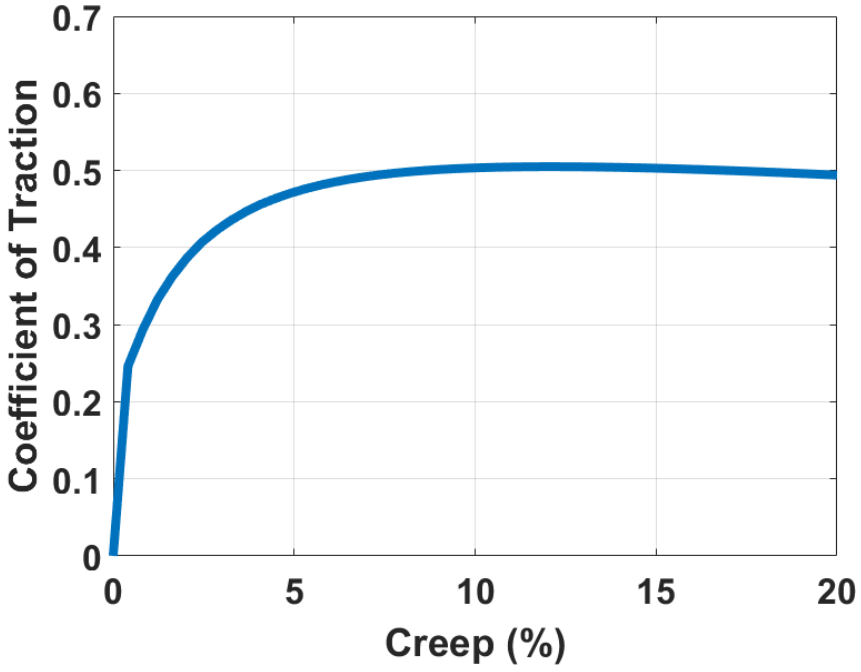

Figure 7.18. ECF Prediction of Full-Scale Rig Traction Data for Wet, Sanded Conditions.

Figure 7.19 illustrates the relationship between conditions and coefficient of traction, where both dry and wet data have been normalised against dry unsanded traction values (FSR data has been normalised against dry, unsanded FSR traction values, and ECF predictions have been normalised against dry, unsanded ECF predictions). This comparison demonstrates that the ECF has been successful at predicting changes in traction when contact conditions are varied.

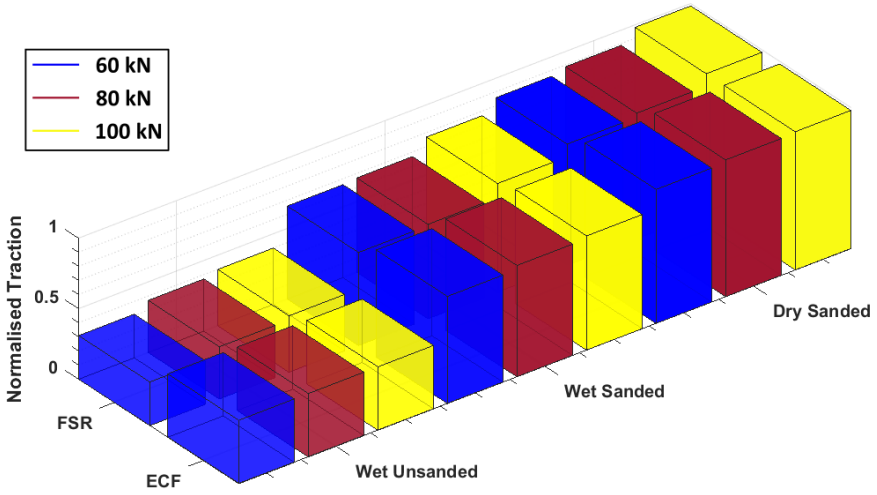

Figure 7.19. Coefficient of Traction when Normalised against Dry Traction Values from FSR Data & ECF Predictions respectively.

As opposed to the aforementioned, laboratory-based FSR data, the data included in Figure 7.20 comes from field tests conducted by Knorr-Bremse [155]. The first sanded axle in these tests was axle 03, where an increase in traction up to ~0.16 was observed. This is very similar to the ECF predicted creep curve produced from sanded, leaf contaminated HPT data, this creep curve has been included in Figure 7.21 where a peak coefficient of traction of ~0.14 was predicted. It should be noted, that the ECF predictions were made without knowing all salient facts regarding the Knorr-Bremse testing, however the wheel load of ~70 kN and vehicle speed of 100 km/h were known. In addition, the type of sand being used in the Knorr-Bremse testing is not known.

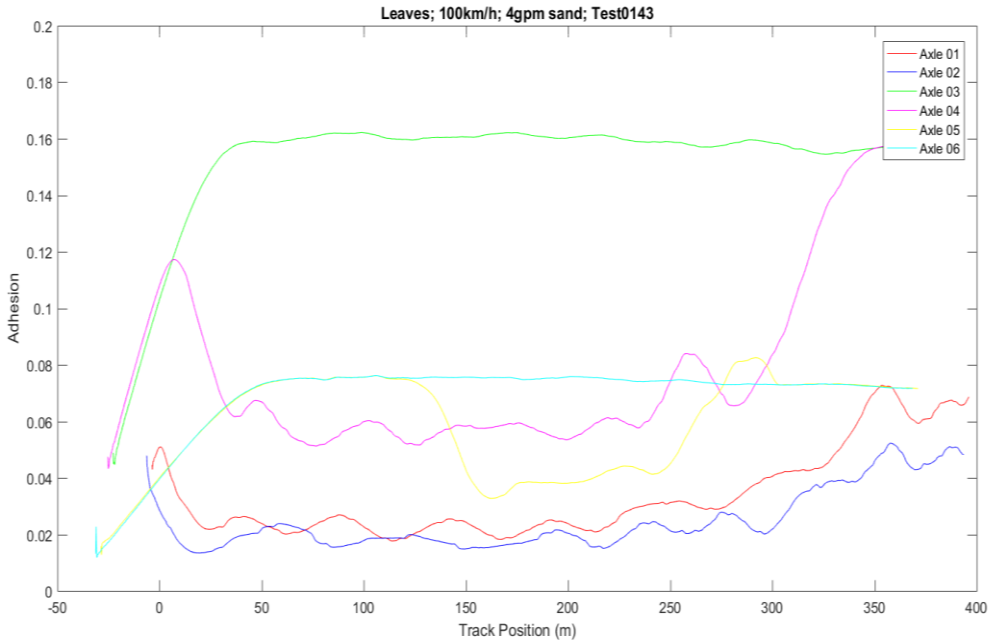

Figure 7.20. Field Data from Sanded Tests conducted in Leaf Contaminated Conditions [155].

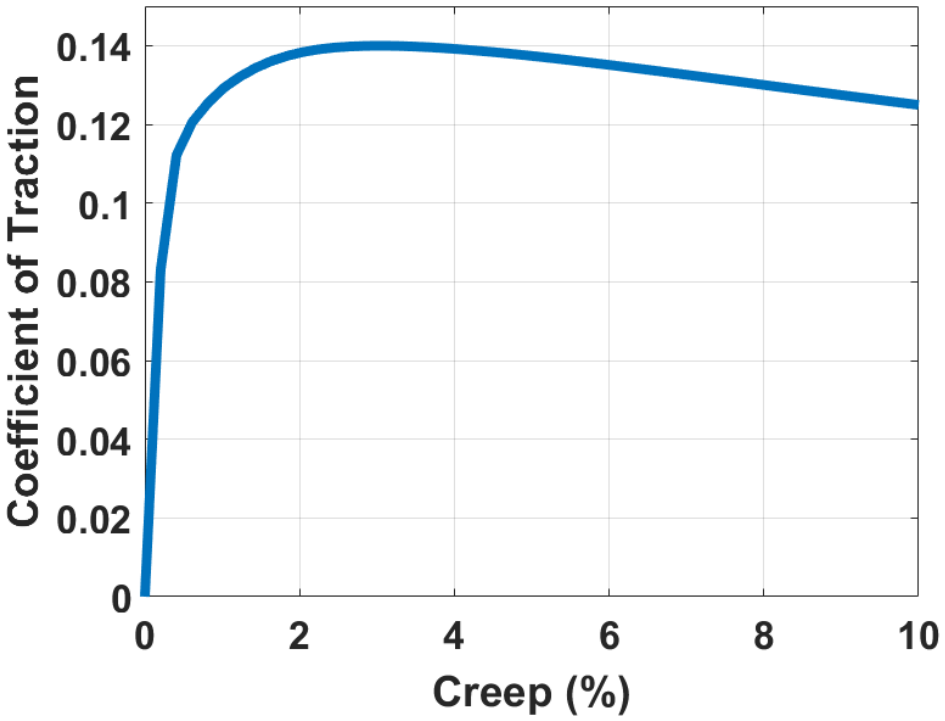

Figure 7.21. ECF Predicted Creep Curve of a Sanded, Leaf Contaminated Contact where Contact Conditions were set to Mimic Knorr-Bremse Testing.

The field testing from Knorr-Bremse also measured traction values in leaf contaminated conditions with no application of sand, the results of which are included in Figure 7.22. The traction values measured from these field tests range from 0.02-0.04, the ECF predicted creep curve predicts very similar traction values

to this. In Figure 7.23, the ECF generated creep curve predicts a maximum coefficient of traction of ~0.04, a very similar value to the field data. Again, it should be noted that not all salient details of the testing methodology were known, including the type of leaf used in these tests.

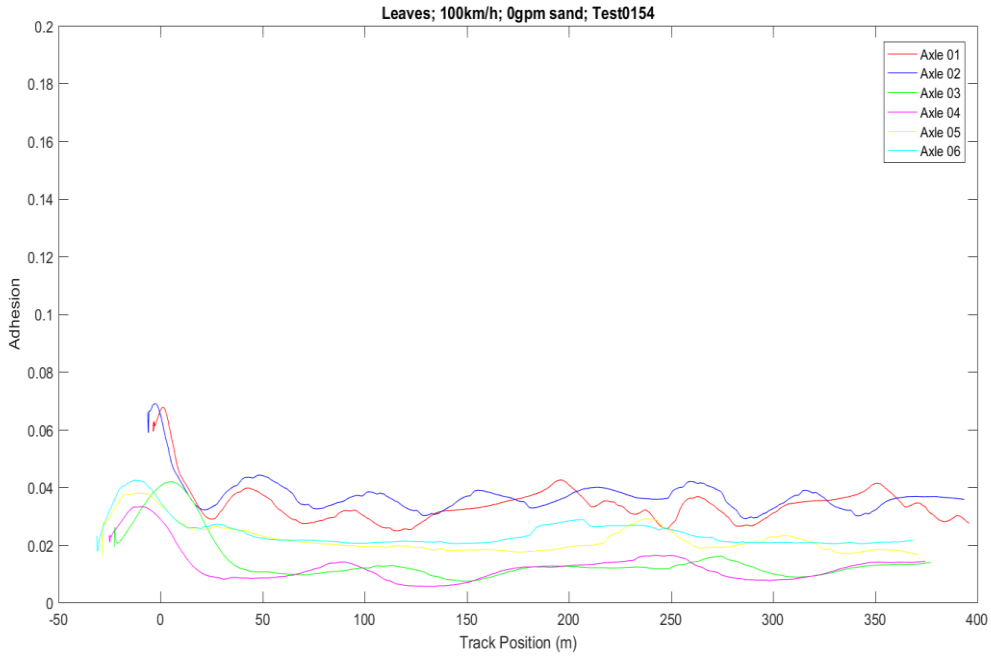

Figure 7.22. Field Data from Unsanded Tests conducted in Leaf Contaminated Conditions [155].

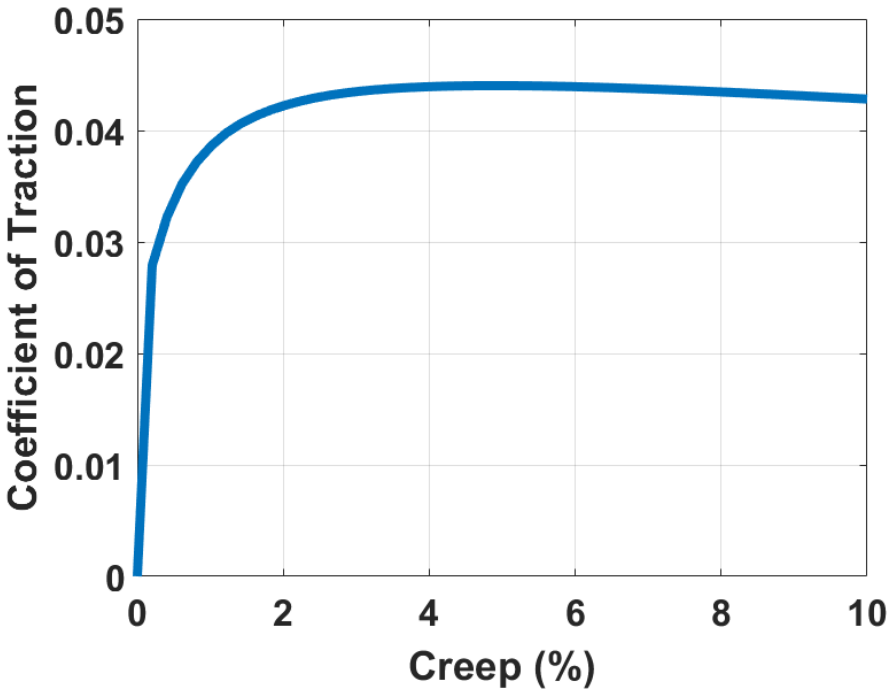

Figure 7.23. ECF Predicted Creep Curve of a Leaf Contaminated Contact where Contact Conditions were set to Mimic Knorr-Bremse Testing.

Overall, the validation of the ECF model with sanded data was hindered by low FSR traction values measured as part of this project. However, when using previously conducted FSR values in conjunction with observations about the overall trend in traction values between dry and wet, sanded and unsanded conditions, then the ECF generated creep curves appear to sensibly predict full-scale behaviour.

This is further corroborated by field data produced by Knorr-Bremse, where traction values measured in sanded and unsanded, leaf contaminated conditions matched very well with ECF predictions of these traction values.

7.5 Summary

In this chapter, data from HPT tests concerning LB rail sand were used to parameterise the ECF model and predicted creep curves were produced. The parameterisation process produced an ECF model that fitted well to HPT data at different normal pressures and contact conditions.

Creep curves generated from the parameterised ECF model predicted adhesion levels for a typical train: between 0.4-0.5 for a dry, sanded contact; between 0.3-0.4 for a wet, sanded contact; and between 0.1-0.2 for a leaf contaminated, sanded contact. A creep curve was also generated using data from unsanded, leaf contaminated HPT tests that predicted adhesion levels between 0.04-0.05.

Full-scale validation of the ECF predictions was hampered by unusually low traction measurements on the FSR, however the trends between contact conditions and normal loads were similar to the ECF predictions. In addition, field data from unsanded and sanded leaf contaminated conditions matched up very well with ECF predictions. In future, more full-scale data would be beneficial for further validation of the ECF model.

8 GENERAL DISCUSSION

This chapter discusses the work included in preceding chapters, with an emphasis on how each chapter relates to one another and what observations can be made based on work across multiple chapters. The project aims and objectives will be evaluated against the outcomes of this project and test methodologies assessed to highlight associated challenges and help identify future improvements.

Findings from high pressure torsion (HPT) testing suggested that a "good" traction enhancing particle should be relatively hard (at least harder than wheel and rail steels), with particle shape and size also being important properties. In the case of particle shape and size, the definition of a "good" particle depends on the contaminant in the contact and how important low surface damage is in any particular operation.

The particle characteristics that best restore traction may however, be in contradiction to the best particle characteristics for other parts of the sanding process. For example, GMRT 2461 [11] calls for "rounded" particles as this is thought to provide the best flow of sand from the sand hopper, however in HPT testing less circular particles were linked with increasing traction in leaf contaminated contacts. This may mean that a trade-off exists between certain particle characteristics when analysing the whole sanding process.

In dry HPT tests it was observed that harder particles tended to remain in the contact less than softer particles; in tests with the scaled-wheel rig (SWR) there was evidence that particles could ping out of the contact upon crushing. Therefore, it could be that as harder particles require greater crushing energy to fracture [105], the fracture of a harder particle will be more severe and more material will be expelled from the contact. The expulsion of material was not as apparent in the presence of water and leaf contaminant (the former case being observed in both HPT and SWR testing) and no obvious link between particle hardness and particle retainment was noted in these conditions. This suggests that when low adhesion contaminants exist, and where the presence of traction restoring material is most necessary, the hardness of the particle should not have as pronounced an effect on the amount of material being expelled.

In both HPT and SWT tests the effect of moisture on particle entrainment was noticeable, with wet conditions appearing to retain more material in the contact. Full-scale rig (FSR) tests quantified this, finding that a greater proportion of material was retained on the rail head in wet conditions. The inference that the presence of

moisture retains crushed particles was seen across multiple scales of testing and in literature [19], increasing the confidence of this observation.

8.1 Fulfilment of Aims & Objectives

The stated aim of this project was to develop an understanding of how to optimise the sanding process, with an emphasis on what makes an ideal traction enhancing particle. This section addresses the completion of this aim through assessing the fulfilment of the project's five objectives.

8.1.1 Objective 1

Literature surrounding the sanding process was reviewed and a gap analysis performed as part of sub-chapter 3.2. Knowledge gaps concerning the effect of particle characteristics (especially non-sand particles) on the wheel/rail contact were identified. It was also observed that there was no in-depth understanding as to how particles were behaving within the contact, as well as little modelling to predict how particles affect the wheel/rail contact.

The literature review also provided information on the key particle characteristics for traction enhancement: particle size and shape, hardness, adhesion, and coefficient of restitution; in addition bulk properties, such as flowability and bulk compressive strength were also identified. This was summarised in sub-chapter 3.3.1.

This objective was fulfilled satisfactorily and the outcomes of it guided the further objectives in this project.

8.1.2 Objective 2

As key particle properties were identified using the review of the literature, another literature review was conducted to identify the best characterisation methods for measuring these properties, this formed sub-chapter 3.3.

The most suitable technique for measuring each key particle property was ascertained through comparing methods according to six criteria, designed to ascertain the practicality and accuracy of the method. The outcome of this produced the particle characterisation framework presented in Table 4.1.

The particle characterisation framework was used on a variety of different particles, including international rail sands and industry abrasives. These results were used to assess the effect of particle characteristics on performance in the wheel/rail contact, which was measured as part of the remaining project.

The literature review and particle characterisation technique selection was successful at identifying key particle properties and forming a particle characterisation framework, the measurements arising from this form chapter 4.

Not all particles were fully characterised (the reasons for this will be discussed when assessing methodologies used in this project), but all particles had some characteristics relating to geometric and physical properties measured, allowing for comparison as part of this project. To this extent, the objective as fulfilled but with the caveat that fully characterising all particles would have been ideal.

8.1.3 Objective 3

HPT testing was conducted on a range of particles with their respective effects on traction and surface damage in the contact measured. Through this, a direct comparison between different particles' performance in dry, wet, and leaf contaminated conditions could be made. The HPT work forms chapter 5.

In addition, the acquired results were used to create ordinary least squares models to assess the relationship between particle characteristics and traction and damage in dry, wet, and leaf contaminated conditions respectively. These models are included in sub-chapter 5.4.6.

In addition to the effect of particle characteristics on performance, tests were also conducted to assess the effect of multiple passes and varying normal pressure in sub-chapter 5.3.5 and sub-chapter 5.3.6 respectively.

As significant trends between particle characteristics and performance were identified and mechanisms underlying these relationships proposed, the objective was fully satisfied.

8.1.4 Objective 4

Particle entrainment into a scaled-wheel contact was observed using high speed videography for three different rail sands. In addition, the effect of moisture on particle entrainment was also observed. This work formed chapter 6.

Quantifiable data on the spread of crushed particles would have been beneficial, however the stated objective of this project was met and can be used as the basis for further work in this area.

8.1.5 Objective 5

The extended creep-force (ECF) model was parameterised in chapter 7 for one type of rail sand in dry, wet, and leaf contaminated conditions. Error between the ECF

model and HPT data was <15% in all cases. The parameterised ECF model was used to generate creep curve predictions for full-scale wheel/rail contacts.

The full-scale rig (FSR) was used to collect data on the effect of one type of rail sand in dry and wet conditions at a range of creep values and normal pressures, to allow for comparison with ECF predictions. These measurements were included in sub-chapter 7.3. Good agreement regarding the relative effect of normal pressure on traction was observed in comparison to ECF predictions, though measured traction values were generally lower than predicted. A possible explanation for this discrepancy will be discussed as part of the evaluation of the FSR methodology.

In addition, data from sanded and unsanded, leaf contaminated field trials was sourced for comparison with ECF outputs. These real world results compared very favourably with ECF predictions.

The objective was met in this case, though there was issue with the FSR which negatively impacted the strength of this part of the project.

8.2 Evaluation of Methodology

This section assesses the practical issues of the test methodologies employed in this project. The limitations and possible improvements for each methodology will be discussed.

8.2.1 Particle Characterisation Framework

As the framework was made up of many tests, most of which could be considered standard, only those tests which limit the characterisation of particles for the use of rail sanding will be discussed.

2D image analysis for assessing particle shape and size is not as descriptive as 3D measurements would have been, however the increase in complexity of 3D measurements is something that needed to be taken into account. If fewer types of particle were being characterised or greater resources were at hand, 3D image analysis would be preferable.

In a similar vein, measurements of the coefficient of restitution would be improved by taking 3D footage of the bouncing particle. A similar balance between added complexity and more descriptive measurements is also present here.

The measurement of particle adhesion using the drop test was the simplest available method, however the work needed to set up the test (e.g. dispersing particles on a substrate, design of the rig, high speed video set-up) increased the complexity and limited the number of tested particles. There is no currently obvious alternative, but

it is instead something that should be taken into account when performing this methodology.

Single particle crushing is a very simple test, to both set up and perform, however the number of tests needed to fully characterise the crushing strength of a material is not trivial. The effect of particle size on crushing strength means the number of tests for one material was ~120. Future use of this methodology will need to take this into consideration and possibly reduce the number of tests, at the cost of losing some information on how the crushing strength of the material changes with particle size.

Holistically, the particle characterisation framework was effective at obtaining the necessary measurements, however the initial work needed to set up the various measurement apparatus was time consuming and resulted in some particles not being fully characterised.

8.2.2 High Pressure Torsion Rig

The HPT methodology was able to provide repeatable measurements under a range of different contact conditions and significant trends between particle characteristics were drawn out from analysing the acquired data.

A practical improvement that could be made to the HPT rig would be to implement a new controller with greater control of the rotational displacement. In wet conditions, the removal of the effect of gross stick-slip events was not entirely achieved, it may be that a newer controller with faster computation times could further reduce the stick-slip effect. However, an entirely new test script may be and post-processing method may have to be implemented, not a trivial process.

An intrinsic limitation of the HPT method is the different entrainment mechanisms of crushed particles compared to a full-scale contact. Whilst there is no trivial method for increasing the realism of this aspect of the HPT rig, further work on understanding the exact mechanisms of particle crushing, and their relation to particle characteristics, would greatly benefit a fuller understanding of the sanding process, from the hopper to the wheel/rail nip to the actual wheel/rail contact.

Further research into the evolution of roughness in an unsanded contact would also help guide aspects of the HPT methodology, especially with regard to surface damage accrued through the test.

8.2.3 Scaled-Wheel Rig

Whilst tests conducted with the SWR provided information on what could be happening when particles meet the wheel/rail nip, the test was limited to only

qualitative information. The test methodology would be improved by more quantitative image analysis of the pre-crushed particle vs its debris, thereby allowing more accurate comparisons to be made between entrainment of different particles.

Further progression would be to implement a similar method for a full-scale contact, with particles being propelled via an air stream, thereby coming closer to the real-world application.

8.2.4 Full-Scale Rig

The traction values measured during FSR testing were lower than previously experienced [144]. The complexity of calibrating the rig, especially the load cell attached to the chain (the measure of slip load), means accurate measurements are particularly difficult to acquire from the test rig. Future efforts on using the FSR rig for measuring full-scale traction should focus on creating bespoke calibration set-ups to reduce the complexity, time, and expense of calibrating attached load cells. In addition, future tests could attempt to create a similar leaf layer to that created in the HPT rig to measure traction in leaf contaminated contacts.

8.3 Summary

In this chapter the overall project has been assessed, with findings from separate chapters used to form an all-inclusive discussion of the work. The aims and objectives of the project were discussed based on their outputs and test methodologies were evaluated with emphasis on practical improvements.

9 CONCLUSIONS

The overarching aim of this project was to investigate what makes a "good" particle for restoring adhesion in the wheel/rail contact. To achieve this, a review of sanding literature was undertaken to identify knowledge gaps and key particle properties in the sanding process.

A new particle characterisation framework had to be designed to assess the key particle properties for use in sanding. In addition, tribological testing was undertaken at a small scale and at full scale, thereby allowing for the comparison between different particle characteristics and their effect on the wheel/rail interface.

A scaled-wheel rig (SWR) was used to assess the crushing of particles at the wheel/rail nip through the use of high speed videography.

Lastly, a predictive model for generating creep curves based off small-scale tribological measurements was parameterised with high pressure torsion (HPT) data and full-scale predictions made concerning traction.

This chapter will summarise the findings, industry benefits, and future work that form the outcomes of this project. The wider impact of this work (academic papers, industry presentations etc.) will also be presented.

9.1 Findings & Benefits

The findings of this project have been attributed to an initial project objective, outlined in sub-chapter 1.2. The overall benefits of the project have also been included in this sub-chapter.

The overall aim of this project has been broadly met, an idea of what makes a "good" adhesion restoring particle has been identified according to their ability to restore traction in the high pressure torsion test; generally, harder particles are better in all conditions, with particle size and circularity also important. In addition, a process for assessing a new prospective particle has been presented i.e. particle characterisation framework, then HPT tests, then ECF predictions.

The findings accrued from the literature review of previous sanding research, forming the output of objective 1 (sub-chapter 3.2), included:

- The identification of knowledge gaps concerning the effect of varying particle characteristics in the wheel/rail contact and the mechanisms behind the restoration of traction;

- The identification of key particle properties, including mineralogy, geometry, physical properties, and bulk behaviour.

The particle characterisation process, generated from completion of objective 2 (sub-chapter 3.3 & chapter 4), gave the following outputs:

- The formulation of a particle characterisation framework, through which prospective sanding particles can be subjected to and initial assessments about suitability for traction enhancement made;
- The characterisation of a range of particles; notably, there were differences in the geometric and physical properties of international rail sands, the latter of which could be mainly attributed to the amount of quartz content.

The range of characterised particles were then tested in the HPT rig, this work formed objective 3 (chapter 5). From the HPT testing, the following findings have been split into those that further the understanding of the sanding process and those that advance new practical techniques:

- Sanding process findings:
    - In both dry and wet conditions, increasing traction was found to be significantly linked ($p<0.001$) to increasing particle hardness and circularity, the former being more strongly linked;
    - In leaf contaminated conditions, increasing particle hardness and decreasing circularity were significantly linked ($p<0.001$) to increasing traction, however particle size was the most important characteristic, with results suggesting the existence an optimum particle size for increasing traction;
    - In all conditions, increasing surface roughness was significantly linked ($p<0.001$) to decreasing particle circularity and in the case of the roughness of the wheel specimen also linked to increasing particle size;
    - When multiple passes over an applied material were conducted, traction data did not appear to change in dry or wet conditions, though decreased in sanded, leaf contaminated conditions;
    - When normal pressure was varied in dry and wet, sanded conditions, the traction increased with increasing normal pressure, however in sanded, leaf contaminated conditions the inverse was found to be true;
- Advancements in tribological testing:
    - A revised test method was implemented in the test script, that minimised the effect of stick-slip, whilst retaining control of angular displacement;

- A new methodology was formulated to test particles in amounts similar to that seen in real-world applications and across dry, wet, and leaf contaminated conditions;
- A novel method for creating a leaf layer was produced, with low adhesion being achieved and a black leaf layer formed.

As previous chapters observed that there was a link between contact conditions and the entrainment of the particle upon crushing, SWR tests were conducted with high speed videography, thereby fulfilling objective 4 (chapter 6). Findings from this work included:

- The observation that in dry conditions a significant amount of the material is expelled away from the contact upon crushing;
- The observation that in wet conditions, more material was retained upon crushing due to the surface tension of the water.

Finally, data from HPT testing was used to parameterise the extended creep-force (ECF) model, producing creep curve predictions that were then compared to full-scale data, thus completing objective 5 (chapter 7). The outputs from this chapter encompassed:

- Parameterisation of the ECF model for sanded contacts, thus allowing the generation of creep curve predictions of full-scale behaviour;
- Comparison of ECF outputs with data acquired from the full-scale rig, which showed good agreement regarding the relative change in traction with pressure and contact conditions, though overall traction predictions were higher than this full-scale data.
- Comparison of ECF outputs with data sourced from field trials showed very good agreement for both sanded and unsanded leaf contaminated contacts;
- A prediction from the ECF model that in dry, sanded conditions the peak coefficient of traction of a typical train would be between 0.4-0.5;
- A prediction from the ECF model that in wet, sanded conditions the peak coefficient of traction of a typical train would be between 0.3-0.4;
- A prediction from the ECF model that in sanded, leaf contaminated conditions the peak coefficient of traction of a typical train would be between 0.1-0.2.

Overall, this project has contributed to the wider rail industry via the following benefits:

- The literature review has provided a basis for understanding sanding research that can be used in railway academia and industry;

- The particle characterisation framework can be used as a means of assessing future, prospective particles by adhesion material suppliers and approvers;
- The analysis of trends observed between particle characteristics have identified what makes a "good" particle in dry, wet, and leaf contaminated conditions, thus allowing particle suppliers to design the most effective particle for restoring adhesion whilst keeping surface damage to a minimum;
- The HPT work also gave inferences for the mechanisms by which particles restore adhesion in the wheel/rail contact, creating a better understanding of the process that may be used to optimise sanding products and systems.
- The high speed videos of SWR activities demonstrates the effect different contact conditions have on particle entrainment, something which could potentially be exploited by sanding system manufacturers.
- The ECF model, combined with inputted data from HPT tests, allows for a very simple, quick, and inexpensive method of predicting the effect of different adhesion restoring particles on wheel/rail traction, thus allowing for different particles to be tested more efficiently.

9.2 Future Work

By analysing HPT data with respect to data accrued from the particle characterisation framework, inferences have been made between a particle's characteristics and its effect on adhesion and damage in a range of conditions. This process may prove very beneficial for also analysing the effect of particle characteristics on wheel/rail isolation. This work would allow a fuller idea of what type of particle is most compatible with track circuits, and what possible compromises may have to be made with respect to what particle characteristics are most effective for restoring adhesion.

Another area of potential future work would be to expand the range of particles being used to parameterise the ECF model. This expansion would create a wider range of data for comparing different types of particles, that can be used to predict full-scale behaviour.

More full-scale validation of the ECF predictions would be an area of future interest. Either through more accurate laboratory testing or by the acquisition of field data using sand in arrange of contact conditions.

Further full-scale work assessing different particles would also be of interest, both as further validation of the ECF model and to further assess different particles' effect on full-scale wheel/rail adhesion behaviour. This full-scale work could also be used as an opportunity to more closely study observations on particle entrainment

into the wheel/rail contact. Similarly, further tests with adhesion restoring particles on a real-world train would also be beneficial.

9.3 Wider Impact

Journal Papers Directly linked with Thesis Work

Skipper WA, Chalisey A, Lewis R. A Review of Railway Sanding System Research: Adhesion Restoration and Leaf Layer Removal. Tribol - Mater Surfaces Interfaces. 2018;12(4):237-251. doi:10.1080/17515831.2018.1542791

Skipper WA, Chalisey A, Lewis R. A Review of Railway Sanding System Research: Wheel/Rail isolation, Damage, and Particle Application. J Rail Rapid Transit. 2019;234(6):567-583.

Skipper WA, Nadimi S, Chalisey A, Lewis R. Particle Characterisation of Rail Sands for Understanding Tribological Behaviour. Wear. 2019;432-433(202960). doi:10.1016/j.wear.2019.202960

Evans M, Skipper WA, Buckley-Johnstone L, Meierhofer A, Six K, Lewis R. The development of a high pressure torsion test methodology for simulating wheel/rail contacts. Tribol Int. 2021;156(106842). doi:10.1016/j.triboint.2020.106842

Other Journal Papers

Watson M, Christoforou P, Herrera P, et al. An Analysis of the Quality of Experimental Design and Reliability of Results in Tribology Research. Wear. 2019;426-427:1712-1718. doi:10.1016/j.wear.2018.12.028

Suhr B, Skipper WA, Lewis R, Six K. Shape Analysis of Railway Ballast Stones: Curvature-based Calculation of Particle Angularity. Sci Rep. 2020;10(6045). doi:10.1038/s41598-020-62827-w

Conference Paper

Skipper WA, Chalisey A, Lewis R. Particle Characterisation of Rail Sand for Understanding Tribological Behaviour. In: Proceedings of the 11th International Conference on Contact Mechanics and Wear of Rail/Wheel Systems, CM 2018.; 2018:886-895

Presentations & Posters

- The IET: Challenges in Tribology, Birmingham, March 2017, Poster
- CM2018, Delft, September 2018, Presentation
- TriboUK 2019, Leeds, July 2019, Presentation
- 28th Mission of Tribology, London, December 2019, Presentation

- IoP Tribology Fair, Sheffield, January 2020, Presentation

Direct Industrial Impacts

- Multiple poster presentations to a wide range of members of the wider tribology industry as part of my responsibilities as a member of the integrated tribology centre for doctoral training.
- Multiple presentations of PhD work to the adhesion research group, a cross-industry group set up to promote the understanding of wheel/rail adhesion.
- Membership of working group 38, a European committee tasked with writing CEN standards concerning adhesion materials. Contributions were made to PD CEN/TS 15427-1-3:2021 & PD CEN/TS 15427-2-3:2021.
- Follow-on work with the Rail Safety and Standards Board, using high pressure torsion and field testing to assess the effect of different particles on the likelihood of wheel/rail isolation occurring.

REFERENCES

[1] P. Gray, “T1107 Sander Trials Dissemination Event,” 2018. [Online]. Available: https://www.rssb.co.uk/Pages/adhesion.aspx.

[2] C. R. Fulford, “Review of low adhesion research (T354) (RSSB Report),” 2004. [Online]. Available: https://www.sparkrail.org/Lists/Records/DispForm.aspx?ID=9539.

[3] Rail Accident Investigation Branch, “Autumn Adhesion Investigation Part 3: Review of adhesion-related incidents Autumn 2005 (RAIB Report),” 2007.

[4] T. M. Beagley, I. J. Mcewen, and C. Pritchard, “Wheel/Rail Adhesion-Boundary Lubrication by Oily Fluids,” *Wear*, vol. 31, pp. 77–88, 1975.

[5] T. M. Beagley and C. Pritchard, “Wheel/rail adhesion - the overriding influence of water,” *Wear*, vol. 35, no. 2, pp. 299–313, 1975.

[6] L. Buckley-Johnstone, R. Lewis, K. Six, and G. Trummer, “Modelling and quantifying the influence of water on wheel / rail adhesion levels (RSSB Rport),” 2016. [Online]. Available: https://www.sparkrail.org/Lists/Records/DispForm.aspx?ID=24280.

[7] K. Ishizaka, S. R. Lewis, and R. Lewis, “The low adhesion problem due to leaf contamination in the wheel/rail contact: Bonding and low adhesion mechanisms,” *Wear*, vol. 378–379, pp. 183–197, 2017.

[8] R. Lewis and R. Dwyer-Joyce, “Wheel/Rail Tribology,” in *Handbook of Lubrication and Tribology: Volume I Application and Maintenance*, 2006.

[9] Rail Accident Investigation Branch, “Rail Accident Report: Near Miss Between a Passenger Train and Cars at Norwich Road Level Crossing, New Rackheath, Norfolk, 24 November 2019 (Report 15/2020),” 2020.

[10] Rail Safety and Standards Board, “Performance and Installation Criteria for Sanding Systems (T797),” 2013.

[11] Rail Safety and Standards Board, “GMRT2461 Sanding Equipment (Issue 3).” pp. 1–24, 2018.

[12] Z. Li, O. Arias-Cuevas, R. Lewis, and E. A. Gallardo-Hernández, “Rolling–Sliding Laboratory Tests of Friction Modifiers in Leaf Contaminated Wheel–Rail Contacts,” *Tribol. Lett.*, vol. 33, no. 2, pp. 97–109, 2009.

[13] I. . Hutchings, “Wear by Hard Particles,” in *Tribology - Friction and Wear of Engineering Materials*, Butterworth-Heinemann, 1992, pp. 135–141.

[14] Société Nationale des Chemins de fer Français, “Regelwerk Infrastruktur - Verfahren: Fahrzeugzulassungsspezifikation SAM S 901 Sandungsanlage,” 2004.

[15] DB/EBA/VDB/VDV Working Group, “Supplementary Regulation No. B 011 to ‘Sanding,’” 2016.

[16] Australian Rail Track Corporation, “Route Access Standard: General Information,” 2017.

[17] Rail Safety and Standards Board, “Understanding the current use of sanders on multiple units (T796),” 2009. [Online]. Available: https://www.sparkrail.org/Lists/Records/DispForm.aspx?ID=629.

[18] A. Meierhofer, “A New Wheel-Rail Creep Force Model based on Elasto-Plastic Third Body Layers,” TU Graz, 2015.

[19] R. Lewis, R. S. Dwyer-Joyce, and J. Lewis, “Disc machine study of contact isolation during railway track sanding,” *J. Rail Rapid Transit*, vol. 217, no. 1, pp. 11–24, 2003.

[20] O. Arias-Cuevas, Z. Li, and R. Lewis, “Investigating the lubricity and electrical insulation caused by sanding in dry wheel-rail contacts,” *Tribol. Lett.*, vol. 37, no. 3, pp. 623–635, 2010.

[21] S. R. Lewis, R. Lewis, J. Cotter, X. Lu, and D. T. Eadie, “A new method for the assessment of traction enhancers and the generation of organic layers in a twin-disc machine,” *Wear*, vol. 366–367, pp. 258–267, 2016.

[22] R. Lewis and R. S. Dwyer-Joyce, “Wear at the wheel/rail interface when sanding is used to increase adhesion,” *J. Rail Rapid Transit*, vol. 220, no. 1, pp. 29–41, 2006.

[23] O. Arias-Cuevas, Z. Li, R. Lewis, and E. A. Gallardo-Hernández, “Rolling–sliding laboratory tests of friction modifiers in dry and wet wheel–rail contacts,” *Wear*, vol. 268, no. 3–4, pp. 543–551, 2009.

[24] S. R. Lewis, S. Riley, D. I. Fletcher, and R. Lewis, “Optimisation of a Railway Sanding System for Optimal Grain Entrainment into the Wheel/Rail Contact,” *J. Rail Rapid Transit*, vol. 232, no. 1, pp. 43–62, 2016.

[25] I. D. Pollicott, “Review of service trails with the high velocity sander (IM-TRIB-029) (British Rail Report),” 1977. [Online]. Available: https://www.sparkrail.org/Lists/Records/DispForm.aspx?ID=8138.

[26] I. D. Pollicott and R. K. Taylor, “Assessment of the Southern Region Water Cannon on Leaf Affected Track in 1976 (TM-TRIB-19) (British Rail Report),” 1977. [Online]. Available: https://www.sparkrail.org/Lists/Records/DispForm.aspx?ID=5120.

[27] R. Taylor and I. D. Pollicott, “Assessment of the cleaning of leaf affected track on Southern region - 1977 (TM-TRIB-29) (British Rail Report),” 1978. [Online]. Available: https://www.sparkrail.org/Lists/Records/DispForm.aspx?ID=16453.

[28] R. K. Taylor and I. D. Pollicott, “Assessment of the Cleaning of Leaf Affected Track on Southern Region - 1978 (TM-TRIB-35) (British Rail Report),” 1979. [Online]. Available: https://www.sparkrail.org/Lists/Records/DispForm.aspx?ID=16456.

[29] I. J. McEwen, “Service Experience with Sandite - South Devon Banks, Autumn 1976 (TM-TRIB-020) (British Rail Report),” 1977. [Online]. Available: https://www.sparkrail.org/Lists/Records/DispForm.aspx?ID=8314.

[30] I. J. McEwen and R. K. Taylor, “Adhesion and Leaves: Wet Abrasive Blasting Tests on Southern Region 1974 (TM-TRIB-7) (British Rail Report),” 1975. [Online]. Available:

https://www.sparkrail.org/Lists/Records/DispForm.aspx?ID=5127.

[31] F. G. R. Zobel, “Effect of ‘slipmaster’ on track circuit operation. Tests using the ‘silica gun’ and high speed tribometer train (IM-ADH-004) (British Rail Report),” 1972. [Online]. Available: https://www.sparkrail.org/Lists/Records/DispForm.aspx?ID=12925.

[32] J. Tunley, “A successful approach to rail operations in low adhesion conditions,” in *World Congress for Railway Research*, 1999.

[33] K. G. Schofield, A. C. Wayte, and J. R. Waring, “The emergency one shot sander (RR-SAM-056) (British Rail Report),” 1995. [Online]. Available: https://www.sparkrail.org/Lists/Records/DispForm.aspx?ID=15017.

[34] E. R. C. Marks, “Emergency Sanding Device: Class 159 Fleet Trial (RR-PRJ-ESDM-RP-3) (British Rail Report),” 1996. [Online]. Available: https://www.sparkrail.org/Lists/Records/DispForm.aspx?ID=14798.

[35] J. R. Waring, “Sanding to Assist Braking in Low Adhesion: Class 318 Feasibility Study (RR-SAM-158) (British Rail Report),” 1996. [Online]. Available: https://www.sparkrail.org/Lists/Records/DispForm.aspx?ID=4792.

[36] W. Wang, T. Liu, H. Wang, Q. Liu, M. Zhu, and X. Jin, “Influence of friction modifiers on improving adhesion and surface damage of wheel/rail under low adhesion conditions,” *Tribiology Int.*, vol. 75, pp. 16–23, 2014.

[37] S. R. Lewis, S. Riley, D. I. Fletcher, and R. Lewis, “Optimisation of a Railway Sanding System , Part 2 : Adhesion Tests,” in *Conference: 10th International Conference on Contact Mechanics and Wear of Rail/Wheel Systems (CM 2015), August 30th – September 3rd, Colorado Springs, Colorado, USA, 2015.*, 2015.

[38] E. A. Gallardo-Hernandez and R. Lewis, “Twin disc assessment of wheel/rail adhesion,” *Wear*, vol. 265, no. 9–10, pp. 1309–1316, 2008.

[39] O. Arias-Cuevas, Z. Li, R. Lewis, and E. a Gallardo-Hernández, “Laboratory investigation of some sanding parameters to improve the adhesion in leaf-contaminated wheel–rail contacts,” *J. Rail Rapid Transit*, vol. 224, no. 3, pp. 139–157, 2010.

[40] Rail Safety and Standards Board, “GE/GN8540 Guidance on Low Adhesion between the Wheel and the Rail – Managing the Risk (Issue 2),” 2015. [Online]. Available: https://www.rssb.co.uk/rgs/standards/gegn8540 iss 2.pdf. [Accessed: 09-May-2017].

[41] S. Kumar, P. K. Krishnamoorthy, and D. L. Prasanna Rao, “Wheel-Rail Wear and Adhesion With and Without Sand for a North American Locomotive,” *J. Eng. Ind.*, vol. 108, no. 2, pp. 141–147, 1986.

[42] W. J. Wang, H. F. Zhang, H. Y. Wang, Q. Y. Liu, and M. H. Zhu, “Study on the adhesion behavior of wheel/rail under oil, water and sanding conditions,” *Wear*, vol. 271, no. 9–10, pp. 2693–2698, 2011.

[43] O. Arias-Cuevas and Z. Li, “Field investigations into the adhesion recovery in leaf-contaminated wheel–rail contacts with locomotive sanders,” *J. Rail Rapid*

Transit, vol. 225, no. 5, pp. 443–456, 2011.

[44] W. Huang *et al.*, "A Subscale Experimental Investigation on the Influence of Sanding on Adhesion and Rolling Contact Fatigue of Wheel/Rail under Water Condition," *J. Tribol.*, vol. 139(1), no. 011401, 2017.

[45] O. Arias-Cuevas, Z. Li, and R. Lewis, "A laboratory investigation on the influence of the particle size and slip during sanding on the adhesion and wear in the wheel-rail contact," *Wear*, vol. 271, no. 1–2, pp. 14–24, 2010.

[46] M. Omasta, M. Machatka, D. Smejkal, M. Hartl, and I. Křupka, "Influence of sanding parameters on adhesion recovery in contaminated wheel–rail contact," *Wear*, vol. 322–323, pp. 218–225, 2014.

[47] F. G. R. Zobel, "Development of Remedies for Poor Adhesion (IM-ADH-019) (British Rail Research)," 1974. [Online]. Available: https://www.sparkrail.org/Lists/Records/DispForm.aspx?ID=9038.

[48] L. B. Shi *et al.*, "Laboratory investigation on the particle-size effects in railway sanding: Comparisons between standard sand and its micro fragments," *Tribol. Int.*, vol. 146, p. 106259, Jun. 2020.

[49] X. Cao *et al.*, "The effect of alumina particle on improving adhesion and wear damage of wheel/rail under wet conditions," *Wear*, vol. 348–349, pp. 98–115, Feb. 2016.

[50] L. B. Shi *et al.*, "Study on the wheel/rail adhesion restoration and damage evolution in the single application of alumina particles," *Wear*, vol. 426–427, pp. 1807–1819, Apr. 2019.

[51] C. Wang *et al.*, "Adhesion and damage characteristics of wheel/rail using different mineral particles as adhesion enhancers," *Wear*, vol. 477, no. 203796, Mar. 2021.

[52] W. A. Skipper, A. Chalisey, and R. Lewis, "A Review of Railway Sanding System Research: Wheel/Rail isolation, Damage, and Particle Application," *J. Rail Rapid Transit*, vol. 234, no. 6, pp. 567–583, 2019.

[53] P. R. Cooper, "An investigation into the relationship between the Particle Size and the Frictional Performance of Sand (IM-ADH-011) (British Rail Report)," 1972. [Online]. Available: https://www.sparkrail.org/Lists/Records/DispForm.aspx?ID=10483.

[54] M. A. Tanvir, "Frictional performance of abrasive fines (IM-ADG-10) (British Rail Report)," 1972. [Online]. Available: https://www.sparkrail.org/Lists/Records/DispForm.aspx?ID=10522.

[55] J. D. Tunley, "Safety Submission for Class 165 Automatic Sander (Part 1: Overview & Evaluation of Braking Performance) (RR-TRS-96-044 Issue 1)." pp. 1–15, 1996.

[56] J. D. Tunley, "Safety Submission for Automatic Sanders Fitted To Class 165/166 3-Car Stock (RR-TRS-96-047 Issue 1)," 1996.

[57] D. M. Peat, "Class 165 Automatic Sander Braking & Track Circuit Tests for a 2-car Train (RR-TRS-96-016 Issue 1)," Derby, 1996.

[58] L. Purcell and A. Lightroller, “Trial of Sander Configurations and Sand Laying Rates (T1107) (RSSB Report),” 2018. [Online]. Available: https://www.rssb.co.uk/AdhesionContent/T1107-Sander-Trials-Research-Report-Issue1.pdf.pdf.

[59] X. Lu, J. Cotter, and D. T. Eadie, “Laboratory study of the tribological properties of friction modifier thin films for friction control at the wheel/rail interface,” *Wear*, vol. 259, no. 7–12, pp. 1262–1269, Aug. 2005.

[60] R. Lewis, E. A. Gallardo, J. Cotter, and D. T. Eadie, “The effect of friction modifiers on wheel/rail isolation,” *Wear*, vol. 271, no. 1–2, pp. 71–77, May 2011.

[61] C. Hardwick, S. Lewis, and R. Lewis, “The effect of friction modifiers on wheel/rail isolation at low axle loads,” *Proc. Inst. Mech. Eng. Part F J. Rail Rapid Transit*, vol. 228, no. 7, pp. 768–783, Sep. 2014.

[62] S. R. Lewis, R. Lewis, P. Richards, and L. E. Buckley-Johnstone, “Investigation of the isolation and frictional properties of hydrophobic products on the rail head, when used to combat low adhesion,” *Wear*, vol. 314, no. 1–2, pp. 213–219, Jun. 2014.

[63] R. Galas, M. Omasta, I. Krupka, and M. Hartl, “Laboratory investigation of ability of oil-based friction modifiers to control adhesion at wheel-rail interface,” *Wear*, vol. 368–369, pp. 230–238, Dec. 2016.

[64] R. Galas, D. Kvarda, M. Omasta, I. Krupka, and M. Hartl, “The role of constituents contained in water–based friction modifiers for top–of–rail application,” *Tribol. Int.*, vol. 117, pp. 87–97, Jan. 2018.

[65] T. Marshall, “Six Sigma project: WSP5.4 LNE Static Sandite Units (Network Rail Report),” 2006.

[66] L. Garner, “Investigation into the Benefits Afforded by Traction Gel Applicators and the Traction Enhancers Alleviate® and U5®,” Liverpool John Moores University, 2011.

[67] Rail Safety and Standards Board, “Research brief: Review of the risks and opportunities from the application of sand during braking (T1046),” 2015.

[68] R. Lewis and J. Masing, “Static wheel / rail contact isolation due to track contamination,” *J. Rail Rapid Transit*, vol. 220, no. 1, pp. 43–53, 2006.

[69] F. P. Bowden and D. Tabor, “The Friction and Lubrication of Solids,” *Am. J. Phys.*, vol. 19, p. 428, 1951.

[70] M. Broster and R. K. Taylor, “Investigation of Electrical Resistance of Some Suspensions in Glycol (IM-ADH-5),” 1972.

[71] M. S. Sutton, “Class 165 Automatic Sander Track Circuit Performance (RR: STG-D-REF-RP-1 Issue 1),” Derby, 1996.

[72] M. S. Sutton, “Class 165 Automatic Sander Track Circuit Performance (RR-STG-D-SND-RP-008 Issue 1),” 1996.

[73] R. A. Wood, “Safety Submission for Class 165 Automatic Sander (Part 2: Evaluation of Track Circuit Performance) (RR: STG-D-SND-RP-10 Issue 1).” pp. 1–20, 1996.

[74] A. Lindsay, “Site Report Track Circuit Shunting Effects of 142 and 153 Class Trains During Sander Trials (TR580038885A4),” Plymouth, 2011.

[75] M. Faccoli, C. Petrogalli, M. Lancini, A. Ghidini, and A. Mazzù, “Effect of desert sand on wear and rolling contact fatigue behaviour of various railway wheel steels,” *Wear*, vol. 396–397, pp. 146–161, Feb. 2018.

[76] D. G. Grieve, R. S. Dwyer-Joyce, and J. H. Beynon, “Abrasive wear of railway track by solid contaminants,” *J. Rail Rapid Transit*, vol. 215, no. 3, pp. 193–205, 2001.

[77] I. D. Pollicott, “Advantages of a high speed sanding device in overcoming the adverse effects of air-flow near wheels (IM-TRIB-017) (British Rail Report),” 1974. [Online]. Available: https://www.sparkrail.org/Lists/Records/DispForm.aspx?ID=9054.

[78] F. . Gay, D. Constantiner, J. T. Champa, K. Hutchings, and D. G. Millette, “Transport of solid particulates,” US 6,297,295 B1, 2001.

[79] S. Barnard and J. Cooke, “Summary Report : Low Adhesion project – Technologies and Solutions for more reliable and predictable braking (RSSB Report),” 2014. [Online]. Available: https://www.sparkrail.org/Lists/Records/DispForm.aspx?ID=15152.

[80] M. Gorbunov *et al.*, “Estimation of sand electrification influence on locomotive wheel/rail adhesion processes,” *Maint. Reliab.*, vol. 21, no. 3, pp. 460–467, 2019.

[81] M. Harmon and R. Lewis, “Top of Rail Friction Modifier Review Paper,” *Tribol. - Mater. Surfaces Interfaces*, vol. 10, no. 3, pp. 150–162, 2016.

[82] The Editors of Encyclopaedia Brittanica, “Mineralogy,” *Encyclopaedia Britannica*. 2008.

[83] C. Klein, “Mineral,” *Encyclopaedia Britannica*. 2013.

[84] R. Siever, *Sand*. 1988.

[85] R. Pettijohn, F.J.; Potter, Paul Edwin; Siever, *Sand and Sandstone*. Berlin, Heidelberg, New York: Springer-Verlag, 1972.

[86] W. W. Emmett, “The Channels and Waters of the Upper Salom River, Idaho,” 1975.

[87] Mindat.org, “Quartz.” [Online]. Available: https://www.mindat.org/min-3337.html. [Accessed: 24-Feb-2017].

[88] The Editors of Encyclopaedia Brittanica, “Moh’s Hardness,” *Encyclopaedia Britannica*. 1998.

[89] Industrial Minerals Association North America, “What is Feldspar?” [Online]. Available: http://www.ima-na.org/?page=what_is_feldspar. [Accessed: 24-Feb-2017].

[90] M. D. Dyar and M. E. Gunter, *Mineralogy and Optical Mineralogy*. Chantilly: Mineralogical Society of America, 2008.

[91] British Geological Survey, “X-ray diffraction (XRD) analysis.” [Online]. Available: http://www.bgs.ac.uk/scienceFacilities/laboratories/mpb/xrd_tech.html.

[Accessed: 07-Feb-2017].

[92] V. S. Shrivastava, "X- ray Diffraction and Mineralogical Study of Soil : A Review," *J. Appl. Chem. Res.*, vol. 9, pp. 41–51, 2009.

[93] ASTM C136, "Standard Test Method for Sieve Analysis of Fine and Coarse Aggregates," *Annu. B. ASTM Stand.*, pp. 3–7, 2006.

[94] P. Vangla, N. Roy, K. Mendu, and G. M. Latha, "Digital Image Analysis for the Determination of Size and Shape Parameters of Sand Grains," *Geo-Innovations*, 2014.

[95] M. Langton and A.-M. Hermansson, "Image analysis determination of particle size distribution," *Food Hydrocoll.*, vol. 7, no. 1, pp. 11–22, 1993.

[96] S. J. Blott and K. Pye, "Particle size distribution analysis of sand-sized particles by laser diffraction: An experimental investigation of instrument sensitivity and the effects of particle shape," *Sedimentology*, vol. 53, no. 3, pp. 671–685, 2006.

[97] W. C. Krumbein and L. L. Sloss, *Stratigraphy & Sedimentation*, 2nd ed. San Francisco: Freeman and Company, 1963.

[98] A. G. Cho, J. Dodds, and J. C. Santamarina, "Particle Shape Effects on Packing Density , Stiffness and Strength – Natural and Crushed Sands- Document Summary Number of Words : 4 , 266 Number of Tables : 2 Number of Figures : 11," *J. Geotech. Geoenvironmental Eng.*, vol. 132, no. May, pp. 591–602, 2006.

[99] H. Wadell, "Volume , Shape , and Roundness of Rock Particles," *J. Geol.*, vol. 40, no. 5, pp. 443–451, 1932.

[100] W. C. Krumbein, "Measurement and geological significance of shape and roundness of sedimentary particles," *J. Sediment. Petrol.*, vol. 11, no. 2, pp. 64–72, 1941.

[101] ASTM, "ASTM D 4791-10: Standard Test Method for Flat Particles, Elongated Particles, or Flat and Elongated Particles in Coarse Aggregate." .

[102] G. W. Stachowiak, "Particle angularity and its relationship to abrasive and erosive wear," *Wear*, vol. 241, no. 2, pp. 214–219, 2000.

[103] Malvern Instruments Ltd., "Morphologi G3 User Manual," 2008.

[104] J. C. Jaeger, "Failure of Rocks Under Tensile Conditions," *Int. J. Rock Mech. Min. Sci.*, vol. 4, pp. 219–227, 1967.

[105] Y. Nakata, A. F. L. Hyde, M. Hyodo, and H. Murata, "Discussion: A probabilistic approach to sand particle crushing in the triaxial test," *Géotechnique*, vol. 49, no. 5, pp. 567–583, 2001.

[106] A. K. Dutta and D. Penumadu, "Hardness and Modulus of Individual Sand Particles Using Nanoindentation," *Adv. Meas. Model. Soil Behav.*, vol. 236, pp. 1–10, 2007.

[107] N. P. Daphalapurkar, F. Wang, B. Fu, H. Lu, and R. Komanduri, "Determination of Mechanical Properties of Sand Grains by Nanoindentation," *Exp. Mech.*, vol. 51, no. 5, pp. 719–728, 2011.

[108] W. C. Oliver and G. M. Pharr, “An improved technique for determining hardness and elastic modulus using load and displacement sensing indentation experiments,” *J. Mater. Res.*, vol. 7, no. 6, pp. 1564–1583, 1992.

[109] M. Sebastiani, K. E. Johanns, E. G. Herbert, and G. M. Pharr, “Measurement of fracture toughness by nanoindentation methods: Recent advances and future challenges,” *Curr. Opin. Solid State Mater. Sci.*, vol. 19, pp. 324–333, 2015.

[110] B. Crüger *et al.*, “Coefficient of restitution for particles impacting on wet surfaces: An improved experimental approach,” *Particuology*, vol. 25, pp. 1–9, 2016.

[111] D. B. Hastie, “Experimental measurement of the coefficient of restitution of irregular shaped particles impacting on horizontal surfaces,” *Chem. Eng. Sci.*, vol. 101, pp. 828–836, 2013.

[112] H. Krupp, “Particle adhesion theory and experiment,” *Adv. Colloid Interface Sci.*, vol. 1, no. 2, pp. 111–239, 1967.

[113] H. J. Butt and M. Kappl, “Normal capillary forces,” *Adv. Colloid Interface Sci.*, vol. 146, no. 1–2, pp. 48–60, 2009.

[114] U. Zafar, C. Hare, A. Hassanpour, and M. Ghadiri, “Drop test: A new method to measure the particle adhesion force,” *Powder Technol.*, vol. 264, pp. 236–241, 2014.

[115] K. Hein, T. Hucke, M. Stintz, and S. Ripperger, “Analysis of adhesion forces between particles and wall based on the vibration method,” *Part. Part. Syst. Charact.*, vol. 19, no. 4, pp. 269–276, 2002.

[116] G. R. Salazar-Banda, M. A. Felicetti, J. A. S. Gonçalves, J. R. Coury, and M. L. Aguiar, “Determination of the adhesion force between particles and a flat surface, using the centrifuge technique,” *Powder Technol.*, vol. 173, no. 2, pp. 107–117, 2007.

[117] M. Takeuchi, “Adhesion forces of charged particles,” *Chem. Eng. Sci.*, vol. 61, no. 7, pp. 2279–2289, 2006.

[118] N. Shukla and K. H. Henthorn, “Effect of relative particle size on large particle detachment from a microchannel,” *Microfluid. Nanofluidics*, vol. 6, no. 4, pp. 521–527, 2009.

[119] M. E. Mullins, L. P. Michaels, V. Menon, B. Locke, and M. B. Ranade, “Effect of Geometry on Particle Adhesion,” *Aerosol Sci. Technol.*, vol. 17, no. 2, pp. 105–118, 1992.

[120] S. Ripperger and K. Hein, “Measurement of adhesion forces in air with the vibration method,” *China Particuology*, vol. 3, no. 1–2, pp. 3–9, 2005.

[121] V. Ganesan, K. A. Rosentrater, and K. Muthukumarappan, “Flowability and handling characteristics of bulk solids and powders – a review with implications for DDGS,” *Biosyst. Eng.*, vol. 101, no. 4, pp. 425–435, 2008.

[122] D. Geldart, E. C. Abdullah, A. Hassanpour, L. C. Nwoke, and I. Wouters, “Charcterization of Powder Flowability Using Measurement of Angle of Repose,” *China Particuology*, vol. 4, no. 3–4, pp. 104–107, 2006.

[123] H. M. B. Al-Hashemi and O. S. B. Al-Amoudi, “A review on the angle of repose of granular materials,” *Powder Technol.*, vol. 330, pp. 397–417, 2018.

[124] A. Hassanpour and M. Ghadiri, “Distinct element analysis and experimental evaluation of the Heckel analysis of bulk powder compression,” *Powder Technol.*, vol. 141, no. 3, pp. 251–261, Mar. 2004.

[125] J. J. Kalker, “A Fast Algorithm for the Simplified Theory of Rolling Contact,” *Veh. Syst. Dyn.*, 1982.

[126] O. Polach, “Creep forces in simulations of traction vehicles running on adhesion limit,” in *Wear*, 2005.

[127] C. Tomberger, P. Dietmaier, W. Sextro, and K. Six, “Friction in wheel-rail contact: A model comprising interfacial fluids, surface roughness and temperature,” *Wear*, 2011.

[128] A. Mazzù and D. Battini, “A Model for the Assessment of Wheel–Rail Contact in the Presence of Solid Contaminants,” *Tribol. Trans.*, vol. 62, no. 2, pp. 230–238, Mar. 2019.

[129] K. Six *et al.*, “Plasticity in wheel–rail contact and its implications on vehicle–track interaction,” *Proc. Inst. Mech. Eng. Part F J. Rail Rapid Transit*, vol. 231, no. 5, pp. 558–569, 2017.

[130] S. Alexandrov, “A Property of Equations of Rigid/Plastic Material Obeying a Voce-Type Hardening Law,” *Meccanica*, vol. 34, pp. 349–356, 1999.

[131] ASTM, “ASTM C702-18: Standard Practice for Reducing Samples of Aggregate to Testing Size.” 2018.

[132] T. Allen, *Particle Size Measurement, 3rd Edition*. Chapman & Hall, 1981.

[133] British Standards Institution, “BS 1377-2:1990 Methods of test for soils for civil engineering purposes. Part 2: Classification tests,” *British Standard*. 1990.

[134] M. de Berg, O. Cheong, M. van Kreveld, and M. Overmars, *Computational Geometry: Algorithms and Applications, 3rd Edition*, 3rd ed. Springer-Verlag Berlin Heidelberg, 2008.

[135] G. R. Anstis, P. Chantikul, B. R. Lawn, and D. B. Marshall, “A Critical Evaluation of Indentation Techniques for Measuring Fracture Toughness: I, Direct Crack Measurements,” *J. Am. Ceram. Soc.*, vol. 64, no. 9, pp. 533–538, 1981.

[136] U. Sandberg and J. Ejsmont, “Influence of tyre rubber hardness on tyre/road noise emission,” in *Inter-Noise 2006*, 2007.

[137] F. Hussain and A. Ali, “Elastic and plastic properties of Soda Lime Glass by micro-indentation,” *Key Eng. Mater.*, vol. 442, no. March, pp. 294–300, 2010.

[138] K. L. Johnson, K. Kendall, and A. D. Roberts, “Surface Energy and the Contact of Elastic Solids,” in *Proceedings of the Royal Society A: Mathematical, Physical and Engineering Sciences*, 1971, vol. 324, no. 1558, pp. 301–313.

[139] W. Weibull, “A Statistical Distribution Function of Wide Applicability,” *J. Appl. Mech.*, vol. 18, pp. 293–297, 1951.

[140] L. Zhou, H. Brunskill, M. Pletz, W. Daves, S. Scheriau, and R. Lewis, “Real-Time

Measurement of Dynamic Wheel-Rail Contacts Using Ultrasonic Reflectometry," *J. Tribol.*, vol. 141, no. 6, Jun. 2019.

[141] T. Fujioka and Z. Horita, "Development of High-Pressure Sliding Process for Microstructural Refinement of Rectangular Metallic Sheets," 2009.

[142] K. Edalati and Z. Horita, "A review on high-pressure torsion (HPT) from 1935 to 1988," *Mater. Sci. Eng. A*, vol. 652, pp. 325–352, 2015.

[143] F. Wetscher, A. Vorhauer, and R. Pippan, "Strain hardening during high pressure torsion deformation," *Mater. Sci. Eng. A*, pp. 410–411, 2005.

[144] M. D. Evans, "Performance Assessment of Friction Management Products in the Wheel-Rail Interface," University of Sheffield, 2018.

[145] M. Evans, W. A. Skipper, L. Buckley-Johnstone, A. Meierhofer, K. Six, and R. Lewis, "The development of a high pressure torsion test methodology for simulating wheel/rail contacts," *Tribol. Int.*, vol. 156, no. 106842, Apr. 2021.

[146] K. Ishizaka, B. White, M. Watson, S. R. Lewis, and R. Lewis, "Influence of temperature on adhesion coefficient and bonding strength of leaf films: A twin disc study," *Wear*, vol. 454–455, p. 203330, Aug. 2020.

[147] M. Watson, B. White, J. Lanigan, T. Slatter, and R. Lewis, "The composition and friction-reducing properties of leaf layers," *Proc. R. Soc. A Math. Phys. Eng. Sci.*, vol. 476, no. 2239, p. 20200057, Jul. 2020.

[148] B. Bhushan and A. V. Kulkarni, "Effect of normal load on microscale friction measurements," *Thin Solid Films*, vol. 278, no. 1–2, pp. 49–56, May 1996.

[149] Y. Nakata, Y. Kato, M. Hyodo, A. F. L. Hyde, and H. Murata, "One-Dimensional Compression Behaviour of Uniformly Graded Sand Related to Single Particle Crushing Strength," *Soils Found.*, vol. 41, no. 2, pp. 39–51, 2001.

[150] D. Jones, "Investigating grease pick-up and carry down using laboratory and field measurements.," University of Sheffield, 2014.

[151] M. Harmon *et al.*, "Optimisation of Grease Application to Railway Track," *J. Rail Rapid Transit*, vol. 232, no. 5, pp. 1514–1527, 2017.

[152] K. Six, A. Meierhofer, G. Müller, and P. Dietmaier, "Physical processes in wheel–rail contact and its implications on vehicle–track interaction," *Veh. Syst. Dyn.*, vol. 53, no. 5, pp. 635–650, May 2014.

[153] A. Meierhofer, C. Hardwick, R. Lewis, K. Six, and P. Dietmaier, "Third body layer-experimental results and a model describing its influence on the traction coefficient," *Wear*, vol. 314, no. 1–2, pp. 148–154, 2014.

[154] M. Harmon, J. F. Santa, J. A. Jaramillo, A. Toro, A. Beagles, and R. Lewis, "Evaluation of the coefficient of friction of rail in the field and laboratory using several devices," *Tribol. - Mater. Surfaces Interfaces*, vol. 14, no. 2, pp. 119–129, Apr. 2020.

[155] M. Fisher, "VT605 Trial at xnH Conditions (Shift2Rail, PINTA2, WP7/WP15) - Overview Presentation for ARG." 2020.

APPENDIX A

HPT Test Procedure

1) Enter test name, test date, 3rd body conditions, ambient humidity, ambient temperature, nominal contact dimensions (ID=10.5 mm, OD=18 mm), and test sweep length into test script.
2) Place the rail specimen (made from R260 steel) into the square pocket of the bottom specimen holder.
3) Place the wheel specimen (made from R8T steel) screwed into top specimen holder.
4) Start the test script.
5) Conduct alignment check between the faces of the specimens at 0°, 40°, -40°. Place contact paper between the faces and visually inspect to make sure the pressure is constant in the contact at all angles.
6) Measure inner and outer diameters the impression on the contact paper. If different from the nominal contact dimensions input these measured dimensions into the script instead.
7) Clean specimen faces thoroughly with acetone.
8) Run in specimen to prevent strain hardening occurring during the test runs. Run in procedure as follows:
    a) Bottom specimen rotated to a position at 0° and brought up till contact is made with the top specimen.
    b) Contact pressure increased to 900 MPa.
    c) Bottom specimen begins to rotate in a +ve° direction.
    d) Rotation finishes when either:
        i) Shear stress in contact reaches a maximum (±950 MPa).
        ii) Sweep angle moves ± 2°.
        iii) Slip between faces has been detected (rapid movement in angular position with little increase in shear stress). This final condition is almost always the condition triggered.
    e) When rotation in the +ve° has finished the bottom specimen begins to rotate back in the -ve° direction, with rotation ending according to the same criteria used in the +ve° case.
    f) This process is repeated with the bottom specimen starting at -30° and 30°.
9) Perform two dry test sweeps at -30° and -20° to ensure the surfaces are fully run in and to allow comparison between the effect of a dry interface and one with a 3rd body layer present. Dry test sweep procedure is as follows:
    a) Bottom specimen raised till contact is made with the top specimen.

b) Contact pressure increased to 900 MPa.
c) Data logging commences.

d) Bottom specimen rotated in the +ve° direction through the test sweep length of 0.4 mm at a rate of 0.1 °/s.
e) When the test sweep length has been met data logging ends.
f) The shear stress in the contact is brought down to zero and the bottom specimen is lowered.

10) When both dry runs have been completed, then apply the requisite material to the contact. The material application procedures are as follows:
a) Dry Particles; place 0.025 g of particles into the contact whilst taking care to try and evenly space the particles. 0.025 g of material was selected as this created a sand density in the contact of 150 g/m^2, the amount currently specified by British standards as a maximum.
b) Liquids; apply 20 µl of liquid onto the contact via a syringe, take care to fully cover the contact. 20 µl was selected as the minimum needed to fully cover the contact.
c) Liquids and Dry Particles; place the particles into the contact as described in 10.a. Then apply the liquid in the same way as 10.b. Take care to try and ensure even particle spacing after liquid application.
d) Leaves; place 0.025 g of leaf powder into the contact, then apply 20 µl of distilled water on top, then perform one extra test run to condition the leaf layer. Before the next test run, apply another 20 µl of water.
e) Leaves and Dry Particles; apply leaf powder as described in 10.d. Before applying the last 20 µl of water, apply the dry particles as described in 10.a.

11) Conduct three more test runs with the bottom specimen at -10°, 0°, and 10°. Run these tests in the same manner as the dry tests as outlined in 9.
12) After all tests are complete analyse the specimens' surfaces using an optical 3D profilometer.